Towards More Efficient and Economical Phosphorus and Bioenergy Recovery from Source-Diverted Blackwater

by

Huijuan Sun

A thesis submitted in partial fulfillment of the requirements for the degree of

Doctor of Philosophy

in

Environmental Engineering

Department of Civil and Environmental Engineering
University of Alberta

ABSTRACT

Decentralized source-diverted blackwater resource recovery represents an attractive wastewater management approach. Source-diverted blackwater refers to toilet wastewater, with or without kitchen wastewater, containing over half of the domestic biochemical oxygen demand (BOD) load and over 90% of PO_4-P and NH_4-N contents. Blackwater has strong buffering capacity as a result of high alkalinity and high pH close to 9. Without the addition of waste streams collected from laundry, washing, showering, and other household wastewaters (i.e., grey water), source-diverted blackwater, especially concentrated blackwater collected from low-flush vacuum toilet systems, is ideal for nutrient and energy recovery. In particular, phosphorus (P) recovery from blackwater helps relieve the dependence on phosphate rock reserves, which is becoming crucial for sustainable waste management in the context of both environment protection and future availability of P. Biogas recovery from blackwater represents a source of renewable energy, which helps increase energy security, reduce the reliance on non-renewable energy, and reduce greenhouse gas emission from non-renewable energy utilization.

This thesis aims to evaluate, develop, and optimize biological and chemical processes to achieve enhanced P and biomethane recovery from source-diverted blackwater. Specifically, this thesis focuses on three aspects: (i) assessing and developing cost-effective and efficient P recovery from raw blackwater without chemical addition, (ii) evaluating and modelling the role of bioreactor microbiome on biomethane recovery from blackwater; and (iii) developing and optimizing bioreactors for simultaneous P and biomethane recovery from blackwater.

This thesis successfully demonstrated the feasibility of P recovery through high-quality struvite precipitation from raw concentrated blackwater, which achieved >90% P recovery without

any alkali addition. Operational conditions for blackwater biomethane recovery from upflow anaerobic sludge blanket (UASB) reactors were optimized, and the importance of low-abundance microorganisms in UASB reactors was demonstrated. Lastly, simultaneous P and biomethane recovery from source-diverted blackwater was demonstrated, and the mechanisms involved in P precipitation in bioreactors were clarified. Overall, this research developed and optimized blackwater P and biomethane recovery technologies and contributed to the development of more sustainable resource recovery-based wastewater management.

PREFACE

The contents of this thesis are my original work, with the contributions of several individuals. The research shown in this thesis was conducted under the supervision of Dr. Yang Liu. I was responsible for experiment design and execution, data collection and analysis, formal analysis, and manuscript writeup and revision. Dr. Liu contributed to conceptualization, formal analysis, supervision, review and editing of the manuscripts, project administration, and funding acquisition. The contributions of other individuals are listed below.

A version of **Chapter 3** has been published as Sun, H., Mohammed, A.N., and Liu, Y., 2020, Phosphorus recovery from source-diverted blackwater through struvite precipitation, Science of the Total Environment, 743, 140747. Mohammed, A.N. contributed to conceptualization and validation.

A version of **Chapter 4** has been published as Sun, H., Chuquihuaccha Hernandez, V.L., Mohammed, A.N., and Liu, Y., 2021, Impact of total suspended solids on struvite from source-diverted blackwater, Journal of Environmental Engineering, 147 (3), 04020157. Chuquihuaccha Hernandez, V.L. was involved in conducting experiments. Mohammed, A.N. contributed to conceptualization and validation.

A version of **Chapter 5** has been published as Sun, H., Yu, N., Mou, A., Yang, X., Liu, Y., 2022, Effluent recirculation weakens the hydrolysis of high-solid content feeds in upflow anaerobic sludge blanket reactors, Journal of Environmental Chemical Engineering, 10 (3), 107913. Yu, N. had the equal contribution to first authorship. Mou, A. and Yang, X. were involved in the chemical analysis of effluent quality.

A version of **Chapter 6** has been published as Sun, H., Zhang, L., Zhang, Y., Guo, B., Liu, Y., 2021, A new non-steady-state mass balance model for quantifying microbiome responses to disturbances in wastewater bioreactors, Journal of Environmental Management, 296, 113370. Zhang, L. provided the experimental data for the model validation. Zhang, Y. and Guo, B. gave constructive suggestions on the model development.

A version of **Chapter 7** has been published as Sun, H., Yu, N., and Liu, Y., 2022, Importance of low-abundance microbial species in response to disturbances in wastewater bioreactors, Process Safety and Environmental Protection, 162, 663–671. Yu, N. contributed to the experimental design and execution.

A version of **Chapter 8** has been published as Sun, H., Yang, X., Yu, N., Gong, X., Zhang, L., and Liu, Y., 2021, Impact of feedwater protein contents on calcium phosphate mineralization in anaerobic digesters, Journal of Environmental Chemical Engineering, 9, 106445. Yang, X. was involved in feeding reactors and monitoring reactor performance. Yu, N. helped assemble reactors and tackle technical problems encountered in the reactor operation. Gong, X. was involved in sludge characterization including Fourier Transform Infrared spectroscopy and zeta potential tests. Zhang, L. contributed to conceptualization, formal analysis, and validation.

A version of **Chapter 9** has been published in the as Sun, H., Yang, X., Zhang, L., and Liu, Y., 2023, The role of protein contents in promoting wastewater phosphorus and bioenergy recovery during anaerobic digestion, Biomass and Bioenergy, 169, 106694. Yang, X. was involved in feeding reactors and monitoring reactor performance. Zhang, L. contributed to conceptualization, formal analysis, and validation.

Chapter 1 summarizes the research background, research objectives, and thesis structure. **Chapter 2** presents the literature review. **Chapter 10** summarizes the conclusions reached in this thesis as well as the recommendations for future research. **Chapters 1, 2** and **10** are originally written by Huijuan Sun and have never been published elsewhere.

DEDICATION

To love, bravery, and peace

"I see tress of green, red roses too

I see them bloom for me and you

And I think to myself what a wonderful world.

I see skies of blue and clouds of white

The bright blessed day, the dark sacred night

And I think to myself what a wonderful world.

The colors of the rainbow so pretty in the sky

Are also on the faces of people going by

I see friends shaking hands saying how do you do

They're really saying I love you.

I hear babies crying, I watch them grow

They'll learn much more than I'll never know

And I think to myself what a wonderful world

Yes I think to myself what a wonderful world."

—Louis Armstrong

ACKNOWLEDGMENTS

The work presented in this thesis could not have been accomplished without the support and expertise of a large number of people in my life. First and foremost, I would like to express my appreciation to my supervisor Dr. Yang Liu for her supervision, advice, and guidance from the early stages of my Ph.D. research to putting this thesis together. Thank Dr. Liu for providing me this precious opportunity to study at the University of Alberta and work in her excellent research group. The past five years' study and research experience will be a milestone in my life. Thank Dr. Liu for inspiring, encouraging, and supporting me continuously during my research. She is positive, affirmative, kind, and fair and has set an excellent example for me to follow forever. Thank Dr. Liu for allowing me to develop skills such as reactor assembly, lab-scale and pilot-scale reactor operation and maintenance, use of microbial analysis software, operation of characterization techniques, etc. Grasping and be proficient in these skills will be beneficial to my future career. Dr. Liu enlightens my life, and my life has more possibilities because of her.

I am grateful to Dr. Jay Cheng, Dr. Hongbo Zeng, Dr. Zaher Hashisho, and Dr. Wenming Zhang for serving as my examination committee members as well as providing constructive comments/suggestions. I also thank Dr. Lijun Deng for his contributed time to serve as the Chair.

A big thanks to all past and present group members in Dr. Liu's group for the support throughout my time in the lab. Special thanks to the postdoctoral fellow Dr. Lei Zhang, Dr. Najiaowa Yu, and the PhD student Abdul Mohammed. Dr. Zhang is proficient in anaerobic digester operation and excellent at tackling technical problems encountered in reactor operation. His critical thinking always inspires me. He gave me many good suggestions when I faced challenges. Dr. Zhang spent a lot of time in serving our students. Dr. Yu gave me great support in

my research. She taught me how to assemble reactors, how to do the sludge tests, how to do microbial community analysis, etc. Abdul always supported me since I joined in Dr. Liu's group. He is enthusiastic about research and provided many valuable suggestions about my experiments. My experiments could not have been conducted smoothly without their contributions.

I would like to thank the past members in Dr. Liu's group, Dr. Bing Guo, Dr. Yun Zhou, Miss Mozhu Li, Dr. Qianyi Zhang, Dr. Xiaoyu Gong, Dr. Mengjiao Gao, and Dr. Hongyu Dang, for their suggestions that always inspired me. Thank the PhD students Miss Anqi Mou, Miss Xinya Yang, Miss Yiyang Yuan, and the visiting student Mr. Victor Leonardo Chuquihuaccha Hernandez for their involvement in conducting my experiments. Thank Dr. Huixin Zhang, Dr. Yingdi Zhang, Miss Xin Zou, Miss Qi Huang, and Ms. Sandra Ukaigwe for their suggestions and continuous support. Thank our administrative assistant Alice Da Silva for her efforts to help create an organized and enjoyable working environment. Thank these lovely group members for their friendship.

Special thanks to our technician Dr. David (Yupeng) Zhao for training and technical support. Dr. Zhao is very warm-hearted and always ready to help.

I would like to acknowledge the financial support for this project from the Natural Sciences and Engineering Research Council of Canada (NSERC) Alliance Project, the City of Edmonton, the NSERC Discovery project, the Alberta Innovates Clean Technology Facilities Support Program, and the Canada Research Chairs (CRC) Program in Future Water Services to Dr. Liu.

I would like to thank all my teachers from kindergarten to university and from China to Canada. Teaching is one of the most rewarding and meaningful professions because their teaching equipped people with humanity, knowledge, enlightenment, and hope. I cannot type all their names

one by one, nevertheless, I will remember them forever. Thank my supervisor Dr. Bofeng Bai at the Xi'an Jiaotong University. Dr. Bai led me to the scientific research, and thereby I found a different and more wonderful world. Thank my supervisor Dr. Tony Yang at the University of Regina. Dr. Yang's attitude toward teaching and research had profound effect on me. Thank the outstanding professors in our Environmental Engineering at the University of Alberta who have taught me. Their excellent teaching laid a solid foundation for my research and future career.

I would not be here without my family's love. My dearest grandpa and parents supported me through everything I have pursued. Although they bid farewell to this world, they never ever leave me even for a second. I would also like to thank my beloved husband for his never-ending support, encouragement, and love. I could not have asked for a better partner to share my accomplishments and life with. I want to be a better person because of him. I must also thank our sweet kids for their accompany in the difficult times.

Last but not least, I also want to express my special thanks to two great friends, Wenyuan Wang and Shuang Li, for their friendship.

TABLE OF CONTENTS

LIST OF TABLES

LIST OF FIGURES

LIST OF ABBREVIATIONS

ACP	amorphous calcium phosphate
AD	anaerobic digestion
ADBW	anaerobically digested blackwater
Alk	alkalinity
BMP	biomethane potential
BOD	biochemical oxygen demand
BSA	bovine serum albumin
BW	blackwater
CaP	calcium phosphate
C/N	ratio: carbon/nitrogen ratio
COD	chemical oxygen demand
CODs	soluble chemical oxygen demand
CODt	total chemical oxygen demand
DCP	monetite
DCPD	brushite

DI	deionized
EDC	endocrine-disrupting compound
EPS	extracellular polymeric substances
FBR	fluidized bed reactor
FTIR	Fourier transform infrared
HAP	hydroxyapatite
HRT	hydraulic retention time
HS	high-solid content substrate
ICP-MS	inductively coupled plasma mass spectrometry
ICSD	Inorganic Crystal Structure Database
LS	low-solid content substrate
MBM	mass balance model
N	nitrogen
OCP	octacalcium phosphate
OLR	organic loading rate
OTU	operational taxonomic unit
P	phosphorus

PCoA	principal coordinates analysis
SBW	blackwater supernatant
SEM-EDX	scanning electron microscope-energy dispersive X-ray spectroscopy
SI	supersaturation index
SMA	specific mehanogenic activity
SRT	solid rention time
SSR	supersautration ratio
TCP	tricalcium phosphate
TP	total phosphorus
TS	total solids
TSS	total suspended solids
UASB	upflow anaerobic sludge blanket
VFA	volatile fatty acid
VS	volatile solids
VSS	volatile suspended solids
VT	vacuum toilet
XRD	X-ray diffraction

CHAPTER 1 INTRODUCTION AND RESEARCH OBJECTIVES

1.1 Background and Motivations

In cities, household wastewater is usually collected and treated at centralized wastewater treatment plants using a range of physiochemical and biological treatment processes. The treated water is then discharged to the environment. Centralized wastewater treatment plants are essential for protecting public health and the environment by ensuring that wastewater is properly treated and managed before being released. However, the capital cost, operating and maintenance cost, and energy consumption of these centralized wastewater treatment systems are extremely high (Maurer et al., 2015). These conventional systems consume a large amount of energy in the long underground collection systems and the biological treatment processes accompanied by sludge generation and post treatment requirements. To provide a sense of scale, wastewater collection and treatment contribute to at 1% of each nation's energy cost (Gao, 2020). To tackle these challenges, water reclamation and resource recovery from wastewater are important steps to develop more sustainable wastewater services and contribute to the circular economy.

Source separation at the household level has been recognized as one of the most promising new sanitation concepts to rebuild the balance of carbon, nutrients, and water cycles (Tervahauta et al., 2013; Gao et al., 2019; Capodaglio, 2020). Under this concept, blackwater and greywater are the two main categories of household wastewater. Blackwater, collected from flush toilets, consists of urine, feces, and optionally organic kitchen waste. Blackwater is considered as high-strength wastewater which is rich in organics [5,000 – 93,000 mg/L of chemical oxygen demand

(COD)] and nutrients [e.g., 1,500 – 16,000 mg/L of nitrogen (N) and 500 – 3,000 mg/L of phosphorus (P)] (Capodaglio, 2020). Greywater, collected from hand basins, washing machines, showers, and baths, however, has large water volume, low COD, and low nutrients. Different characteristics between blackwater and greywater make them suitable for different treatment processes, in order to maximize energy and nutrient recovery and water reuse.

Compared to traditional centralized wastewater management, source separation and decentralized treatment systems allow for maximized local resource recovery and help save cost and energy associated with wastewater collection and conveyance networks. For instance, co-digesting source-diverted concentrated blackwater and wet organic wastes can recover approximately 90% of the N, 74% of the P, and 79% of the potassium (K) (Moges et al., 2018). By virtue of the source separation system, blackwater may provide not only a source of variable valuable resources, but also multiple benefits to society (Wang et al., 2023).

Among the resources, P is an essential element to sustain all forms of life on Earth. For instance, P is fundamental for fruit and crop growth because it takes part in major processes such as photosynthesis, energy transfer, cell division, and cell growth. P is a building block of DNA, RNA, and energy storage ATP in animals. It also helps build strong bones and teeth and is related to mineral metabolism as well (Theregowda et al., 2019). As the global population grows, the increased agricultural demand is an imminent threat to the world's P supply (Cordell et al., 2009; Daneshagr et al., 2018). Commercial phosphate fertilizers mainly come from natural phosphate rock (Samreen and Kausar, 2019), but phosphate rock reserves are limited around the world, and they distribute unevenly (Daneshgar et al., 2018). The quality and accessibility of currently available phosphate rock reserves are declining, while the costs associated with mining, refining, storage, and transportation are rising (International Energy Agency, 2021). One strategy for

relieving the dependence on phosphate rock reserves is to recover P from various waste sources, which is becoming crucial for sustainable waste management in the context of both environment protection and future availability of P (Egle et al., 2016; Cunha et al., 2018). Although many technologies are available for P recovery from wastewater, the requirement of chemical addition makes the P recovery in an up-scaled process costly. Economical strategies for P recovery from wastewater are required for sustainable wastewater management. Source-diverted blackwater could provide a solution to efficient and economical resource recovery.

In addition to P recovery, bioenergy recovery in the form of biomethane from blackwater could serve as another core component to re-establish the balance of energy production and consumption for the decentralized sanitation system. The most effective approach is to produce bioenergy from blackwater through anaerobic digestion (AD) that converts biodegradable organics into biogas (mainly contains CH_4 of higher than 70% and CO_2). AD has been widely applied to treat wastewater due to the bioenergy recovery, the small amount of sludge production, and the small footprint. Over the past years, Dr. Liu's group has made significant efforts in developing bioenergy recovery technology from source-diverted blackwater (Florentino et al., 2019; Gao et al., 2019a; Gao et al., 2019b; Zhang et al., 2019; Gao, 2020; Yu et al., 2020; Guo et al., 2021; Huang et al., 2021; Boiocchi et al., 2022; Dang et al., 2022; Zhang et al., 2022), while a deeper understanding of bioreactor design, operational condition selection, reaction mechanisms, and AD process limitation is still required. New AD processes (developed by Dr. Liu's group) (Zhang et al., 2021a; 2021b) that can achieve simultaneous biomethane and P recovery will significantly improve process simplicity, reduce operating costs, and achieve great environmental benefits. The new AD processes should be further studied.

1.2 Research Objectives and Approaches

The main objectives of this thesis were to achieve P and biomethane recovery from blackwater through chemical and biological processes. The specific objectives and approaches are described as follows.

Objective 1. To develop and optimize P recovery processes from blackwater

P recovery from blackwater is still limited. These limited studies mainly focused on P recovery from anaerobically digested blackwater (ADBW), and none studied P recovery from raw blackwater. ADBW has similar phosphate-phosphorus (PO_4-P) concentration as raw blackwater before AD, but with a relatively lower pH value (commonly around neutral pH), hence pH adjustment by adding alkali is required for efficient P recovery. To reduce the chemical cost associated with pH adjustment, recovering P directly from raw blackwater before AD can be an option. Source-diverted blackwater, especially concentrated blackwater collected from vacuum toilet systems, typically has moderate PO_4-P content, high ammonia-nitrogen (NH_4-N) content, strong buffering capacity as a result of high alkalinity, and a high pH value close to 9.0. It was hypothesized that concentrated blackwater is a potentially good source for P recovery through struvite precipitation without pH adjustment.

Objective 1.1 To assess the feasibility of P recovery from raw blackwater through struvite precipitation

The feasibility of producing high-quality struvite directly from raw concentrated blackwater without pH adjustment was examined by conducting batch experiments. Three types of raw blackwater flushed with 0.5 L, 1.0 L, and 5.0 L tap water per flush were used. Anaerobically

digested blackwater flushed with 1.0 L tap water per flush was also used to compare its P recovery potential with that of raw blackwater.

Objective 1.2 To evaluate the role of blackwater solids in P recovery effectiveness

In addition to pH, blackwater solid content was identified as one major operation parameter for the struvite precipitation directly from blackwater. Therefore, the role of blackwater solids in struvite production was further evaluated. Specifically, the P recovery efficiency and struvite purity and size were assessed at different blackwater solid concentrations.

Objective 2. To assess and develop biomethane recovery processes from blackwater

Dr. Liu's group has investigated biomethane recovery from source-diverted blackwater using a range of bioreactor types, blackwater sources and operational conditions (Gao et al., 2019a; Gao et al., 2019b; Zhang et al., 2019; Yu et al., 2020; Huang et al., 2021; Zhang et al., 2022). One operational condition, effluent recirculation, in an upflow anaerobic sludge blanket (UASB) reactor is a commonly used strategy to improve both mixing and upflow velocity of the reactor. Although it is considered as an important strategy, the benefits to bioreactor performance of mixing depend on bioreactor design, substrate characteristics, operational conditions, and the ratio between recirculation volume and influent volume. It was hypothesized that although mixing can improve sludge mixing and substrate uptake by microorganisms, mixing will also lead to the disturbance of the localized syntrophic interactions and thus negatively impact the biomethane yield. Further, additional studies are needed to link AD microbial community dynamics and bioreactor treatment efficiency, and another hypothesis was that a non-steady-state mass balance model can be developed to better evaluate the role of bioreactor microbes.

Objective 2.1 To reveal the role of UASB reactor mixing condition in biomethane recovery

One of the most important operation parameters for UASB reactor operation is the mixing condition, which can impact the contact between microorganisms/enzymes and substrates. The impact of effluent recirculation on biomethane production from a UASB reactor treating substrates of different solid contents was assessed.

Objective 2.2 To evaluate and model the role of UASB microbial community during blackwater biomethane recovery

Bioreactors are often subject to various physical, chemical, and biological disturbances, such as operational condition changes. The adaptation of the microbial community to disturbances (rather than recovery to the original state) determines the stability of wastewater treatment performance. An ecology model, based on the non-steady-state mass balance (16S rRNA MiSeq reads normalized by volatile suspended solids), was proposed to quantify microbiome responses to disturbances in wastewater bioreactors. Rather than focusing on the most abundant microbial groups commonly used in the literature, the model helps to identify the role of active species within the community.

Objective 2.3 To demonstrate the impact of low-abundance microorganisms in UASB reactor on biomethane recovery

The novel non-steady-state mass balance model developed in Objective 2.2 was applied to identify active low-abundance species that responded to an operational disturbance, which was induced by turning on-or-off effluent recirculation in UASB reactors (based on the experiments in Objective 2.1).

Objective 3. To develop and enhance simultaneous P and biomethane recovery processes from blackwater

The biological process offers the strongest promise for economical P recovery. The previous studies in Dr. Liu's group found calcium phosphate (CaP) precipitation in the UASB reactor treating blackwater (Zhang et al., 2021a; 2021b). How the characteristics of blackwater (other than chemical conditions) affect the CaP formation was not clear. It was hypothesized that proteins in blackwater contribute to the CaP precipitation and impact the biomethane generation as well.

Objective 3.1 To assess the feasibility of simultaneous P and biomethane recovery from blackwater

Blackwater contains about 40% proteins; the hydrolysis of proteins in AD causes the OH^- generation. The produced OH^- could help build a localized supersaturation environment to facilitate the CaP precipitation. This study was designed to demonstrate the feasibility of simultaneous P and biomethane recovery with the presence of proteins as the carbon source.

Objective 3.2 To explore the role of protein content in P and biomethane recovery from blackwater

The impact of feedwater protein content on CaP and biomethane production was further examined in the UASB reactors. This study aimed to evaluate the role of protein contents (a series of protein: carbohydrate ratios) in the efficiency of blackwater P and biomethane recovery. It also determined the optimum feedwater protein content for maximized CaP and biomethane production.

1.3 Thesis Structure

This thesis is a paper-based thesis. A total of ten chapters are presented and organized as follows. **Fig. 1–1** shows the overview of the thesis structure.

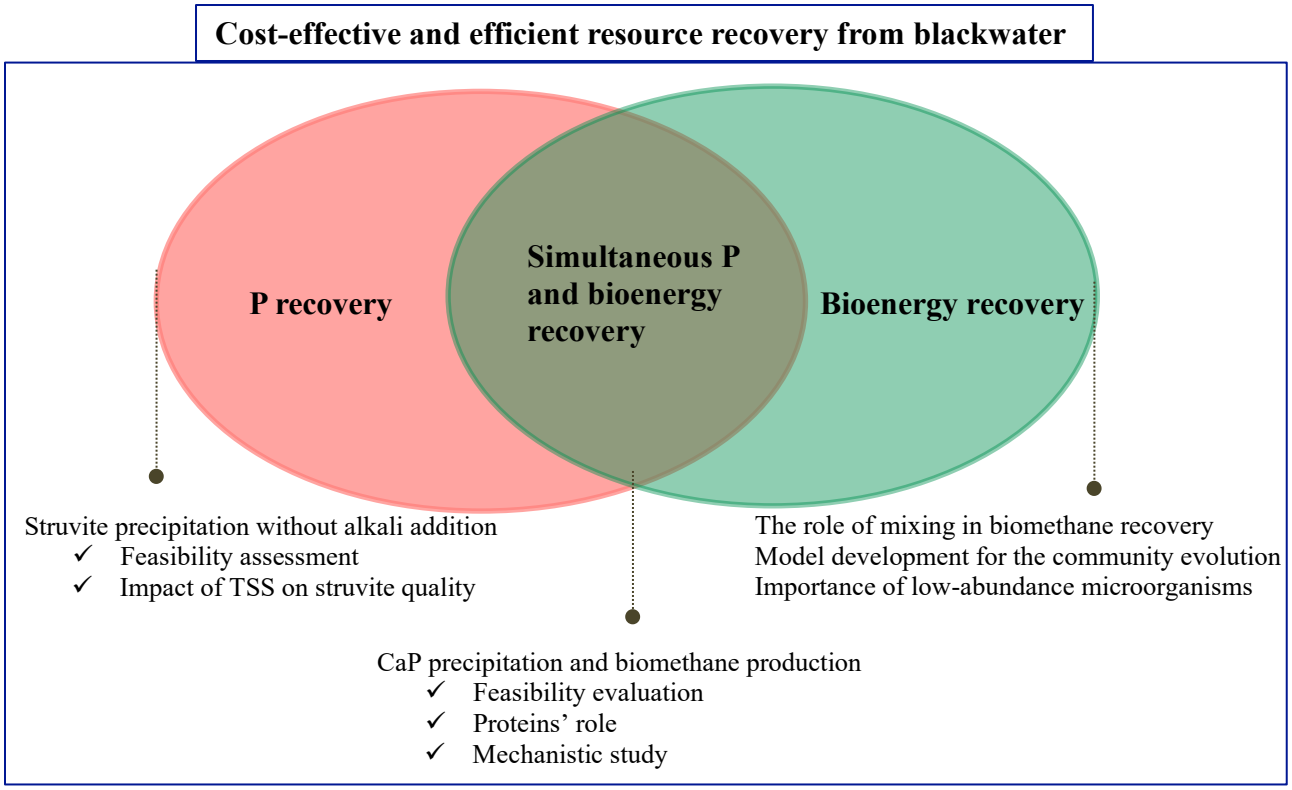

Figure 1-1. Overview of the thesis structure.

Chapter 1 introduces the research background, motivations, objectives, and approaches. The importance of resource recovery from blackwater in decentralized sanitation systems was emphasized.

Chapter 2 presents a literature review on P and bioenergy recovery from blackwater. Typically, this chapter summarized the important factors affecting the P recovery through struvite precipitation and CaP precipitation, respectively. This chapter highlighted the research achievements and research challenges/gaps in the P and bioenergy recovery from blackwater.

Chapter 3 assesses the feasibility of recovering P through struvite precipitation from raw concentrated blackwater via batch experiments. The quality of produced struvite in terms of purity,

Mg/P/N ratio, and heavy-metal content was examined. This chapter demonstrated the feasibility of high-quality struvite production from raw blackwater without alkali addition.

Further, Chapter 4 evaluates the impact of blackwater TSS on struvite quality. A fluidized bed reactor (FBR) was operated in a batch mode. An optimum Mg/P molar ratio and operating time of the FBR were determined. The influence of blackwater TSS level (120 mg/L–1,600 mg/L) and upflow velocity of the FBR (18–90 m/h) on P recovery efficiency and struvite purity and size was studied. The impact of TSS concentration on struvite growth was discussed. The hypothesis in Objective 1 is verified by the work in Chapter 3 and Chapter 4.

Chapter 5 examines the impact of effluent recirculation on biomethane production of the UASB reactors fed with substrates of high and low solid contents. The layered microbial communities were identified. The effects of mixing due to effluent recirculation on community structure, hydrolysis efficiency of particulate organic matter, and biomethane inhibition were clarified. This chapter could provide guidance on how to select an operational strategy for a UASB reactor treating wastewater containing solids.

Chapter 6 describes a novel non-steady-state mass balance model used to quantify the microbial responses to the operational disturbance applied to a wastewater bioreactor. The model incorporated the temporal changes of operational taxonomic units following a disturbance, through considering the density and type of genotypes in the influent entering the bioreactor, in the effluent leaving the bioreactor, growing in the bioreactor, and in the waste sludge discharged from the bioreactor continuously or instantaneously, as well as the prior microbial community and the sludge characteristics. This model provided a solution to calculate the individual microbe growth rate during the community evolution.

Based on the experiments carried out in Chapter 5 and the methodology developed in Chapter 6, Chapter 7 highlights the importance of low-abundance microbial species in response to an operational disturbance applied to a bioreactor to maintain the biosystem stability. Objective 2 is completed in Chapter5, Chapter 6, and Chapter 7.

Chapter 8 assesses the feasibility of simultaneous CaP and biomethane production from blackwater in a UASB reactor. The requirements of CaP nucleation from a solution were clarified. The role of proteins in CaP formation was elucidated. The well-developed microbial community for a stabilized local pH environment was analyzed.

Chapter 9 further explores the role of protein contents in CaP and biomethane production under a low supersaturation condition. The influence of protein content (0%–100%) on Ca and P removals was examined. Two mechanisms underlying the CaP precipitation induced by the protein degradation were highlighted. The microbial communities built in the UASB reactors in the presence of different-content proteins were identified. An optimum protein content that was favorable to the methanogenesis was found. Objective 3 is fulfilled by Chapter 8 and Chapter 9.

Finally, Chapter 10 highlights the conclusions drawn from this thesis and provides the recommendations for future research.

References

Boiocchi, R., Zhang, Q., Gao, M., Liu, Y., 2022. Modeling and optimization of an upflow anaerobic sludge blanket (UASB) system treating blackwater. J. Environ. Chem. Eng. 10 (3), 107614.

Capodaglio, A.G., 2020. Taking the water out of "wastewater": an ineluctable oxymoron for urban water cycle sustainability. Water Environ. Res. 92 (12), 2030–2040.

Cordell, D., Drangert, J.-O., White, S., 2009. The story of phosphorus: global food security and food for thought. Global Environ. Change 19 (2), 292–305.

Cunha, J.R., Schott, C., van der Weijden, R.D., Leal, L.H., Zeeman, G., Buisman, C., 2018. Calcium addition to increase the production of phosphate granules in anaerobic treatment of black water. Water Res. 130, 333–342.

Daneshgar, S., Callegari, A., Capodaglio, A.G., Vaccari, D., 2018. The potential phosphorus crisis: resource conservation and possible escape technologies: a review. Resources 7 (2), 37.

Dang, H., Yu, N., Mou, A., Zhang, L., Guo, B., Liu, Y., 2022. Metagenomic insights into direct interspecies electron transfer and quorum sensing in blackwater anaerobic digestion reactors supplemented with granular activated carbon. Bioresour. Technol. 352, 127113.

Egle, L., Rechberger, H., Krampe, J., Zessner, M., 2016. Phosphorus recovery from municipal wastewater: an integrated comparative technological, environmental and economic assessment of P recovery technologies. Sci. Total Environ. 571, 522–542.

Florentino, A.P., Sharaf, A., Zhang, L., Liu, Y., 2019. Overcoming ammonia inhibition in anaerobic blackwater treatment with granular activated carbon: the role of electroactive microorganisms. Environ. Sci.: Water Res. Technol. 5, 383.

Gao, M., 2020. Anaerobic Treatment of Source-diverted Blackwater-maximizing Biomethane Recovery. University of Alberta, Canada.

Gao, M., Guo, B., Zhang, L., Zhang, Y., Liu, Y., 2019a. Microbial community dynamics in anaerobic digesters treating conventional and vacuum toilet flushed blackwater. Water Res. 160 (1), 249–258.

Gao, M., Zhang, L., Florentino, A.P., Liu, Y., 2019b. Performance of anaerobic treatment of blackwater collected from different toilet flushing systems: can we achieve both energy recovery and water conservation? J. Hazard. Mater. 365, 44–52.

Guo, B., Yu, N., Weissbrodt, D.G., Liu, Y., 2021. Effects of micro-aeration on microbial niches and antimicrobial resistances in blackwater anaerobic digesters. Water Res. 196, 117035.

Huang, Q., Zakaria, B.S., Zhang, Y., Zhang, L., Liu, Y., Dhar, B.R., 2021. A high-rate anaerobic biofilm reactor for biomethane recovery from source-separated blackwater at ambient temperature. Water Environ. Res., 93 (1), 61–74.

International Energy Agency, 2021. The Role of Critical Minerals in Clean Energy Transitions. IEA Publications.

Maurer, M., Rothenberger, D., Larsen, T.A., 2005. Decentralised wastewater treatment technologies from a national perspective: at what cost are they competitive? Water Supply 5 (6), 145–154.

Moges, M.E., Todt, D., Heistad, A., 2018. Treatment of source-separated blackwater: a decentralized strategy for nutrient recovery towards a circular economy. Water 10, 463.

Samreen, S., Kausar, S., 2019. Phosphorus fertilizer: the original and commercial sources, in: Zhang, T. (Ed.), Phosphorus-Recovery and Recycling. IntechOpen, London, UK.

Tervahauta, T., Trang, H., Hernández, L., Zeeman, G., Buisman, C.J.N., 2013. Prospects of source-separation-based sanitation concepts: a model-based study. Water 5, 1006–1035.

Tervahauta, T., van der Weijden, R.D., Flemming, R.L., Leal, L.H., Zeeman, G., Buisman, C.J.N., 2014. Calcium phosphate granulation in anerobic treatment of black water: a new approach to phosphorus recovery. Water Res. 48, 632–642.

Theregowda, R.B., González-Mejía, A.M., Ma, X., Garland, J., 2019. Nutrient recovery from municipal wastewater for sustainable food production systems: an alternative to traditional fertilizers. Environ. Eng. Sci. 36 (7), 833–842.

Wang, X., Chen, J., Li, Z., Cheng, S., Mang, H.-P., Zheng, L., Jan, I., Harada, H., 2023. Nutrient recovery technologies for management of blackwater: a review. Front. Environ. Sci. 10, 1080536.

Yu, N., Guo, B., Zhang, Y., Zhang, L., Zhou, Y., Liu, Y., 2020. Different micro-aeration rates facilitate production of different end-products from source-diverted blackwater. Water Res. 177, 115783.

Zhang, L., Guo, B., Zhang, Q., Florentino, A., Xu, R., Zhang, Y., Liu, Y., 2019. Co-digestion of blackwater with kitchen organic waste: effects of mixing ratios and insights into microbial community. J. Clean. Prod. 236, 117703.

Zhang, L., Mou, A., Guo, B., Sun, H., Anwar, M.N., Liu, Y., 2021a. Simultaneous phosphorus recovery in energy generation reactor (SPRING): high rate thermophilic blackwater treatment. Resour. Conserv. Recycl. 164, 105163.

Zhang, L., Mou, A., Sun, H., Zhang, Y., Zhou, Y., Liu, Y., 2021b. Calcium phosphate granules formation: key to high rate of mesophilic UASB treatment of toilet wastewater. Sci. Total Environ. 773, 144972.

Zhang, L., Zhang, Y., Yuan, Y., Mou, A., Park, S., Liu, Y., 2022. Impacts of granular activated carbon addition on anaerobic granulation in blackwater treatment. Environ. Res. 206, 112406.

CHAPTER 2 LITERATURE REVIEW ON PHOSPHORUS AND BIOENERGY RECOVERY FROM BLACKWATER

As mentioned in Chapter 1, source-diverted blackwater, especially concentrated blackwater collected from vacuum toilet systems, has moderate PO_4-P content, high NH_4-N content, strong buffering capacity as a result of high alkalinity, and high pH close to 9. Blackwater is also high strength wastewater that has high concentration of biochemical oxygen demand (BOD). These characteristics make blackwater to be a good source for P and biomethane recovery. Chapter 2 mainly reviews: (i) P recovery from blackwater through struvite precipitation, (ii) biomethane recovery from blackwater through anaerobic digestion (AD), and (iii) simultaneous P and biomethane recovery from blackwater through AD.

2.1 P Recovery from Blackwater through Struvite Precipitation

Due to the political, economic, geographical, climate change, and world population growth, people are facing a P resource crisis in the future. P recovery from wastewater provides a way to relieve the dependence on phosphate rock reserves and to increase the future P availability.

P can be recovered as various forms like struvite ($NH_4MgPO_4 \cdot 6H_2O$), K-struvite ($KMgPO_4 \cdot 6H_2O$), calcium phosphate (CaP), aluminum phosphate, iron phosphate, phosphoric acid, elemental P, and polyphosphates depending on the waste source, recovery process, and target product.

Among the products, struvite ($NH_4MgPO_4 \cdot 6H_2O$, also as MAP) is a competitive form which is produced through chemical precipitation (illustrated in **Fig. 2–1**). Struvite precipitation is a promising strategy due to its low energy requirement and high P recovery efficiency

(Theregowda et al., 2019). Moreover, struvite represents a valuable multi-nutrient slow-release fertilizer. Many efforts have been made on struvite precipitation from various waste sources, such as domestic wastewater, animal manures, sludge liquor, and sewage sludge ash.

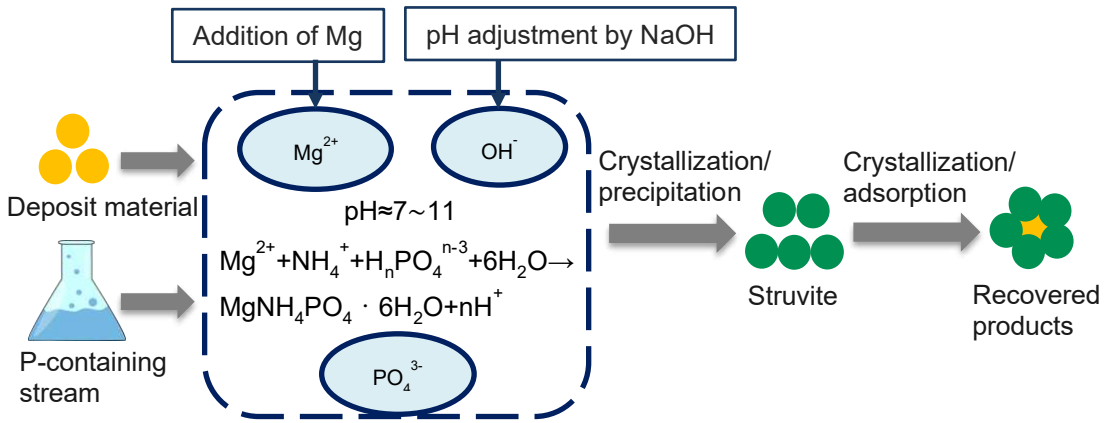

Figure 2-1. Schematic of struvite precipitation from wastewater.

2.1.1 Requirements for P product precipitation

The precipitation of a P product [Eq. (2–1)] must meet two requirements: (i), a supersaturation index [SI, calculated by Eq. (2–2)] above 0 based on the water quality to satisfy the thermodynamic requirement; and (ii), a higher SI to overcome the activation energy barrier and to trigger the nucleation.

$$aA + bB + cC \leftrightarrow dD \tag{2–1}$$

$$SI = \log\frac{IAP}{K_{sp}} \tag{2–2}$$

$$IAP = \{A\}^a\{B\}^b\{C\}^c \tag{2–3}$$

For a precipitation reaction shown in Eq. (2–1), *SI* is the supersaturation index to be determined, *IAP* is the ion activity product which can be calculated by Eq. (2–3), K_{sp} is the equilibrium constant of the Precipitate D, and {} is the activity of a target species.

The wastewater matrix determines whether the first requirement is met or not, which can usually be satisfied for the wastewater to be treated. To meet the second requirement, engineers usually increase pH, add ions like Ca or Mg that are needed for the precipitation, or choose a waste stream with a high P concentration. For instance, for the struvite production from blackwater, pH adjustment and Mg supplementation are commonly applied to achieve the second requirement (Zeeman et al., 2008; de Graaff et al., 2010; Alp, 2010; de Graaff et al., 2011; Gell et al., 2011; Yee et al., 2019).

2.1.2 Potential for struvite precipitation from blackwater

Domestic wastewater is a rich source of P, with a theoretical capacity of replacing 40–50% of the mineral P fertilizer consumed annually by the agriculture industry (Egle et al., 2016). In particular, household blackwater (i.e., toilet wastewater containing urine and feces) contributes 70–90% of P in domestic wastewater (Kujawa-Roeleveld and Zeeman, 2006; Meinzinger and Oldenburg, 2009; Todt et al., 2015). Decentralized source-diverted blackwater treatment has been suggested as an alternative to centralized wastewater treatment. Without the addition of other waste streams, source-diverted blackwater, especially concentrated blackwater collected from low-flush vacuum toilet systems, has an increased potential to recover energy and nutrients (de Graaff et al. 2011; Gao et al. 2019a). AD of blackwater is a commonly applied technique to recover energy, but PO_4-P and NH_4-N concentrations in the effluent are usually high. In this regard, this anaerobically digested blackwater (ADBW) can be further treated to recover nutrients like P and N.

The initial PO_4-P concentration of blackwater is an important parameter influencing the economically feasibility and efficiency of P recovery. An economically feasible P recovery requires the PO_4-P concentration of at least 50 mg/L in waste streams (Cornel and Schaum, 2009). The PO_4-P concentration in raw blackwater collected from low flush vacuum toilets can reach 53.3 mg/L (Alp, 2010) or 79 mg/L (de Graaff et al., 2010), and that in ADBW is slightly higher, for instance, 92 mg/L (de Graaff et al., 2010). Raw blackwater collected from low flush vacuum toilets satisfies the requirement of economical P recovery. However, this type of blackwater with relatively low PO_4^{3-} concentration does not benefit the supersaturation ratio [Eqs. (2–2) and (2–3)]. Nevertheless, the PO_4^{3-} concentration is not the only factor affecting the *IAP*; the NH_4^+ concentration, Mg^{2+} concentration, and pH should be taken into account together with the PO_4^{3-} concentration.

Among the factors affecting the *IAP*, pH is the most important factor due to its ability to change the free concentrations of Mg^{2+}, NH_4^+, and PO_4^{3-}. The concentrations of free Mg^{2+} and NH_4^+ decrease with the increase in pH as a result of the formation of magnesium hydroxide complexes and volatilization in the form of gaseous NH_3, respectively (Uludag-Demirer and Othman, 2009). In addition, pH controls the solubility of struvite, which is the minimum within the range of 9.0–11.7 (Nelson et al., 2003). It has been demonstrated that even a waste stream with a low PO_4-P concentration was able to achieve P recovery efficiency of 90% at an appropriate condition (Alp et al., 2010; Uludag-Demirer and Othman, 2009). If the initial PO_4-P concentration in blackwater is too low, one way to increase it can be the use of combined technologies such as biological processes (Campos et al., 2019). Apart from inorganic P, blackwater also contains large content of organic P which is not suitable for direct chemical precipitation. The release of organic

P and its conversion into inorganic P by virtue of pre-treatment techniques before chemical precipitation will enhance the struvite production.

Although struvite can precipitate in a wide range of pH values, an optimum pH level usually falls into the range of 9.0–9.5 (de Graaff et al., 2010; Alp, 2010; Yee et al., 2019). One fact is that pH will drop during the reaction of struvite precipitation due to the release of protons. Therefore, an external alkali source is usually required to maintain an optimum pH level if the waste stream to be treated does not have an appropriate initial pH value or adequate buffer capacity. Blackwater collected from low flush vacuum toilets (1 L water per flush) after the anaerobic treatment has high PO_4-P and NH_4-N concentrations, but its pH value is usually lower than 8.0 (de Graaff et al., 2010; Zeeman et al., 2008). The alkali source is often added to increase the pH level of anaerobically digested blackwater for enhanced P recovery (Gell et al., 2011; de Graaff et al., 2011; Yee et al., 2019). The use of alkali will increase the operating cost. For instance, de Graaff et al. (2011) examined P recovery as struvite from ADBW. In the study, with sodium hydroxide (NaOH; for pH adjustment) and magnesium chloride ($MgCl_2$; to achieve target Mg/P molar ratios) additions, the optimal P recovery efficiency of 90% was achieved with a pH value of 9.0 and a Mg/P molar ratio of 1.3.

From the perspectives of both environmental sustainability and economy, raw concentrated blackwater collected from low-flush vacuum toilets has a pH value in the range of 8.6–9.0 (de Graaff et al. 2010; Knerr et al. 2011; Gao et al. 2019b) and is potentially ideal for struvite production due to the free use of alkali for pH adjustment. To date, there are only a few studies (Alp 2010; Gell et al. 2011; de Graaff et al. 2011; Yee et al. 2019) pertinent to struvite precipitation from blackwater (including both raw blackwater and ADBW), with PO_4-P concentration ranging from 53.3 to 92 mg/L (shown in **Table 2–1**). Only one study was reported to recover P from raw

blackwater. By using raw blackwater collected from low-flush vacuum toilets (0.7 L/per flush), Alp (2010) conducted batch experiments to determine the optimum conditions for P recovery through struvite precipitation. It was found that the highest P removal was achieved at a pH value of 9.5 (NaOH was used to adjust pH) and a Mg/P molar ratio of 1.3 (magnesium oxide, MgO, was used as the external source for Mg supplementation). However, whether struvite can be produced from raw blackwater with high purity, reasonable Mg/P/N mass ratio, and low heavy-metal contents is still unknown.

2.1.3 Challenges for struvite precipitation from blackwater

For specific blackwater having complex characteristics, a big challenge can be to ensure both production purity and enhanced P recovery efficiency. The presence of other cations, such as Ca^{2+}, K^{+} and Al^{3+}, and anions like HCO_3^{-}/CO_3^{2-} in blackwater will interfere with struvite precipitation by competing for Mg^{2+} and PO_4^{3-} to from different species. These coprecipitations such as calcium phosphate and magnesium carbonate will affect the purity of produced struvite. Other heavy metals such as Fe, Zn, Cu, and Cr may also be found in produced struvite. The ratio of Mg^{2+}: NH_4^{+}: PO_4^{3-} at different pH levels and the ratio between other cations (such as Ca^{2+}) and Mg^{2+} should be studied to determine their influences on both P recovery efficiency and struvite purity. Generally, Mg^{2+} concentration in blackwater is as low as 10 mg/L; an external Mg source is usually added to achieve a higher supersaturation index. However, the Mg supplementation will greatly increase the operating cost of struvite precipitation. The use of low-cost Mg source such as industrial grade MgO or $Mg(OH)_2$, seawater or bittern instead of expensive $MgCl_2$ can significantly reduce the operating cost (Campos et al., 2019).

Blackwater also has high levels of total suspended solids (TSS) and complex species. High TSS concentration in raw blackwater can be a challenge for high-quality struvite production, and its general impact has not been well understood or agreed upon by the scientific community. For instance, Ping et al. (2016) found that the TSS concentration above 153 mg/L negatively affected the struvite pellet growth. Tarragó et al. (2018) found that even at high solid concentrations (e.g., TSS concentration of 1,000–3,000 mg/L), more than 95% of P was recovered as struvite. The authors also proposed that solids facilitated struvite crystallization, acting as nuclei favoring heterogeneous nucleation. Hence, prior to the use of raw blackwater as a potential waste source for struvite production, the role of blackwater TSS in struvite production also needs to be addressed.

The safety of struvite product from blackwater can be one concern for its agricultural use as fertilizer. Based on one previous study (Gell et al., 2011), the heavy metal and pathogen contents in struvite recovered from anaerobically treated blackwater did not exceed the Dutch regulation limits. But for struvite produced from raw blackwater, it still needs to examine the heavy metal and pathogen contents.

Table 2-1. Previous studies relevant to struvite production from source-diverted blackwater.

Waste sources	Jar test or reactor	PO_4-P concentration, mg/L	pH	Mg/P molar ratio	P recovery efficiency	References
Raw concentrated blackwater collected from vacuum toilet systems	Jar test	53.3 ± 14.8	9.5 (with pH adjustment)	1.5	87%	Alp, 2010
Anaerobically digested concentrated blackwater	Continuously stirred tank	Not reported	8.6 (with pH adjustment)	Not reported	Not reported	Gell et al., 2011
Anaerobically digested concentrated blackwater	Jar test	92.0	8.0 and 9.0 (with pH adjustment)	1.3 (pH=9.0) and 1.5 (pH=8.0)	> 90%	de Graaff et al., 2011
Synthetic anaerobically digested blackwater	Jar test	41.2	9.0 (With pH adjustment)	1.5	> 83%	Yee et al., 2019

2.2 Biomethane Recovery from Blackwater

Biogas produced through AD is a source of energy, which helps increase energy security, reduce the reliance on non-renewable energy, and reduce greenhouse gas emission from non-renewable energy utilization (Maleki et al., 2018; Obileke et al., 2021). The conversion of organics into biogas goes through four major steps including hydrolysis, acidogenesis, acetogenesis, and methanogenesis. An effective AD process requires a well-developed microbial community to fulfill the four steps. Generally, biogas production through AD is affected by the substrate type (e.g., carbohydrates, proteins, and fats), bioreactor type [e.g., batch reactor, continuous stirred tank reactor (CSTR), and upflow anaerobic sludge blanket reactor (UASB)], and operational condition [e.g., temperature, pH, hydraulic retention time (HRT), organic loading rate (OLR), buffering capacity, and effluent recirculation strategy]. Bioenergy recovery from blackwater has been extensively studied in Dr. Liu's group (e.g., Florentino et al., 2019a; Florentino et al., 2019b; Gao et al., 2019a; Gao et al., 2019b; Gao, 2020; Zhang et al., 2020; Huang et al., 2021; Zhang et al., 2021a; Zhang et al., 2021b; Zhang et al., 2022). This study will not provide a detailed review on biogas recovery from blackwater but focus on the impact of mixing on biogas recovery, which is one research gap when treating blackwater using a UASB reactor.

Blackwater, especially concentrated blackwater collected from vacuum toilet systems, contains high solid content. When treating a high-solid content substrate in a UASB reactor, effluent recirculation is commonly employed to improve both mixing and upflow velocity of the reactor (Buzzini et al., 2007; López-López et al., 2015; Zamanzadeh et al., 2016). Mixing, for instance, helps reduce toxicity and volatile fatty acid (VFA) accumulation, which often lead to the instability and deterioration of an anaerobic digester. Effluent recirculation can also create favorable hydrodynamic conditions, facilitating heat and mass transfer in the sludge bed (Speece,

2008; Singh et al., 2020). However, the benefits to bioreactor performance of effluent recirculation depend on bioreactor design, substrate characteristics, operational conditions, and the ratio between recirculation volume and influent volume. Excessive mixing due to effluent recirculation can adversely affect biogas production due to changes in the distribution of enzymes and microorganisms (Singh et al., 2020).

Recent studies show that the effluent recirculation applied to a UASB reactor may reduce biomethane production (Kim et al., 2002; Zamanzadeh et al., 2016; Zhang et al., 2020). In these studies, different types of wastewater with high solid content (e.g., dog food, food waste, blackwater) were used as the substrates, and the effluent recirculation was thought to disturb the close spatial associations and syntrophic relationships between microbial consortia (Stroot et al., 2001; Zhang et al., 2020). However, the impact of effluent recirculation on the performance of a UASB reactor treating low-solid content substrates has not been elucidated, which represent as a key parameter on the selection of operational conditions (with or without recirculation) when treating blackwater by UASB reactors to achieve both maximized bioenergy recovery.

2.3 Simultaneous P and Biomethane Recovery from Blackwater

Although many technologies are contributing to overcoming the challenges of P recovery from wastewater, the biological process offers the strongest promise for economical P recovery. Recent studies demonstrated that simultaneous bioenergy recovery and P recovery through calcium phosphate (CaP) precipitation can be achieved in a UASB reactor (Tervahauta et al., 2014; Cunha et al., 2018; Zhang et al., 2021a; Zhang et al., 2021b). However, the mechanisms underlying the bio-induced CaP precipitation still need to be clarified.

No matter recovering P through struvite precipitation from anaerobically digested blackwater (AD followed by struvite precipitation) or recovering P from raw blackwater (struvite precipitation followed by AD), the use of Mg supplement and/or alkali increase chemical cost, and the two-stage design increases operational complexity and cost. Anaerobic treatment of blackwater has been a competitive strategy due to low cost, operational simplicity, low production of sludge, and most importantly, maximized bioenergy recovery (Chernicharo, 2006; Batstone et al., 2015; Zhang et al., 2018). If P and bioenergy can be simultaneously recovered in an AD process without chemical addition, the treatment process could be more compact and more economical in comparison to the treatment design for struvite production. Recent studies (**Table 2–2**) demonstrated that simultaneous bioenergy recovery in the form of biomethane and P recovery in the form of CaP granules from blackwater can be achieved in UASB reactors with (Cunha et al., 2018a; 2018b; 2019a; 2019b) or without Ca addition (Zhang et al., 2021a; 2021b).

2.3.1 Mechanisms for bio-induced CaP precipitation

CaP is a mixture consisting of different compositions depending on the blackwater characteristics and the reactor operational conditions. It may contain hydroxyapatite (HAP, $Ca_{10}(PO_4)_6(OH)_2$), calcium phosphate (TCP, $Ca_3(PO_4)_2$), octacalcium phosphate (OCP, $Ca_8(HPO_4)_2(PO_4)_4$), monetite (DCP, $CaHPO_4$), brushite ($CaHPO_4 \cdot 2H_2O$), amorphous calcium phosphate (ACP, $Ca_3(PO_4)_2 \cdot xH_2O$), and even calcite ($CaCO_3$) and struvite ($MgNH_4PO_4 \cdot 6H_2O$) (Daneshgar et al., 2018a; Zhang et al., 2021a).

Table 2-2. Summary of CaP precipitation in anaerobic digesters.

Waste source	Operation	Influent pH	Ca concentration, mg/L	PO_4-P concentration, mg/L	Mechanisms	References
Vacuum black water	One 50 L UASB reactor (25°C) and a 2.4 m^3 UASB reactor (35°C)	8.1	62	149	1. Supersaturation of minerals caused the formation of seed crystals. 2. Biofilm surrounding the granules created a micro-environment that controlled the diffusion of ions and elevated the local pH.	Tervahauta et al., 2014
Vacuum black water	Two 5.1 L UASB reactors (25°C)	7.9	144–460	50 (TP: 176)	1. Adding Ca increased the concentration of seed crystals that served as initial nuclei for CaP granulation. 2. Adding Ca stimulated the biomass agglomeration that strengthened the granular structure. 3. Complexation of Ca with biomass created local conditions for CaP precipitation and subsequent formation of CaP granules.	Cunha et al., 2018a; 2018b
1. Glucose 2. VFA mixture (60% acetate, 20% propionate, and 20% butyrate)	Four 2 L UASB reactors (25°C)	7.49–8.20	112–120	100–111	1. The produced extracellular biopolymers contributed to biofilm formation, trapping microorganisms, and combing CaP particles. 2. The local microbial syntrophy caused the pH gradient between bulk and granule center, which was crucial to CaP enrichment in granules.	Cunha et al., 2019a
Vacuum black water	One 2 L UASB reactor (52°C)	6.5–7.1	168.0–268.2	98.7–210.6	Hydrolysis of protein and urea triggered a fast pH increase, facilitating CaP precipitation.	Zhang et al., 2021a

Note: VFA is the abbreviation of volatile fatty acid.

TP is the abbreviation of total phosphorus.

As mentioned above, there are two requirements for P product formation. To meet the second kinetic requirement, Ca is usually replenished to achieve a high supersaturation level of CaP (Cunha et al., 2018a), triggering the formation of CaP. CaP precipitation occurring in an anaerobic reactor is thought to involve a series of bio-induced chemical reactions favored by a local microenvironment involving the pH gradient and the extracellular polymeric substances (EPS) (**Fig. 2–2**) (Tervahauta et al., 2014; Cunha et al., 2018a; Cunha et al., 2018b; Zhang et al., 2021a). One of the CaP species, HAP, is easily supersaturated even at a low pH level of 6.0 due to the low solubility product constant (**Table 2–3**), however, the precipitation of HAP is not kinetically favorable without interventions (Cunha et al., 2018b; Daneshgar et al., 2018b). The detection of HAP granules in anaerobic reactors (Tervahauta, 2014; Cunha et al., 2018b) indicates that the local microenvironment built in anaerobic reactors can overcome the activation energy barrier, triggering the formation of HAP nuclei.

However, the formation of CaP granules from blackwater was also observed below the supersaturation requirement without any chemical addition in our group (Zhang et al., 2021b). It was thought that a localized supersaturation condition in the vicinity of biomass must be created; the pH level and the Ca concentration in the local environment were different from that were observed in the effluent or in the influent.

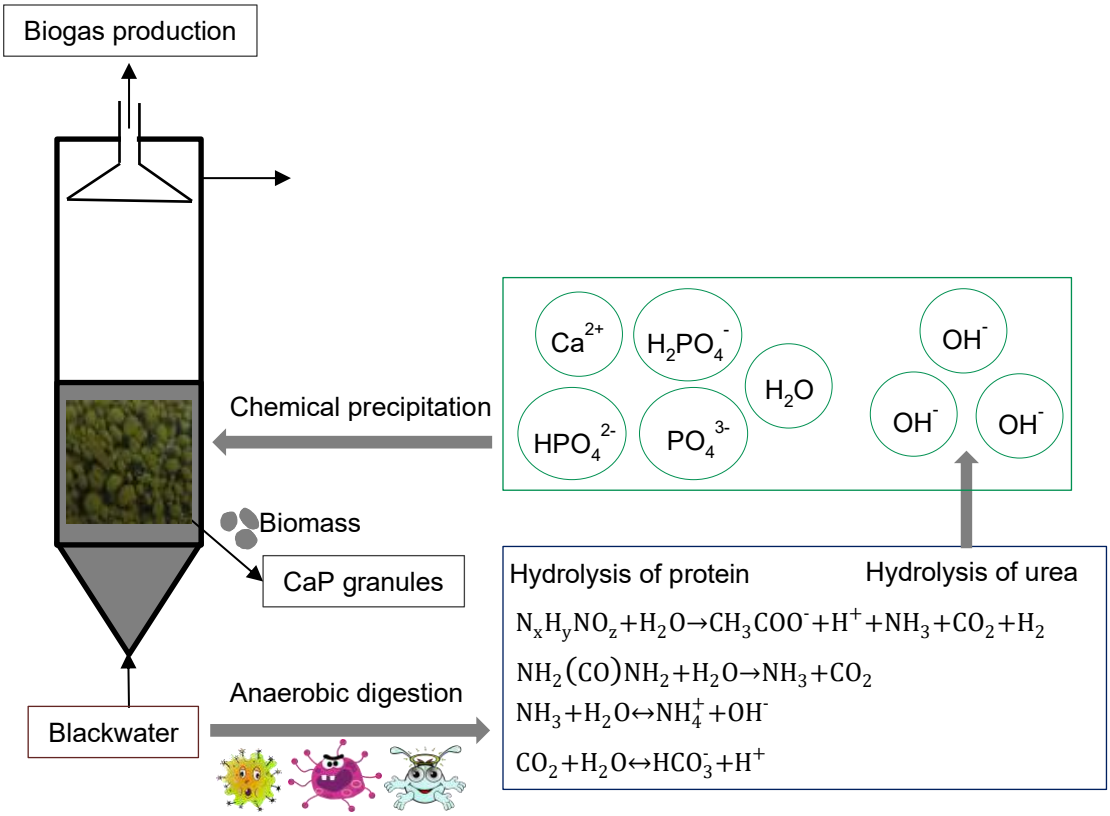

Figure 2-2. Schematic of bio-induced CaP precipitation in an AD process treating blackwater.

Table 2-3. Possible CaP species produced in the P recovery process in an anaerobic digester (Siegel, 1961; Daneshgar et al., 2018b).

Possible CaP species	Reaction	Produce condition	pK_{sp} (25ºC)
HAP	$10Ca^{2+}+6PO_4^{3-}+2OH^- \leftrightarrow Ca_{10}(PO_4)_6(OH)_2$	Slow formation from ACP, DCPD	58.62
TCP	$3Ca^{2+}+2PO_4^{3-} \leftrightarrow Ca_3(PO_4)_2$	Slow formation from ACP, DCPD	32.63
OCP	$8Ca^{2+}+2HPO_4^{2-}+4PO_4^{3-} \leftrightarrow Ca_8(HPO_4)_2(PO_4)_4$	Hydrolysis of DCPD at pH = 5–6	36.48
DCP	$Ca^{2+}+HPO_4^{2-} \leftrightarrow CaHPO_4$	Fast formation from ACP, DCPD	6.81
DCPD	$Ca^{2+}+HPO_4^{2-}+2H_2O \leftrightarrow CaHPO_4 \cdot 2H_2O$	pH < 7	6.6
ACP	$3Ca^{2+}+2PO_4^{3-}+xH_2O \leftrightarrow Ca_3(PO_4)_2 \cdot xH_2O$	pH > 6	25.46
Calcite	$Ca^{2+}+CO_3^{2-} \leftrightarrow CaCO_3$	Stable at 25ºC and atmospheric pressure	8.22–8.48
Dolomite	$Ca^{2+}+Mg^{2+}+CO_3^{2-} \leftrightarrow MgCa(CO_3)_2$	pH > 9.7	12.53
$Ca(OH)_2$	$Ca^{2+}+2OH^- \leftrightarrow Ca(OH)_2$	pH > 9.5	5.2

Note: K_{sp} is the solubility product constant. pK_{sp}=-log(K_{sp}).

2.3.2 Research gaps for simultaneous P and biomethane recovery from blackwater

Blackwater is a complex mixture; its characteristics (other than Ca concentration) and operational conditions required to develop such localized favorable microenvironment for CaP formation have not been explored. Blackwater consists of organics including carbohydrates, lipids, proteins, and urea. Zhang et al. (2021a) proposed that protein and urea hydrolysis promoted CaP precipitation in the AD process. However, the impact of feedstock composition on CaP precipitation during AD has not been elucidated.

In addition to the feedstock composition, other factors such as the reactor configuration and the operational condition can also affect the local environment. For instance, CaP can form in a UASB reactor, but cannot form in a CSTR. Too much mixing in the CSTR may destroy the local environment. The reactor operational condition like recirculation, temperature, and OLR may also affect the localized supersaturation. The maintenance and deterioration of local environment deserve further investigation.

CaP production does not only rely on a high P concentration and/or chemical additions, an alternative economical way can be to achieve an optimum feedstock or a propriate operational condition to create a localized supersaturation condition, triggering the CaP precipitation at a low or even below supersaturation requirement. Co-digestion of blackwater and other streams with considerable P and Ca concentration and complex organic constituents is potentially feasible for simultaneous CaP precipitation and bioenergy recovery in an efficient and economical way. For instance, whey processing effluent and soybean protein wastewater with considerable PO_4-P and protein contents, starch processing wastewater with considerable PO_4-P contents, and protein-enriched poultry processing wastewater may be good sources for simultaneous recovery of

biomethane and CaP. While the ratio of different sources should be further investigated for achieving both bioenergy and P recovery efficiently and economically.

References

Alp, Ö., 2010. Further Treatment of Digested Blackwater for Extraction of Valuable Components. PhD Thesis, Hamburg University of Technology, Germany.

Batstone, D.J., Hülsen, T., Mehta, C.M., Keller, J., 2015. Platforms for energy and nutrient recovery from domestic wastewater: a review. Chemosphere 140, 2–11.

Buzzini, A.P., Pires, E.C., 2007. Evaluation of a upflow anaerobic sludge blanket reactor with partial recirculation of effluent used to treat wastewaters from pulp and paper plants. Bioresour. Technol. 98, 1838–1848.

Campos, J.L., Crutchik, D., Franchi, Ó., Pavissich, J.P., Belmonte, M., Pedrouso, A., Mosquera-Corral, A., Val del Río, Á., 2019. Nitrogen and phosphorus recovery from anaerobically pretreated agro-food wastes: a review. Front. Sustain. Food Syst. 2, 91.

Chernicharo, C.A.L., 2006. Post-treatment options for the anaerobic treatment of domestic wastewater. Rev. Environ. Sci. Biotechnol. 5, 73–92.

Cornel, P., Schaum, C., 2009. Phosphorus recovery from wastewater: needs, technologies and costs. Water Sci. Technol. 59 (6), 1069–1076.

Cunha, J.R., Schott, C., van der Weijden, R.D., Leal, L.H., Zeeman, G., Buisman, C., 2018a. Calcium addition to increase the production of phosphate granules in anaerobic treatment of black water. Water Res. 130, 333–342.

Cunha, J.R., Tervahauta, T., van der Weijden, R.D., Temmink, H., Leal, L.H., Zeeman, G., Buisman, C.J.N., 2018b. The effect of bioinduced increased pH on the enrichment of calcium phosphate in granules during anaerobic treatment of black water. Environ. Sci. Technol. 52, 13144–13154.

Cunha, J.R., Schott, C., van der Weijden, R.D., Leal, L.H., Zeeman, G., Buisman, C., 2019a. Recovery of calcium phosphate granules from black water using a hybrid upflow anaerobic sludge bed and gas-lift reactor. Environ Res. 178, 108671.

Cunha, J.R., Morais, S., Silva, J.C., van der Weijden, R.D., Leal, L.H., Zeeman, G., Buisman, C., 2019b. Bulk pH and carbon source are key factors for calcium phosphate granulation. Environ. Sci. Technol. 53, 1334–1343.

Daneshgar, S., Callegari, A., Capodaglio, A.G., Vaccari, D., 2018a. The potential phosphorus crisis: resource conservation and possible escape technologies: a review. Resources 7 (2), 37.

Daneshgar, S., Buttafava, A., Capsoni, D., Callegari, A., Capodaglio, A.G., 2018b. Impact of pH and ionic molar ratios on phosphorus forms precipitation and recovery from different wastewater sludges. Resources 7 (4), 71.

de Graaff M.S., Temmink, H., Zeeman, G., Buisman, C.J.N., 2010. Anaerobic treatment of concentrated blackwater in a UASB reactor at a short HRT. Water 2 (1), 101–119.

de Graaff M.S., Temmink, H., Zeeman, G., Buisman, C.J.N., 2011. Energy and phosphorus recovery from black water. Water Sci. Technol. 63 (11), 2759–2765.

Egle, L., Rechberger, H., Krampe, J., Zessner, M., 2016. Phosphorus recovery from municipal wastewater: an integrated comparative technological, environmental and economic assessment of P recovery technologies. Sci. Total Environ. 571, 522–542.

Florentino, A.P., Sharaf, A., Zhang, L., Liu, Y., 2019a. Overcoming ammonia inhibition in anaerobic blackwater treatment with granular activated carbon: the role of electroactive microorganisms. Environ. Sci.: Water Res. Technol. 5, 383.

Florentino, A.P., Xu, R., Zhang, L., Liu, Y., 2019b. Anaerobic digestion of blackwater assisted by granular activated carbon: from digestion inhibition to methanogenesis enhancement. Chemosphere 233, 462–471.

Gao, M., 2020. Anaerobic Treatment of Source-diverted Blackwater-maximizing Biomethane Recovery. University of Alberta, Canada.

Gao, M., Zhang, L., Guo, B., Zhang, Y., Liu, Y., 2019a. Enhancing biomethane recovery from source-diverted blackwater through hydrogenotrophic methanogenesis dominant pathway. Chem. Eng. J. 378, 122258.

Gao, M., Guo, B., Zhang, L., Zhang, Y., Liu, Y., 2019b. Microbial community dynamics in anaerobic digesters treating conventional and vacuum toilet flushed blackwater. Water Res. 160 (1), 249–258.

Gell, K., de Ruijter, F.J., Kuntke, P., de Graaff, M., Smit, A.L., 2011. Safety and effectiveness of struvite from black water and urine as a phosphorus fertilizer. J. Agric. Sci. 3 (3), 67–80.

Huang, Q., Zakaria, B.S., Zhang, Y., Zhang, L., Liu, Y., Dhar, B.R., 2021. A high-rate anaerobic biofilm reactor for biomethane recovery from source-separated blackwater at ambient temperature. Water Environ. Res., 93 (1), 61–74.

Kim, M., Ahn, Y.-H., Speece, R.E., 2002. Comparative process stability and efficiency of anaerobic digestion; mesophilic vs. thermophilic. Water Res. 36 (17), 4369–4385.

Knerr, H., Rechenburg, A., Kistemann, T., Schmitt, T.G., 2011. Performance of a MBR for the treatment of blackwater. Water Sci Technol. 63 (6), 1247–1254.

Kujawa-Roeleveld, K., Zeeman, G., 2006. Anaerobic treatment in decentralised and source-separation-based sanitation concepts. Rev. Environ. Sci. Biotechnol. 5 (1), 115–139.

López-López, A., León-Becerril, E., Rosales-Contreras, M. E., Villegas-García, E., 2015. Influence of alkalinity and VFAs on the performance of an UASB reactor with recirculation for the treatment of Tequila vinasses. Environ. Technol. 36 (19), 2468–2476.

Maleki, E., Bokhary, A., Liao, B.Q., 2018. A review of anaerobic digestion bio-kinetics. Rev. Environ. Sci. Biotechnol. 17, 691–705.

Meinzinger, F., Oldenburg, M., 2009. Characteristics of source-separated household wastewater flows: a statistical assessment. Water Sci. Technol. 59 (9), 1785–1791.

Nelson, N. O., Mikkelsen, R.L., Hesterberg, D.L., 2003. Struvite precipitation in anaerobic swine lagoon liquid: effect of pH and Mg:P ratio and determination of rate constant. Bioresour. Technol. 89 (3), 229-236.

Obileke, K., Nwokolo, N., Makaka, G., Mukumba, P, Onyeaka, H., 2021. Anaerobic digestion: technology for biogas production as a source of renewable energy- a review. Energy Environ. 32 (2), 191–225.

Ping, Q., Li, Y., Wu, X., Yang, L., Wang, L., 2016. Characterization of morphology and component of struvite pellets crystallized from sludge dewatering liquor: effects of total suspended solid and phosphate concentrations. J. Hazard. Mater. 310, 261–269.

Siegel, F.R., 1961. Factors influencing the precipitation of dolomitic carbonates. State Geol. Surv. Kansas Bull. 152 (Pt. 5), 127–158.

Singh, B., Szamosi, Z., Siménfalvi, Z., 2020. Impact of mixing intensity and duration on biogas production in an anaerobic digester: a review. Crit. Rev. Biotechnol. 40 (4), 508–521.

Speece, R.E., 2008. Anaerobic Biotechnology and Odor/Corrosion Control for Municipalities and Industries. Archae Press, Tennessee, US.

Stroot, P.G., McMahon, K.D., Mackie, R.I., Raskin, L., 2001. Anaerobic codigestion of municipal solid waste and biosolids under various mixing conditions–I. digester performance. Water Res. 35 (7), 1804–1816.

Tarragó, T., Sciarria, T.P., Ruscalleda, M., Colprim, J., Balaguer, M.D., Adani, F., Puig, S., 2018. Effect of suspended solids and its role on struvite formation from digested manure. J. Chem. Technol. Biotechnol. 93, 2758–2765.

Tervahauta, T., van der Weijden, R.D., Flemming, R.L., Leal, L.H., Zeeman, G., Buisman, C.J.N., 2014. Calcium phosphate granulation in anerobic treatment of black water: a new approach to phosphorus recovery. Water Res. 48, 632–642.

Theregowda, R.B., González-Mejía, A.M., Ma, X., Garland, J., 2019. Nutrient recovery from municipal wastewater for sustainable food production systems: an alternative to traditional fertilizers. Environ. Eng. Sci. 36 (7), 833–842.

Todt, D., Heistad, A., Jenssen, P.D., 2015. Load and distribution of organic matter and nutrients in a separated household wastewater stream. Environ. Technol. 36 (12), 1584–1593.

Uludag-Demirer, S., Othman, M., 2009. Removal of ammonium and phosphate from the supernatant of anaerobically digested waste activated sludge by chemical precipitation. Bioresour. Technol. 100 (13), 3236-3244.

Yee, R.A., Alessi D.S., Ashbolt, N.J., Hao, W., Konhauser, K., Liu, Y., 2019. Nutrient recovery from source-diverted blackwater: optimization for enhanced phosphorus recovery and reduced co-precipitation. J. Clean. Prod. 235 (20), 417–425.

Zamanzadeh, M., Hagen, L.H., Svensson, K., Linjordet, R., Horn, S.J., 2016. Anaerobic digestion of food waste–effect of recirculation and temperature on performance and microbiology. Water Res. 96, 246–254.

Zeeman, G., Kujawa, K., de Mes, T., Hernandez, L., de Graaff, M., Abu-Ghunmi, L., Abu-Ghunmi, L., Mels, A., Meulman, B., Temmink, H., Buisman, C., van Lier, J., Lettinga, G., 2008. Anaerobic treatment as a core technology for energy, nutrients and water recovery from source separated domestic waste(water). Water Sci. Technol. 57 (8), 1207-1212.

Zhang, L., Vrieze, J.D., Hendrickx, T.L.G., Wei, W., Temmink, H., Rijnaarts, H., Zeeman, G., 2018. Anaerobic treatment of raw domestic wastewater in a UASB-digester at 10°C and microbial community dynamics. Chem. Eng. J. 334, 2088–2097.

Zhang, L., Guo, B., Mou, A., Li, R., Liu, Y., 2020. Blackwater biomethane recovery using a thermophilic upflow anaerobic sludge blanker reactor: impacts of effluent recirculation on reactor performance. J. Environ. Manage. 274, 111157.

Zhang, L., Mou, A., Guo, B., Sun, H., Anwar, M.N., Liu, Y., 2021a. Simultaneous phosphorus recovery in energy generation reactor (SPRING): high rate thermophilic blackwater treatment. Resour. Conserv. Recycl. 164, 105163.

Zhang, L., Mou, A., Sun, H., Zhang, Y., Zhou, Y., Liu, Y., 2021b. Calcium phosphate granules formation: key to high rate of mesophilic UASB treatment of toilet wastewater. Sci. Total Environ. 773, 144972.

Zhang, L., Zhang, Y., Yuan, Y., Mou, A., Park, S., Liu, Y., 2022. Impacts of granular activated carbon addition on anaerobic granulation in blackwater treatment. Environ. Res. 206, 112406.

CHAPTER 3 FEASIBILITY ASSESSMENT OF PHOSPHORUS RECOVERY FROM SOURCE-DIVERTED BLACKWATER THROUGH STRUVITE PRECIPITATION

A version of this chapter has been published in the *Science of the Total Environment*.

3.1 Synopsis

P recovery from wastewater through struvite precipitation is becoming a promising strategy to both mitigate eutrophication risk due to excess P discharge into water bodies and alleviate the global P crisis by producing value-added fertilizer. However, the composition and quality of wastewater differ among regions and home to home. Source-diverted blackwater, especially concentrated blackwater collected from vacuum toilet systems, typically has a moderate PO_4-P content, high NH_4-N content, strong buffering capacity as a result of high alkalinity, and a high pH close to 9. Thus, concentrated blackwater is a potential source for P recovery through struvite precipitation.

Chapter 3 aims to examine the feasibility of P recovery from raw blackwater through struvite precipitation in terms of both P recovery efficiency and struvite characterization. In this Chapter, P recovery efficiencies for different raw blackwater flushed with 0.5 L, 1.0 L, and 5.0 L of tap water per flush were obtained via batch experiments. Correspondingly, ADBW flushed with 1.0 L of tap water per flush was examined to compare its P recovery potential with that of raw blackwater. The characterization of the struvite produced from concentrated blackwater was performed via X-ray diffraction (XRD) and scanning electron microscopy-energy dispersive X-ray spectroscopy (SEM-EDS) techniques. The metal contents of the struvite product were analyzed by inductively coupled plasma mass spectrometry (ICP-MS), and its purity was determined. The feasibility study in Chapter 3 is expected to provide evidence for the efficacy of P recovery from concentrated blackwater through struvite precipitation without any alkali addition for pH adjustment.

3.2 Experimental Method

3.2.1 Blackwater collection and sample preparation

Blackwater (feces and urine) samples from vacuum toilets (0.5 L and 1 L water per flush) and dual-flush (5 L water per flush) toilets were collected from the University of Alberta (Edmonton, Canada) campus over a two-week period. The blackwater samples were stored at 4 ºC for at least 24 h to allow for a pH increase. The blackwater supernatants were examined within 12 h to ensure that water quality was consistent between analyses. Supernatants of three types of blackwater (categorized by flush volume), SBW-0.5, SBW-1, and SBW-5, were used in the experiments. In addition, struvite recovery from anaerobically digested vacuum toilets (1L water per flush) collected blackwater (ADBW-1) was examined. More information about the UASB reactor where blackwater was digested can be found elsewhere (Gao et al., 2019a).

3.2.2 Batch experiments

The experiments were conducted using jar tests; magnetic stir bars facilitated the mixing of blackwater sample and added reagents. All tests were carried out in triplicate at room temperature (21 ± 0.5 ºC) with 50 mL of each sample. NaOH (2.0 M) was used to adjust the original pH of the selected samples for comparison. Prior to each test, $MgCl_2$ (1.0 M) was used as the external magnesium source for the samples to achieve the required Mg/P molar ratio of 1.1, 1.3, and 1.5. The magnetic stir bar in the jar started at 200 rpm for 5 min before slowing to 60 rpm for 30 min; the solution was then allowed to settle for at least 30 min for the collection of produced precipitates.

3.2.3 Precipitates collection

After the 30-min settlement of the precipitates, the supernatant was transferred out of the jar. Subsequently, the precipitates were washed by deionized (DI) water at least three times to remove loosely attached compounds, such as NaCl and NH_4Cl, from the produced precipitate surface. Finally, the washed precipitates were dried in the fume hood at room temperature overnight.

To evaluate the kinetics associated with struvite precipitation, the supersaturation ratio (SSR) was calculated following Eqs. (3–1) and (3–2) described below.

$$Mg^{2+}+NH_4^{+}+H_nPO_4^{n-3}+6H_2O \rightarrow MgNH_4PO_4\cdot 6H_2O+ nH^{+} \quad (3–1)$$

$$SSR = \left(\frac{\{Mg^{2+}\}\{NH_4^{+}\}\{PO_4^{3-}\}}{K_{sp}}\right)^{1/3} \quad (3–2)$$

where {} denotes the ionic activity of ionic species, and K_{sp} is the thermodynamic solubility product of struvite depending on the waste source where it is produced. In this study, a value of 3.89×10^{-10} for digested wastewater was used for K_{sp} (Bhuiyan et al., 2008; Borgerding, 1972).

The activity {} can be calculated by Eq. (4–3).

$$\{i\} = \gamma_i[i] \quad (3–3)$$

where i represents NH_4^{+}, Mg^{2+}, and PO_4^{3-}, respectively. γ_i is the activity coefficient of species i, which can be estimated by Güntelberg approximation of the Debye-Hückel equation when the ionic strength is less than 0.1 M (Sawyer et al., 2003).

$$\log \gamma_i = -0.5 z_i^2 \left(\frac{\sqrt{\mu}}{1+\sqrt{\mu}}\right) \quad (3–4)$$

where μ is the ionic strength and z_i is the charge of species i. Ionic strength can be calculated using Eq. (3–5).

$$\mu = \frac{1}{2}\sum_j c_j z_j^2 \quad (3\text{–}5)$$

where *j* represents all the ions in the water sample to be determined, and c_j is the concentration of species *j*.

3.2.4 Water quality analysis

Water quality of blackwater samples, defined by parameters including pH, chemical oxygen demand (COD), PO_4-P concentration, NH_4-N concentration, alkalinity, total suspended solids (TSS), and metal contents were examined. The pH value was measured by a pH meter (VWR SympHony, Avantor Inc., Radnor, PA, USA). COD, TSS, and NH_4-N concentration were determined by standard methods (Baird et al., 2017). PO_4-P concentration and alkalinity were tested by HACH kits (HACH, Loveland, Colorado, USA). Metal contents were measured by the ICP-MS method. The P recovery efficiency, η, was calculated based on the initial PO_4-P concentration of the sample, $[PO_4\text{-}P]_{initial}$, and the final PO_4-P concentration after the reaction, $[PO_4\text{-}P]_{final}$, as shown in Eq. (3–6).

$$\eta = \frac{[PO_4\text{–}P]_{initial} - [PO_4\text{–}P]_{final}}{[PO_4\text{–}P]_{initial}} \times 100\% \quad (3\text{–}6)$$

3.2.5 Struvite purity determination

The purity of the produced struvite was determined by analyzing its NH_4-N concentration. The principle behind this method is that NH_4^+ only participates during the reaction producing struvite, and it is not involved in producing any other possible components that compete for phosphate ions with struvite. The precipitates (50 mg) were dissolved in hydrochloric acid (HCl, 3.0 M), and diluted with DI water until the meniscus was at the 250 mL mark of a volumetric flask. NH_4-N

concentration of this diluted solution was then determined by the standard method (Baird et al., 2017). Eq. (3–7) was used to calculate the purity of the produced struvite based on weight.

$$p_{\mathrm{MAP}} = \frac{n_{\mathrm{NH_4-N}} \times MW_{\mathrm{MAP}}}{m_{\mathrm{p}}} \times 100\% \quad (3\text{–}7)$$

where p_{MAP} is the purity of struvite, $n_{\mathrm{NH_4-N}}$ is the mole of NH_4-N in the dissolved precipitates obtained from the measurement, MW_{MAP} is the molecular weight of struvite, and m_{p} is the mass of dissolved precipitates.

3.2.6 Characterizations

Heavy metal contents of blackwater supernatant samples and the produced precipitates were characterized by the ICP-MS (Elan 6000, Perkin Elmer, Oshawa, Ontario, Canada) method. The components of produced precipitates were detected by XRD (Ultimate IV, Rigaku Tokyo, Japan) technique to examine the presence of the co-precipitates. The structure morphology of the precipitates was observed by SEM (Zeiss Sigma 300 VP, FELMI-ZFE, Graz, Austria), and the distribution of elements in the precipitates was determined by EDS (Bruker EDS system, USA).

3.3 Results

3.3.1 Characterization of raw blackwater and ADBW samples

Water quality of the blackwater samples was examined and compared with the studies reported in the literature. As shown in **Table 3–1**, the pH values for BW-0.5, BW-1, BW-5, and ADBW-1 in this study were 8.7, 8.6, 8.3, and 7.8, respectively. PO_4-P concentrations for these types of blackwater were 88.8 mg/L, 70.4 mg/L, 29.2 mg/L, and 78.8 mg/L, respectively. NH_4-N

concentrations were 1,520 mg/L, 1,053 mg/L, 338 mg/L, and 1,280 mg/L, respectively. It can be noted that after blackwater was anaerobically digested, total chemical oxygen demand (COD_t) decreased significantly, and its pH dropped to below 8.0. Besides, the PO_4-P concentration maintained relatively stable since COD_t was not associated with P. Overall, blackwater characteristics observed in the present study were comparable to those found in the literature (Palmquist and Hanæus, 2005; de Graaff et al., 2010; Alp, 2010; Gao et al., 2019a; Gao et al., 2019b).

3.3.2 P recovery efficiency for blackwater collected from various flushing systems

Fig. 3–1 shows the P recovery efficiencies achieved with the supernatants of three types of blackwater (SBW-0.5, SBW-1, and SBW-5) and the anaerobically digested blackwater (ADBW-1). During these experiments, the pH values of all the four samples were not adjusted, and a fixed Mg/P molar ratio of 1.3 was used to replenish the magnesium in the samples. As shown in **Fig. 3–1**, the P recovery efficiencies reached 93.8% ± 0.9%, 92.4% ± 2.6%, 53.3% ± 1.2%, and 85.8% ± 1.2% for SBW-0.5, SBW-1, SBW-5, and ADBW-1, respectively.

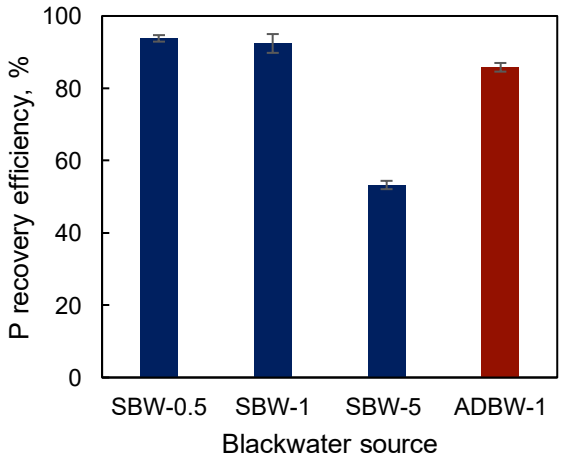

Figure 3-1. P recovery efficiency for blackwater collected from different flush systems.

The highest P recovery efficiency was achieved for SBW-0.5 and SBW-1, which may be attributed to the high pH of 8.6–8.7 and the high PO_4-P concentration of 70.4–88.8 mg/L as compared to other blackwater sources. Although the initial PO_4-P concentration for ADBW-1 was as high as 78.8 mg/L, its lower initial pH of 7.8 was not favorable for a high P removal. Despite the relatively high pH of 8.3 for SBW-5, the low PO_4-P concentration of 29.2 mg/L resulted in an inefficient P removal. According to Cornel and Schaum (2009), the economically feasible P recovery requires an aqueous phase containing PO_4-P higher than 50 mg/L. Hence, raw concentrated blackwater (e.g., BW-0.5 and BW-1) with both high initial pH and high PO_4-P content achieved higher P recovery efficiency than less concentrated blackwater (e.g., SBW-5) and ADBW, enabling it to be an ideal candidate for P recovery.

Table 3-1. Characterization of raw blackwater and ADBW samples.

	This study				(de Graaff et al., 2010)		(Gao et al., 2019a; Gao et al., 2019b)			(Alp, 2010)	(Palmquist and Hanæus, 2005)
	BW-0.5	BW-1	BW-5	ADBW-1	BW-VT	ADBW-VT	BW-1	BW-6	ADBW-1	BW-VT	BW-VT
COD_t, mg/L	12,328	9,583	3,952	913	9,800	2,400	9,492	4,710	1,190	5,461	
pH	8.7	8.6	8.3	7.8	8.8	7.6	8.7	8.5	7.9	7.1	
Alk., mg $CaCO_3$/L	2,140	914	358	2,550	5,000	5,833					
PO_4-P, mg/L	88.8	70.4	29.2	78.8	79	92				59.6	
NH_4-N, mg/L	1,520	1,053	338	1,280	1,400	1,500	1,040	182		1,002	
Na, mg/L	421.0	272.0	81.9	483.0							97.7
K, mg/L	275.0	180.0	91.7	179.0						429	75
Ca, mg/L	58.2	53.1	50.8	55.9						148	68.6
Mg, mg/L	6.1	14.9	21.4	10.5						111	17
Fe, mg/L	1.350	0.945	0.606	0.495							1.28
Al, mg/L	0.665	0.316	0.211	0.229							0.54
Zn, mg/L	0.598	0.419	0.270	0.085							
Cu, mg/L	0.367	0.336	0.366	0.145							0.126
Mg/P/N molar ratio	0.1:1.0: 30.9	0.3:1.0: 33.1	0.9:1.0: 25.7	0.2:1.0: 36.0							

Note: Alk. represents alkalinity.
BW-0.5, -1, -5, and -6 represent blackwater with 0.5 L, 1 L, 5 L, and 6 L of water per flush, respectively.
VT represents blackwater collected from vacuum toilet.

3.3.3 Effect of Mg/P molar ratio of concentrated blackwater on P recovery efficiency

The molar ratio between Mg and P is another critical factor impacting the P recovery from blackwater; this ratio is 1 theoretically based on the reaction shown in Eq. (3–1). In practice, a Mg/P molar ratio greater than 1 is commonly employed to increase the SSR [shown in Eq. (3–2)], facilitating the struvite precipitation.

Fig. 3–2 shows the influence of the Mg/P molar ratio (1.1, 1.3, and 1.5) on the P recovery efficiency for SBW-0.5, SBW-1, and ADBW-1. Similar to the results demonstrated in Section 2.3.2, SBW-0.5 achieved a higher P recovery, in comparison to SBW-1 and ADBW-1. The highest P recovery for SBW-0.5 was achieved under a Mg/P ratio of 1.3, while the best P recovery for SBW-1 and ADBW-1 was obtained under a Mg/P molar ratio of 1.5, which was possible due to the great supersaturation capacity obtained. Overall, our results showed that the impact of three Mg/P molar ratios (i.e., 1.1, 1.3, 1.5) on improving the SSR and P recovery was limited, and the differences among P recovery efficiency for all three types of blackwater were less than 5%.

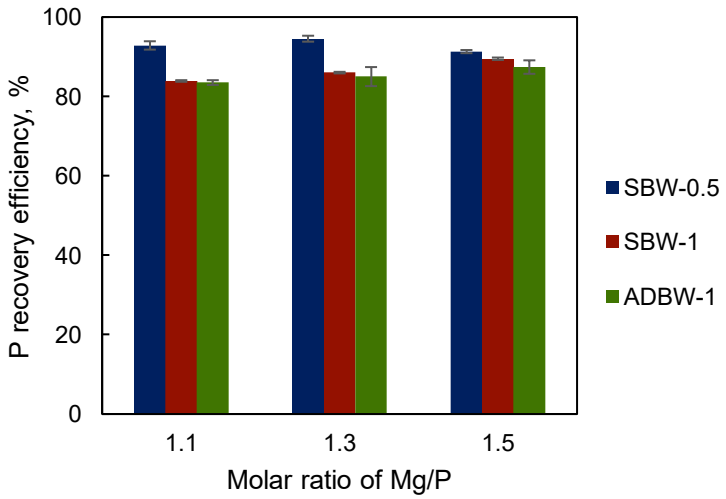

Figure 3-2. Influence of Mg/P molar ratio on P recovery efficiency.

Based on a specific K_{sp} value of 3.89×10^{-10} for a digested wastewater (Bhuiyan et al., 2008; Borgerding, 1972), SSRs for the three types of blackwater at different Mg/P molar ratios can be estimated (**Table 3–2**). In this study, an SSR higher than 4.0 was able to achieve a P recovery efficiency higher than 90%. Ghosh et al. (2019) found that an SSR of 5.5–6.0 was optimum for an efficient P removal based on an experimental study using synthetic anaerobic digestate. In raw wastewater, the activities of NH_4^+, Mg^{2+}, and PO_4^{3-} can be affected greatly by various ions with various concentrations and thus should be determined accordingly. Therefore, the determination of an optimum SSR largely depends on a specific wastewater source.

Table 3-2. SSRs of three types of blackwater.

	Mg/P molar ratio	Ionic strength	SSR
SBW-0.5	1.1	0.0828	4.1
	1.3	0.0836	4.3
	1.5	0.0843	4.5
SBW-1	1.1	0.0544	3.7
	1.3	0.0551	3.9
	1.5	0.0557	4.1
ADBW-1	1.1	0.0906	3.4
	1.3	0.0913	3.6
	1.5	0.0920	3.8

3.3.4 Effect of pH of concentrated blackwater on P recovery efficiency

Fig. 3–3 shows the influence of the initial pH of blackwater on P recovery efficiency. It is shown that a higher pH led to higher P recovery in all blackwater samples. For instance, a pH of 9.0 for SBW-0.5 achieved the highest P recovery efficiency of 95%, and a pH of 9.0 for SBW-1 achieved a P removal of 92%. After pH adjustment using NaOH, a pH of 9.0 and 9.5 for ADBW-1 achieved a P removal of 93% and 95%, respectively. However, without pH adjustment, it was observed that the initial pH of ADBW-1 resulted in a P removal of only 87%. It should be noted that a higher

pH of raw concentrated blackwater can be achieved after being stored for an extended period. A pH value of 9.0 or even higher can be achieved after 1–3 d storage of blackwater due to the hydrolysis of proteins, lipids, creatinine, and uric acid and ammonium release (Nsavyimana et al., 2020). Therefore, when concentrated blackwater is used to produce struvite, storage with a proper period is ideal for achieving a maximum initial pH close to 9.0.

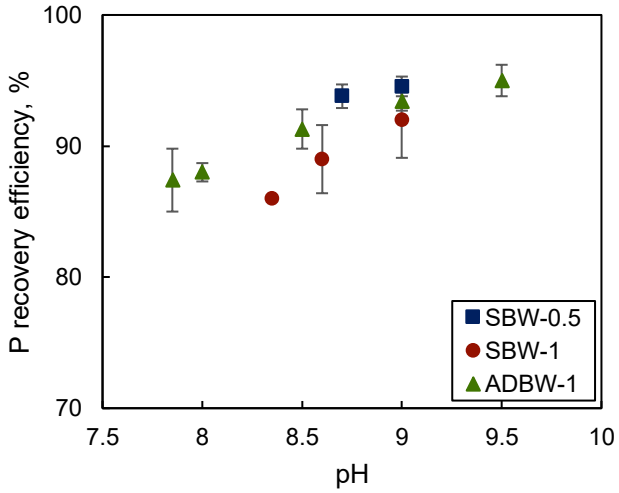

Figure 3-3. Influence of initial pH on P recovery efficiency (Error bars represent the standard deviations of the triplicated experiments).

3.3.5 Characterization of produced struvite

The XRD diffractogram in **Fig. 3–4** shows the detected intensities from XRD measurements for the struvite precipitates produced from SBW-0.5 with Mg/P molar ratios of 1.3 and initial pH values of 9.0 after storage. In comparison to the reference powder diffraction file of pure struvite (PDF 97-001-4269), most intensity peaks of the struvite were detected from the precipitates. A similar observation was obtained for the struvite produced from SBW-1 under Mg/P molar ratios of 1.3 and pH values of 9.0. No other components were detected by XRD characterization, likely

because their contents were lower than the detection limit (1–5 wt. %), indicating the high purity of struvite produced from concentrated blackwater. The color of the produced struvite was ivory and can be observed in **Fig. 3–4**.

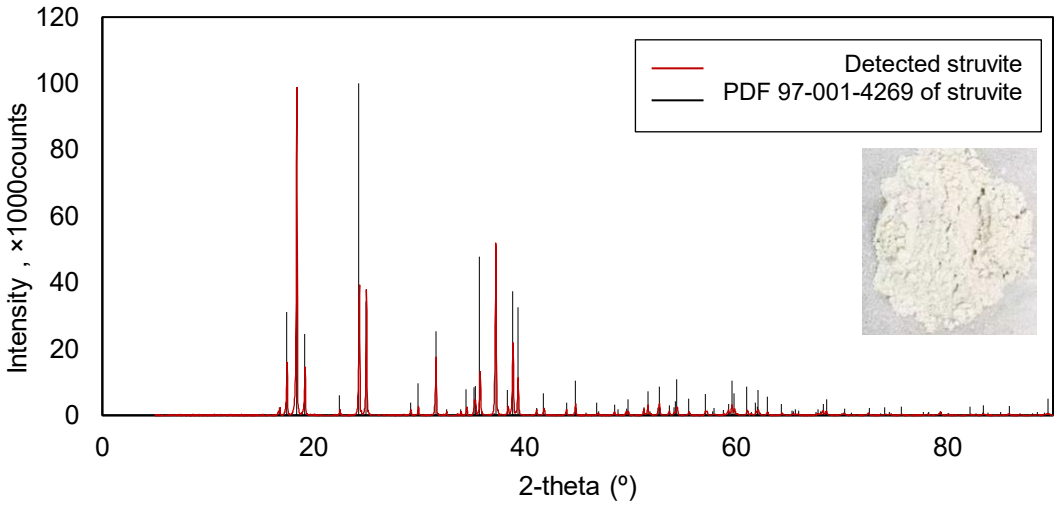

Figure 3-4. XRD pattern for struvite produced from concentrated blackwater.

SEM images of the struvite produced from SBW-0.5 with Mg/P molar ratios of 1.3 and pH values of 9.0 are shown in **Fig. 3–5(a)**. Typically, the crystal structures of struvite mainly include orthorhombic prism and tabular structures, indicating regular growth of struvite crystals. The crystal structure of struvite is similar to that produced from synthetic ADBW (Yee et al., 2019a; 2019b). As demonstrated in the literature, at a very early growth stage, the small pyramid-shaped crystals can often be formed, and then transformed to arrowhead-shaped crystals displaying well-defined faces, where they grew uniformly in each direction (Manzoor et al., 2018). In the present study, the crystals had a typical orthorhombic prism structure with different amounts of faces, as shown in **Fig. 3–5(b)**. Precipitated struvite crystals in the batch experiments reached lengths as

large as 40–50 μm. The growth of the crystals, illustrated in **Fig. 3–5(b)**, coincides with the morphological evolution revealed by Manzoor et al. (2018).

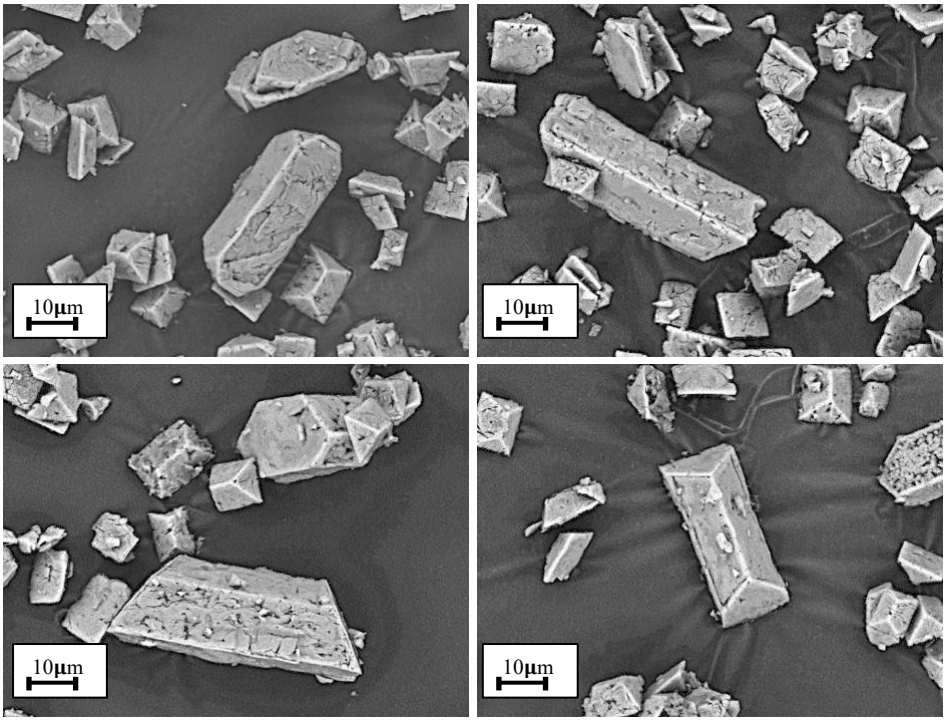

(a)

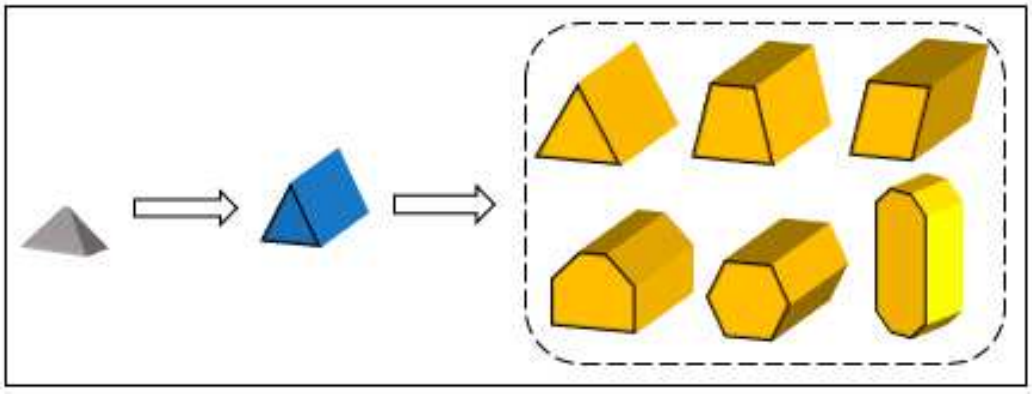

(b)

Figure 3-5. Characterization of struvite produced from concentrated blackwater.

The EDS technique was used to obtain the mass ratio between Mg, P, and N of the produced struvite, and the results are shown in **Table 3–3**. The average mass ratio was obtained based on at least 30 struvite samples produced from both SBW-0.5 and SBW-1. Compared to the theoretical mass ratio of Mg/P/N of 10:12.6:5.7 for pure struvite, an average mass ratio of 10:12:4.7 based on EDS results, confirms the high purity of the struvite produced from concentrated blackwater (SBW-0.5 and SBW-1). The Mg/P/N mass ratio in this study is also comparable with that achieved by using ADBW and urine as the waste source (Gell et al., 2011). Moreover, the average purity of the struvite produced from SBW-0.5 and SBW-1, as determined by the direct NH_4-N test method, reached values as high as 94.9%.

Table 3-3. Purity of struvite produced from concentrated blackwater.

	This study	Theoretical value	(Gell et al., 2011)
Mass ratio of Mg/P/N	10:12:4.7	10:12.6:5.7	10:10:5
Purity	94.9 ± 1.5 %	100 %	---

3.3.6 Heavy-metal contents of produced struvite

The presence of heavy metals (*e.g.*, Cu, Pb, Cr, Cd, As) in the struvite is the main concern for its utilization as a fertilizer because they can accumulate and impose risks on animal and human health *via* the food-chain or direct exposure (Li et al., 2019). However, there are currently no legislative standards with respect to heavy-metal contents for commercial struvite produced from waste when it is used as a fertilizer. **Table 3–4** summarizes light and heavy -metal contents of the struvite produced from concentrated blackwater (SBW-0.5 and SBW-1) in this study, and they are compared to literature values, which include the heavy-metal contents of the struvite formed from ADBW and urine (Gell et al., 2011). Heavy-metal contents of the struvite produced from other waste sources can be found elsewhere (Li et al., 2019). Calcium (Ca) and potassium (K) are two

dominant metals among all the metals being detected; nevertheless, they are present in a small amount relative to the struvite. The heavy-metal contents of common concern (*i.e.,* Zn, Cu, Ni, Cr, Cd, Pb, As) were all at relatively low levels, enabling the possible use of the struvite produced from concentrated blackwater as a fertilizer. This is consistent with the previous finding that heavy metals in struvite precipitated from stored urine were not detected (Ronteltap et al., 2007).

Table 3-4. Metal contents in the struvite produced from concentrated blackwater.

Metal content, mg/kg	This study	(Gell et al., 2011)
Ca	6,444 ± 1,172	Not reported (NR)
K	2,103 ± 386	NR
Na	274.00 ± 21.00	NR
Fe	150.00 ± 14.00	NR
Al	78.70 ± 32.30	NR
Mn	52.10 ± 10.00	NR
Zn	22.90 ± 3.70	<59
Rb	15.20 ± 5.30	NR
Ba	13.80 ± 1.50	NR
Cu	7.93 ± 3.17	134
Sr	5.96 ± 2.50	NR
Ni	1.42 ± 0.37	<2
Ga	1.01 ± 0.16	NR
Mo	0.78 ± 0.32	NR
Cr	0.67 ± 0.34	<4
Se	0.60 ± 0.10	NR
Ag	0.53 ± 0.20	NR
Sn	0.12 ± 0.01	NR
Co	0.10 ± 0.02	NR
Cd	<Detected limitation (DL)	<4
Pb	<DL	<59
As	<DL	<24

3.4 Discussion

Coprecipitates compete for magnesium and phosphate with struvite and are usually the main concern when producing struvite from wastewater since calcium is often present in tap water; these

compounds typically consist of calcium and include HAP [$Ca_5(PO_4)_3(OH)$], $Ca_3(PO_4)_2$, and $CaCO_3$, etc. HAP crystals have a typical spherical structure (Martinez et al., 2015), $Ca_3(PO_4)_2$ crystals have a round edge (Boanini et al., 2019), and $CaCO_3$ crystal can have rhombic, needle-like, or spherical structures (Ni and Ratner, 2008). In this study, neither the XRD technique nor the SEM technique detected the presence of calcium compounds with significant amounts (below 5 wt. %).

Further, the formation of coprecipitates is highly dependent on the dominant factors such as pH, Mg/P molar ratio, and Mg/Ca molar ratio (Zhang et al., 2019; Yee et al., 2019a). At a higher pH, NH_4^+ consumes OH^- to form NH_3, resulting in the potential release of NH_4^+ from struvite and the formation of $Mg_3(PO_4)_2$ [Eq. (3–8)]. Nevertheless, this phenomenon is more significant for wastewater containing lower NH_4^+ content. In blackwater, NH_4^+ concentrations are typically greater than 1,000 mg/L, which is more than enough to precipitate PO_4^{3-} with a concentration of approximately 100 mg/L. Meanwhile, a higher pH can break the equilibrium of triprotic phosphate, causing the formation of $Ca_3(PO_4)_2$ [Eq. (3–9)]. In addition, HCO_3^- consumes OH^- to generate more CO_3^{2-}, leading to the potential formation of $CaCO_3$ [Eq. (3–10)]. As such, although alkalinity helps maintain stable pH, too high alkalinity tends to cause undesired formation of $CaCO_3$. In this study, an initial pH of close to 9.0 for concentrated blackwater effectively mitigated the formation of impurities.

$$MgNH_4PO_4 \cdot 6H_2O + OH^- \rightarrow Mg_3(PO_4)_2 + NH_3 + 7H_2O \quad (3–8)$$

$$HPO_4^{2-} + 2OH^- + Ca^{2+} \rightarrow Ca_3(PO_4)_2 + 2H_2O \quad (3–9)$$

$$HCO_3^- + OH^- + Ca^{2+} \rightarrow CaCO_3 + H_2O \quad (3–10)$$

According to Zhang et al. (2019), calcite co-precipitation was significant when the Mg/P molar ratio was below 1.8. Nevertheless, the Mg/P molar ratio alone is not sufficient to determine

the tendency of coprecipitation occurrence, and the calcium concentration in the waste source must be taken into account. In their study (Zhang et al., 2019), the calcium concentration was as high as 124.81 mg/L, and the PO_4-P concentration was only 52.82 mg/L; therefore, when adding the external magnesium source to achieve the Mg/P molar ratio of 1.8, the molar ratio of Ca/Mg was close to 1.0. In this study, when the molar ratio of Mg/P was 1.3, the molar ratio of Ca/Mg was an average of 0.35; this low Ca/Mg molar ratio was unfavorable to the formation of $CaCO_3$. It was consistent with the finding that a Ca/Mg molar ratio of higher than 0.5 contributed to the early formation of coprecipitates (Lee et al., 2016). Mitani et al. (2003) found that the coexistence of calcium in wastewater containing low PO_4-P concentration (40 mg/L) interfered with struvite precipitation and recommended that the Ca/Mg molar ratio should be lower than 0.25 to prevent calcium phosphate precipitation prior to struvite precipitation. Hence, both the molar ratios of Mg/P and Ca/Mg should be considered for estimating the co-precipitation of calcium compounds.

In addition to the formation of coprecipitates, the possible presence of pathogens and endocrine-disrupting compounds (EDCs) in the produced struvite is another concern for its use as the commercial fertilizer (Yee et al., 2019b). The optimization of post-precipitation treatment, such as washing and drying, is beyond the scope of the present study.

3.5 Conclusions

The prospect of recovering P directly from source-diverted blackwater through struvite precipitation without pH adjustment was successfully demonstrated in this chapter. Chapter 3 completed Objective 1.1. Among various blackwater sources, including concentrated blackwater collected from vacuum toilet systems, low-dilution blackwater collected from dual-flush toilet

systems, and low-dilution blackwater anaerobically digested by the UASB reactor, P recovery percentage was the highest from concentrated blackwater. The moderate PO_4-P concentration, high NH_4-N concentration, relatively low calcium concentration, strong buffering capacity, and ideal pH enable concentrated blackwater to be a potential source candidate for producing struvite. When the supersaturation ratio of struvite was maintained above 4.0, P recovery efficiency exceeding 90% was achieved for concentrated blackwater. The produced struvite had high quality in terms of purity (nearly 95%) and low heavy-metal concentrations. This study puts forward an economical method for struvite production from concentrated blackwater through saving costs associated with pH adjustment and suggests strategies to enhance nutrient recovery in decentralized wastewater management systems.

References

Alp, Ö., 2010. Further treatment of digested blackwater for extraction of valuable components. PhD Thesis, Hamburg University of Technology, Germany.

Baird, R.B., Eaton, A.D., Rice, E.W., 2017. Standard Methods for the Examination of Water and Wastewater, 23rd ed. American Public Health Association, Washington.

Bhuiyan, M.I.H., Mavinic, D.S., Koch, F.A., 2008. Thermal decomposition of struvite and its phase transition. Chemosphere 70 (8), 1347–1356.

Boanini, E., Gazzano, M., Nervi, C., Chierotti, M.R., Rubini, K., Gobetto, R., Bigi, A., 2019. Strontium and zinc substitution in *ß*-tricalcium phosphate: an X-ray diffraction, solid state NMR and ATR-FTIR study. J. Funct. Biomater. 10 (2), 20.

Borgerding, J., 1972. Phosphate deposits in digestion systems. J. Water Pollut. Control Fed. 44, 813–819.

de Graaff M.S., Temmink, H., Zeeman, G., Buisman, C.J.N., 2010. Anaerobic treatment of concentrated blackwater in a UASB reactor at a short HRT. Water 2 (1), 101–119.

Gao, M., Guo, B., Zhang, L., Zhang, Y., Liu, Y., 2019a. Microbial community dynamics in anaerobic digesters treating conventional and vacuum toilet flushed blackwater. Water Res. 160 (1), 249–258.

Gao, M., Zhang, L., Zhang, H., Florentino, A.P., Liu, Y., 2019b. Energy recovery from municipal wastewater: impacts of temperature and collection systems. J. Environ. Eng. Sci. 141 (1), 24–31.

Gell, K., de Ruijter, F.J., Kuntke, P., de Graaff, M., Smit, A.L., 2011. Safety and effectiveness of struvite from black water and urine as a phosphorus fertilizer. J. Agric. Sci. 3 (3), 67–80.

Ghosh, S., Lobanov, S., Lo, V.K., 2019. Impact of supersaturation ratio on phosphorus recovery from synthetic anaerobic digester supernatant through a struvite crystallization fluidized bed reactor. J. Environ. Technol. 40 (15), 2000–2010.

Lee, S.-H., Kumar, R., Jeon, B.-H., 2016. Struvite precipitation under changing ionic conditions in synthetic wastewater: experiment and modeling. J. Colloid Interface Sci. 474, 93–102.

Li, B., Boiarkina, I., Yu, W., Huang, H., Munir, T., Wang, G., Yong, B.R., 2019. Phosphorus recovery through struvite crystallization: challenges for future design. Sci. Total Environ. 648, 1244–1256.

Manzoor, M.A.P., Singh, B., Agrawal, A.K., Arun, A.B., Mujeeburahiman, M., Rekha, P.-D., 2018. Morphological and micro-tomographic study on evolution of struvite in synthetic urine infected with bacteria and investigation of its pathological biomineralization. PLoS One 13 (8), e0202306.

Martinez, C., La Gattina, G., Garrido, L., Gilabert, U., Ozols, A., 2015. Hydroxyapatite microsphere production by plasma spray. Procedia Mater. Sci. 8, 319–323.

Mitani, Y., Sakai, Y., Mishina, F., Ishiduka, S., 2003. Struvite recovery from wastewater having low phosphate concentration. J. Water Environ. Technol. 1 (1), 13–18.

Ni, M., Ratner, B.D., 2008. Differentiation of calcium carbonate polymorphs by surface analysis techniques-an XPS and TOF-SIMS study. Surf. Interface Anal. 40 (10), 1356–1361.

Nsavyimana, G., Kaboneka, S., Bigumandondera, P., Ngahane, E.L., Ndikumana, T., Vasel, J.L., 2020. Exploring a new approach of the population equivalent concept through a detailed characterization of grey and black waters. IJASRE 6 (1), 32–49.

Palmquist, H., Hanæus, J., 2005. Hazardous substances in separately collected grey- and blackwater from ordinary Swedish households. Sci. Total Environ. 348 (1–3), 151–163.

Ronteltap, M., Maurer, M., Gujer, W., 2007. The behaviour of pharmaceuticals and heavy metals during struvite precipitation in urine. Water Res. 41 (9), 1859–1868.

Sawyer, C.N., McCarty, P.L., Parkin, G.F., 2003. Chemistry for Environmental Engineering and Science, fifth ed., McGraw-Hill Inc.

Yee, R.A., Alessi D.S., Ashbolt, N.J., Hao, W., Konhauser, K., Liu, Y., 2019a. Nutrient recovery from source-diverted blackwater: optimization for enhanced phosphorus recovery and reduced co-precipitation. J. Clean. Prod. 235 (20), 417–425.

Yee, R.A., Leifels, M., Scott, C., Ashbolt, N.J., Liu, Y., 2019b. Evaluating microbial and chemical hazards in commercial struvite recovered from wastewater. Environ. Sci. Technol. 53 (9), 5378–5386.

Zhang, H., Gong, W., Luo, X., Xie, B., Li, G., Liang, H., 2019. Obtaining high-purity struvite from anaerobically digested wastewater: effects of pH, Mg/P, and Ca^{2+} interactions. Environ. Eng. Sci. 36 (1), 102–113.

CHAPTER 4 EVALUATION OF ROLE OF BLACKWATER SOLIDS IN STRUVITE PRODUCTION EFFECTIVENESS

A version of this chapter has been published in the *Journal of Environmental Engineering*.

4.1 Synopsis

In Chapter 3, source-diverted blackwater, especially concentrated blackwater collected from vacuum toilet systems, has been demonstrated to be an ideal source for struvite production without pH adjustment. However, the impact of total suspended solids (TSS) in blackwater towards struvite quality are not well addressed.

Though raw blackwater has an ideal pH for struvite precipitation, it also has high levels of TSS and complex species. High TSS concentrations in raw blackwater can be a challenge for high-quality struvite production, and their general impacts are not well understood or agreed upon by the scientific community. For instance, Ping et al. (2016) found that TSS concentrations above 153 mg/L negatively affected the struvite pellet growth. Tarragó et al. (2018) found that even at high solids concentrations (*e.g.*, 1000–3000 mg/L TSS), more than 95% of P was recovered as struvite. The authors also proposed that solids facilitated struvite crystallization, acting as nuclei favoring heterogeneous nucleation. Hence, prior to the use of raw blackwater as a potential waste source for struvite production, the role of blackwater TSS in struvite production needs to be addressed.

Fluidized bed reactor (FBR) has been demonstrated as a competitive process for struvite production due to its high mixing energy, easy particle classification, and simple process control (Ohlinger et al. 2000; Iqbal et al. 2008; Rahaman 2009; Shim et al. 2020). It is easier to achieve crystal-size classification through the inverted telescope design of the FBR and by controlling the upflow velocity in the FBR (Fattah et al. 2008; Fattah et al. 2012; Rahaman et al. 2014). In Chapter 4, an FBR was operated in a batch mode to examine the influence of TSS in raw concentrated blackwater on P recovery efficiency as well as the purity and size of the produced struvite. The impact of upflow velocity of the FBR on struvite quality was also assessed. The produced struvite

was characterized via XRD and SEM techniques. The metal contents of the struvite product were determined by ICP-MS.

4.2 Experimental Method

4.2.1 Preparation for blackwater samples with various TSS concentrations

Blackwater (feces and urine) from vacuum toilets (0.5–1 L water per flush) was collected from the University of Alberta (Edmonton, Canada) campus every day over a two-week period. Upon collection, blackwater was well-mixed and stored at 4 ºC for 24 h, allowing large solids to settle and the pH value to reach 8.5–9.0. Prior to the experiments, the supernatant of the blackwater was then centrifuged to obtain supernatants with different TSS concentrations. Six TSS levels were tested in this study, including 1,600 mg/L, 620 mg/L, 520 mg/L, 340 mg/L, 220 mg/L, and 120 mg/L.

4.2.2 Batch FBR experiments

The experiments were conducted in an FBR in a batch mode. All tests were carried out in triplicate with 80 mL of each sample at room temperature (21 ± 0.5 °C). A schematic of the experimental setup is shown in **Fig. 4–1**. Prior to the feeding of FBR, magnesium chloride ($MgCl_2$, 1.0 M) was added to the blackwater sample to achieve the target Mg/P molar ratio. Subsequently, the sample was fed into the FBR from its lower part. After the sample was pumped into the FBR, this pump was stopped, and meanwhile, another pump in the recirculation line started to work. After the target-period of operation, the precipitates were collected from the bottom of the FBR. The upflow

velocity of the sample in the FBR was adjusted by tuning the flow rate of the pump in the recirculation line. The upflow velocity, u, was calculated by Eq. (4–1).

$$u = Q/A \tag{4–1}$$

where Q is the flow rate of the pump in recirculation line, and A is the cross-sectional area of FBR.

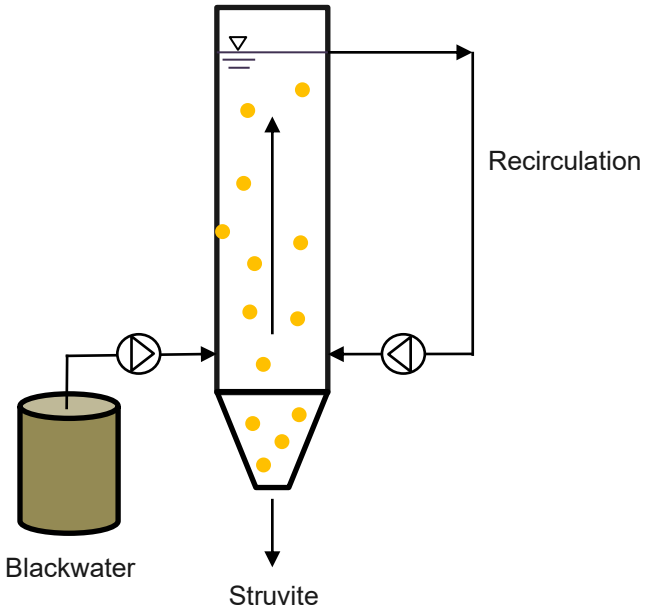

Figure 4-1. Schematic of FBR experimental setup.

4.2.3 Drying precipitates

The produced precipitates were collected from the bottom of the FBR. Solids were washed by deionized water at least three times to remove the loosely attached compounds, such as NaCl and NH_4Cl, from the precipitate surfaces. Finally, the washed precipitates were dried in the fume hood at room temperature over night for further characterization.

4.2.4 Water quality analysis

Blackwater samples were tested for pH, PO_4-P concentration, NH_4-N concentration, TSS concentration, and alkalinity. pH values were measured by a B40PCID pH meter (VWR SympHony, Avantor Inc., Radnor, PA, USA). NH_4-N and TSS concentrations were examined by the Standard Methods (Baird et al., 2017). PO_4-P concentration and alkalinity were determined by HACH kits (HACH, Loveland, Colorado, USA). The P recovery efficiency (η), as shown in Eq. (4–2), was calculated based on the initial ($[PO_4\text{-}P]_{initial}$) and final PO_4-P ($[PO_4\text{-}P]_{final}$) concentrations, before and after operation, respectively.

$$\eta = \frac{[PO_4\text{-}P]_{initial} - [PO_4\text{-}P]_{final}}{[PO_4\text{-}P]_{initial}} \times 100\% \quad (4\text{–}2)$$

4.2.5 Struvite purity determination

The struvite purity of the produced precipitates was determined by analyzing the NH_4-N concentration of the precipitates. This is based on the principle that NH_4^+ only participates in reaction producing struvite [See Eq. (4–3)], but it does not participate in other reactions producing possible components which compete for Mg^{2+} and PO_4^{3-} with struvite.

$$Mg^{2+} + NH_4^+ + H_nPO_4^{n-3} + 6H_2O \rightarrow MgNH_4PO_4 \cdot 6H_2O + nH^+ \quad (4\text{–}3)$$

The precipitates (50 mg) were dissolved in hydrochloric acid (HCl, 3.0 M) and diluted with deionized water to obtain 250 mL solution. The NH_4-N concentration of this diluted solution was then determined by the Standard Method (Baired et al., 2017). The struvite purity of the precipitates based on weight was calculated by Eq. (4–4).

$$p_{MAP} = \frac{n_{NH_4\text{-}N} \times MW_{MAP}}{m_p} \times 100\% \quad (4\text{–}4)$$

where p_{MAP} is the struvite purity, n_{NH_4-N} is the number of NH_4-N moles in the dissolved precipitates obtained from the measurement, MW_{MAP} is the molecular weight of struvite, and m_p is the mass of the dissolved precipitates.

4.2.6 Characterization

Metal contents of the produced precipitates were characterized by the ICP-MS (Elan 6000, Perkin Elmer, Oshawa, Ontario, Canada) method. The components of produced precipitates were detected by XRD (Ultimate IV, Rigaku Tokyo, Japan) to examine the presence of coprecipitates. The morphology structures of the precipitates were observed by SEM (Zeiss Sigma 300 VP, FELMI-ZFE, Graz, Austria).

4.2.7 Struvite size determination

In order to measure the sizes of the struvite crystals collected from the triplicate experiments, at least 30 SEM images were captured, and the sizes of at least 150 crystals were determined. The average size of the struvite crystals collected from the triplicate experiments was calculated based on the measured 150 crystal sizes.

4.2.8 Statistical analysis

Student's t-test was performed to determine the p-value. A p-value less than 0.05 indicates statistical difference between two groups of data.

4.3. Results

4.3.1 Characterization of blackwater sample

Table 4–1 shows the characteristics of the raw concentrated blackwater samples. After blackwater was stored for 24 h, its average pH, NH_4-N concentration, and alkalinity were 8.9, 1,025.5 mg/L, and 3,145.0 mg/L, respectively. A pH value of 8.9 fell in the optimum pH range (8.5–9.5) for struvite precipitation reported elsewhere (Alp, 2010; Shih and Yan, 2016; Daneshgar et al., 2018; Yee et al., 2019a). This high NH_4-N concentration can also contribute to a high supersaturation ratio of struvite. The high alkalinity brought about sufficient buffer capacity, which was able to maintain a stable pH value. In comparison to the three parameters mentioned above, the PO_4-P concentration was much more stable during the short storage time, and remained at 76.9 mg/L, which is a typical concentration for concentrated blackwater collected from vacuum toilet system (de Graaff et al., 2011). The metal-content analysis of the blackwater sample showed that Na, K, and Ca were the three dominant metals. Although other metals such as Al, Fe, Zn, Cu, and Cr were also present, their concentrations were less than 1.0 mg/L. After 24-h storage, the TSS of original blackwater supernatant was 1,600 mg/L. Other typical composition of concentrated blackwater such as COD, total solids (TS), and volatile solids (VS) can be found elsewhere (Kujawa-Roeleveld and Zeeman, 2006; de Graaff et al., 2011; Gao et al., 2019).

Table 4-1. Characteristics of blackwater samples. The results are presented as mean ± standard deviation.

Parameter	Supernatant of blackwater
pH	8.9 ± 0.3
TSS, mg/L	1,600, 620, 520, 340, 220, 120 (obtained by centrifugation)
PO_4-P, mg/L	76.9 ± 14.5
NH_4-N, mg/L	1,025.5 ± 235.5
Alkalinity, mg $CaCO_3$/L	3,145.0 ± 415.0
Na, mg/L	530.0 ± 80.0
K, mg/L	203.8 ± 23.7
Ca, mg/L	54.2 ± 4.0
Mg, mg/L	1.9 ± 0.4

4.3.2 Determination of Mg/P molar ratio and operating time of FBR

The optimum Mg/P molar ratio for struvite production varies from waste source to waste source. For this specific blackwater, a reasonable Mg/P molar ratio was determined. **Fig. 4–2** shows the influences of Mg/P molar ratio on P recovery efficiency at different operating times of FBR. When the Mg/P molar ratio increased from 1.1 to 1.5, the P recovery efficiency increased from 87% to 94% with an operating time of 60 min. For all the five Mg/P molar ratio levels, increasing the FBR operating time from 60 to 120 min did not significantly improve the P recovery efficiency since the increment of P recovery efficiency was less than 2% (p value = 0.80–0.96 for Mg/P molar ratio of 1.1–1.5). Therefore, in this study, a Mg/P molar ratio of 1.5 and an FBR operating time of 60 min were employed for all the experiments for achieving high P recovery efficiency. This Mg/P molar ratio was consistent with that reported by Yee et al. (2019a). The authors concluded that a

pH value of 9.0 for ADBW and a Mg/P molar ratio of 1.5 were the optimal conditions in terms of both enhanced P recovery efficiency and minimized co-precipitation potential.

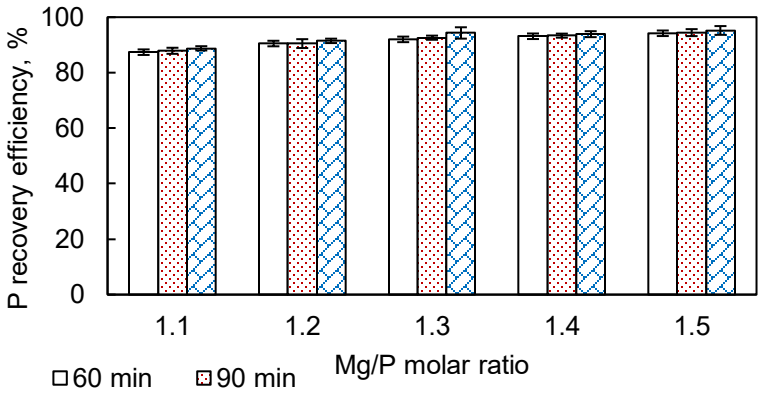

Figure 4-2. Impacts of Mg/P molar ratio on P recovery efficiency at different FBR operating times. Blackwater with TSS of 120 mg/L was used. Error bars represent the standard deviations of the triplicate experiments.

Under the same upflow velocity, a lower TSS level resulted in slightly higher P recovery efficiency, but this contribution was limited (P value = 0.24 for upflow velocity of 18–90 m/h). With the TSS level ranging from 200 to 1,600 mg/L, the P recovery efficiency ranged from 90.4 to 94.5% at an upflow velocity of 30 m/h. Therefore, it can be concluded that, under the premise that the appropriate wastewater quality (e.g., pH, PO_4-P concentration, and NH_4-N concentration) and the operating conditions (e.g., Mg/P molar ratio and reaction time) were used, neither TSS concentration nor FBR upflow velocity significantly affected P recovery efficiency. A similar conclusion was also reported by Tarragó et al. (2018), who found that even at the high TSS concentrations (1,000–3,000 mg/L), the P recovery efficiency from digested swine manure (PO_4-P concentration of 328–488 mg/L) was 95%. Tarragó et al. (2018) suggested that TSS acted as nuclei favoring heterogeneous nucleation, hence, it did not interfere with struvite formation.

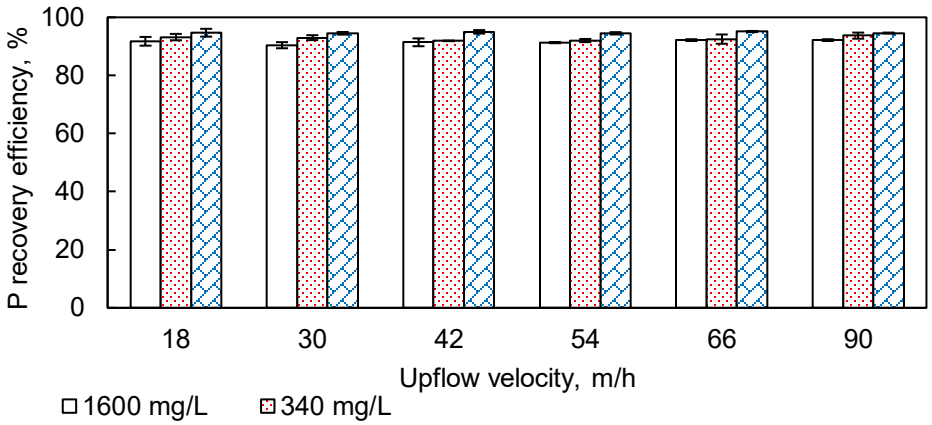

Figure 4-3. Impacts of blackwater TSS on P recovery efficiency at different FBR upflow velocities. Error bars represent the standard deviations of the triplicate experiments.

4.3.4 Influence of blackwater TSS on struvite size

Typical struvite morphology revealed by SEM imaging is shown in **Fig. 4–4**. Within the upflow velocity range studied and under the high TSS conditions (520, 620, and 1,600 mg/L), almost all crystals exhibited an orthorhombic shape that was less than 5 μm. In comparison, the crystals collected under the low TSS conditions (120 and 220 mg/L) were considerably larger, with more rod-shaped crystals detected. Our observation demonstrated that although TSS did not have a negative effect on the P recovery efficiency, it hindered the continuous growth of struvite crystals. Similarly, Ping et al. (2016) found that the average struvite size decreased greatly with the increase of TSS concentration (31–251 mg/L). Tarragó et al. (2018) also stated that smaller particles were obtained when the TSS concentration was higher.

Fig. 4–5 shows the size distribution of the struvite produced from blackwater with the TSS concentration of 120 mg/L under different FBR upflow velocities. As shown in **Fig. 4–5(a)**, the average crystal size was the largest at the lowest upflow velocity, *i.e.*, 18 m/h. The results indicated

that a higher upflow velocity was unfavorable to the agglomeration of the fine crystals and tended to break the larger crystals. One explanation for this phenomenon is the high shear force exerted on the struvite crystal (Wang et al., 2006). Tarragó et al. (2016) also found that the struvite size was correlated with the upflow velocity.

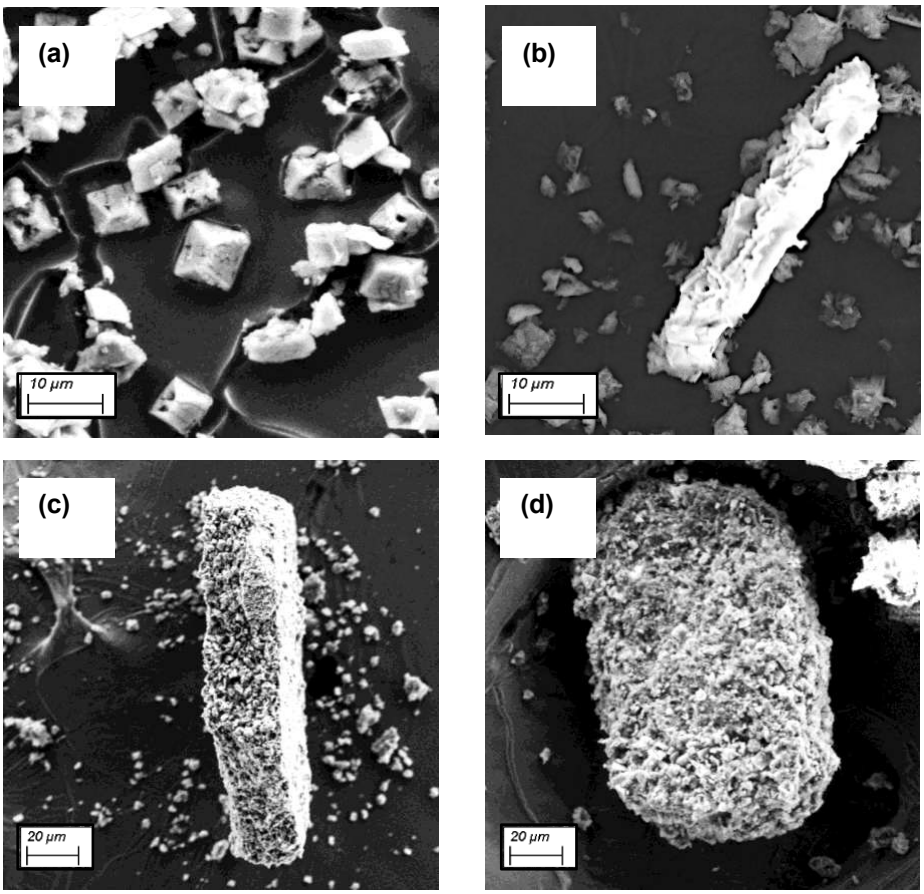

Figure 4-4. Typical SEM images of struvite produced from blackwater with TSS of (a) 1,600 mg/L at upflow velocity from 18 to 90 m/h, (b) 340 mg/L at upflow velocity of 18 m/h, (c) 220 mg/L at upflow velocity of 18 m/h, and (d) 120 mg/L at upflow velocity of 18 m/h.

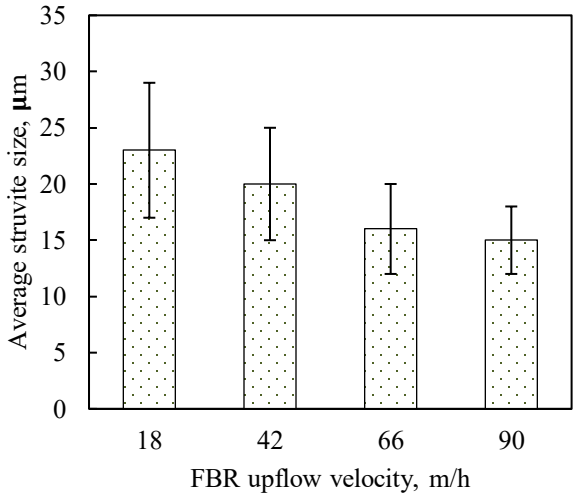

(a) Average struvite size

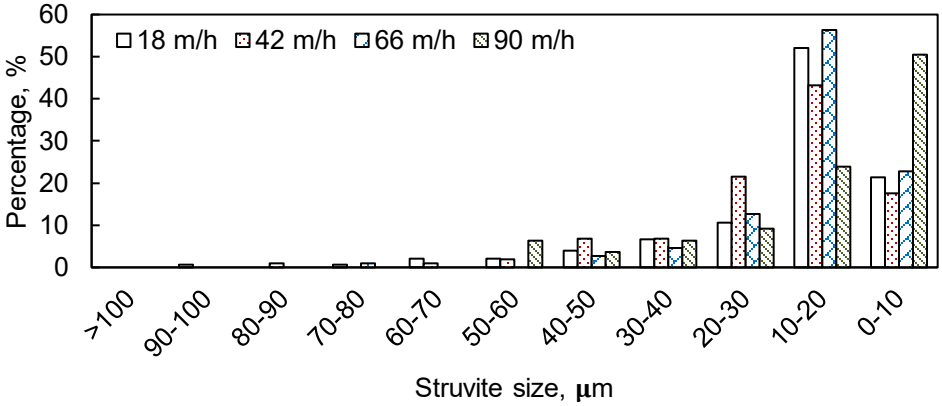

(b) Struvite size distribution

Figure 4-5. Size of struvite produced from blackwater with TSS of 120 mg/L: (a) average struvite size, and (b) struvite size distribution.

4.3.5 Influence of blackwater TSS on struvite purity

Fig. 4–6 shows the influences of blackwater TSS concentration on purity of the produced struvite.

At the high TSS level of 1,600 mg/L, the struvite purity was only 40%. With the decrease of TSS

concentration, the struvite purity increased. When the TSS concentration was 220 mg/L, the struvite purity reached 81%. An even lower TSS concentration did not further increase struvite purity (P value = 0.22). The influences of blackwater TSS concentration on struvite purity obtained in this study coincided with that reported by Ping et al. (2016). It was found that struvite purity was linearly related to TSS level with a negative slope when the TSS level ranged from 31 mg/L to 251 mg/L. Although TSS provided a deposit site for struvite nucleation, the trapping of TSS in the struvite embryo led to low-quality struvite, and the presence of TSS in the bulk phase hindered the continuous growth of crystal. TSS is not the only factor for controlling struvite purity; co-precipitation of other compounds plays a more important role when TSS is not a limiting factor for struvite purity. Source-diverted blackwater has low heavy-metal contaminations (Cunha et al., 2019; Yee et al., 2019b; Zhang et al., 2021), and calcium could be the dominant cation that competes for PO_4^{3-} with struvite. The chemical reactions that produce possible calcium compounds can be found in **Table 4–2**.

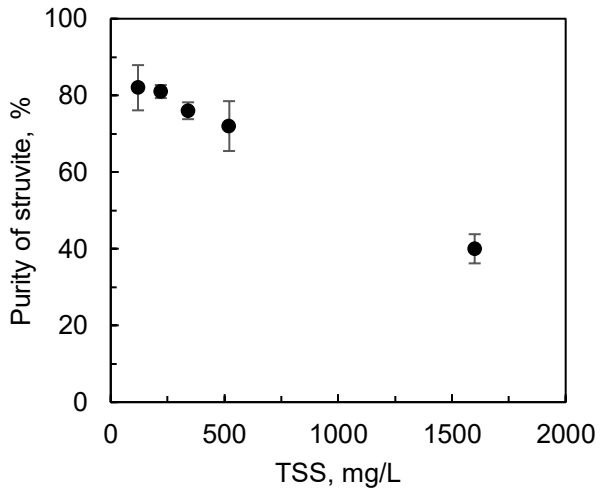

Figure 4-6. Influence of blackwater TSS on the struvite purity. Error bars represent the standard deviations of the triplicate experiments.

Table 4-2. Possible calcium compounds producing in the struvite precipitation process from blackwater (Lei et al., 2017; Daneshgar et al., 2018).

Precipitates	Chemical reaction
Hydroxyapatite (HAP)	$10Ca^{2+} + 6PO_4^{3-} + 2OH^- \rightarrow Ca_{10}(OH)_2(PO_4)_6$
Tricalcium phosphate (TCP)	$3Ca^{2+} + 2PO_4^{3-} \rightarrow Ca_3(PO_4)_2$
Amorphous calcium phosphate (ACP)	$3Ca^{2+} + 2PO_4^{3-} + xH_2O \rightarrow Ca_3(PO_4)_2 \cdot xH_2O$
Calcite	$Ca^{2+} + CO_3^{2-} \rightarrow CaCO_3$

4.3.6 Quality of produced struvite

The quality of the produced struvite was further examined by the XRD technique and ICP-MS method. The XRD pattern for the precipitates produced from blackwater with the TSS concentration of 120 mg/L is illustrated in **Fig. 4–7**. As compared to the Inorganic Crystal Structure Database (ICSD), the detected peaks aligned with crystalline struvite as indicated by the middle panel. However, in addition to struvite, calcite ($CaCO_3$, indicated by the bottom panel) was detected in the precipitates. No other calcium compounds such as $Ca_3(PO_4)_2$ (TCP) or $Ca_5(PO_4)_3(OH)$ (HAP) were detected, likely because their contents were lower than the detection limit (1–5 wt.%). The occurrence of coprecipitates driven by reaction kinetics is more related to the quality of blackwater such as pH and existing species. The presence of $CaCO_3$ was probably a result of the high alkalinity of blackwater, which was 3,145 mg $CaCO_3$/L in this study as shown in **Table 4–3**. Dai et al. (2018) found that addition of Ca^{2+} at high concentrations in an alkaline environment resulted in $CaCO_3$ precipitation. Wei et al. (2019) pointed out that 35 mmol/L of carbonate, *i.e.*, 1,750 mg $CaCO_3$/L, could cause the formation of flocs on the struvite crystal surfaces. In addition, the blackwater pH value of 8.9 and the low Ca/P molar ratio (0.5 in this study) suppressed the formation of TCP and HAP. According to Yee et al. (2019a), a pH value of 9.0 was able to minimize the occurrence of co-precipitates. Hallas et al. (2019) also demonstrated that a pH range of 8.0–10.0 impeded the potential formation of $CaHPO_4 \cdot 2H_2O$ and $Mg(OH)_2$.

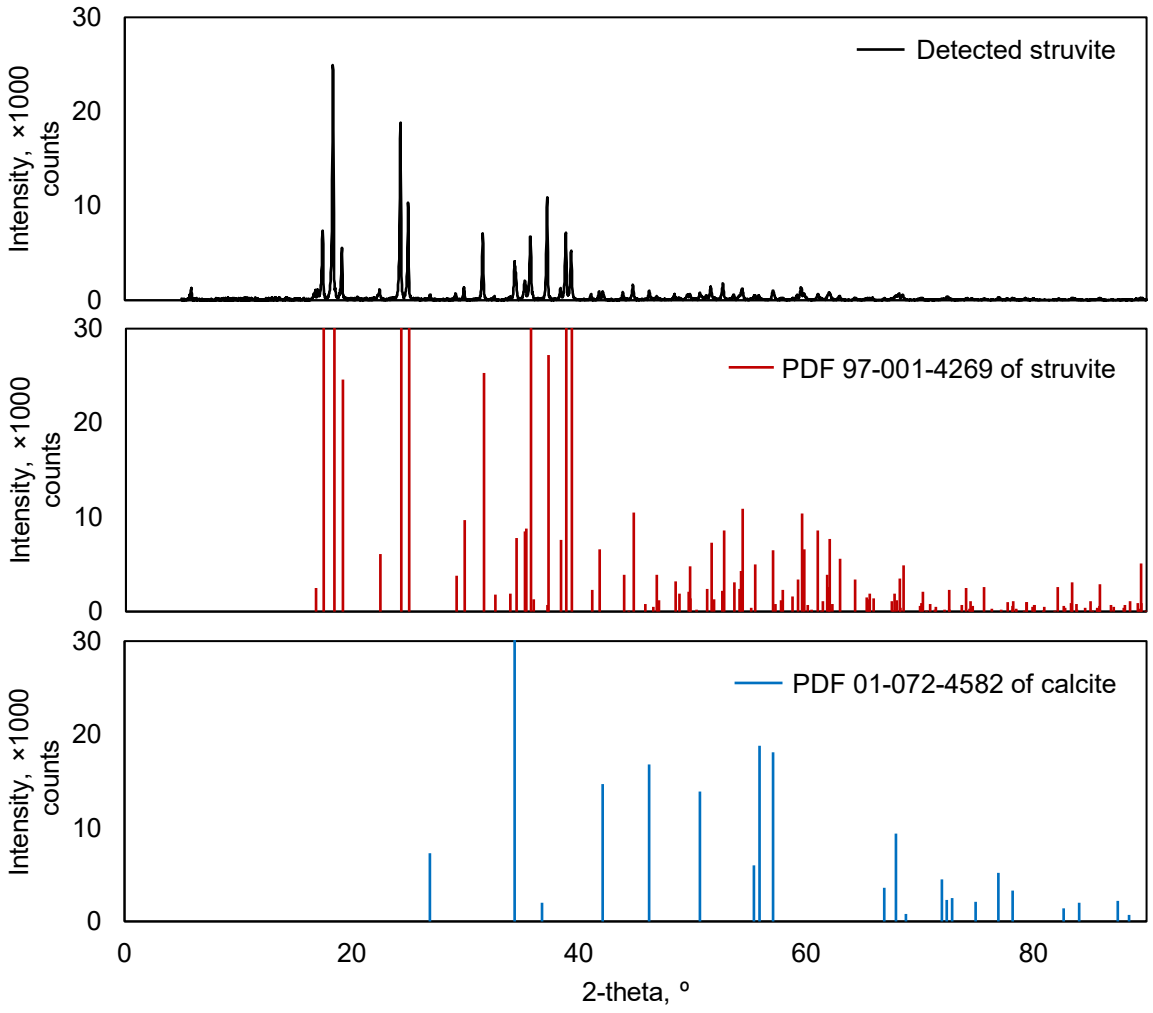

Figure 4-7. XRD pattern for the precipitate produced from blackwater with TSS of 120 mg/L.

In order to further assess the quality of the produced precipitates and to examine the metal contents, the authors determined the contents of calcium and other metals existing in the precipitates by applying the ICP-MS method; the results are shown in **Table 4–3**. Ca, K, and Na were three dominant co-existing metals among all the metals detected. Heavy metals such as Sr, Mn, Cu, Ti, Ba, and Sn were also present, but only in relatively small amounts. The metal contents of the struvite produced in this study were compared with that of the commercial struvite produced from ADBW (Yee et al., 2019b) in **Table 4–3**. It demonstrates that although high alkalinity

resulted in the occurrence of $CaCO_3$, the quality of the produced struvite was still comparable with that of the commercial struvite in terms of metal contents (Yee et al., 2019b).

Table 4-3. Metal contents in the struvite produced from blackwater with TSS of 120 mg/L. The results are presented as mean ± standard deviation.

Metal, mg/kg	This study	Yee et al. (2019b)
Ca	24723.00 ± 296.00	22100
K	2243.00 ± 50.00	10000
Na	952.00 ± 18.00	3300
Fe	600.00 ± 40.00	20100
Zn	345.00 ± 7.00	240
Al	121.00 ± 7.00	Not reported (NR)
Sr	111.00 ± 14.00	NR
Mn	86.10 ± 12.90	205
Cu	80.90 ± 0.10	60
Ti	64.90 ± 4.40	NR
Ba	32.80 ± 2.00	NR
Sn	5.95 ± 2.62	NR
Ce	5.85 ± 0.75	NR
Rb	4.18 ± 0.58	NR
Ni	3.94 ± 0.14	Not detected (ND)
Cr	2.26 ± 0.43	14
Pd	1.50 ± 0.76	NR
Mo	1.49± 0.09	NR
Se	1.48 ± 0.25	NR
La	1.18 ± 0.51	NR
Pb	0.93 ± 0.17	ND
Cd	0.84 ± 0.02	ND
As	0.75 ± 0.23	ND
Ga	0.58 ± 0.02	NR
Co	0.39 ± 0.02	NR
Ag	0.32 ± 0.10	NR

4.4 Discussion

4.4.1 Impact of blackwater quality on P recovery efficiency

P recovery efficiency, potential of coprecipitation, and coprecipitate species are directly related to the reaction kinetics that are affected by a number of factors including water quality of waste (*e.g.*,

pH, PO_4-P concentration, NH_4-N concentration, and alkalinity) and operating conditions (*e.g.*, Mg/P molar ratio and temperature). From the perspective of pH, a short-period storage of raw concentrated blackwater allows the hydrolysis of proteins, lipids, creatinine, and the release of uric acid and NH_3, and hence, leads to an increased pH value (Nsavyimana et al., 2020). The appropriate pH (close to 9.0) of raw concentrated blackwater contributes to the economic viability of P recovery from blackwater due to the absence of alkali utilization. More importantly, this pH value is favorable to high P recovery efficiency and minimized coprecipitation potential (Yee et al., 2019a).

From the perspective of alkalinity, a higher pH value is accompanied by a higher level of alkalinity. The release and dissolution of NH_3 generated from the hydrolysis process contributes to an increased pH value and alkalinity. Meanwhile, the dissolution of CO_2 results in the availability of CO_3^{2-} in the bulk liquid phase. Although the alkalinity helps maintain a stable pH value, high alkalinity can cause the formation of $CaCO_3$, decreasing the purity of the produced struvite. Nevertheless, according to the metal-content analysis, the quality of the struvite product in this study was comparable with the quality of the commercial struvite produced from ADBW (Yee et al., 2019b).

4.4.2 Impact of blackwater TSS on struvite growth

The growth of struvite crystals is governed by growth kinetics, which can be expressed by various models. Among these models, the two-step growth model is considered the most useful (Tai et al., 1999; Bhuiyan et al., 2008). The two steps include the diffusion and reaction processes. In the diffusion process, solute molecules are transported from the bulk fluid phase to the solid surface. In the reaction process, the solute molecules arrange themselves into the crystal lattice driven by

a localized supersaturation ratio. The colloidal particles of blackwater are primarily negatively-charged (Garcia et al., 2007; Hjorth et al., 2008; Christensen et al., 2009; Capdevielle et al., 2016) and can trap positively-charged ions like NH_4^+ and Mg^{2+}. This process provides a localized site which is favorable for PO_4^{3-} deposit. The presence of TSS with a high concentration can effectively reduce the diffusion process where NH_4^+, Mg^{2+}, and PO_4^{3-} are transported to the nucleic sites. This is why a high TSS level does not affect the P recovery efficiency. However, the colloidal particles can also trap other impurity ions to form complexes (Capdevielle et al., 2016), which together with the colloidal particle itself, bring about low-quality struvite.

High TSS contents provide sufficient nucleic sites, and thus large amounts of fine crystals are formed. According to Capdevielle et al. (2016), the agglomeration of crystals mainly includes three steps: the collision of crystals (aggregation), the association of crystals, and the formation of a crystalline bridge between them (agglomeration). Although aggregation is strong between small particles, the presence of colloidal particles can also increase the fluid viscosity, which lowers aggregation (Capdevielle et al., 2016). Hence, high TSS contents eventually hinder the continuous growth of the struvite crystal, resulting in struvite of small size. Another possible explanation is the repulsive force between the TSS and the struvite crystal. TSS, which is negatively-charged, can disrupt the aggregation potential of crystals, which have a negative surface charge (Shaddel et al., 2019).

After the induction period preceding the onset of crystallization, the growth of struvite in an FBR is mainly transport-controlled (Bhuiyan et al., 2008); in other words, it is dependent on hydrodynamic conditions. As stated by Tai et al. (1999), crystal growth in an FBR is independent of superficial velocity. However, once a critical crystal size is achieved, individual crystals cannot grow larger by themselves, and a crystal net in which particles act as linking bonds is formed to

allow for a bigger crystalline structure, also known as agglomeration (Tarragó et al., 2018). When TSS is not a limiting factor for struvite growth, a high superficial velocity caused by a high upflow velocity leads to a great shear force exerted on the crystal. The shear force adversely affects the aggregation and/or agglomeration of struvite crystals driven by the three steps mentioned above.

4.4.3 Quality of struvite produced from raw blackwater

In addition to an appropriate pH value of blackwater, the fact that source-diverted blackwater has low heavy-metal contaminations (Cunha et al., 2019; Yee et al., 2019b; Zhang et al., 2021) makes it an ideal source for struvite precipitation. Although calcium-related impurities are inevitably present in the struvite producing from blackwater, the occurrence of coprecipitates could be reduced by tuning the operating conditions including the pH value, the Mg/P molar ratio, and the Ca/Mg molar ratio. More details can be found in Chapter 3.

4.4.4 Practical applications of producing struvite from raw blackwater

Producing struvite from ADBW has been implemented at a commercial scale (Yee et al., 2019b). To the best of the authors' knowledge, however, producing struvite directly from raw blackwater at a commercial scale has never been reported. Source-diverted concentrated blackwater collected from vacuum toilet systems has an appropriate pH value (close to 9.0) after short-period storage. The reduced chemical cost pertinent to the elimination of the pH adjustment makes it economically feasible to produce struvite directly from raw blackwater. The low heavy-metal contents in blackwater help to ensure the quality of the produced struvite, making its utilization as the commercial fertilizer viable. Producing struvite directly from raw blackwater provides an alternative means to the P recovery in a decentralized wastewater management system.

4.4.5 Future research directions for producing struvite from raw blackwater

As demonstrated from this study, the presence of TSS with a concentration lower than 220 mg/L did not pose a negative influence on the struvite purity or size. As such, pre-treatment of raw blackwater to reduce TSS contents can improve struvite quality. Further studies on continuous operation of struvite reactors for P recovery from raw blackwater should also be conducted to identify the operation conditions at a commercial scale.

4.5 Conclusions

Raw concentrated blackwater collected from vacuum toilet systems is an economically-viable and environmentally-sustainable source for P recovery through struvite precipitation. The appropriate blackwater pH of close to 9.0, which was achieved after a short storage-period, contributed to both high P recovery efficiency and low co-precipitation potential in an economic way. A high TSS level provided localized sites favorable to ions deposit, so it did not significantly affect the phosphorus recovery efficiency. However, high TSS content was a limiting factor for the struvite purity and size. At a TSS concentration lower than 220 mg/L, TSS was no longer an important factor for the struvite purity and size, while the upflow velocity of the fluidized bed reactor showed a direct relationship with the struvite size. A smaller upflow velocity (e.g., 18 m/h) allowed for the agglomeration and continuous growth of the struvite crystals, and a greater upflow velocity was unfavorable to the steady growth of the struvite crystals due to the higher shear force exerted on them. Chapter 4 completed Objective 1.2. Chapter 3 and Chapter 4 are expected to provide the possibility for P recovery directly from source-diverted blackwater, aiming at more sustainable wastewater management.

References

Alp, Ö., 2010. Further Treatment of Digested Blackwater for Extraction of Valuable Components. PhD Thesis, Hamburg University of Technology, Germany.

Baird, R.B., Eaton, A.D., Rice, E.W., 2017. Standard Methods for the Examination of Water and Wastewater, 23rd ed. American Public Health Association, Washington.

Bhuiyan, M.I.H., Mavinic, D.S., Beckie, R.D., 2008. Nucleation and growth kinetics of struvite in a fluidized bed reactor. J. Cryst. Growth 310 (6), 1187–1194.

Capdevielle, A., Sýkorová, E., Béline, F., Daumer., M.L., 2016. Effects of organic matter on crystallization of struvite in biologically treated swine wastewater. Environ. Technol. 37 (7), 880–892.

Christensen, M.L., Hjorth, M., Keiding, K., 2009. Characterization of pig slurry with reference to flocculation and separation. Water Res. 43 (3), 773–783.

Cunha, J.R., Schott, C., van der Weijden, R.D., Leal, L.H., Zeeman, G., Buisman, C., 2019. Recovery of calcium phosphate granules from black water using a hybrid upflow anaerobic sludge bed and gas-lift reactor. Environ. Res. 178, 108671.

Dai, H., Tan, X., Zhu, H., Sun, T., Wang, X., 2018. Effects of commonly occurring metal ions on hydroxyapatite crystallization for phosphorus recovery from wastewater. Water 10 (11), 1619.

Daneshgar, S., Buttafava, A., Capsoni, D., Callegari, A., Capodaglio, A.G., 2018. Impact of pH and ionic molar ratios on phosphorus forms precipitation and recovery from different wastewater sludges. Resources 7 (4), 71.

de Graaff, M.S., Temmink, H., Zeeman, G., Buisman, C.J.N., 2011. Energy and phosphorus recovery from black water. Water Sci. Technol. 63 (11), 2759–2765.

Fattah, K.P., Mavinic, D.S., Koch, F.A., 2012. Influence of process parameters on the characteristics of struvite pellets. J. Environ. Eng. 138 (12), 1200–1209.

Fattah, K.P., Mavinic, D.S., Koch, F.A., Jacob, C., 2008. Determining the feasibility of phosphorus recovery as struvite from filter press centrate in a secondary wastewater treatment plant. J. Environ. Sci. Health Part A 43, 756–764.

Gao, M., Zhang, L., Zhang, H., Florentino, A.P., Liu, Y., 2019. Energy recovery from municipal wastewater: impacts of temperature and collection systems. J. Environ. Eng. Sci. 14 (1), 24–31.

Garcia, M.C., Vanotti, M.B., Szogi, A.A., 2007. Simultaneous separation of phosphorus sludge and manure solids with polymers. Trans. ASABE 50 (6), 2205–2215.

Hallas, J.F., Mackowiak, C.L., Wilkie, A.C., Harris, W.G., 2019. Struvite phosphorus recovery from aerobically digested municipal wastewater. Sustainability 11 (2), 376.

Hjorth, M., Christensen, M.L., Christensen, P.V., 2008. Flocculation, coagulation, and precipitation of manure affecting three separation techniques. Bioresour. Technol. 99 (18), 8598–8604.

Iqbal, M., Bhuiyan, H., Mavinic, D.S., 2008. Assessing struvite precipitation in a pilot-scale fluidized bed crystallizer. Environ. Technol. 29 (11), 1157–1167.

Kujawa-Roeleveld, K., Zeeman, G., 2006. Anaerobic treatment in decentralised and source-separation-based sanitation concepts. Rev. Environ. Sci. Biotechnol. 5 (1), 115–139.

Lei, Y., Song, B., van der Weijden, R.D., Saakes, M., Buisma, C.J.N., 2017. Electrochemical induced calcium phosphate precipitation: importance of local pH. Environ. Sci. Technol. 51 (19), 11156–11164.

Nsavyimana, G., Kaboneka, S., Bigumandondera, P., Ngahane, E.L., Ndikumana, T., Vasel, J.L., 2020. Exploring a new approach of the population equivalent concept through a detailed characterization of grey and black waters. IJASRE 6 (1), 32–49.

Ohlinger, K.N., Young, T.M., Schroeder, E.D., 2000. Postdigetion struvite precipitation using a fluidized bed reactor. J. Environ. Eng. 126 (4), 361–368.

Ping, Q., Li, Y., Wu, X., Yang, L., Wang, L., 2016. Characterization of morphology and component of struvite pellets crystallized from sludge dewatering liquor: effects of total suspended solid and phosphate concentrations. J. Hazard. Mater. 310, 261–269.

Rahaman, Md.S., 2009. Phosphorus Recovery from Wastewater through Struvite Crystallization in a Fluidized Bed Reactor: Kinetics, Hydrodynamics and Performance. PhD Thesis, University of British Columbia, Canada.

Rahaman, Md.S., Mavinic, D.S., Ellis, N., 2014. Fluidisation behaviour of struvite recovered from wastewater. J. Environ. Eng. Sci. 9 (2), 137–149.

Shaddel, S., Ucar, S., Andreassen, J.-P., Østerhus, S.W., 2019. Engineering of struvite crystals by regulating supersaturation-correlation with phosphorus recovery, crystal morphology and process efficiency. J. Environ. Chem. Eng. 7 (1), 102918.

Shih, K., Yan, H., 2016. The crystallization of struvite and its analog (K-struvite) from waste streams for nutrient recycling, in: Prasad, M.N.V., Shih, K. (Eds.), Environmental Material and Waste. Academic Press, Elsevier, pp. 665–686.

Shim, S., Won, S., Reza, A., Kim, S., Ahmed, N., Ra, C., 2020. Design and optimization of fluidized bed reactor operating conditions for struvite recovery process from swine wastewater. Processes 8, 422.

Tai, C.Y., Chien, W.-C., Chen, C.Y., 1999. Crystal growth kinetics of calcite in a dense fluidized-bed crystallizer. AIChE J. 45 (8), 1605–1614.

Tarragó, E., Puig, S., Ruscalleda, M., Balaguer, M.D., Colprim, J., 2016. Controlling struvite particles' size using the up-flow velocity. Chem. Eng. J. 302, 819–827.

Tarragó, T., Sciarria, T.P., Ruscalleda, M., Colprim, J., Balaguer, M.D., Adani, F., Puig, S., 2018. Effect of suspended solids and its role on struvite formation from digested manure. J. Chem. Technol. Biotechnol. 93, 2758–2765.

Wang, J., Burken, J.G., Zhang, X., 2006. Effect of seeding materials and mixing strength on struvite precipitation. Water Environ. Res. 78 (2), 125–132.

Wei, J., Ge, J., Rouff, A.A., Wen, X., Meng, X., Song, Y., 2019. Phosphorus recovery from wastewater using light calcined magnesite, effects of alkalinity and organic acids. J. Environ. Chem. Eng. 7 (5), 103334.

Yee, R.A., Alessi, D.S., Ashbolt, N.J., Hao, W., Konhauser, K., Liu, Y., 2019a. Nutrient recovery from source-diverted blackwater: optimization for enhanced phosphorus recovery and reduced co-precipitation. J. Clean. Prod. 235 (20), 417–425.

Yee, R.A., Leifels, M., Scott, C., Ashbolt, N.J., Liu, Y., 2019b. Evaluating microbial and chemical hazards in commercial struvite recovered from wastewater. Environ. Sci. Technol. 53 (9), 5378–5386.

Zhang, L., Mou, A., Guo, B., Sun, H., Anwar, M.N., Liu, Y., 2021. Simultaneous phosphorus recovery in energy generation reactor (SPRING): high rate thermophilic blackwater treatment. Resour. Conserv. Recycl. 164, 105163.

CHAPTER 5 THE ROLE OF EFFLUENT RECIRCULATION APPLIED TO UPFLOW ANAEROBIC SLUDGE BLANKET REACTORS IN BIOMETHANE RECOVERY FROM BLACKWATER

A version of this chapter has been published in the *Journal of Environmental Chemical Engineering*.

5.1 Synopsis

Sustainable waste management can be achieved using anaerobic digestion (AD). In addition to the advantages such as low sludge yield, low energy input, and high treatment capacity, AD processes provide the possibility for energy and resource recovery from wastes (Maleki et al., 2018; Gao et al., 2019a; Cunha et al., 2020; Zhang et al., 2021). Biogas produced from AD processes is a source of renewable energy, which helps increase energy security, reduce the reliance on non-renewable energy, and reduce greenhouse gas emission from non-renewable energy utilization (Kuo and Dow, 2017; Obileke et al., 2021).

In anaerobic digesters such as continuous stirred-tank reactors (CSTR) and moving bed biofilm reactors (MBBR), mechanical mixing is widely introduced to facilitate substrate mixing in the digesters (Ma et al., 2019; Singh et al., 2020; Swain et al., 2022). Effluent recirculation applied to an upflow anaerobic sludge blanket (UASB) reactor is also commonly used to improve both mixing and upflow velocity of the reactor (Buzzini and Pires, 2007; López-López et al., 2015; Zamanzadeh et al., 2016; Lukitawesa et al., 2018; Zhang et al., 2020). However, it is difficult to make a general statement about whether effluent recirculation should be applied to a UASB reactor operated under a specific scenario.

Chapter 5 aims to assess the impact of effluent recirculation on biomethane production of an UASB reactor treating substrates of different solid contents, providing scientific basis on the selection of operational conditions for an AD process. Two 2.0 L UASB reactors were operated for 219 d under a mesophilic condition. A type of synthetic blackwater, dog food wastewater, was used as the feeds. The high-solid content feed consisted the original dog food which was ground followed by sieving before use. The low-solid content feed was prepared by autoclaving the high-

solid content feed at 121.1 ºC at 30.2 psi for 90 min in a vacuum/gravity steam sterilizer to allow for its prehydrolysis. Reactor performance, in terms of effluent pH value, effluent chemical oxygen demand (COD) concentration, and methane production, was monitored every 2–3 d. The hydrolysis efficiency of the substrate was calculated, and the layered microbial communities in the sludge beds of both reactors were analyzed.

5.2 Experiments and Analysis

5.2.1 Experimental setup and reactor operation

Two UASB reactors with 2.0 L working volume, R1 and R2, were operated for 219 d under mesophilic conditions (35 ± 2 °C) controlled by water baths. The reactors were made of polymethyl methacrylate (PMMA) and had dimensions of 36.5 cm × 8 cm (height × diameter). Three peristaltic pumps (BT100–2J, Longer, China) were used to feed the two reactors and recirculate effluent in one reactor, respectively. A schematic of the two reactors can be found in the supplementary material (**Fig. 5–1**).

The operation was divided into four phases: Phase I, 42 d (Day 0–Day 42), Phase II, 81 d (Day 42–Day 123), Phase III, 51 d (Day 123–Day 174), and Phase IV, 45 d (Day 174–Day 219). **Table 5–1** shows the operation differences among the four phases. In Phases I and II, a high-solid content substrate (HS) was used as the substrate, and effluent recirculation was applied only to R2, where the upflow velocity was maintained at 10 cm/h. Phase I was the start-up period when the performances of both reactors were not stable; Phase I results were not considered in the analysis. To validate the observations in Phase II, effluent recirculation was switched between R1 and R2 in Phase III, with recirculation only applied to R1, where the upflow velocity was maintained at

10 cm/h. To further demonstrate the impact of solid contents, a low-solid content substrate (LS) was used as the substrate in both R1 and R2 in Phase IV.

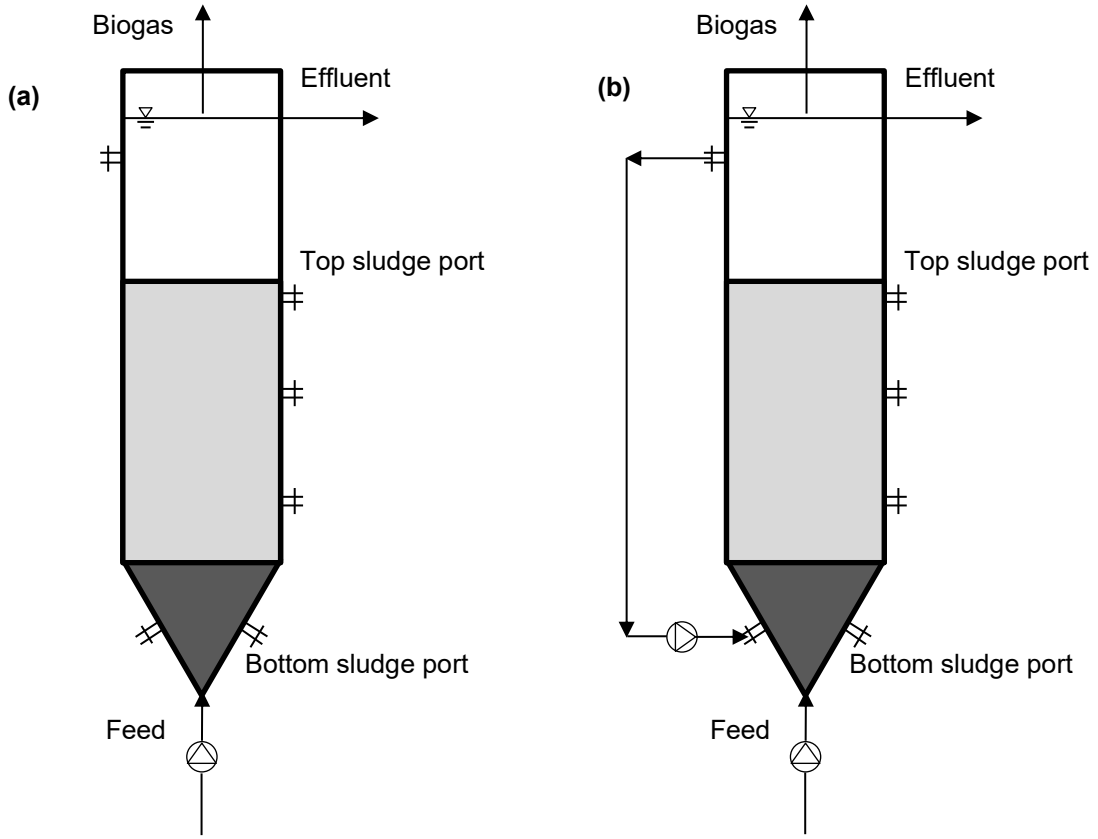

Figure 5-1. Configurations of UASB reactors: (a) reactor without effluent recirculation and (b) reactor with effluent recirculation.

The HS consisted ground dog food (Salmon and Sweet Potato Dog Food, Kirkland Signature, USA) (11.5 g/L), urea (0.23 g/L), KH_2PO_4 (0.11 g/L), K_2HPO_4 (0.17 g/L), Na_2CO_3 (0.5 g/L), and tap water. The original dog food was ground for 1 min by an electric grinder (2500 W, 50 Hz), followed by sieving before use (**Fig. 5–2**). The LS was prepared by autoclaving the HS at 121.1 ºC at 30.2 psi for 90 min in a vacuum/gravity steam sterilizer (Model 733LS, Getinge, US) to allow for its prehydrolysis.

R1 and R2 were seeded with 1.5 L digested sludge collected from a stably operated anaerobic digester with volatile suspended solid (VSS) concentration of 13.5 g/L. Reactor feeds were mixed using magnetic stirrers before they were added to the reactors, and reactor feeds were replenished every 2 d. Based on previous studies treating similar high-solid content feeds (Dębowski et al., 2013; Gao et al., 2019b; Zhang et al., 2020), a representative organic loading rate (OLR) was selected to be 1.9 g COD/L/d. The hydraulic retention time (HRT) was 8.0 d for both reactors. Waste sludge was collected from the top sampling port (**Fig. 5–1**) to maintain the volume of sludge in the reactor less than 1.4 L. The volume and COD concentration of waste sludge were tested before discharge.

Table 5-1. Reactor operation in four phases.

Reactors at different phases		Effluent recirculation	Without effluent recirculation	HS	LS
Phase I	R1		✓	✓	
	R2	✓		✓	
Phase II	R1		✓	✓	
	R2	✓		✓	
Phase III	R1	✓		✓	
	R2		✓	✓	
Phase IV	R1	✓			✓
	R2		✓		✓

Figure 5-2. (a) Synthetic blackwater (original) and (b) Synthetic blackwater (ground).

Reactor performance, in terms of effluent pH value, effluent chemical oxygen demand (COD) concentration, and methane production, was monitored every 2–3 d. During Phase II, the hydrolysis efficiencies of the HS in R1 and R2 were calculated, and at the end of Phase II, the layered microbial communities in the sludge beds of both reactors were analyzed.

5.2.2 Chemical analysis

Feed and effluent pH values were measured with a pH meter (SympHony B40PCID, VWR, Radnor, US). Feed and effluent COD concentrations and sludge VSS concentrations were tested following Standard Methods (Rice et al., 2017). Concentrations of VFAs (acetate, propionate, butyrate) in the sludge were measured using ionic chromatography (IC) equipped with a conductivity detector (DIONEX ICS-2100, ThermoFisher, US). All the chemical tests were conducted in triplicate, and averages with standard deviations were presented. The biogas generated was collected in a 10 L foil sampling bag (Chromatographic Specialties Inc., Brockville, Canada), and its volume was measured with a syringe every 2–3 d. The biogas composition was identified with a gas chromatograph (7890B, Agilent Technologies, Santa Clara, US). The

methanisation rate shown in Eq. (5–1) was calculated by dividing the produced methane measured in the reactor by the theoretical methane that can be produced from the feed (Gao et al., 2019a).

$$r = \frac{V_{CH4,measured}}{V_{CH4,theoretical}} \times 100\% \quad (5–1)$$

where r is the methanisation rate, $V_{CH4,\ measured}$ is the measured CH_4 yield (in mL/d), and $V_{CH4,\ theoretical}$ is the theoretical methane that can be produced from the feed (in mL/d). In this study, the theoretical methane was 395 mL/g feed COD, calculated with the standard equation of state.

Theoretically, the influent COD has three fates. First, it can be converted to methane. Second, it is discharged in effluent. Third, it accumulates in discharged waste sludge and reactor sludge bed. The mass balance for influent COD is shown in Eq. (5–2) (Zhang et al., 2021). The theoretical COD mass balance was determined in Phase II.

$$COD_{inf} Q\Delta t = \sum_{i=1}^{i=\Delta t} COD_{methane} V_i + COD_{eff} Q\Delta t + COD_{dis} V_{dis} + \left(COD_{slu,\Delta t} V_{\Delta t} - COD_{slu,0} V_0\right) \quad (5–2)$$

where Δt is the duration of COD mass balance test in d. COD_{inf}, COD_{eff}, and COD_{dis} are the CODs of influent, effluent, and discharged sludge in g/L. $COD_{slu,0}$ is the COD of sludge in the reactor sludge bed at t=0, and $COD_{slu,\Delta t}$ is the COD of sludge in the reactor sludge bed at $t = \Delta t$. $COD_{methane}$ is the COD of methane in g/L. Q is the volumetric flow rate in L/d. V_i is the methane volume in L at t=i. V_{dis} is the volume of discharged waste sludge in L. $V_{\Delta t}$ and V_0 are the volumes of sludge in the reactor in L at $t = \Delta t$ and t=0, respectively.

5.2.3 Biomethane potential (BMP) test for high solid-content substate and low-solid content substrate (Gao et al., 2019a)

The BMP is an important index to evaluate the ultimate biomethane potential for the feed, which is expressed as the ratio of the produced methane COD and the feed COD (g CH_4 COD/g feed COD). The BMPs for the HS and the LS were evaluated. The BMP tests were conducted in 120 mL serum bottles being stored in a shaker incubator (120 rpm) (New Brunswick™ Innova® 44, Eppendorf, Canada) under a dark condition. The temperature of the incubator was 35 °C. All tests were conducted in triplicate. Each serum bottle was added in 10 mL inoculum and 10 mL feed, followed by being flushed with nitrogen gas. After being sealed with a butyl rubber stopper and an aluminum cap, the serum bottle was stored in the shaker incubator. Produced methane was monitored through measuring the bottle headspace pressure with a pressure gauge (GMH 3100, Greisinger, Germany) and the gas composition with a gas chromatography (7890B, Agilent Technologies, Santa Clara, US). The tests were terminated when daily methane production during three consecutive days was less than 1% of the accumulated volume of methane.

5.2.4 Specific methanogenic activity (SMA) test for sludge samples

At the end of Phase II, sludge samples were collected from the top and bottom sampling ports of R1 and R2 (**Fig. 5–1**). The SMA and the sludge stability for the samples were tested.

The SMA determines the sludge capability to produce methane from a specific substrate when the substrate availability is not limited (Hussain and Dubey, 2014). SMA is expressed as the maximum ratio of the daily produced methane COD and the sludge VS (g CH_4 COD/g sludge VS/d). In this study, the sludge samples collected from the top and bottom sludge beds of both reactors at the end of Phase II and the specific substrates H_2/CO_2 and acetate were used in the SMA

assays. The SMA tests were conducted in 120 mL serum bottles being stored in a shaker incubator (120 rpm) under a dark condition. The temperature of the incubator was 35°C. All tests were conducted in triplicate. Prior to the SMA tests, the accumulated COD in the sludge samples were consumed, and then the VS concentrations of the sludge samples were measured. For each serum bottle, 4 mL sludge sample was added and then diluted by 16 mL deionized water. The pH of the mixed sludge and substrate was adjusted to 7.5. When H_2/CO_2 was used as the substrate, a ratio of 80%/20% of H_2/CO_2 content was applied to flush the headspace of the bottles. When acetate was applied, its initial COD concentration in the bottles was 1 g/L, and the bottles were flushed with nitrogen gas. Produced methane was monitored as described in the BMP tests. The SMA test was stopped when the maximum daily produced methane was obtained.

5.2.5 Sludge stability test for sludge samples

The sludge stability determines the amount of biodegradable substrate presented in the sludge, and it is expressed as g CH_4 COD/g sludge COD (Gao et al., 2019b). The sludge stability test was conducted using the sludge samples collected from the top and bottom sludge beds of both reactors at the end of Phase II. The set-up procedure for the sludge stability test was the same as that for the BMP test, except that each 120 mL serum bottle was added in 10 mL sludge sample to be determined. Produced methane was monitored until no more methane production can be detected.

5.2.6 Calculation of particulate COD hydrolysis efficiency in the reactor

The particulate COD hydrolysis efficiency evaluates the percentage of the feed particulate COD that is hydrolyzed, which can be determined using Eq. (5–3) (Gao et al., 2020). The particulate COD hydrolysis efficiency during Phase II was determined in triplicate.

$$\eta = \frac{COD_{CH4} + sCOD_{eff} - sCOD_{inf}}{tCOD_{inf} - sCOD_{inf}} \times 100\% \quad (5\text{–}3)$$

where η is the hydrolysis efficiency, $tCOD_{inf}$, $sCOD_{inf}$, $sCOD_{eff}$, and COD_{CH4} are the total COD in the reactor feed, the soluble COD in the reactor feed, the soluble COD in the effluent, and the COD converted from the produced methane (in g/d), respectively.

5.2.7 Microbial community analysis

The microbial community in the sludge samples collected at the end of Phase II were identified by DNA extraction followed by 16S rRNA sequencing. A 2 mL sludge sample was centrifuged at 4000 *g* for 10 min, and the supernatant was discarded. Genomic DNA was extracted from the retained sludge with a DNeasy Power-Soil Kit (QIAGEN, Hilden, Germany), and its concentration was measured with NanoDrop One (ThermoFisher, Waltham, USA). 16S rRNA genes were amplified with the universal primer pair 515F (GTGCCAGCMGCCGCGG) and 806R (GGACTACHVGGGTWTCTAAT). Pooled PCR products were sequenced on an Illumina MiSeq platform. Sequence analyses were performed following the DADA2 algorithm (Callahan et al., 2016) in the Qiime2 workflow (Caporaso et al., 2010). Operational taxonomic units (OTUs) were clustered with 99% similarity with respect to the Greengenes database, version 13_8 (McDonald et al., 2012; Werner et al., 2012). Heatmaps were generated using the "pheatmap" package, version 1.0.12 (Kolde, 2019) in RStudio, version 3.6.3 (R Core Team, 2020). The predicted metagenome and functional genes were determined using the Phylogenetic Investigation of Communities by Reconstruction of Unobserved States (PICRUSt) (Langille et al., 2013).

5.2.8 Statistical analysis

Student's t-test was performed to determine the p-value. A p-value less than 0.05 indicates statistical difference between two groups of data.

5.3 Results and Discussion

5.3.1 UASB reactor performance in Phase II

Fig. 5–3 shows the reactor performance in terms of effluent pH, effluent COD concentration, and methanisation rate during Phase I to Phase IV. During Phase II to Phase IV, compared with the feed pH value (7.75 ± 0.14), the effluent pH values for both reactors slightly increased (7.81 ± 0.23) and did not present significant difference (p value = 0.79 > 0.05) [**Fig. 5–3**(a)]. The stable effluent pH indicated that VFAs did not accumulate in either reactor.

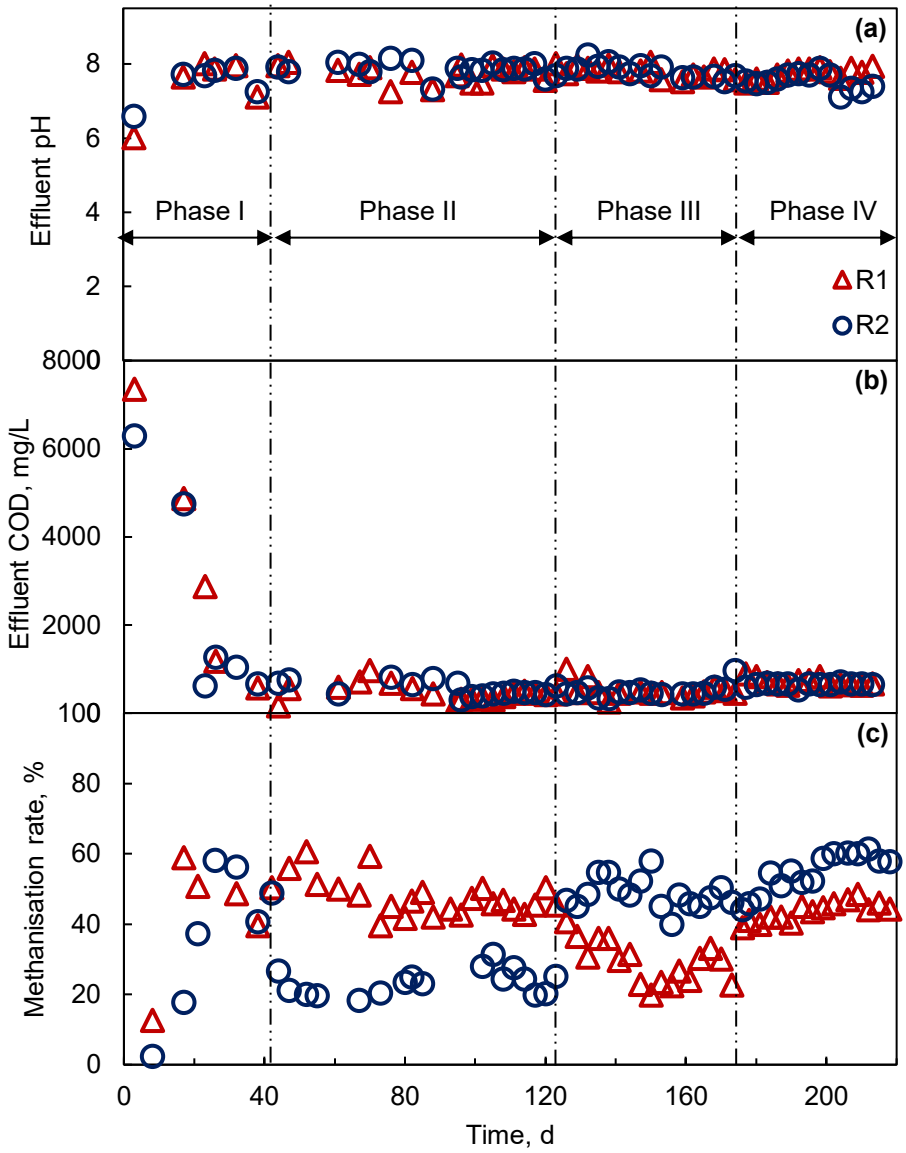

Figure 5-3. Performances of the two UASB reactors (R1 and R2): (a) effluent pH, (b) effluent COD concentration, and (c) methanisation rate. The red triangles represent the performance data for R1 without effluent recirculation in Phases I and II and with effluent recirculation in Phases III and IV. The blue circles represent the performance data for R2 with effluent recirculation in Phases I and II and without effluent recirculation in Phases III and IV. High-solid content substrate (HS) was used in Phases I, II, and III, and low-solid content substrate (LS) was used in Phase IV.

In Phase II, R1 was operated without effluent recirculation, and R2 was operated with effluent recirculation. The purpose of Phase II was to examine the role of effluent recirculation on

microbial community development and biogas production. **Fig. 5–3**(b) shows that both reactors achieved a COD removal higher than 90% (p value = 0.38 > 0.05). Although the effluent COD concentrations were low, the "removed" COD was not all converted to biomethane. **Fig. 5–4**(a) shows the feed COD conversion in both reactors. Theoretically, the feed COD has three fates. First, it can be converted to biomethane. Second, it is discharged in effluent. Third, it accumulates in discharged waste sludge and reactor sludge bed. These three fates account 100% feed COD. Practically, the feed COD and that detected in the three fates are unbalanced due to occasional sludge washout, unknown metabolism, analytical errors, etc. Therefore, an unknown conversion is usually introduced to compensate the unbalance between feed COD and its conversion. In Phase II, in the absence of effluent recirculation (R1), 50% of the feed COD was converted to methane, 16% of the feed COD accumulated in the reactor sludge, 10% of the feed COD was discharged with waste sludge, and 5% of the feed COD was discharged in the effluent. With effluent recirculation (R2), 26% of the feed COD was converted to methane, 27% of the feed COD accumulated in the reactor sludge, 19% of the feed COD was in the waste sludge, and 7% of the feed COD was in the effluent. A small fraction of the feed COD was used for biomass growth (reflected by the accumulated COD in the sludge bed); however, large amount of the feed COD accumulating in the reactor sludge and the waste sludge was caused by the particulate COD that cannot be hydrolyzed. It can be observed that, in comparison to R1, with effluent recirculation (R2), larger amount of COD accumulated in the reactor sludge, which coincided with the higher sludge stability indices of the sludge at both top and bottom of R2 [**Fig. 5–4**(b)]. As demonstrated previously, a higher sludge stability index represents a higher fraction of biodegradable substrate present in the sludge and a lower hydrolysis efficiency of particulate COD in the reactor (Gao et al., 2020).

To further assess the substrate hydrolysis efficiency in the reactors, the hydrolysis efficiencies of the HS in both R1 and R2 in Phase II were calculated with Eq. (5–3) and are shown graphically in **Fig. 5–5**(a). The hydrolysis efficiency reached 45.5% in R1 (without effluent recirculation), whereas the hydrolysis efficiency reached only 22.0% in R2 (with effluent recirculation). The lower hydrolysis efficiency in R2 was accompanied by the lower concentrations of VFAs (acetate, propionate, and butyrate) in the R2 sludge bed [**Fig. 5–5**(b)]. Hydrolysis is often the rate-limiting step in AD for substrates with high solid content (Jolis, 2008; Guo et al., 2021). The results showed that hydrolysis deteriorated in the presence of effluent recirculation in the UASB reactor, and insufficient VFAs could have led to a low methane yield. The average methanisation rate in R1 without effluent recirculation was 47.9%, whereas the average methanisation rate in R2 with effluent recirculation was as low as 25.5% [**Fig. 5–3**(c)].

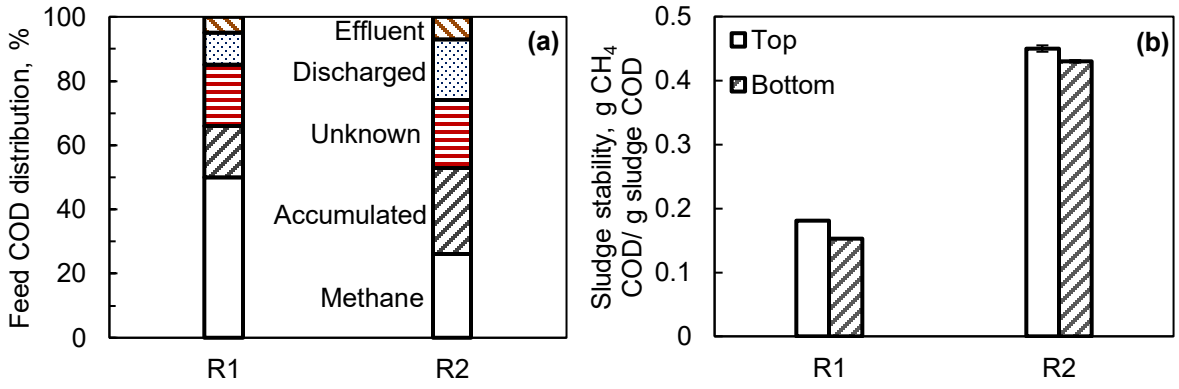

Figure 5-4. (a) Feed COD mass balance and (b) sludge stability in R1 (without effluent recirculation) and R2 (with effluent recirculation) in Phase II.

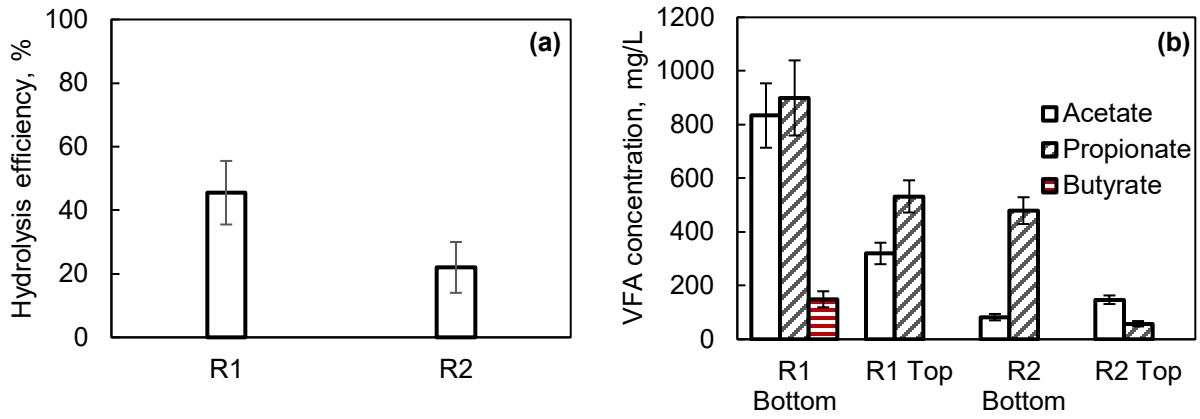

Figure 5-5. (a) Hydrolysis efficiency and (b) concentrations of VFAs in terms of acetate, propionate, and butyrate for in R1 (without effluent recirculation) and R2 (with effluent recirculation) in Phase II.

5.3.2 UASB reactor performance in Phase III and Phase IV

To validate the impact of effluent recirculation on UASB reactor performance, in particular, methane production, effluent recirculation was switched between R1 and R2 (applied to R1 and discontinued in R2) in Phase III. After the effluent recirculation was terminated in R2, the methane production rose immediately (within 2 d) from 25.5% to 47.9%. Conversely, after the effluent recirculation was imposed on R1, the methane generation dropped gradually from 47.9% to 25.5%. The fact that effluent recirculation was unfavorable to methane production was also reported in a recent study that treated blackwater using a thermophilic UASB reactor (Zhang et al., 2020).

To further demonstrate whether the lower methane production of the reactor with effluent recirculation was related to inefficient hydrolysis of the substrate, reactor feed was switched to the LS ($sCOD_{inf}/tCOD_{inf}$ ratio = 35.2%) in R1 and R2 in Phase IV, as compared to the HS ($sCOD_{inf}/tCOD_{inf}$ ratio = 13.5%) used in Phases I–III. It should be noted that both types of substrates had the same BMP value (1.51 ± 0.24 g CH_4 COD/g VSS) and total COD concentration,

hence only soluble COD concentration of the LS was increased. The use of LS with a higher soluble COD concentration increased the methanisation rate from 47.9% to 54.5% (a 6.6% increase) in the reactor without effluent recirculation, but it increased the methanisation rate from 25.5% to 43.5% (a 18.0% increase) in the reactor with effluent recirculation. The results indicated that the adverse impact of effluent recirculation on methane production was less significant for a low-solid content substrate. Hence, once the hydrolysis inhibition was mitigated, the methane production rose, even in the presence of effluent recirculation.

5.3.3 Microbial community analysis

Figs. 5–6(a) and **(b)** show the archaeal and bacterial community richness indicated by the number of archaeal genera and bacterial genera, respectively, in the top and bottom sludge beds of R1 and R2 at the end of Phase II. Bacterial community richness was similar in the bottom sludge beds of R1 and R2. In comparison, bacterial community in the top sludge bed of R2 was also rich but had significantly reduced richness in R1, which may be explained by the effluent recirculation that increased mixing. Archaeal genera dominated in the top sludge beds of both reactors. It was noted that archaeal community richness was significantly higher in R1 without effluent recirculation than in R2 with effluent recirculation. **Figs. 5–6(a)** and **(b)** illustrate higher archaeal and bacterial segregation, especially archaeal segregation, along the sludge bed of R1 in the absence of effluent recirculation.

Figs. 5–6(c) and **(d)** the relative abundances of archaeal and bacterial genera in the top and bottom sludge beds of R1 and R2 at the end of Phase II. Since archaeal species mainly grew in the top sludge bed of both reactors, archaeal species in the bottom sludge bed were not considered herein. In both reactors, the genera *Methanosaeta* (56.72% in R1 and 46.52% in R2),

Methanospirillaceae (16.30% in R1 and 20.46% in R2), *Methanobacterium* (5.74% in R1 and 8.57% in R2), and an undefined species in the family *WSA2* (11.62% in R1 and 15.00% in R2), were the major archaeal species in the top sludge bed. As compared to R2, both acetoclastic and hydrogenotrophic methanogenesis were more active (**Figs. 5–7**) in the top sludge bed of R1, the reactor without effluent recirculation.

In the bottom sludge bed of R1, *Prevotella* (75.36%), *Veillonella* (6.97%), *Lactococcus* (3.32%), and *Anaerovibrio* (2.46%) comprised 88.11% of the total bacteria. *Prevotella* was reported to play a particularly important role in the metabolism of proteins and peptides (Flint and Stewart, 1999). *Veillonella* can use lactate, pyruvate, and succinate to release acetate, propionate, and CO_2 (Xu et al., 2011). *Lactococcus* is a homofermenter that ferments sugars, producing lactic acid (Bartkiene et al., 2020). *Anaerovibrio* ferments glycerol to generate propionate, cell matter, and H_2 (Schauder and Schink, 1989). In the top sludge bed of R1, *Prevotella* accounted for only 3.65%, and diverse species were identified (Shannon's diversity index was 1.44 for bacteria in the bottom sludge bed of R1 and 3.66 for bacteria in the top sludge bed of R1). *T78*, an undefined genus in the order *RB046*, an undefined genus in the order *Bacteroidales,* and an undefined genus in the family *Thermovirgaceae* had relative abundances of 16.79%, 10.22%, 5.49%, and 5.15%, respectively, in the top sludge bed of R1.

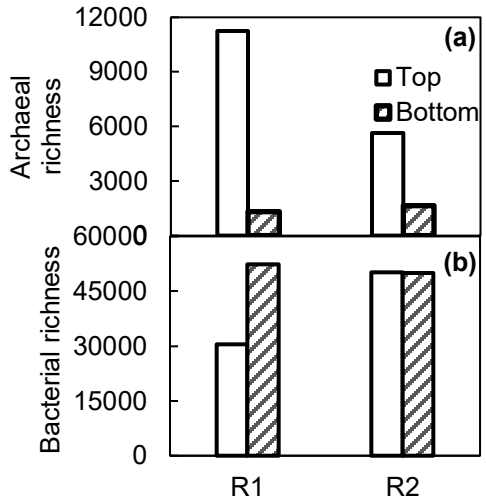

Relative abundances of archaeal genera, %

(c)

56.72	16.30	5.74	4.28	0.67	11.62	3.22	1.26	R1 Top
44.60	19.50	12.80	7.16	5.57	4.85	4.17	0.45	R1 Bottom
46.52	20.46	8.57	4.19	1.15	15.00	1.61	1.45	R2 Top
42.27	11.92	10.30	5.93	1.89	24.66	1.89	1.07	R2 Bottom
Methanosaeta	f_Methanospirillaceae	Methanobacterium	Methanosarcina	Methanobrevibacter	f_WSA2	Methanolinea	Methanomassiliicoccus	

Relative abundances of bacterial genera, %

(d)

3.65	0.41	0.16	1.12	1.67	5.15	2.02	16.79	10.22	5.49	0.01	1.73	3.13	3.58	1.90	1.40	2.06	3.06	4.56	2.13	R1 Top
75.38	6.97	3.32	2.46	0.47	0.41	0.41	0.36	0.33	0.32	0.28	0.25	0.25	0.24	0.19	0.15	0.15	0.08	0.06	0.06	R1 Bottom
16.73	4.04	0.48	7.70	2.51	2.44	2.70	4.99	4.24	2.76	0.41	0.73	2.38	11.82	0.65	2.48	1.33	0.52	1.05	1.17	R2 Top
53.47	3.86	1.03	7.88	0.75	0.64	1.37	1.45	1.66	1.45	2.29	0.23	0.81	6.07	0.36	0.97	0.58	0.24	0.52	0.29	R2 Bottom
Prevotella	Veillonella	Lactococcus	Anaerovibrio	o_Clostridiales	f_Thermovirgaceae	vadinCA02	T78	o_RB046	o_Bacteroidales	f_Enterobacteriaceae	Pelotomaculum	Syntrophomonas	HA73	o_SHA-98	p_OP8	f_Dethiosulfovibrionaceae	f_Sediment-4	Blvii28	f_Syntrophorhabdaceae	

Figure 5-6. Microbial community analysis for two UASB reactors, R1 (without effluent recirculation) and R2 (with effluent recirculation), at the end of Phase II: (a) the richness of archaeal genera, (b) the richness of bacterial genera, (c) the relative abundances of archaeal genera, and (d) the most abundant bacterial genera (relative abundance > 1%). Undefined genera were named using higher taxonomic levels such as family (f_) and order (o_). "Top" means top sludge bed of one reactor, and "bottom" means bottom sludge bed of one reactor.

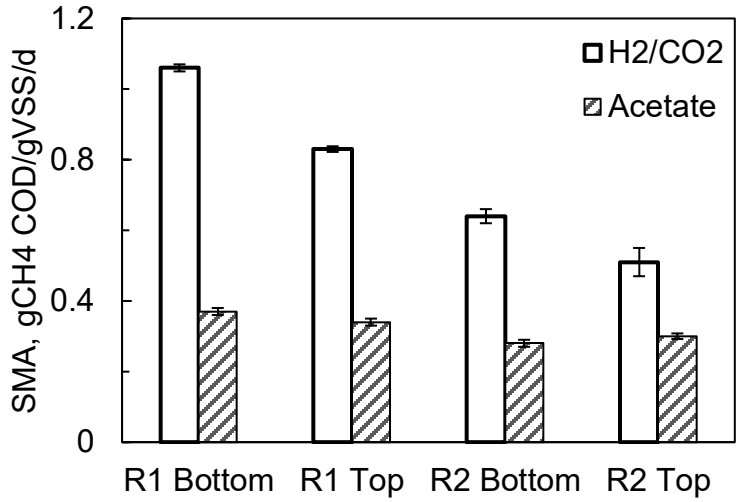

Figure 5-7. SMA tests of sludge collected from R1 (without effluent recirculation) and R2 (with effluent recirculation) at the end of Phase II. "Bottom" means sludge sampled from the bottom sludge bed of one reactor, and "top" means sludge sampled from the top sludge bed of one reactor.

In the bottom sludge bed of R2, ten dominant genera (relative abundances greater than 1%) were identified. Four genera were the same as that detected in the bottom sludge bed of R1, and six other genera included *HA73* (6.07%), an undefined species in the family *Enterobacteriaceae* (2.29%), two undefined species in the orders *RB046* (1.66%) and *Bacteroidales* (1.45%), *T78* (1.45%), and *vadinCA02* (1.37%). *HA73* is an uncultured bacterial genus belonging to the *Synergistetes* phylum. *HA73* oxidizes acetate syntrophically, followed by hydrogenotrophic methanogenesis (Ito et al., 2011; Sitthi et al., 2020). In the top sludge bed of R2, *Prevotella* was present at 16.73%. Almost all other genera were more abundant in the top sludge bed of R2 than in the bottom sludge bed of R2 (Shannon's diversity index was 2.46 for bacteria in the bottom sludge bed of R2 and 3.77 for bacteria in the top sludge bed of R2).

It was noticed that effluent recirculation increased sludge mixing, hence reduced the community segregation as observed in R1, where bacteria dominated bottom sludge and archaea dominated top sludge. Enhanced biomass transport due to the turbulence caused by effluent recirculation may have reduced the contact time between sludge particles and microorganisms, limiting the hydrolase accessibility to substrates and microorganisms and inhibiting the hydrolysis of particulate organic matter.

Two models have been proposed previously to describe the hydrolysis of organic materials: (1) microorganisms secrete enzymes in the bulk liquid, and these enzymes are adsorbed onto organic particles or react with soluble substrates, and (2) microorganisms attach to organic particles, produce enzymes in the vicinity of these particles, then utilize soluble products released by enzymatic reactions (Batstone et al., 2002; Vavilin et al., 2008). Both models require the attachment of microorganisms and/or enzymes to particles. In the reactor with effluent recirculation, turbulent transport would decrease the contact time of microorganisms and/or

enzymes and particles, making sludge adsorption sites less accessible to microorganisms and/or enzymes. Considerations of particle surface area and transport phenomena would provide a deeper understanding of hydrolysis kinetics.

The metagenome and functional genes were predicted based on the 16S rRNA gene amplicon data for the communities in R1 and R2 at the end of Phase II. It was observed that functional gene groups differed in the presence (R2) and absence (R1) of effluent recirculation (**Fig. 5–8**). Higher metabolism was apparent in almost all substrates in the absence of effluent recirculation (R1); carbohydrate, amino acid, lipid, and xenobiotic metabolism was higher in the top sludge bed of both reactors, whereas vitamins, nucleotides, terpenoids, polyketides, and enzyme metabolism were more prevalent in the bottom sludge bed of both reactors. The absence of effluent recirculation led to more efficient genetic information, including replication and repair, translation, folding, sorting, and degradation in the bottom sludge bed of R1, possibly due to greater VFA concentrations (Yu et al., 2020), whereas effluent recirculation contributed to more active cellular signaling and cell motility in R2.

5.4 Implication

Effluent recirculation strategy creates substrate-dilution and enhanced heat and mass transfer conditions in anaerobic digesters; however, whether effluent recirculation can be employed in a wastewater engineering process relies on various conditions. In this lab-scale study, when a mesophilic UASB reactor treated high-solid content and high-strength wastewater, effluent recirculation adversely affected the biomethane yield through inhibiting the particulate COD hydrolysis. In one previous study where a thermophilic UASB reactor treated high-strength

blackwater, effluent recirculation also reduced biomethane production (Zhang et al., 2020). We may deduce that, under a mesophilic or thermophilic condition, the mixing in the sludge bed of a UASB reactor due to the upflow velocity and the biogas generation is sufficient for the substrate diffusion. Nevertheless, the impact of effluent recirculation on performance of an up-scaling UASB reactor deserves further investigation.

5.5 Conclusions

This study assessed the impact of effluent recirculation applied to a UASB reactor on the hydrolysis of blackwater with high and low solid contents. Effluent recirculation adversely impacted the methane production of the reactor treating a high-solid content substrate due to the inefficient hydrolysis of particulate organic matter. This adverse impact of effluent recirculation became less significant for a low-solid content substrate, likely because the hydrolysis inhibition was mitigated. Effluent recirculation increased the sludge mixing and thus reduced the microbial community segregation in the reactor. Effluent recirculation could limit accessibility of particle adsorption sites, through which inhibited the hydrolysis of particulate organic matter. However, hydrolysis kinetics deserve further research with regard to particle surface and particle transport phenomena. Chapter 5 completed Objective 2.1.

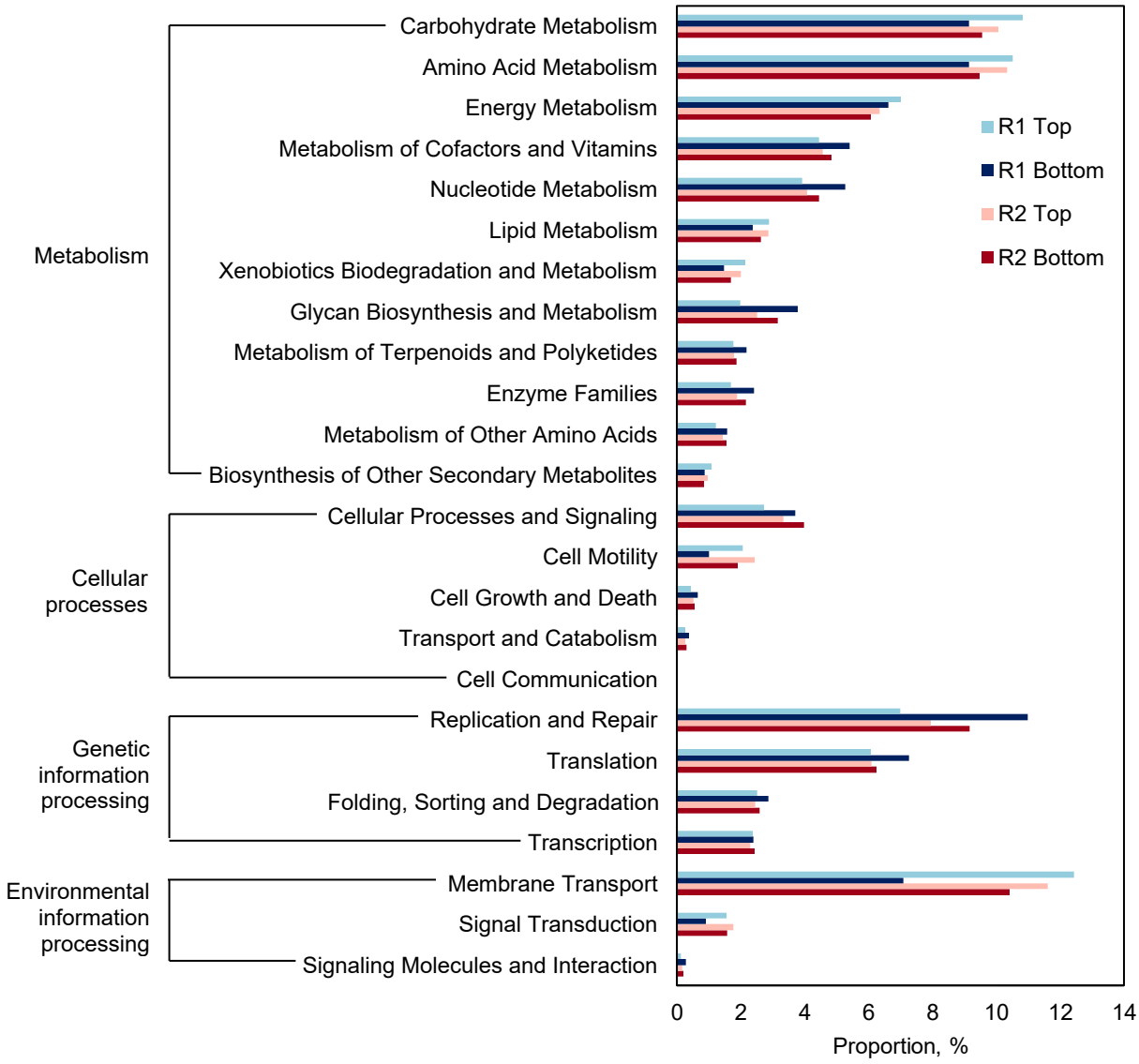

Figure 5-8. Predicted metagenome functions based on the microbial community identified in R1 (without effluent recirculation) and R2 (with effluent recirculation) at the end of Phase II. "Top" means top sludge bed of one reactor, and "bottom" means bottom sludge bed of one reactor.

References

Bartkiene, E., Lele, V., Ruzauskas, M., Domig, K.J., Starkute, V., Zavistanaviciute, P., Bartkevics, V., Pugajeva, I., Klupsaite, D., Juodeikiene, G., Mickiene, R., Rocha, J.M., 2020. Lactic acid bacteria isolation from spontaneous sourdough and their characterization including antimicrobial and antifungal properties evaluation. Microorganisms 8, 64.

Batstone, D.J., Keller, J., Angelidaki, R.I., Kalyuzhnyi, S.V., Pavlostathis, S.G., Rozzi, A., Sanders, W.T.M., Siegrist, H., Vavilin, V.A., 2002. The Anerobic Digestion Model No 1(ADM1). Water Sci. Technol. 45 (10), 65-73.

Buzzini, A.P., Pires, E.C., 2007. Evaluation of a upflow anaerobic sludge blanket reactor with partial recirculation of effluent used to treat wastewaters from pulp and paper plants. Bioresour. Technol. 98, 1838–1848.

Callahan, B.J., McMurdie, P.J., Rosen, M.J., Han, A.W., Johnson, A.M.A., Holmes, S.P., 2016. DADA2: high resolution sample inference from Illumina amplicon data. Nat. Methods 13 (7), 581–583.

Caporaso, J.G., Kuczynski, J., Stombaugh, J., Bittinger, K., Bushman, F.D., Costello, E.K., Fierer, N., Peña, A.G., Goodrich, J.K., Gordon, J.I., Huttley, G.A., Kelley, S.T., Knights, D., Koenig, J.E., Ley, R.E., Lozupone, C.A., McDonald, D., Muegge, B.D., Pirrung, M., Reeder, J., Sevinsky, J.R., Turnbaugh, P.J., Walters, W.A., Widmann, J., Yatsunenko, T., Zaneveld, J., Knight, R. 2010. QIIME allows analysis of high-throughput community sequencing data. Nat. Methods 7 (5), 335–336.

Cunha, J.R., Schott, C., van der Weijden, R.D., Leal, L.H., Zeeman, G., Buisman, C., 2020. Calcium phosphate granules recovered from black water treatment: a sustainable substitute for mined phosphorus in soil fertilization. Resour. Conserv. Recycl. 158, 104791.

Flint, H.J., Stewart, C.S., 1999. Bacteroides and Prevotella, in Robinson, R.K. (Ed.): Encyclopedia of Food Microbiology, pp. 198–203.

Gao, M., Zhang, L., Florentino, A.P., Liu, Y., 2019a. Performance of anaerobic treatment of blackwater collected from different toilet flushing systems: can we achieve both energy recovery and water conservation? J. Hazard. Mater. 365, 44–52.

Gao, M., Zhang, L., Guo, B., Zhang, Y., Liu, Y., 2019b. Enhancing biomethane recovery from source-diverted blackwater through hydrogenotrophic methanogenesis dominant pathway. Chem. Eng. J. 378, 122258.

Gao, M., Zhang, L., Liu, Y., 2020. High-loading food waste and blackwater anaerobic co-digestion: maximizing bioenergy recovery. Chem. Eng. J. 394, 124911.

Guo, H., Oosterkamp, M.J., Tonin, F., Hendriks, A., Nair, R., van Lier, J.B., de Kreuk, M., 2021. Reconsidering hydrolysis kinetics for anaerobic digestion of waste activated sludge applying cascade reactors with ultra-short residence times. Water Res. 202, 117398.

Hussain, A., Dubey, S.K., 2014. Specific methanogenic activity test for anaerobic treatment of phenolic wastewater. Desalin. Water Treat. 52 (37–39), 7015–7025.

Ito, T., Yoshiguchi, K., Ariesyady, H., Okabe, S., 2011. Identification of a novel acetate-utilizing bacterium belonging to Synergistes group 4 in anaerobic digester sludge. ISME J. 5, 1844-1856.

Jolis, D., 2008. High-solids anaerobic digestion of municipal sludge pretreated by thermal hydrolysis. Water Environ. Res. 80 (7), 654–662.

Kolde, R., 2019. Package 'pheatmap'. https://cran.r-project.org/package=pheatmap.

Kuo, J., Dow, J., 2017. Biogas production from anaerobic digestion of food waste and relevant air quality implications. J. Air Waste Manag. Assoc. 67, 1000–1011.

Langille, M.G., Zaneveld, J., Caporaso, J.G., McDonald, D., Knights, D., Reyes, J.A., Clemente, J.C., Burkepile, D.E., Vega Thurber, R.L., Knight, R., Beiko, R.G., Huttenhower, C., 2013. Predicted functional profiling of microbial communities using 16S rRNA marker gene sequences. Nat. Biotechnol. 31 (9), 814–821.

López-López, A., León-Becerril, E., Rosales-Contreras, M. E., Villegas-García, E., 2015. Influence of alkalinity and VFAs on the performance of an UASB reactor with recirculation for the treatment of Tequila vinasses. Environ. Technol. 36 (19), 2468–2476.

Lukitawesa, Wikandari, R., Millati, R., Taherzadeh, M.J., Niklasson, C., 2018. Effect of effluent recirculation on biogas production using two-stage anaerobic digestion of citrus waste. Molecules 23 (12), 3380.

Ma, S., Ma, H., Hu, H., Ren, H., 2019. Effect of mixing intensity on hydrolysis and acidification of sewage sludge in two-stage anaerobic digestion: characteristics of dissolved organic matter and the key microorganisms. Water Res. 148, 359–367.

Maleki, E., Bokhary, A., Liao, B.Q., 2018. A review of anaerobic digestion bio-kinetics. Rev. Environ. Sci. Biotechnol. 17, 691–705.

McDonald, D., Price, M.N., Goodrich, J., Nawrocki, E.P., DeSantis, T.Z., Probst, A., Andersen, G.L., Knight, R., Hugenholtz, P., 2012. An improved Greengenes taxonomy with explicit ranks for ecological and evolutionary analyses of bacteria and archaea. ISME J. 6 (3), 610–618.

Obileke, K., Nwokolo, N., Makaka, G., Mukumba, P, Onyeaka, H., 2021. Anaerobic digestion: technology for biogas production as a source of renewable energy- a review. Energy Environ. 32 (2), 191–225.

R Core Team, 2020. R: A Language and Environment for Statistical Computing. R Foundation for Statistical Computing, Vienna, Austria.

Rice, E.W., Baird, R.B., Eaton. A.D., 2017. Standard Methods for the Examination of Water and Wastewater, twenty third ed., American Public Health Association (APHA), American Water Works Association, Water Environment Federation (WEF), Washington, DC.

Schauder, R., Schink, B., 1989, *Anaerovibrio glycerini* sp. nov., an anerobic bacterium fermenting glycerol to propionate, cell matter, and hydrogen. Arch. Microbiol. 152, 473–478.

Singh, B., Szamosi, Z., Siménfalvi, Z., 2020. Impact of mixing intensity and duration on biogas production in an anaerobic digester: a review. Crit. Rev. Biotechnol. 40, 508–521.

Sitthi, S., Hatamoto, M., Watari, T., Yamaguchi, T., 2020. Enhancing anaerobic syntrophic propionate degradation using modified polyvinyl alcohol gel beads. Heliyon 6, e05665.

Swain, G., Maurya, K.L., Sonwani, R.K., Singh, R.S., Jaiswal, R.P., Nai, B.N., 2022. Effect of mixing intensity on biodegradation of phenol in a moving bed biofilm reactor: process optimization and external mass transfer study. Bioresour. Technol. 351, 126921.

Vavilin, V.A., Fernandez, B., Palatsi, J., Flotats, X., 2008. Hydrolysis kinetics in anaerobic degradation of particulate organic material: an overview. Waste Manage. 28 (6), 939–951.

Werner, J.J., Koren, O., Hugenholtz, P., DeSantis, T.Z., Walters, W.A., Caporaso, J.G., Angenent, L.T., Knight, R., Ley, R.E., 2012. Impact of training sets on classification of high-throughput bacterial 16s rRNA gene surveys. ISME J. 6 (1), 94–103.

Yu, N., Guo, B., Zhang, Y., Zhang, L., Zhou, Y., Liu, Y., 2020. Different micro-aeration rates facilitate production of different end-products from source-diverted blackwater. Water Res. 177, 115783.

Zamanzadeh, M., Hagen, L.H., Svensson, K., Linjordet, R., Horn, S.J., 2016. Anaerobic digestion of food waste–effect of recirculation and temperature on performance and microbiology. Water Res. 96, 246–254.

Zhang, L., Guo, B., Mou, A., Li, R., Liu, Y., 2020. Blackwater biomethane recovery using a thermophilic upflow anaerobic sludge blanker reactor: impacts of effluent recirculation on reactor performance. J. Environ. Manage. 274, 111157.

Zhang, L., Mou, A., Sun, H., Zhang, Y., Zhou, Y., Liu, Y., 2021. Calcium phosphate granules formation: key to high rate of mesophilic UASB treatment of toilet wastewater. Sci. Total Environ. 773, 144972.

CHAPTER 6 DEVELOPING A NEW NON-STEADY-STATE MASS BALANCE MODEL AND ITS APPLICATION FOR QUANTIFYING MICROBIOME RESPONSES TO DISTURBANCES IN A UASB REACTOR TREATING BLACKWATER

A version of this chapter has been published in the *Journal of Environmental Management*.

6.1 Synopsis

Ecological wastewater treatment processes are subject to various physical, chemical, and biological disturbances, such as operating-condition changes, chemical pollution, and shock flows (Vuono et al., 2015). Disturbances play a significant role in temporal and spatial heterogeneity in the structure and dynamics of an ecological community (Seifan et al., 2012). Faced with sudden disturbances, an ecological community may stabilize, alternatively stabilize, or shift to a new regime (Shade et al., 2012). The adaptation of the ecological community to disturbances (rather than recovery to the original state) determines the stability of wastewater treatment performance.

In the microbial community analysis, scientists usually study how different microorganisms contribute to the function of an ecosystem and compare different communities shaped in different ecosystems (Li et al., 2016). Under disturbances, a microbial community may adapt to a newly built environment or deteriorate. In addition to determining individual microbe's abundance and community richness and diversity, understanding how a microbial community responds to disturbances can help know better the evolution and adaptivity of the community. Omics tools, such as shotgun metagenomic whole-genome sequencing, provide ways to determine the functional output of the target microbiome (Shade et al., 2012). However, comparing the functional output of a community (e.g., relative abundance) before and after disturbances alone cannot fully describe the community dynamics in response to the disturbances, and it cannot distinguish active populations (not prevailing populations identified by relative abundances) from inactive species (Mei and Liu, 2019).

The neutral community model (Sloan et al., 2006; Ofiţery et al., 2010), the mass balance model (Saunders et al., 2016; Mei et al., 2016), and the mass-flow immigration model (Frigon and

Well, 2019; Guo, 2019) have been developed to quantify population dynamics in wastewater treatment communities. The neutral community model is employed to estimate the community-level migration probability, and the mass-flow immigration model is used to assess the immigration rates of specific operational taxonomic units (OTUs). The mass balance model (MBM) is used to calculate the net (or observed) growth rates of individual microbes in bioreactors (e.g., activated sludge and anaerobic digestion systems) (Saunders et al., 2016; Mei et al., 2016; Ali et al., 2019; Cheng et al., 2019). According to this MBM, an individual microbe's net growth rate can be calculated with Eq. (6–1) (Saunders et al., 2016; Mei et al., 2016):

$$\mu_x = \frac{1}{SRT} - \frac{p_{x,inf} VSS_{inf} Q_{inf}}{p_{x,BS} VSS_{BS} V_{BS}}, \quad (6–1)$$

where μ_x is the net growth rate (1/d), SRT is the solid retention time (d), $p_{x,inf}$ and $p_{x,BS}$ are the relative abundances of microbe x in all OTUs for the influent and the bioreactor system (*i.e.*, activated sludge and anaerobic digestion bioreactors), respectively, VSS_{inf} and VSS_{BS} are the volatile suspended solid concentrations in the influent and the bioreactor system, respectively (g/L), Q_{inf} is the daily volume of the influent (L/d), and V_{BS} is the volume (L) of the bioreactor system.

The MBM is a steady-state approach, assuming the microbial cell numbers in the bioreactor are temporally consistent. The net growth rates of microbes calculated with Eq. (6–1) are determined by the SRT and the cell numbers of microbes entering the bioreactor (e.g., immigration). The MBM has been successfully applied to describe the relative importance of microbial immigration in engineered water systems (Mei and Liu, 2019). However, when a bioreactor is subject to disturbances, how to quantify the community responses to the disturbances is still unclear.

Chapter 6 aims to develop a methodology to quantify microbiome responses to disturbances in wastewater bioreactors. Herein the author proposed an ecology model, based on a non-steady-state mass balance (16S rRNA MiSeq reads normalized by volatile suspended solids), to quantify microbiome responses to disturbances in wastewater bioreactors. Rather than focusing on the most abundant microbial groups commonly used in the literature, the goal of the model was to identify active species within the community. The model incorporated the temporal changes of OTUs following a disturbance, through considering the density and type of genotypes in the influent entering the bioreactor, in the effluent leaving the bioreactor, growing in the bioreactor, and in the waste sludge discharged from the bioreactor continuously or instantaneously, as well as the prior microbial community and the sludge characteristics. One application of this model demonstrated that significant differences existed between the key populations responding to an increasing organic loading rate (OLR) and the dominant species in a high-rate thermophilic UASB reactor.

6.2 Non-Steady-State Mass Balance Model Development

In a bioreactor operated under a disturbance, the growth and decay of microbes are assumed to obey the first-order kinetics (Saunders et al., 2016). The mass balance based on the cell numbers of individual microbes in the reactor is expressed by:

$$\frac{dN_{x,BS}}{dt} = \mu_x N_{x,BS} + n_{x,inf} - n_{x,eff} - n_{x,waste}, \quad (6\text{–}2)$$

where $N_{x,BS}$ is the cell number of an individual microbe x in the bioreactor system, t is the test duration (d), $n_{x,inf}$ is the cell number of microbe x in the influent entering the system per day (1/d),

$n_{x,eff}$ is the cell number of microbe x in the effluent exiting the system per day (1/d), and $n_{x,waste}$ is the cell number of microbe x in the sludge discharged from the system per day (1/d).

Eq. (6–2), when divided by $N_{x,BS}$, can be rewritten as:

$$\frac{1}{N_{x,BS}}\frac{dN_{x,BS}}{dt} = \mu_x + \frac{n_{x,inf}}{N_{x,BS}} - \frac{n_{x,eff}}{N_{x,BS}} - \frac{n_{x,waste}}{N_x,BS}. \quad (6–3)$$

The cell concentration is assumed to be proportional to the volatile (or volatile suspended) solid concentration (Mei et al., 2016). Therefore, for microbe x,

$$\frac{n_{x,inf}}{N_{x,BS}} = \frac{p_{x,inf}VSS_{inf}Q_{inf}}{p_{x,BS}VSS_{BS}V_{BS}}. \quad (6–4)$$

Similarly,

$$\frac{n_{x,eff}}{N_{x,BS}} = \frac{p_{x,eff}VSS_{eff}Q_{eff}}{p_{x,BS}VSS_{BS}V_{BS}} = \frac{p_{x,eff}VSS_{eff}Q_{inf}}{p_{x,BS}VSS_{BS}V_{BS}}, \quad (6–5)$$

where $p_{x,eff}$ is the relative abundance of microbe x in all OTUs for the effluent, VSS_{eff} is the volatile suspended solid concentration in the effluent (g/L), Q_{eff} is the daily volume of the effluent (L/d), and for the continuous bioreactor, $Q_{inf} = Q_{eff}$.

If the sludge is discharged continuously from the bioreactor, the term $\frac{n_{x,waste}}{N_{x,BS}}$ can be represented by the solid retention time (SRT) of the bioreactor, where

$$\frac{n_{x,waste}}{N_{x,BS}} = \frac{1}{SRT}. \quad (6–6)$$

When Eqs. (6–4) – (6–6) are substituted into Eq. (6–3), Eq. (6–7) can be obtained.

$$\frac{1}{p_{x,BS}VSS_{BS}V_{BS}}\frac{d(p_{x,BS}VSS_{BS}V_{BS})}{dt} = \mu_x + \frac{p_{x,inf}VSS_{inf}Q_{inf}}{p_{x,BS}VSS_{BS}V_{BS}} - \frac{p_{x,eff}VSS_{eff}Q_{eff}}{p_{x,BS}VSS_{BS}V_{BS}} - \frac{1}{SRT} \quad (6–7)$$

If the sludge is not continuously removed from the bioreactor, the sludge can be discharged at certain sludge-wasting times. During a test duration of t_s, if the sludge is discharged n times, and the volume of the discharged sludge is V_i (i=1, 2 … n), the term $\frac{n_{x,waste}}{N_{x,BS}}$ can be calculated approximately with Eq. (6–8):

$$\frac{n_{x,waste}}{N_{x,BS}} = \frac{\sum_{i=1}^{n} p_{x,i} VSS_i V_i}{t_s \times (p_{x,BS} VSS_{BS} V_{BS})} \approx \frac{\sum_{i=1}^{n} V_i}{t_s V_{BS}}. \quad (6–8)$$

Therefore, in the scenario of instantaneous sludge discharge from the bioreactor, the microbial net growth rate can be calculated with Eq. (6–9):

$$\frac{1}{p_{x,BS} VSS_{BS} V_{BS}} \frac{d(p_{x,BS} VSS_{BS} V_{BS})}{dt} = \mu_x + \frac{p_{x,inf} VSS_{inf} Q_{inf}}{p_{x,BS} VSS_{BS} V_{BS}} - \frac{p_{x,eff} VSS_{eff} Q_{eff}}{p_{x,BS} VSS_{BS} V_{BS}} - \frac{\sum_{i=1}^{n} V_i}{t_s V_{BS}}. \quad (6–9)$$

The differential equations, Eqs. (6–7) and (6–9), can be solved by MATLAB programming to obtain the net growth rate of microbe x. The influences of the microbial community and the sludge characteristics before the disturbance are considered in the initial condition.

6.3 Application of Non-Steady-State Mass Balance Model

6.3.1 Thermophilic UASB reactor operation

The newly developed non-steady-state MBM was applied to quantify the microbiome responses to a disturbance due to an increased OLR in a UASB reactor. A 2 L thermophilic UASB reactor (52 ºC) was fed with high-solid content blackwater collected from the University of Alberta (Edmonton, Canada) campus. The OLRs of the thermophilic UASB reactor were selected based on previous blackwater treatment studies (Gao et al., 2019; Gao et al., 2020). A double OLR of

12.4 g COD/L/d was considered a disturbance (test duration of 22 d) to the current operation of the UASB reactor at an OLR of 5.9 g COD/L/d. The OLR increase was achieved by decreasing the hydraulic retention time (HRT) from 5 d to 2.5 d (**Table 6–1**). More details about the UASB reactor setup, its performances, the chemical analysis methods, and the community analysis method can be found in Zhang et al. (2021). The sensitivity analysis of the non-steady-state MBM is shown in **Fig. 6–1**. The top four parameters, to which the non-steady-state MBM model is most sensitive, include test duration, sludge volume, and VSS of sludge at both previous and current stages.

Table 6-1. VSS concentrations in the influent (inf), effluent (eff), and reactor (AD) before and after the disturbance. The results are presented as mean ± standard deviation.

Disturbance	OLR, g COD/L/d	HRT, d	VSS_{AD}, g/L	VSS_{inf}, g/L	VSS_{eff}, g/L
Before	5.9	5.0	39.8±1.4	11.4±1.6	2.1±0.0
After	12.4	2.5	38.9±0.6	13.0±1.9	1.9±0.1

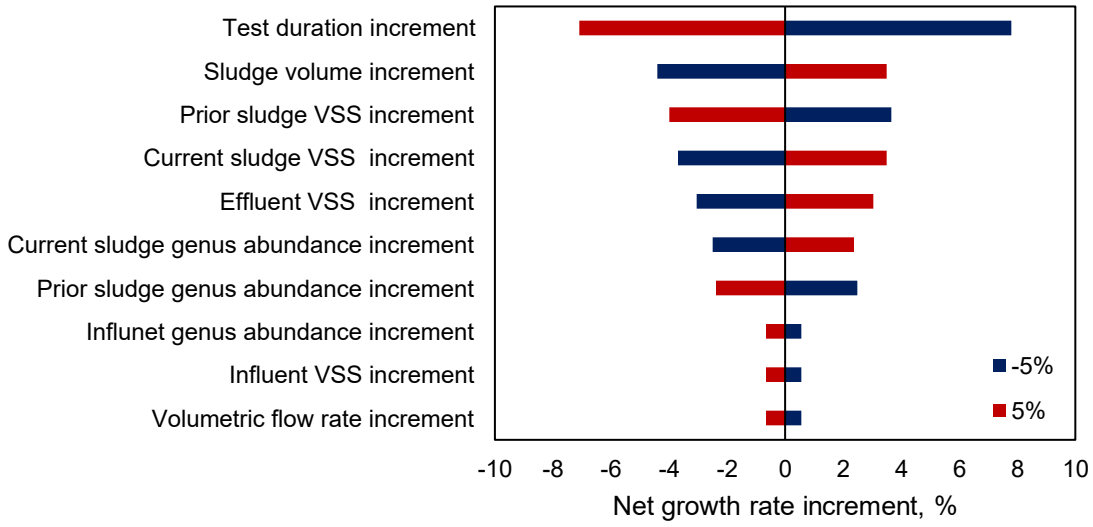

Figure 6-1. Sensitivity analysis of the non-steady-state mass balance model.

6.3.2 Activities of archaeal genera

The relative abundances of the archaeal genera before and after the disturbance are shown in **Fig. 6–2**. The activities of the archaeal genera calculated with the non-steady-state MBM and the steady-state MBM are also shown in **Fig. 6–2**. Based on the 16S rRNA amplicon analysis, the most abundant archaeal community was *Methanothermobacter* (increased from 65.74% to 79.83%) and *Methanosarcina* (decreased from 32.71% to 15.93%) after the disturbance. However, the most active archaeal genus identified with the non-steady-state MBM was *Methanoculleus* (relative abundance of 2.55%), followed by *Methanomassiliicoccus* (relative abundance of 1.69%) *and Methanothermobacter* (relative abundance of 79.83%). *Methanoculleus* had the highest net growth rate, suggesting its active response to accommodate the stressed OLR. It was coincident with the previous finding that *Methanoculleus* shows greater robustness than *Methanosarcina* under stressed conditions (Wintsche et al., 2018). The most abundant *Methanothermobacter* with a relatively low net growth rate indicated that a microbe with a higher relative abundance does not always mean that it is more active, which is in agreement with previous studies (Campbell and Kirchman, 2013; Silva et al, 2019).

The net growth rates calculated with the non-steady-state MBM and the steady-state MBM did not agree. According to the steady-state MBM, *Methanothermobacter*, *Methanosarcina*, and *Methanoculleus* were the most active genera with the same net growth rate. The steady-state MBM does not consider the microbial community and the sludge characteristics before the disturbance. If a specific microbe does not exist in the influent, its net growth rate is only determined by the SRT. That is why the same growth rate was obtained for *Methanothermobacter*, *Methanosarcina*, and *Methanoculleus*. Actually, *Methanosarcina* had a negative growth rate due to the sharp decrease of its relative abundance after the disturbance. Therefore, the temporal changes of OTUs

before and after the disturbance must be incorporated when quantifying the activities of microbes in a bioreactor undergoing a disturbance.

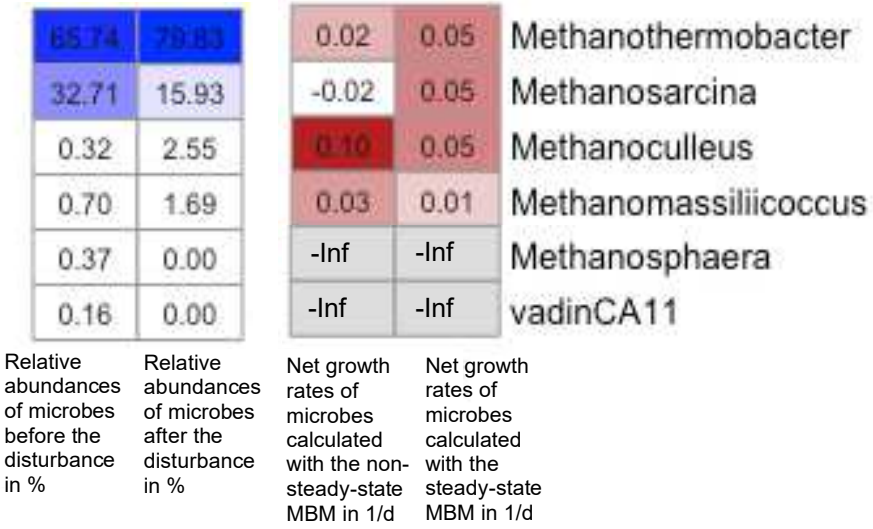

Figure 6-2. Relative abundances and net growth rates of archaeal genera. "-Inf" represents negative infinity.

6.3.3 Activities of bacterial genera

The relative abundances of the bacterial genera before and after the disturbance (relative abundance > 1% after the disturbance) and their net growth rates calculated with the two MBMs are shown in **Fig. 6–3(a)**. In terms of the relative abundances assessed by 16SrRNA amplicon analysis, *S1* and *Coprothermobacter* were dominant, accounting for over 40% of the bacterial genera. However, the net growth rates of *S1* and *Coprothermobacter* calculated with the non-steady-state MBM were moderate. Some abundant genera (e.g., an undefined genus of the order *OPB54* and an undefined genus of the family *TIBD11*) even had a negative growth rate. **Fig. 6–3(b)** shows the top 10 active bacterial genera identified with the non-steady-state MBM. The relative abundances of these 10 microbes after the disturbance ranged from 0.08% to 2.70%. Most

of these active bacteria perform hydrolysis of substrates, which is a rate-limiting step, especially under high OLR conditions. For instance, *Fibrobacter* is a cellulolytic microbe that mainly hydrolyzes cellulose into acetate and propionate (Lissens et al., 2004). *Ruminofilibacter* is capable of hydrolyzing xylan (Weiss et al., 2011). Little information about *W22* has been reported in the literature; it could play a role in hydrolysis and acidogenesis (Jiang et al., 2019). *Treponema* is likely a homoacetogen that consumes H_2 and CO_2 to produce acetate (Wang et al., 2013). Homoacetogenesis provides an alternative pathway to consume H_2 under suppressed methanogenesis (Siriwongrungson et al., 2007). *Treponema* is a key microbial indicator closely related to the AD process stability (Li et al., 2016). When the UASB reactor was disturbed by a higher OLR, the microbes that performed hydrolysis but had relatively small abundances exhibited sharply increased activities to overcome the rate-limiting step. The active *Treponema* also made a positive response to accommodate the stressed OLR, maintaining the process stability.

The steady-state MBM could not distinguish these top 10 active bacteria from each other because their net growth rates calculated with the steady-state MBM were the same. The reason why their net growth rates were the same is referred to Section 6.3.2.

(a)

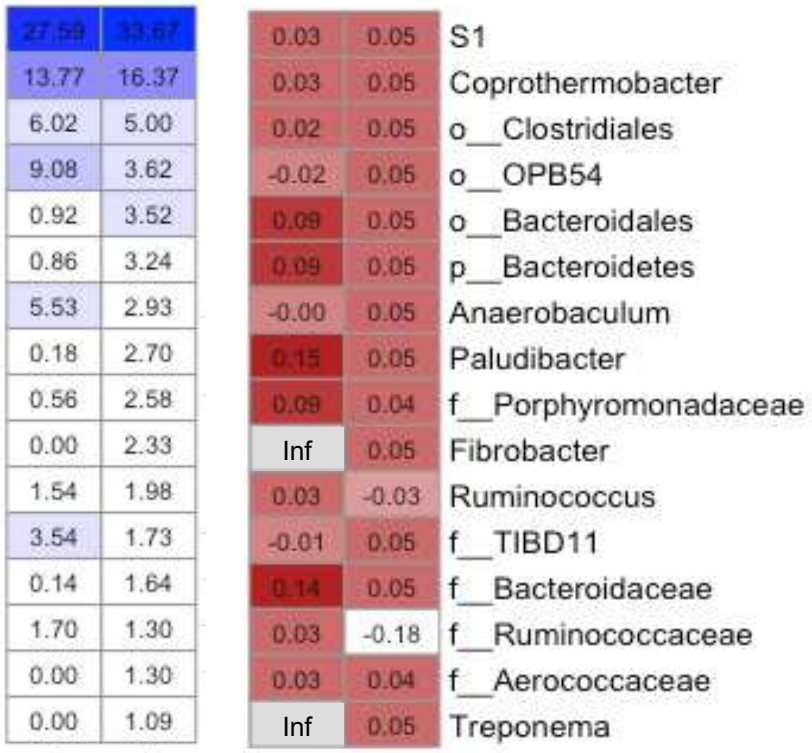

Relative abundances of microbes before the disturbance in %

Relative abundances of microbes after the disturbance in %

Net growth rates of microbes calculated with the non-steady-state MBM in 1/d

Net growth rates of microbes calculated with the steady-state MBM in 1/d

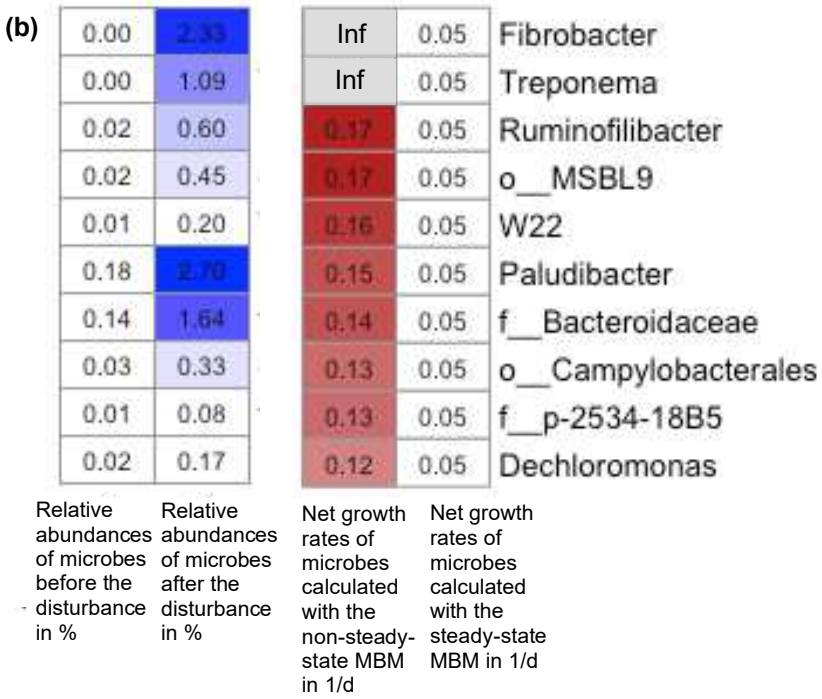

Figure 6-3. (a) The most abundant bacterial genera (relative abundance > 1% after the disturbance). (b) Top 10 active bacterial genera identified with their net growth rates calculated with the non-steady-state MBM. "Inf" represents positive infinity. Undefined genera are named using higher taxonomic levels such as family (f_), order (o_), and phylum (p_).

6.4 Implication of Non-Steady-State Mass Balance Model

Microorganisms can maintain their prevalence in bioreactors because of their immigration from the bioreactor influent microbial community, their growth in the bioreactors, and/or their retention from the seed sludge. However, not all prevalent microorganisms are active at all times, in other words, their abundances do not always reflect their growth rates or activity (Campbell and Kirchman, 2013; Calusinska et al., 2018; Silva et al, 2019). In bioreactors, some low abundant microbes can exert a disproportionately large functional effect through performing a very specific task (Calusinska et al., 2018). As a matter of fact, a substantial fraction of microbes may be dormant or inactive at any given moment, as demonstrated in previous microbial ecology studies

(Lennon and Jones, 2011; Shade et al., 2012). The dormancy has been shown to be important for maintaining overall compositional stability under disturbance scenarios. Rather than only focusing on the dominant microbial groups, the proposed non-steady-state MBM aims to identify active species within the community through normalizing 16S rRNA MiSeq reads by volatile suspended solids. Identifying active species improves the understanding of community dynamics and adaptation to the disturbance exerted on the bioreactor. A microbe's positive net growth rate indicates that this microbe has to work actively to accommodate a stressed (or limiting) condition caused by the disturbance. The functions of the active microbes tell what the limiting condition could be. In comparison, a microbe's negative net growth rate shows that this microbe cannot adapt well to the new environment and tends to decay.

To summarize, the newly developed non-steady-state MBM builds upon the previously steady-state MBM model by incorporating the temporal changes of OTUs following a disturbance, through a mass balance approach (considering cell numbers of individual microbes in the influent, effluent, bioreactor, and waste sludge, as well as the prior microbial community and sludge characteristics). This 'universal ecology model' facilitates a better understanding of microbiome dynamics and microbiome responses to disturbances in wastewater bioreactors.

6.5 Conclusions

For the first time, a universal non-steady-state MBM was developed to elucidate microbiome responses to a disturbance exerting on a UASB reactor treating blackwater for biomethane recovery. In particular, it can be used to identify active and inactive populations. This model was applied in a thermophilic UASB reactor fed with source-diverted blackwater to study the

microbiome responses to an increasing OLR. After the OLR disturbance, the microbes responsible for hydrolysis exhibited sharply increased activities to overcome this rate-limiting step in the anaerobic digestion, arising from the increased OLR. However, these most active species identified with the non-steady-state MBM were not the prevailing species identified with their relative abundances based on OTUs. Chapter 6 completed Objective 2.2.

References

Ali, M., Wang, Z., Salam, K.W., Hari, A.R., Pronk, M., van Loosdrecht, M.C.M., Saikaly, P.E., 2019. Importance of species sorting and immigration in the bacterial assembly of different-sized aggregates in a full-scale aerobic granular sludge plant. Environ. Sci. Technol. 53, 8291–8301.

Calusinska, M., Goux, X., Fossépré, M., Muller, E.E.L., Wilmes, P., Delfosse, P., 2018. A year of monitoring 20 mesophilic full-scale bioreactors reveals the existence of stable but different core microbiomes in bio-waste and wastewater anaerobic digestion systems. Biotechnol. Biofuels 11, 196.

Campbell, B.J., Kirchman, D.L., 2013. Bacterial diversity, community structure and potential growth rates along an estuarine salinity gradient. ISME J. 7 (1), 210–220.

Cheng, H., Cheng, D., Mao, J., Lu, T., Hong, P.-Y., 2019. Identification and characterization of core sludge and biofilm microbiota in anaerobic membrane bioreactors. Environ. Int. 133, 105165.

Frigon, D., Wells, G., 2019. Microbial immigration in wastewater treatment systems: analytical considerations and process implications. Curr. Opin. Biotechnol. 57, 151–159.

Gao, M., Zhang, L., Guo, B., Zhang, Y., Liu, Y., 2019. Enhancing biomethane recovery from source-diverted blackwater through hydrogenotrophic methanogenesis dominant pathway. Chem. Eng. J. 378, 122258.

Gao, M., Zhang, L., Liu, Y., 2020. High-loading food waste and blackwater anaerobic co-digestion: maximizing bioenergy recovery. Chem. Eng. J. 394, 124911.

Guo, B., 2019. Cellular Metabolic Markers and Growth Dynamics Definition of Functional Groups in Activated Sludge Wastewater Treatment Heterotrophic Population. McGill University, Montreal.

Jiang, Y., Dennehy, C., Lawlor, P.G., Hu, Z., McCabe, M., Cormican, P., Zhan, X., Gardiner, G.E., 2019. Exploring the roles of and interactions among microbes in dry co-digestion of food waste and pig manure using high-throughput 16S rRNA gene amplicon sequencing. Biotechnol. Biofuels 12, 5.

Lennon, J.T., Jones, S.E., 2011. Microbial seed banks: the ecological and evolutionary implications of dormancy. Nat. Rev. Microbiol. 9 (2), 119–130.

Li, L., He, Q., Ma, Y., Wang, X., Peng, X., 2016. A mesophilic anaerobic digester for treating food waste: process stability and microbial community analysis using pyrosequencing. Microb. Cell Fact. 15, 65.

Lissens, G., Verstraete, W., Albrecht, T., Brunner, G., Creuly, C., Seon, J., Dussap, G., Lasseur, C., 2004. Advanced anaerobic bioconversion of lignocellulosic waste for bioregenerative life support following thermal water treatment and biodegradation by *Fibrobacter succinogenes*. Biodegradation 15, 173–183.

Mei, R., Liu, W.-T., 2019. Quantifying the contribution of microbial immigration in engineered water systems. Microbiome 7, 144.

Mei, R., Narihiro, T., Nobu, M.K., Kuroda, K., Liu, W.-T., 2016. Evaluating digestion efficiency in full-scale anaerobic digesters by identifying active microbial populations through the lens of microbial activity. Sci. Rep. 6, 34090.

Ofiţeru, I.D., Lunn, M., Curtis, T.P., Wells, G.F., Criddle, C.S., Francis, C.A., Sloan, W.T., 2010. Combined niche and neutral effects in a microbial wastewater treatment community. PNAS 107 (35), 15345–15350.

Saunders, A.M., Albertsen, M., Vollertsen, J., Nielsen, P.H., 2016. The activated sludge ecosystem contains a core community of abundant organisms. ISME J. 10, 11–20.

Seifan, M., Seifan, T., Jeltsch, F., Tielbörger, K., 2012. Combined disturbances and the role of their spatial and temporal properties in shaping community structure. Perspect. Plant Ecol. Evol. Syst. 14 (3), 217–229.

Shade, A., Peter, H., Allison, S.D., Baho, D.L., Berga, M., Bürgmann, H., Huber, D.H., Langenheder, S., Lennon, J.T., Martiny, J.B.H., Matulich, K.L., Schmidt, T.M., Handelsman, J., 2012. Fundamentals of microbial community resistance and resilience. Front. Microbiol. 3, 417.

Silva, L., Calleja, M.L., Huete-Stauffer, T.M., Ivetic, S., Ansari, M.I., Viegas, M., Morán, X.A.G., 2019. Low abundances but high growth rates of coastal heterotrophic bacteria in the red sea. Front. Microbiol. 9, 3244.

Siriwongrungson, V., Zeng, R.J., Angelidaki, I., 2007. Homoacetogenesis as the alternative pathway for H_2 sink during thermophilic anaerobic degradation of butyrate under suppressed methanogenesis. Water Res. 41 (18), 4204–4210.

Sloan, W.T., Lunn, M., Woodcock, S., Head, I.M., Nee, S., Curtis, T.P., 2006. Quantifying the roles of immigration and chance in shaping prokaryote community structure. Environ. Microbiol. 8, 732–740.

Vuono, D.C., Benecke, J., Henkel, J., Navidi, W.C., Cath T.Y., Munakata-Marr, J., Spear, J.R., Drewes, J.E., 2015. Disturbance and temporal partitioning of the activated sludge metacommunity. ISME J. 9, 425–435.

Wang, W., Xie, L., Luo, G., Zhou, Q., Angelidaki, I., 2013. Performance and microbial community analysis of the anaerobic reactor with coke oven gas biomethanation and in situ biogas upgrading. Bioresour. Technol. 146, 234–239.

Weiss, S., Zankel, A., Lebuhn, M., Petrak, S., Somitsch, W., Guebitz, G.M., 2011. Investigation of microorganisms colonising activated zeolites during anaerobic biogas production from grass silage. Bioresour. Technol. 102 (6), 4353–4359.

Wintsche, B., Jehmlich, N., Popp, D., Harms, H., Kleinsteuber, S., 2018. Metabolic adaptation of methanogens in anaerobic digesters upon trace element limitation. Front. Microbiol. 9, 405.

Zhang, L., Mou, A., Guo, B., Sun, H., Anwar, M.N., Liu, Y., 2021. Simultaneous phosphorus recovery in energy generation reactor (SPRING): high rate thermophilic blackwater treatment. Resour. Conserv. Recycl. 164, 105163.

CHAPTER 7 IMPORTANCE OF LOW-ABUNDANCE MICROBIAL SPECIES IN RESPONSE TO DISTURBANCES IN A UASB REACTOR TREATING BLACKWATER

A version of this chapter has been published in the *Process Safety and Environmental Protection*.

7.1 Synopsis

Next-generation amplicon sequencing is widely employed to identify taxa within a microbial community. Currently, there is no consensus on the classification of these taxa. Most studies describe that a small portion of these taxa having individual relative abundances higher than 1% is abundant; the remaining big portion having individual relative abundances less than 1% is usually defined to be low-abundant (de Cena et al., 2021). Patterns of species abundance and distribution can provide insights into community functions and species' competition and predation (Verberk, 2011). Low-abundance taxa are usually thought to be less important for major community functions.

In recent years, scientists paid increasing attention on the importance of low-abundance microorganisms in various ecological habitats such as human bodies (Claussen et al., 2017; Benjamino et al., 2018; de Cena et al., 2021; Pust et al., 2022), marine environments (Jousset et al., 2017; Stępień et al., 2021), soil (Kurm et al., 2017; Dawson et al., 2017; Bickel and Or, 2021), and wastewater bioreactors (Liang et al., 2017; Guo et al., 2022). Low-abundance species have been found to contribute to specific functional traits and exhibit greater sensitivity to environmental factors than abundant species (Li et al., 2019; Bickel and Or, 2021). Detecting low-abundant species and unravelling their yet unknown contributions may be crucial for understanding community assembly and function comprehensively (Jousset et al., 2017).

In wastewater bioreactors, the microbial community regulates bioreactor performance. Microbial species degrade organic matter and maintain biosystem stability. One of the most important challenges facing the microbial community in the sludge is to adapt to changing environments in the bioreactor due to various disturbances (De Vrieze and Verstraete, 2016;

Santillan et al., 2019). Most studies only identify the microbial community developed in a stable environment or compare different representative communities between different operation conditions; however, limited efforts have been made on the microbial community evolution in response to the disturbance at a species level. Low-abundance species are considered to be a functional cache or a diverse source pool that responds to disturbances (Lynch and Neufeld, 2015), which have been found to play critical roles in community-wide species interactions (Hol et al., 2015; Dawson et al., 2017; Guo et al., 2022). When responding to a changing environment, the low-abundance species metabolically active and numerically increased are selected by this specific environment (Lynch and Neufeld, 2015), but the detection of these active low-abundance species is yet to be explored (Claussen et al., 2017).

Based on the methodology developed in Chapter 6 and the experiments conducted in Chapter 5, Chapter 7 identified active low-abundance species that responded to an operational disturbance, which was induced by turning on-or-off effluent recirculation in UASB reactors treating wastewater. Sludge samples were taken from the top and bottom layers of the reactors every half hydraulic retention time (HRT) after the initiation/termination of effluent recirculation, and the microbial community evolution was assessed.

7.2 Methodology

7.2.1 Experimental setup and reactor operation

Two 2.0 L UASB reactors, R1 and R2, were operated under mesophilic conditions (35 ± 2 ºC) for over 174 d. R1 and R2 were fed with synthetic blackwater containing commercial dog food (Salmon and Sweet Potato Dog Food, Kirkland Signature, USA) (11.5 g/L), urea (0.23 g/L),

KH_2PO_4 (0.11 g/L), K_2HPO_4 (0.17 g/L), Na_2CO_3 (0.5 g/L), and tap water (hereafter DFW). The DFW were mixed using magnetic stir bars before being added to the reactors and refilled every 2 d. The DFW had a pH value of 7.75 ± 0.14, a tCOD concentration of 15.6 ± 0.7 g/L, and a sCOD concentration of 2.1 ± 0.1 g/L. The HRT was 8.0 d, and the OLR was 1.9 g COD/L/d in both reactors.

After a 42-d reactor startup period, Stage I operation was carried out for 81 d where both R1 (without effluent recirculation) and R2 (with effluent recirculation) showed stable operation. In Stage II (51 d operation), effluent recirculation was applied to R1 and meanwhile stopped in R2. Sludge samples were taken from the top and bottom layers of sludge beds in R1 and R2 every half HRT (*i.e.,* every 4.0 d) from the initiation of Stage II to 3rd HRT (a total 7 samples for each layer). Performance of the two reactors were monitored through testing effluent pH value, CH_4 production, and COD removal every 2–3 d during the reactor operation.

7.2.2 Performance analysis

Reactor influent and effluent pH values were tested with a pH meter (SympHony B40PCID, VWR, Radnor, US). Influent and effluent COD concentrations were measured according to the Standard Methods (Rice et al., 2017). Biogas produced from reactors was collected in a 10 L foil sampling bag (Chromatographic Specialties Inc., Brockville, Canada), and its volume was measured every 2–3 d. The biogas composition was determined with a gas chromatograph (7890B, Agilent Technologies, Santa Clara, US). The methanisation rate was calculated as the percentage of feed COD that was converted to methane COD (in %).

7.2.3 Microbial community analysis

Microbial communities in the sludge samples were identified by DNA extraction followed by 16S rRNA sequencing. A sludge sample with a volume of 1 mL was centrifuged at 4000 *g* for 10 min, and the supernatant was discarded. Genomic DNA was extracted from the retained sludge with a DNeasy Power-Soil Kit (QIAGEN, Hilden, Germany), and its concentration was measured with NanoDrop One (ThermoFisher, Waltham, USA). 16S rRNA genes were amplified with the universal primer pair 515F (GTGCCAGCMGCCGCGG) and 806R (GGACTACHVGGGTWTCTAAT). Pooled PCR products were sequenced on an Illumina MiSeq platform. Data sets generated by 16S rRNA gene amplicon sequencing were deposited in the NCBI Sequence Read Archive under the accession number PRJNA800755. Sequence analyses were performed following the DADA2 algorithm (Callahan et al., 2016) in the Qiime2 workflow (Caporaso et al., 2010). Operational taxonomic units (OTUs) were clustered with 99% similarity with reference to the Greengenes database, version 13_8 (McDonald et al., 2012; Werner et al., 2012). Alpha diversity represented by the Shannon diversity index and beta diversity based on principal coordinates analysis (PCoA) were calculated using the "vegan" package, version 2.5.7 (Oksanen et al., 2019). Heatmaps were generated using the "pheatmap" package, version 1.0.12 (Kolde, 2019). These analyses were performed in RStudio, version 3.6.3 (R Core Team, 2020).

7.2.4 Calculation of net growth rates

The net growth rates of individual microbes responding to the effluent recirculation application in R1 and its termination in R2 (shift from Stage I to Stage II), were calculated based on the non-steady-state mass balance model shown in Eq. (7–1) (also in Chapter 3):

$$\frac{1}{p_{x,rs}VSS_{rs}V_r}\frac{d(p_{x,rs}VSS_{rs}V_r)}{dt} = \mu_x + \frac{p_{x,inf}VSS_{inf}Q_{inf}}{p_{x,rs}VSS_{rs}V_r} - \frac{p_{x,eff}VSS_{eff}Q_{eff}}{p_{x,rs}VSS_{rs}V_r} - \frac{\sum_{i=1}^{n}V_i}{t_sV_r} \qquad (7–1)$$

where μ_x is the net growth rate of microbe x (1/d), and t is the operation time (d). $p_{x,inf}$, $p_{x,eff}$, and $p_{x,rs}$ are the relative abundances of microbe x in OTUs for the influent, effluent, and reactor sludge, respectively. VSS_{inf}, VSS_{eff}, and VSS_{rs} are the volatile suspended solid concentrations of the influent, effluent, and reactor sludge, respectively (g/L). Q_{inf} and Q_{eff} are the daily volumes of influent and effluent, respectively (L/d). For the continuous bioreactor, $Q_{inf} = Q_{eff}$. V_r is the bioreactor volume (L). t_s is the test duration, during which the waste sludge is discharged n times, and the volume of the discharged sludge is V_i (i = 1, 2 … n).

When Eq. (7–1) was applied to calculate the net growth rates of microbes in the UASB reactors, the community evolution during first 3 HRTs after the initiation (or termination) of effluent recirculation was considered. The net growth rates of individual microbes during four dynamic periods were calculated: from the disturbance initiation to first half HRT (0.5 HRT), from first half HRT to first HRT (1 HRT), from first HRT to second HRT (2 HRT), and from second HRT to third HRT (3 HRT). For instance, when calculating the microbial net growth rates from the disturbance initiation to first half HRT, the community before the disturbance application (in Stage I) was considered as the initial condition. The differential equation was solved by means of Matlab programming.

7.3 Results

7.3.1 UASB reactor performance in Stages I and II

R1 and R2 performance in terms of effluent pH, COD removal efficiency, and methanisation rate are shown in **Fig. 7–1**. During all stages of operation, reactor performance was stabilized within the first 20 d. Over 30 d of stable operation was maintained in both reactor for Stages I and II. By

comparing the results of the two reactors, it was found that UASB effluent recirculation had limited impact on the reactor effluent pH level and COD removal. The average methanisation rates without effluent recirculation (R1 in Stage I and R2 in Stage II) reached 47.9%, whereas that with effluent recirculation (R2 in Stage I and R1 in Stage II) reached only 25.5%. As found in Zhang et al. (2020) and in Chapter 5, with effluent recirculation, a large portion of feed COD accumulated in reactor sludge due to inefficient hydrolysis of high-strength wastewater, resulting in low methane production.

7.3.2 Archaeal and bacterial community diversity

Fig. 7–2 shows the archaea and bacteria richness in sludge at the top and bottom layers of R1 and R2 in Stage I. Without effluent recirculation, archaeal (especially) and bacterial communities were segregated along the sludge bed of R1. In R1 without effluent recirculation, archaeal genera were present mainly in the top layer of sludge, and bacterial genera dominated in the bottom layer of sludge. In R2 with effluent recirculation, bacterial community segregation was not observed, likely due to the mixing condition caused by effluent recirculation. Although archaeal community stratification was observed, archaea richness was much lower than that in R1, which may be attributed to the low VFA production caused by low hydrolysis efficiency of the synthetic blackwater (Chapter 5).

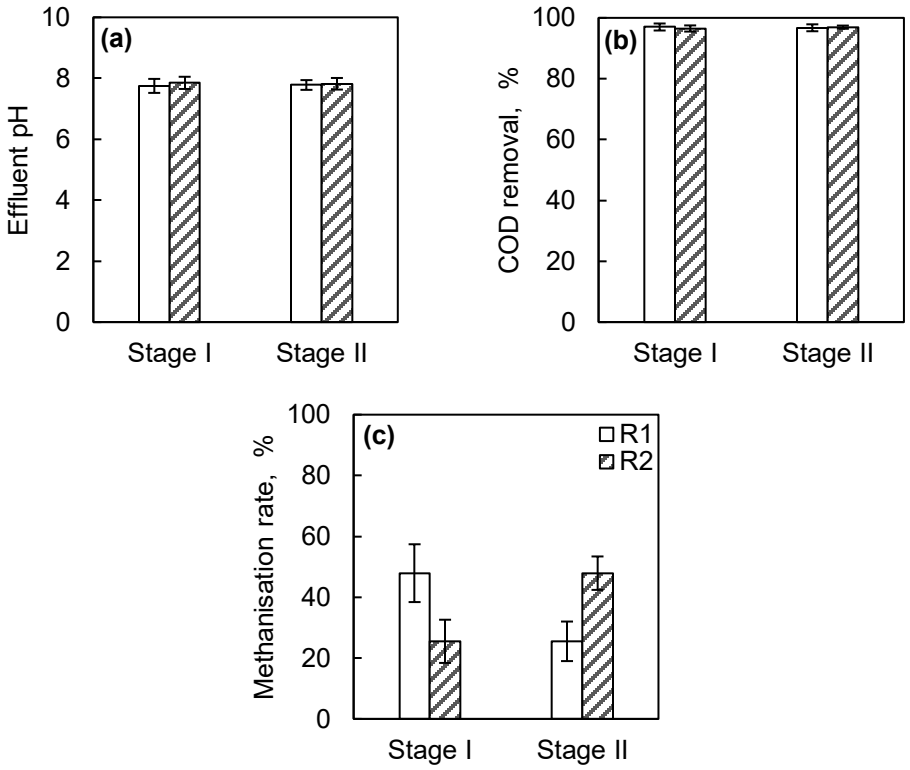

Figure 7-1. R1 and R2 performance in Stages I and II: (a) Effluent pH, (b) COD removal, and (c) methanisation rate. Error bars represent standard deviations. The legend of (a) and (b) are the same as that of (c).

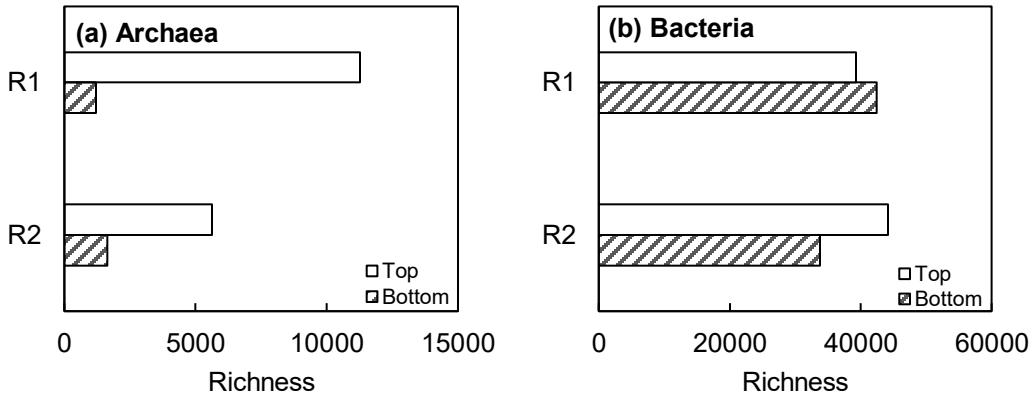

Figure 7-2. (a) Archaea and (b) bacteria in sludge at top and bottom layers of R1 and R2 in Stage II.

Fig. 7–3 shows the alpha diversity of archaea [**Fig. 7–3(a)**] and bacteria [**Fig. 7–3(b)**] represented by the Shannon diversity index, which accounts for both abundance and evenness of species present in a microbial community. Microbial communities in the sludge at both top and bottom layers of R1 and R2 responded quickly to the application (R1) and termination (R2) of effluent recirculation (shift from Stage I to Stage II). After the disturbance initiation in Stage II, the microbial community became more diverse and reached the highest diversity level quickly (within the first half HRT) in response to the changed physical environment. With an increase in test duration, the microbial community diversity became stable. **Fig. 7–3** also shows the beta diversity of archaea [**Fig. 7–3(c)**] and bacteria [**Fig. 7–3(d)**] in terms of PCoA results, illustrating the dissimilarity among microbial communities during community evolution in response to the disturbances. As the layered archaeal and bacterial communities were clustered into groups during their evolution, neither effluent recirculation application nor termination caused significant community separation in the reactor.

7.3.3 Relative abundances of archaea and bacteria

Fig. 7–4 shows the relative abundances of archaea and bacteria present in the sludge at the top and bottom layers of R1 and R2 from the initiation of Stage II to 3rd HRT. **Figs. 7–3(a) – (d**) indicate that in both reactors, *Methanosaeta* and an undefined genus of the family Methanospirillaceae were the two dominant archaeal genera during microbial community evolution. *Methanolinea*, an undefined genus of the family WSA2, and *Methanomassiliicoccus* were the second dominant archaeal genera. The methanogenesis pathway was dependent on substrates, whereas methane production was affected by the reactor operating conditions.

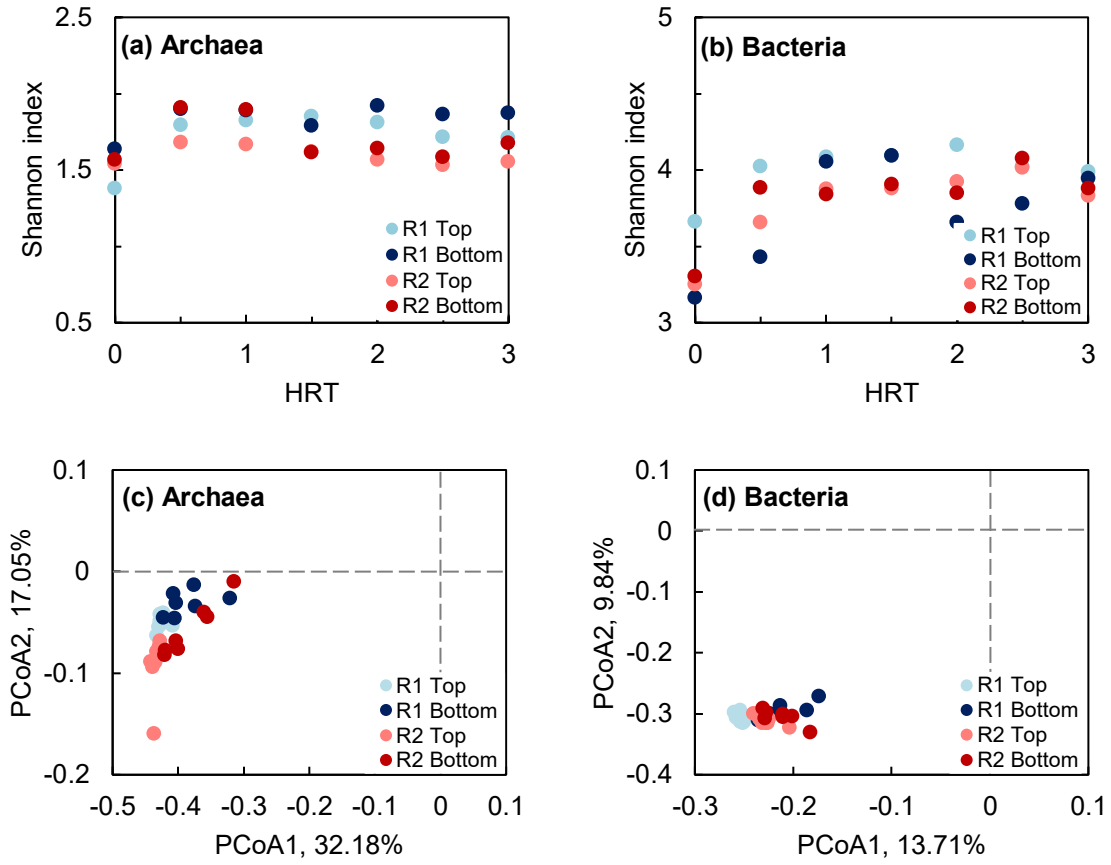

Figure 7-3. Variation in the Shannon diversity index for archaea with test duration in sludge sampled from the top and bottom layers of R1 and R2, (b) variation in the Shannon diversity index for bacteria with test duration in sludge sampled from top and bottom layers of R1 and R2, (c) beta diversity based on PCoA for archaea in sludge sampled from top and bottom layers of R1 and R2 during community evolution, and (d) beta diversity based on PCoA for bacteria in sludge sampled from top and bottom layers of R1 and R2 during community evolution from Stage I to Stage II.

The application/termination of effluent recirculation imposed greater influences on the bacterial community structure and evolution than on the archaeal community structure and evolution. An undefined genus of the order *Bacteroidales* in the top layer of R1 and the genus *Prevotella* in the bottom layer of R1 were the most dominant bacterial genera in the sludge at different test durations during bacterial community evolution. Species of the order *Bacteroidales* have been shown to play an important role in protein and amino acid degradations (Mei et al.,

2020). *Prevotella* has been reported to be involved in protein and peptide metabolism (Flint and Stewart, 1999). An undefined genus of the order *RB046* was the most abundant bacterial genus in the sludge at the top layer of R2 with effluent recirculation, whereas the genus *HA73* became prevalent after effluent recirculation was terminated. Little information can be found for genera of the order *RB046* and the uncultured species *HA73*, nevertheless, *HA73* belongs to the phylum *Synergistetes* that utilizes acetate through syntrophic acetate oxidation (Ito et al., 2011; Sitthi et al., 2020). An undefined genus of the phylum *OP8* was the most major bacterial genus in the sludge at the bottom layer of R2 with effluent recirculation, and the most dominant genus varied at different test durations after the effluent recirculation termination. Within the 2nd HRT and 3rd HRT of Stage II, an undefined genus of the order *Clostridiales* was prevalent. Microbial species of the order *Clostridiales* are involved in carbohydrate hydrolysis (Xia et al., 2015). The hydrolysis of complex organic matter is the rate-limiting step in the anaerobic digestion of high-solid content DFW. Bacterial genera responsible for organic matter hydrolysis prevailed. The overlapping functions of different species tends to maintain system stability (Konopka et al., 2015; García-García, 2019). The disturbance induced by effluent recirculation application or termination played an important role in bacteria selection.

(a) Relative abundances of archaea in R1 Top layer sludge

0 HRT	0.5 HRT	1 HRT	2 HRT	3 HRT	
34.51	29.96	31.19	31.31	39.51	Methanosaeta
20.38	27.19	24.07	27.61	19.25	f_Methanospirillaceae
15.24	13.63	12.88	10.77	11.28	Methanolinea
14.63	13.63	14.35	11.66	12.82	f_WSA2
7.24	7.30	7.30	8.82	7.39	Methanomassiliicoccus
2.86	2.33	3.99	2.55	5.02	o_WCHD3-30
2.85	2.93	3.63	4.11	3.90	Methanobacterium
0.73	0.00	0.71	0.17	0.00	Methanospirillum
0.61	0.79	0.76	0.63	0.43	o_pGrfC26
0.47	0.28	0.57	0.42	0.26	Methanobrevibacter
0.28	0.00	0.09	0.21	0.00	Methanosphaera
0.10	0.27	0.21	0.23	0.14	Methanomethylovorans
0.09	0.30	0.00	0.21	0.00	Methanosarcina
0.00	1.20	0.26	1.32	0.00	f_[Methanomassiliicoccaceae]
0.00	0.10	0.00	0.00	0.00	vadinCA11

(b) Relative abundances of archaea in R1 Bottom layer sludge

0 HRT	0.5 HRT	1 HRT	2 HRT	3 HRT	
30.00	34.79	33.69	37.70	41.39	Methanosaeta
17.08	17.98	22.58	12.03	13.74	f_Methanospirillaceae
9.68	12.44	10.56	10.31	9.51	Methanolinea
11.47	13.84	13.15	12.19	10.62	f_WSA2
5.57	8.14	7.52	7.62	4.64	Methanomassiliicoccus
0.75	2.95	2.84	3.07	4.89	o_WCHD3-30
7.44	4.45	4.41	9.34	6.75	Methanobacterium
0.00	1.11	0.59	0.56	0.00	Methanospirillum
0.00	0.60	0.55	0.22	0.71	o_pGrfC26
4.74	2.34	0.94	4.84	5.46	Methanobrevibacter
2.62	0.58	0.18	1.65	1.59	Methanosphaera
0.21	0.00	0.18	0.34	0.34	Methanomethylovorans
1.37	0.14	0.56	0.15	0.23	Methanosarcina
3.57	0.29	1.84	0.00	0.00	f_[Methanomassiliicoccaceae]
1.16	0.34	0.35	0.00	0.14	vadinCA11

(c) Relative abundances of archaea in R2 Top layer sludge

0 HRT	0.5 HRT	1 HRT	2 HRT	3 HRT	
81.07	33.79	33.00	47.36	38.66	Methanosaeta
9.34	32.29	35.29	22.23	34.03	f_Methanospirillaceae
1.17	5.59	6.06	7.35	6.25	Methanolinea
0.27	12.55	9.60	8.97	8.92	f_WSA2
1.04	8.85	9.15	8.96	6.88	Methanomassiliicoccus
5.39	2.15	2.11	1.82	2.25	Methanobacterium
0.14	1.09	0.78	0.15	0.72	Methanospirillum
0.00	0.52	0.63	0.53	0.24	o_pGrfC26
0.00	0.53	0.90	0.49	0.58	Methanobrevibacter
0.29	0.50	0.33	0.45	0.56	Methanosphaera
0.41	0.20	0.00	0.33	0.00	Methanomethylovorans
0.87	0.83	0.79	0.26	0.50	Methanosarcina
0.00	0.00	0.24	0.20	0.00	f_[Methanomassiliicoccaceae]
0.00	1.10	0.91	0.58	0.32	vadinCA11

(d) Relative abundances of archaea in R2 Bottom layer sludge

0 HRT	0.5 HRT	1 HRT	2 HRT	3 HRT	
26.98	31.45	29.00	43.07	42.89	Methanosaeta
25.43	31.14	32.66	27.79	24.85	f_Methanospirillaceae
3.58	4.44	4.22	5.53	5.40	Methanolinea
11.49	8.27	7.35	2.83	5.50	f_WSA2
9.29	5.98	9.23	8.14	7.30	Methanomassiliicoccus
2.92	3.85	3.00	5.53	8.45	Methanobacterium
3.79	1.47	0.30	0.00	0.00	Methanospirillum
0.00	0.33	0.36	0.00	0.26	o_pGrfC26
5.26	4.78	5.35	0.74	0.52	Methanobrevibacter
2.55	1.70	1.77	1.96	1.57	Methanosphaera
0.28	0.23	0.00	0.30	0.72	Methanomethylovorans
2.75	2.87	3.09	1.96	1.87	Methanosarcina
0.00	0.60	0.57	0.22	0.00	f_[Methanomassiliicoccaceae]
5.68	2.87	2.79	1.92	0.65	vadinCA11

(e) Relative abundances of bacteria in R1 Top layer sludge

0 HRT	0.5 HRT	1 HRT	2 HRT	3 HRT	
6.67	8.15	7.67	8.53	10.09	o_Bacteroidales
6.44	5.25	5.28	4.59	6.77	f_Thermovirgaceae
4.66	3.66	4.59	2.53	2.69	SJA-88
4.54	4.02	3.56	2.14	2.43	Blvii28
4.23	1.07	0.85	2.02	0.31	Prevotella
4.08	3.78	3.14	1.85	2.23	f_Sediment-4
4.08	2.32	2.23	1.22	1.53	HA73
3.80	4.22	4.29	3.06	4.77	f_Syntrophaceae
3.80	7.41	4.79	4.35	2.90	W22
3.47	1.70	1.96	1.05	1.12	Aminiphilus
2.50	2.61	2.30	1.44	3.42	c_Pla3
2.48	3.23	2.47	3.07	2.63	o_SHA-98
2.37	1.92	1.93	1.81	2.65	f_Dethiosulfovibrionaceae
2.21	3.51	3.44	3.01	3.27	o_OPB95
2.21	2.37	1.94	1.70	2.19	T78
2.07	1.35	1.31	0.85	1.26	c_noFP_H4
1.81	1.40	1.37	1.35	2.29	f_Syntrophorhabdaceae
1.58	0.90	1.19	1.40	0.68	p_OP8
1.58	2.05	1.45	2.32	1.92	Syntrophomonas
1.51	1.23	1.66	1.48	2.92	p_Hyd24-12
1.48	1.79	3.76	2.29	3.23	f_GZKB119
1.38	0.33	0.56	0.29	0.34	o_Bacteroidales
1.29	0.74	2.19	1.74	2.25	SC103
1.21	0.49	0.76	0.44	0.31	Lactococcus
1.17	1.69	1.23	1.54	1.15	Syntrophus
1.16	1.16	1.72	3.24	1.70	o_Clostridiales
1.02	2.50	1.51	2.09	1.19	Treponema
0.90	1.81	1.32	3.55	1.60	vadinCA02
0.79	0.50	0.99	1.06	0.96	vadinHB04
0.77	1.25	3.06	3.80	3.15	f_R4-41B
0.70	1.10	0.97	0.65	1.00	f_Syntrophaceae
0.68	1.10	1.08	1.32	1.65	Pelotomaculum
0.61	0.87	1.12	1.47	3.00	o_RB046
0.36	0.76	0.58	1.10	0.72	p_OD1
0.33	1.61	0.66	2.14	0.23	o_GIF10

(f) Relative abundances of bacteria in R1 Bottom layer sludge

[illegible]	[illegible]	13.32	21.68	10.39	Prevotella
13.38	6.50	5.56	8.31	7.80	Lactococcus
2.99	3.53	2.04	6.34	4.16	vadinHB04
2.71	1.94	0.96	1.39	1.39	o_Bacteroidales
2.52	0.82	1.45	2.01	1.38	o_Clostridiales
2.30	1.47	1.04	2.64	0.77	o_Lactobacillales
2.13	1.20	1.03	2.97	1.35	Anaerovibrio
1.98	3.50	5.52	2.38	3.64	o_Bacteroidales
1.79	1.33	0.68	0.30	0.89	f_Enterobacteriaceae
1.69	0.63	0.83	0.55	0.86	p_OP8
1.68	0.81	0.76	1.97	0.91	f_Bifidobacteriaceae
1.59	1.39	1.44	2.05	1.65	Clostridium
1.36	0.30	0.29	0.31	0.73	f_Synergistaceae
1.16	1.33	0.94	1.73	1.40	Ruminococcus
1.03	1.93	3.54	0.77	1.15	W22
1.02	1.15	0.61	3.92	2.12	f_Clostridiaceae
0.95	0.32	0.63	0.70	1.46	Desulfovibrio
0.86	1.80	2.44	0.67	0.80	SJA-88
0.81	0.34	0.19	0.71	1.03	Oscillospira
0.81	0.33	1.04	0.90	1.36	vadinCA02
0.73	0.95	2.59	0.87	4.07	f_R4-41B
0.68	1.99	2.76	2.23	2.73	f_Thermovirgaceae
0.62	1.35	1.86	0.53	0.71	f_Sediment-4
0.61	1.81	1.09	2.21	0.62	f_Lachnospiraceae
0.49	1.19	1.48	1.14	1.86	HA73
0.47	1.25	1.85	0.42	0.84	Blvii28
0.44	1.28	2.47	0.50	2.42	f_GZKB119
0.43	0.55	1.22	0.72	0.76	Syntrophomonas
0.40	2.06	2.03	2.65	2.83	Aminiphilus
0.36	0.37	0.30	0.42	1.47	Bacteroides
0.34	1.32	2.36	0.72	1.21	o_OPB95
0.34	0.73	1.34	0.58	1.02	T78
0.32	0.93	1.29	0.85	1.23	f_Dethiosulfovibrionaceae
0.31	0.97	2.15	0.64	0.71	o_SHA-98
0.26	1.74	2.39	1.04	1.80	f_Syntrophaceae
0.24	1.86	3.17	2.68	9.59	SC103
0 HRT	0.5 HRT	1 HRT	2 HRT	3 HRT	

(g) Relative abundances of bacteria in R2 Top layer sludge

0 HRT	0.5 HRT	1 HRT	2 HRT	3 HRT	
27.21	4.01	4.30	8.21	4.51	o_RB046
7.44	3.55	2.74	4.53	2.93	vadinCA02
6.88	10.61	8.51	8.43	12.98	HA73
4.90	10.94	5.49	3.92	2.09	p_OP8
4.62	1.43	1.64	2.03	1.88	Syntrophomonas
4.23	1.08	1.34	1.94	1.49	f_Syntrophorhabdaceae
4.16	1.51	1.88	2.93	2.50	f_Thermovirgaceae
4.15	3.69	3.42	5.22	3.71	Candidatus
2.92	0.97	1.10	1.40	1.25	f_Dethiosulfovibrionaceae
2.22	0.86	1.07	1.44	1.38	T78
2.20	5.42	7.21	7.53	7.34	o_Bacteroidales
1.64	1.01	0.66	1.03	2.38	Aminiphilus
1.63	0.53	0.66	0.61	0.34	Desulfobulbus
1.59	0.79	1.10	1.19	0.95	f_Pirellulaceae
1.23	0.28	0.47	0.45	0.53	Clostridium
1.17	0.41	0.39	0.59	0.49	PD-UASB-13
1.05	0.25	0.45	0.64	0.54	o_SHA-1
1.04	1.81	1.69	1.57	1.95	o_Clostridiales
0.61	2.66	3.89	2.73	3.23	SJA-88
0.34	1.50	1.81	2.17	1.81	f_Syntrophaceae
0.32	2.03	2.91	2.22	2.30	f_Sediment-4
0.24	5.58	6.06	2.60	1.78	f_GZKB119
0.20	2.24	4.20	4.18	4.93	Blvii28
0.15	5.63	4.19	3.03	6.72	SC103
0.11	0.77	0.52	1.14	0.92	o_SHA-98
0.04	10.24	7.53	3.19	4.23	f_R4-41B
0.00	0.51	1.05	0.69	1.29	f_Holophagaceae

(h) Relative abundances of bacteria in R2 Bottom layer sludge

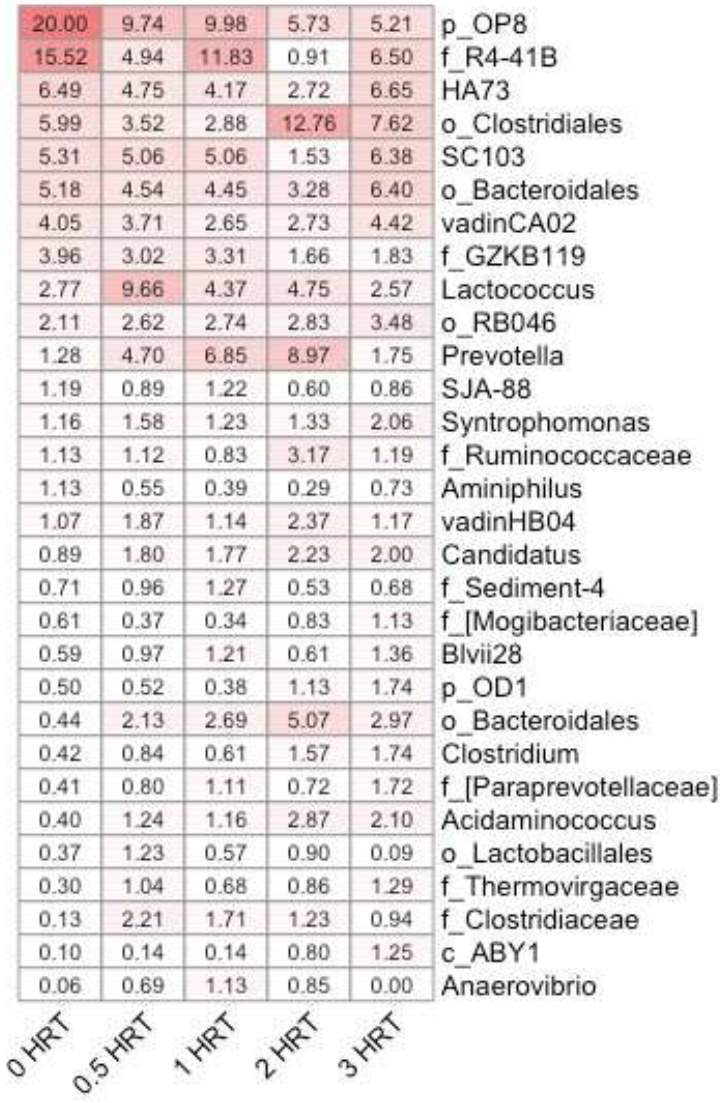

Figure 7-4. Heatmaps for the relative abundances of (a) archaea in R1 top layer sludge, (b) archaea in R1 bottom layer sludge, (c) archaea in R2 top layer sludge, (d) archaea in R2 bottom layer sludge, (e) bacteria in R1 top layer sludge, (f) bacteria in R1 bottom layer sludge, (g) bacteria in R2 top layer sludge, and (h) bacteria in R2 bottom layer sludge at the initial time (0 HRT), first half HRT (0.5 HRT), 1st HRT, 2nd HRT, and 3rd HRT after the initiation of Stage II. The unit of relative abundance is %. Undefined genera were named using higher taxonomic levels such as family (f_), order (o_), class (c_), and phylum (p_).

7.3.4 Net growth rates of archaea and bacteria

To identify active/inactive species when the microbial community responded to the disturbance imposed by effluent recirculation application to R1 or effluent recirculation termination in R2 in Stage II, Eq. (7–1) was used to calculate the net growth rates of individual microbes. In **Fig. 7–5**, a positive net growth rate indicates active growth, and a negative net growth rate indicates inactive growth. The net growth rates achieved their greatest absolute values (positive or negative) right after effluent recirculation application/termination was initiated (e.g., first half HRT). As the test duration increased, the absolute values of microbial net growth rates decreased as the microbial community accommodated to the new environment. The variation in net growth rate and community alpha diversity over the test duration illustrated that the well-developed microbial communities were capable of making quick responses to the disturbance, maintaining reactor stability.

In this study, microbes with relative abundances less than 1% were considered as low-abundance species. Low-abundance microbial species presented greater net growth rates than high-abundance microbial species. In the sludge at the top layer of R1, during the first half HRT of Stage II, *Methanosarcina* was the most active archaeal genus with a net growth rate of 0.39 d^{-1} (**Fig. 7–5(a)**), but its relative abundance was low, increasing from 0.09% (Stage I) to 0.30% (first 0.5 HRT of Stage II) (**Fig. 7–4(a)**). *Methanosarcina* is a versatile methanogen, and robust toward impairments compared with other methanogens (De Vrieze et al., 2012). *Methanomethylovorans* was the second most active archaeal genus with a net growth rate of 0.34 d^{-1}; its relative abundance increased from 0.10% to 0.27%. The net growth rates of *Methanosaeta*, the most dominant archaeal genus, were relatively small, varying from 0.05 to 0.02 d^{-1}. When effluent recirculation was applied to R1, substrate hydrolysis and methane production decreased (Chapter 5). Archaeal

genera, especially robust ones, grew actively to alleviate the negative impact of the challenging environment induced by effluent recirculation. In the sludge at the top layer of R2, during the community shift during a test duration of first half HRT, only three archaeal genera had positive net growth rates (*Methanomassiliicoccus*, *Methanospirillum*, and an undefined genus of the family *WSA2*); all other species presented negative growth. When effluent recirculation was terminated in R2, the new environment in R2 was less stressful for microorganisms and more favourable for organic matter hydrolysis and methane generation. The disturbance shaped the community assembly and can result in fluctuations of functionally similar species (Jarzyna et al., 2021). In spite of some inactive growing genera, the performance of R2 turned better after the disturbance application. It should also be noted that the absolute values of the net growth rates of low-abundance species may be "overrated" just because their lower initial abundances. Hence, further studies should be conducted to clarify the roles of these low-abundance species.

Bacterial community evolution differed between the sludge at the top layer and the sludge at the bottom layer in both R1 and R2 [**Figs. 7–5(e) – (h)**]. Many genera are still uncultured, so their functions are not well understood. Different bacterial genera have overlapping functions and their enrichment relies on specific conditions. *Clostridiales* and *Bacteroidales* dominated the anaerobic digestion of complex organic matter in R1 and R2 (**Fig. 7–4**). Although effluent recirculation/termination enabled more diverse bacterial genera to grow actively, these diverse bacterial genera had low relative abundances. As the active growth of these low-abundance species would provide a higher microbial diversity when effluent recirculation was discontinued (**Fig. 7–3**), the low-abundance species played a vital role in maintaining biosystem stability and in reducing microbial impairments due to the disturbance.

(a) net growth rates of archaea in R1 Top layer sludge

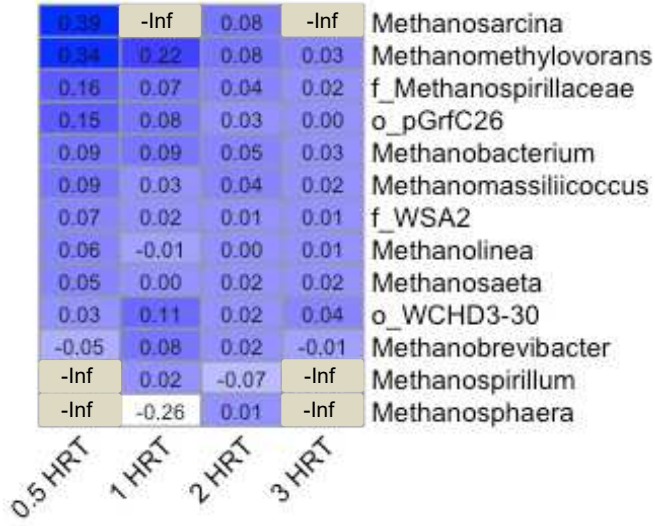

(b) Net growth rates of archaea in R1 Bottom layer sludge

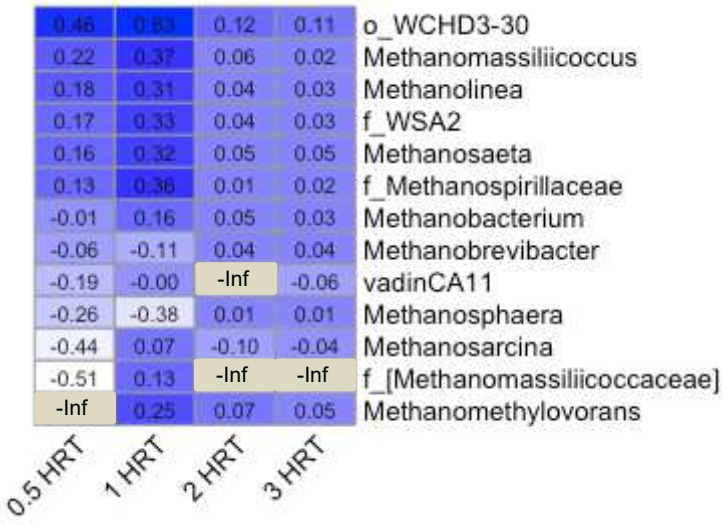

(c) Net growth rates of archaea in R2 Top layer sludge

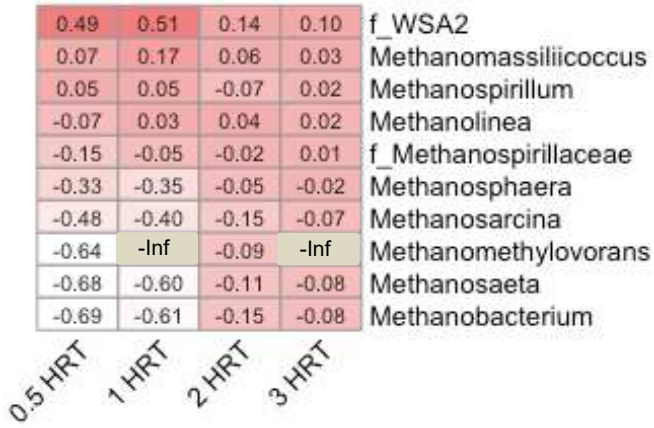

(d) Net growth rates of archaea in R2 Bottom layer sludge

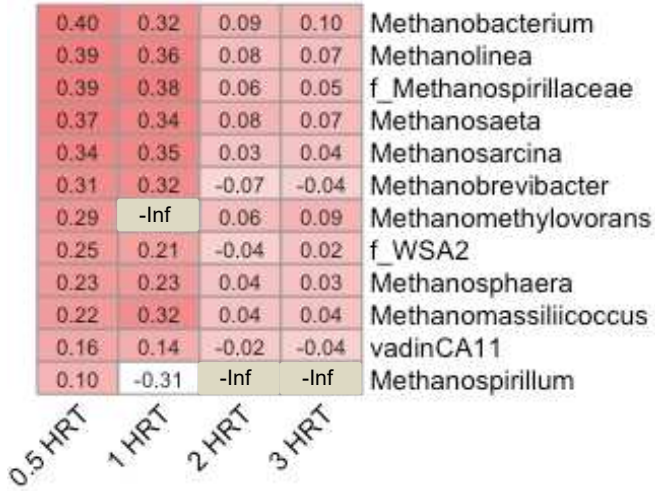

(e) Net growth rates of bacteria in R1 Top layer sludge

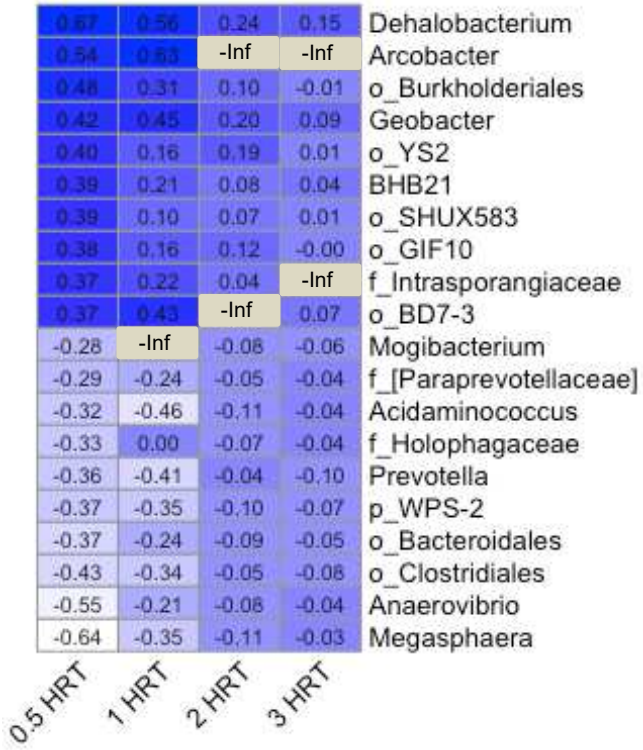

(f) Net growth rates of bacteria in R1 Bottom layer sludge

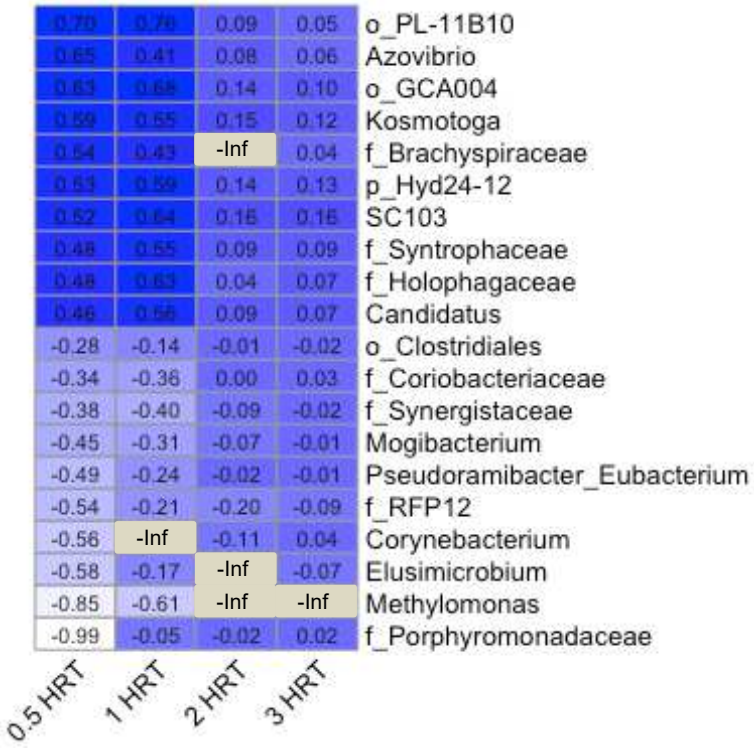

(g) Net growth rates of bacteria in R2 Top layer sludge

0.5 HRT	1 HRT	2 HRT	3 HRT	
1.07	0.98	0.21	0.16	f_R4-41B
0.95	1.01	0.25	0.18	Treponema
0.87	1.04	0.25	0.20	f_Holophagaceae
0.76	0.89	0.22	0.13	Desulfovibrio
0.74	0.72	0.21	0.11	Prevotella
0.61	0.82	0.21	0.13	o_OPB95
0.59	0.51	0.12	0.12	SC103
0.55	0.57	0.07	0.10	W22
0.49	0.42	0.14	0.08	c_Clostridia
0.49	0.58	0.16	0.10	f_Spirochaetaceae
-0.70	-Inf	-0.15	-Inf	f_Helicobacteraceae
-0.71	-0.42	-0.16	-Inf	o_OPB11
-0.76	-0.90	-0.10	-Inf	f_Isosphaeraceae
-0.76	-0.52	-0.11	-0.07	f_SHA-31
-0.78	-1.01	-0.14	-Inf	Planctomyces
-0.79	-0.78	-0.14	-0.11	o_RB046
-0.81	-0.90	-0.19	-Inf	Mycobacterium
-0.83	-0.88	-0.28	-Inf	o_TP122
-0.90	-0.85	-0.18	-0.12	p_WS1
-0.98	-Inf	-0.13	-0.09	C1_B004

(h) Net growth rates of bacteria in R2 Bottom layer sludge

0.5 HRT	1 HRT	2 HRT	3 HRT	
0.89	0.99	0.26	0.14	f_S24-7
0.83	0.62	0.20	0.06	Oscillospira
0.83	0.95	0.23	-Inf	Anaerovibrio
0.71	0.73	0.17	0.13	o_SHA-98
0.67	-Inf	0.13	0.04	k_Bacteria
0.65	0.66	0.08	0.06	f_Ellin515
0.64	0.33	0.19	0.07	f_Veillonellaceae
0.63	1.03	0.22	0.08	o_YS2
0.62	0.68	0.22	0.12	o_Bacteroidales
0.61	0.54	0.12	0.08	Desulfovibrio
-0.06	0.16	-0.11	0.01	f_R4-41B
-0.07	0.10	-Inf	-Inf	c_Endomicrobia
-0.08	0.28	-Inf	-0.01	c_Mollicutes
-0.11	0.28	0.10	0.10	c_OP8_1
-0.12	0.22	-0.08	0.06	Paludibacter
-0.12	-0.15	-0.10	-Inf	f_Puniceicoccaceae
-0.16	-0.12	-Inf	0.03	o_Thermoanaerobacterales
-0.21	0.29	-Inf	-Inf	o_ML615J-28
-0.24	-0.21	-0.08	0.04	f_Ignavibacteriaceae
-0.28	0.32	-0.07	-0.05	Elusimicrobium

Figure 7-5. Heatmaps for the net growth rates of (a) archaea in R1 top layer sludge, (b) archaea in R1 bottom layer sludge, (c) archaea in R2 top layer sludge, (d) archaea in R2 bottom layer sludge, (e) bacteria in R1 top layer sludge, (f) bacteria in R1 bottom layer sludge, (g) bacteria in R2 top layer sludge, and (h) bacteria in R2 bottom layer sludge within first half HRT (0.5 HRT), 1st HRT, 2nd HRT, and 3rd HRT after the initiation of Stage II. The unit of net growth rate is d^{-1}. Undefined genera were named using higher taxonomic levels such as family (f_), order (o_), class (c_), and phylum (p_). "-Inf" means a negatively infinite growth rate.

7.4 Discussion

External disturbances or fluctuations during biological wastewater treatment change the physical/chemical environment in the bioreactor. Disturbances are considered the main factors driving variations in species diversity and microbial community structure (Shade et al., 2012), while a deep understanding of the outcomes due to disturbances is lacking (Santillan et al., 2019). Microbial communities respond to such disturbances in ways that preserve the stability of the biological system (Liu et al., 2018). In this study the microbial community became more diverse when the bioreactor faced a disturbance (initiating or discontinuing effluent recirculation), reaching its highest diversity level directly after disturbance initiation. Microbial biodiversity tended to stabilize over time as microbial communities adapted to the changing environment. Linkage between biodiversity and process stability has been extensively documented in the literature (Yan et al., 2021; Jarzyna et al., 2022). An increase in microbial biodiversity buffers environmental stress on the biological system and helps maintain system functioning-stability (García-García et al., 2019).

Studies of microbial communities in wastewater bioreactors are mainly restricted to the identification of abundant species within the well-developed communities. However, relatively rare or dormant species that can strongly contribute to ecosystem assembly and function (Hooper et al., 2005; Lennon and Jones, 2011; Shade et al., 2012; Zhao et al., 2021; Guo et al., 2022) are

often overlooked. By quantifying the activities of individual microbes within the dynamic community in terms of their net growth rates, this study identified the low-abundance species that actively grew during the community evolution in response to the disturbance. The metabolically active and numerically increased low-abundance species were also detected in bioreactor communities responding to challenging OLR and HRT conditions (Yu et al., submitted). Although it is difficult to reveal microbial community behavior in a disturbed environment (Shade et al., 2012), calculation of the net growth rates of individual microbes provides a way to quantify their growth and decay during community evolution. Low-abundance microbes have been found to have high normalized betweenness and degree based on the co-occurrence network analysis, indicating their importance in maintaining the biosystem stability and functionality (Banerjee et al., 2018; Guo et al., 2022; Pust and Tümmler, 2022). Here, in response to the disturbance induced by initiating or discontinuing effluent recirculation in a reactor treating wastewater, an increase in the growth of some low-abundance species may have led to high biodiversity in the microbial community. Temporal fluctuations in species abundance can help stabilize community properties (Jarzyna et al., 2022). The role of actively growing low-abundance species in maintaining biosystem functioning-stability deserve more comprehensive investigation.

Microbial communities in wastewater bioreactors encompass a large diversity of poorly characterized lineages (Farag et al., 2014; Kristensen et al., 2021). These uncultured microorganisms with unknown functionality could be selected by environment. The identification of activities of low-abundance species in response to a specific bioreactor disturbance may help detect some species having undescribed process-critical functions.

7.5 Conclusions

This study highlighted the importance of low-abundance species within a well-developed microbial community in response to a changing environment in a UASB reactor for blackwater treatment. Chapter 7 completed Objective 2.3. In response to a disturbance in a UASB reactor, such as effluent recirculation application and termination, microbial biodiversity increased to a high level quickly. In addition, some low-abundance species identified by the non-steady-state mass balance model were observed to be more active than dominant species in adapting to the changing environment.

References

Banerjee, S., Schlaeppi, K., van der Heijden, M.G., 2018. Keystone taxa as drivers of microbiome structure and functioning. Nat. Rev. Microbiol. 16 (9), 567–576.

Benjamino, J., Lincoln, S., Srivastava, R., Graf, J., 2018. Low-abundant bacteria drive compositional changes in the gut microbiota after dietary alteration. Microbiome 6, 86.

Bickel, S., Or, D., 2021. The chosen few—variations in common and rare soil bacteria across biomes. ISM J. 15, 3315–3325.

Callahan, B.J., McMurdie, P.J., Rosen, M.J., Han, A.W., Johnson, A.M.A., Holmes, S.P., 2016. DADA2: high resolution sample inference from Illumina amplicon data. Nat. Methods 13 (7), 581–583.

Caporaso, J.G., Kuczynski, J., Stombaugh, J., Bittinger, K., Bushman, F.D., Costello, E.K., Fierer, N., Peña, A.G., Goodrich, J.K., Gordon, J.I., Huttley, G.A., Kelley, S.T., Knights, D., Koenig, J.E.,

Ley, R.E., Lozupone, C.A., McDonald, D., Muegge, B.D., Pirrung, M., Reeder, J., Sevinsky, J.R., Turnbaugh, P.J., Walters, W.A., Widmann, J., Yatsunenko, T., Zaneveld, J., Knight, R., 2010. QIIME allows analysis of high-throughput community sequencing data. Nat. Methods 7 (5), 335–336.

Claussen, J.C., Skiecevičienė, J., Wang, J., Rausch, P., Karlsen, T.H., Lieb, W, Baines, J.F., Franke, A., Hütt, M.-T., 2017. Boolean analysis reveals systematic interactions among low-abundance species in the human gut microbiome. PLoS Comput. Biol. 13 (6), e1005361.

Dawson, W., Hör, J., Egert, M., van Kleunen, M., Pester, M., 2017. A small number of low-abundance bacteria dominate plant species-specific responses during rhizosphere colonization. Front. Microbiol. 8, 875.

de Cena, J.A., Zhang, J., Deng, D., Damé-Teixeira, N., Do, T., 2021. Low-abundant microorganisms: the human microbiome's dark matter, a scoping review. Front. Cell. Infect. Microbiol. 11, 689197.

De Vrieze, J., Hennebel, T., Boon, N., Verstraete, W., 2012. Methanosarcina: the rediscovered methanogen for heavy duty biomethanation. Bioresour. Technol. 112, 1–9.

De Vrieze, J., Verstraete, W., 2016. Perspectives for microbial community composition in anaerobic digestion: from abundance and activity to connectivity. Environ. Microbiol. 18 (9), 2797–2809.

Farag, I.F., Davis, J.P., Youssef, N.H., Elshahed M.S., 2014. Global patterns of abundance, diversity and community structure of the *Aminicenantes* (candidate phylum OP8). PLoS One 9 (3), e92139.

Flint, H.J., Stewart, C.S., 1999. Bacteroides and prevotella, in: Robinson, R.K., Batt, C., Patel, P. (Eds.), Encyclopedia of Food Microbiology, Academic Press, USA, pp. 198–203.

García-García, N., Tamames, J., Linz, A.M., Pedrós-Alió, C., Puente-Sánchez, F., 2019. Microdiversity ensures the maintenance of functional microbial communities under changing environmental conditions. ISME J. 13 (12), 2969–2983.

Guo, B., Zhang, L., Sun, H., Gao, M., Yu, N., Zhang, Q., Mou, A., Liu, Y., 2022. Microbial co-occurrence network topological properties links with reactor parameters and reveals importance of low-abundance genera. npj Biofilms Microbiomes 8, 3.

Hol, W.H.G., Garbeva, P., Hordijk, C., Hundscheid, M.P.J., Gunnewiek, P.J.A.K., van Agtmaal, M., Kuramae, E.E., de Boer, W., 2015. Non-random species loss in bacterial communities reduces antifungal volatile production. Ecology 96 (8), 2042–2048.

Hooper, D.U., Chapin III, F.S., Ewel, J.J., Hector, A., Inchausti, P., Lavorel, S., Lawton, J.H., Lodge, D.M., Loreau, M., Naeem, S., Schmid, B., Setälä, H., Symstad, A.J., Vandermeer J., Wardle, D.A., 2005. Effects of biodiversity on ecosystem functioning: a consensus of current knowledge. Ecol. Monogr. 75(1), 3–35.

Ito, T., Yoshiguchi, K., Ariesyady, H., Okabe, S., 2011. Identification of a novel acetate-utilizing bacterium belonging to Synergistes group 4 in anaerobic digester sludge. ISME J. 5, 1844-1856.

Jarzyna, M.A., Norman, K.E.A., LaMontagne, J.M., Helmus, M.R., Li, D., Parker, S.M., Rocha, M.P., Record, S., Sokol, E.R., Zarnetske, P.L., Surasinghe, T.D., 2022. Community stability is related to animal diversity change. Ecosphere 13 (3), e3970.

Jousset, A., Bienhold, C., Chatzinotas, A., Gallien, L., Gobet, A., Kurm, V., Küsel, K., Rillig, M.C., Rivett, D.W., Salles, J.F., van der Heijden, M.G.A., Youssef, N.H., Zhang, X., Wei, Z., Hol, W.H.G., 2017. Where less may be more: how the rare biosphere pulls ecosystems strings. ISME J. 11 (4), 853–862.

Kolde, R., 2019. Package 'pheatmap'. https://cran.r-project.org/package=pheatmap.

Konopka, A., Lindemann, S., Fredrickson, J., 2015. Dynamics in microbial communities: unraveling mechanisms to identify principles. ISME J. 9, 1488–1495.

Kristensen, J.M., Singleton, C., Clegg, L.-A., Petriglieri, F., Nielsen, P.H., 2021. High diversity and functional potential of undescribed "Acidobacteriota" in Danish wastewater treatment plants. Front. Microbiol. 12, 643950.

Kurm, V., van der Putten, W.H., de Boer, W., Naus-Wiezer, S., Hol, W.H.G., 2017. Low abundant soil bacteria can be metabolically versatile and fast growing. Ecology 98 (2), 555–564.

Lennon, J.T., Jones, S.E., 2011. Microbial seed banks: the ecological and evolutionary implications of dormancy. Nat. Rev. Microbiol. 9 (2), 119–130.

Li, P., Liu, J., Jiang, C., Wu, M., Liu, M., Li, Z., 2019. Distinct successions of common and rare bacteria in soil under humic acid amendment—a microcosm study. Front. Microbiol. 10, 1–14.

Liang, H., Ye, D., Luo, L., 2017. Unravelling diversity and metabolic potential of microbial consortia at each stage of leather sewage treatment. RSC Adv. 7, 41727–41737.

Liu, Z., Cichocki, N., Bonk, F., Günther, S., Schattenberg, F., Harms, H., Centler, F., Müller, S., 2018. Ecological stability properties of microbial communities assessed by flow cytometry. mSphere 3 (1), e00564-17.

Lynch, M.D.J., Neufeld, J.D., 2015. Ecology and exploration of the rare biosphere. Nat. Rev. Microbiol. 13, 217–229.

McDonald, D., Price, M.N., Goodrich, J., Nawrocki, E.P., DeSantis, T.Z., Probst, A., Andersen, G.L., Knight, R., Hugenholtz, P., 2012. An improved Greengenes taxonomy with explicit ranks for ecological and evolutionary analyses of bacteria and archaea. ISME J. 6 (3), 610–618.

Mei, R., Nobu, M.K., Narihiro, T., Liu, W.-T., 2020. Metagenomic and metatranscriptomic analyses revealed uncultured Bacteroidales populations as the dominant proteolytic amino acid degraders in anaerobic digesters. Front. Microbiol. 11, 593006.

Oksanen, J., Blanchet, F.G., Friendly, M., Kindt, R., Legendre, P., McGlinn, D., Minchin, P.R., O'Hara, R. B., Simpson, G.L., Solymos, P., Stevens, M.H.H., Szoecs, E., Wagner, H., 2019. Community Ecology Package. https://cran.r-project.org.

Pust, M.-M., Tümmler, B., 2022. Bacterial low-abundant taxa are key determinants of a healthy airway metagenome in the early years of human life. Comput. Struct. Biotechnol. J. 20, 175–186.

R Core Team, 2020. R: A Language and Environment for Statistical Computing. R Foundation for Statistical Computing, Vienna, Austria.

Santillan, E., Seshan, H, Constancias, F., Drautz-Moses, D.I., Wuertz, S., 2019. Frequency of disturbance alters diversity, function, and underlying assembly mechanisms of complex bacterial communities. npj Biofilms Microbiomes 5, 8.

Rice, E.W., Baird, R.B., Eaton. A.D., 2017. Standard Methods for the Examination of Water and Wastewater, twenty third ed., American Public Health Association (APHA), American Water Works Association, Water Environment Federation (WEF), Washington, DC.

Shade, A., Peter, H., Allison, S.D., Baho, D.L., Berga, M., Bürgmann, H., Huber, D.H., Langenheder, S., Lennon, J.T., Martiny, J.B.H., Matulich, K.L., Schmidt, T.M., Handelsman, J., 2012. Fundamentals of microbial community resistance and resilience. Front. Microbiol. 3, 417.

Sitthi, S., Hatamoto, M., Watari, T., Yamaguchi, T., 2020. Enhancing anaerobic syntrophic propionate degradation using modified polyvinyl alcohol gel beads. Heliyon 6, e05665.

Stępień, A., Pabis, K., Sobczyk, R., Serigstad, B., 2022. High species richness and extremely low abundance of Cumacean communities along the shelf and slope of the Gulf of Guinea (West Africa). Front. Mar. Sci. 8, 703547.

Stroot, P.G., McMahon, K.D., Mackie, R.I., Raskin, L., 2001. Anaerobic codigestion of municipal solid waste and biosolids under various mixing conditions–I. digester performance. Water Res. 35 (7), 1804–1816.

Verberk, W.C.E.P., 2011. Explaining general patterns in species abundance and distributions. Nature Education Knowledge 3(10), 38.

Werner, J.J., Koren, O., Hugenholtz, P., DeSantis, T.Z., Walters, W.A., Caporaso, J.G., Angenent, L.T., Knight, R., Ley, R.E., 2012. Impact of training sets on classification of high-throughput bacterial 16s rRNA gene surveys. ISME J. 6 (1), 94–103.

Xia, Y., Chin, F.Y.L., Chao, Y., Zhang, T., 2015. Phylogeny-structured carbohydrate metabolism across microbiomes collected from different wastewater treatment process. Biotechnol. Biofuels 8, 172.

Yan, Y., Connolly, J., Liang, M., Jiang, L., Wang, S., 2021. Mechanistic links between biodiversity effects on ecosystem functioning and stability in a multi-site grassland experiment. J. Ecol. 109, 3370–3378.

Yu, N., Mou, A., Sun, H., Liu, Y. Anaerobic digestion of thickened waste activated sludge under calcium hypochlorite stress: performance stability and microbial communities. Submitted to Environ. Res. on Mar. 15, 2022 (in revision).

Zhang, L., Guo, B., Mou, A., Li, R., Liu, Y., 2020. Blackwater biomethane recovery using a thermophilic upflow anaerobic sludge blanker reactor: impacts of effluent recirculation on reactor performance. J. Environ. Manage. 274, 111157.

Zhao, X., Yang, Y., Feng, K., Wang, X., Liu, B., Xie, G., Xing, D., 2012. Self-regulating microbiome networks ensure functional resilience of biofilms in sand biofilters during manganese load fluctuations. Water Res. 188, 116473.

CHAPTER 8 FEASIBILITY ASSESSMENT OF SIMULTANEOUS PHOSPHORUS AND BIOMETHANE RECOVERY FROM BLACKWATER

A version of this chapter has been published in the *Journal of Environmental Chemical Engineering*.

8.1 Synopsis

Although struvite precipitation is a competitive method for P recovery from waste streams, the biological process offers the strongest promise for economical P recovery. Our recent studies demonstrated that simultaneous bioenergy recovery and calcium phosphate (CaP) precipitation from blackwater can be achieved in a UASB reactor (Zhang et al., 2021a; Zhang et al., 2021b). Bio-induced CaP precipitation and accumulation in anaerobic digesters represent an attractive approach to recovery P from wastewater. Typically, proteins account for 30–50% of organic contents in domestic wastewater (Yao, 2014; Alisawi, 2020). From the literature, the impact of proteins on CaP recovery during anaerobic digestion has not been elucidated. Factors that trigger the CaP nucleation in anaerobic reactors have not been elucidated.

To improve our understanding on the P recovery through CaP precipitation in anaerobic digesters, Chapter 8 aims to demonstrate the important impact of blackwater organics composition, i.e., proteins, on the development of a favorable microenvironment for the CaP mineralization in anaerobic digesters. Two 3.5 L UASB reactors fed with two types of synthetic wastewater were operated under a mesophilic condition. The feed of one reactor (G reactor) had glucose as the sole carbon source, and the feed of the other reactor (G+B reactor) had glucose (60% COD) and bovine serum albumin (BSA, 40% COD) as the combined carbon sources. The reactor performance was monitored during the operation. At the end of the operation, the sludge samples were characterized using extracellular polymeric substances (EPS) extraction, zeta potential measurement, Fourier transform infrared (FTIR) spectroscopy, and X-ray diffraction (XRD) analysis. The microbial communities developed in the two reactors were analyzed through DNA extraction and 16S rRNA gene sequencing.

8.2 Experiments and Analysis Methods

8.2.1 UASB reactor operation

Two 3.5 L UASB reactors were operated at mesophilic conditions (35 ± 2 ºC) controlled by water baths. The two reactors were fed with synthetic wastewater. The recipes for the two types of synthetic wastewater and their characteristics are shown in **Table 8–1**. Deionized water was used to prepare the synthetic wastewater. The trace mineral supplement stock was prepared based on Wolfe's formulation (ATCC, 2021). The vitamin stock contained in mg/L: 20 biotin, 100 riboflavine, 100 nicotinamide, 100 p-aminobenzoic acid, 100 thiamin, 100 panthotenic acid, 100 pyridoxamine, and 100 cyanocobalamine. One reactor (*i.e.*, G reactor) had glucose as the sole carbon source. The other reactor (*i.e.*, G+B reactor) had glucose and BSA as the carbon sources. The ratio of glucose and BSA for the feed in G+B reactor was 6:4 according to their contributions to the COD. The feeds were stored in a fridge (4 ºC) and refilled every 3 d. Both reactors were inoculated with 2.0 L digested sludge collected from a local wastewater treatment plant (Edmonton, Canada) containing volatile suspended solids (VSS) of 13.1 g/L. Both reactors had an HRT of 7.0 d and an OLR of 0.57 g COD/L/d. The reactors were operated under a steady state-state condition for 60 d. Performances and feed characteristics of the reactors were monitored every 3–6 d. The start-up stages for both reactors (24 d) were not considered in this study.

8.2.2 Chemical analysis

pH values were measured with a pH meter (SympHony B40PCID, VWR, Radnor, US). COD concentrations, TSS concentrations, and VSS concentrations were tested following the Standard Methods (Rice et al., 2017). NH_4-N concentrations were determined using a Nessler ammonia reagent set (Hach, Loveland, US). PO_4-P concentrations were measured using a Hach kit (TNT

844, Hach, Loveland, US). Ca concentrations were determined using a Hach hardness reagent set (Hach, Loveland, US). The produced biogas was collected in a 10 L foil sampling bag (Chromatographic Specialties Inc., Brockville, Canada), and its volume was measured with a syringe every 3–6 d. The biogas composition was quantified with a gas chromatography (7890B, Agilent Technologies, Santa Clara, US). The methanisation rate was calculated based on the amount of methane as COD that was converted from the feed COD, represented as g CH_4·COD/g feed COD (also as %).

Table 8-1. The feed recipes for the G reactor and the G+B reactor.

Chemicals		Characteristics	
G reactor	G+B reactor		
Glucose (100%)	Glucose (60%) BSA (40%)	COD, mg/L	4000
NaH_2PO_4		PO_4-P, mg/L	60
NH_4Cl		NH_4-N, mg/L	300
$CaCl_2$		Ca, mg/L	100
$MgCl_2·6H_2O$		Mg, mg/L	10
KCl		K, mg/L	50
$NaHCO_3$		Alkalinity, mg $CaCO_3$/L	1500
Trace mineral stock, mL/L			10
Vitamin stock, mL/L			1

8.2.3 Supersaturation index (SI)

The SI can be calculated by:

$$SI = log\left(IAP/K_{sp}\right) \quad (8–1)$$

where *IAP* is the ion activity of the associated lattice ions, and K_{sp} is the thermodynamic solubility product. When $SI>0$, the relevant compound has the potential to precipitate in the solution. When

SI<0, the relevant compound is undersaturated. For the calculation of *SI* in MINTEQ, only the inorganic compounds in the synthetic feed (see **Table 8–1**) were considered, and the organic compounds were not considered.

8.2.4 Sludge sampling

At the end of the reactor operation, sludge samples were collected from all sampling ports within the sludge bed height and then mixed well. After the TSS and VSS concentrations of the mixed sludge were determined, the sludge was divided into three parts: 5 mL sludge was used for EPS extraction, 2 mL sludge was used for DNA extraction, and 50 mL sludge was dried overnight in a fume hood at the room temperature (21 ± 0.5 ºC). The dry sludge was milled to fine particles for zeta potential measurement, functional group detection, and XRD analysis.

8.2.5 EPS extraction

The sludge EPS was extracted following the modified formaldehyde–NaOH method (Liu and Fang, 2002). Sludge with a volume of 5 mL was collected in a 15 mL polyethylene centrifuge tube, and 0.06 mL formaldehyde (36.5 wt. %) was added in the tube. The contents were mixed, and then the tube was stored at 4 °C for 1 h. After 1 h, 4 mL NaOH (1 N) was added in the tube, and the tube were stored at 4 °C for 3 h. After 3 h, the tube was centrifuged at 6,000 *g* for 20 min, and the supernatant was retained. The supernatant was filtered through a membrane filter with the pore size of 0.22 μm, and the filtrate was dialysed using a membrane tubing (3500 Dalton MWCO) for 24 h. The EPS polysaccharide content was quantified with the phenol-sulfuric acid method developed by DuBois et al. (1956). The EPS protein content was determined using a Coomassie Protein Assay Kit (Thermo Scientific, Waltham, US) (Bradford, 1976). EPS contents were tested in triplicate.

8.2.6 FTIR analysis

Specific functional groups present in the sludge were detected by an FTIR Spectrometer (Nicolet iS50, Thermo Scientific, Waltham, US). The FTIR spectra (absorbance) were recorded at the 4,000–450 cm^{-1} wavenumber region.

8.2.7 Zeta potential measurement

Zeta potential values of the sludge suspension were measured by a Zetasizer Nano apparatus (ZEN3600, Malvern Instruments Ltd., Worcestershire, UK) at the room temperature (21 ± 0.5 ºC). The sludge suspension was prepared by dispersing 1 mg fine sludge particles in 2 mL deionized water. Zeta potential values were measured in triplicate.

8.2.8 XRD analysis

Potential chemical compositions of the sludge were identified by the XRD (Ultima IV, Rigaku, Tokyo, Japan) analysis. The sludge was examined at room temperature over the scan range of 5º–90º using a Cobalt tube as the radiation source. The accelerating voltage was set at 38 kV and the current was set at 38 mA. The scan step was 0.02º and the scan speed was 2º/min. The powder diffractometer used the Bragg–Brentano geometry. Data conversion was conducted using the Jade MDI 9.6 software. The phase was identified using the DIFFRAC.EVA software based on the 2020 ICDD PDF 4+ and PDF 4+/Organics databases.

8.2.9 Microbial analysis

Centrifuge tube containing 2 mL sludge was centrifuged at 4,000 *g* for 10 min, and the supernatant was discarded. Genomic DNA was extracted from the retained sludge with a DNeasy Power-Soil Kit (QIAGEN, Hilden, Germany), according to the manufacturer's protocol. Extracted DNA

concentrations were measured with NanoDrop One (Thermo Scientific, Waltham, USA). 16S rRNA genes were amplified with the universal forward primer 515F (GTGCCAGCMGCCGCGG) and the reverse primer 806R (GGACTACHVGGGTWTCTAAT), which targeted the V4 region. Pooled PCR products were sequenced on the Illumina MiSeq platform. Sequence analyses were performed based on the DADA2 algorithm (Callahan et al., 2016) using the Qiime2 workflow (Caporaso et al., 2010). OTUs were clustered with a 99% sequence identity threshold with respect to the Greengenes database, version 13_8 (McDonald et al., 2012; Werner et al., 2012). Heatmaps were generated using the "pheatmap" package, version 1.0.12 (Kolde, 2019) in RStuido, version 3.6.3 (R Core Team, 2020).

8.3 Results

8.3.1 UASB reactor performance

The stabilized performance of the two UASB reactors, *i.e.*, G reactor and G+B reactor, are shown in **Fig. 8–1**. Compared to the pH value of the feed (7.3 ± 0.2), the pH value of the G reactor effluent varied within a range of 6.7–7.6 after AD of glucose, while the pH value of the G+B reactor effluent increased significantly (7.3–8.1) as a result of the BSA digestion [**Fig. 8–1(a)**]. The release of NH_3 from amino acids and its dissolution in water produced more NH_4^+ and OH^-, leading to the effluent pH increase in the G+B reactor. The NH_4-N concentration variations with time for both reactors can be found in **Fig. 8–2**.

As shown in **Figs. 8–1(b)** and **(c)**, the COD removal efficiencies in both reactors were higher than 90%. As compared with the G+B reactor, the G reactor achieved higher COD reduction (P value = 0.003 < 0.05) and methanisation rates (P value = 0.0002 < 0.05); which may be

attributed to the more appropriate pH for methanogens' growth in the G reactor (pH range of 6.5–7.8 has been reported to be optimum for methanogens' growth) (Fang et al., 2014). The COD mass balances in both reactors are shown in **Fig. 8–3**.

The P and Ca removals in **Figs. 8–1(d)** and **(e)** show that 16.7% PO_4-P and 20.7% Ca were removed in the G+B reactor, but none was removed in the G reactor. **Fig. 8–4** shows that the PO_4-P and Ca concentrations were stable in both reactor feeds. The average molar ratio of removed Ca and PO_4-P for the G+B reactor was 1.68 [**Fig. 8–1(f)**]. Simultaneous removal of PO_4-P and Ca has been reported in previous studies where elevated pH levels in anaerobic digesters were observed (Zhang et al., 2021a; 2021b). In these studies, high pH was thought to play a significant role in the formation of CaP precipitates in anerobic digesters. Further mechanistic studies on the fate of PO_4-P and Ca in bioreactors are introduced below.

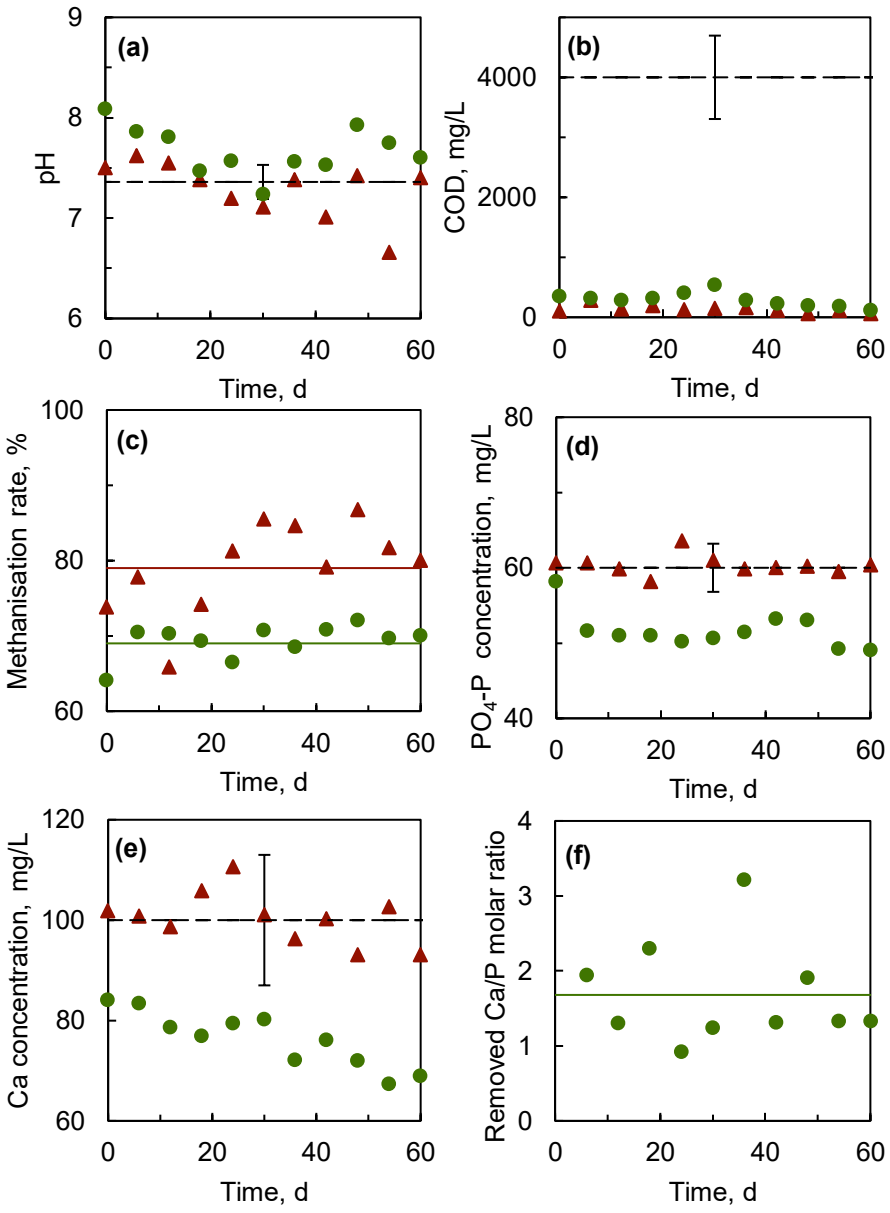

Figure 8-1. Performances of the two UASB reactors: (a) pH value, (b) COD concentration, (c) methanisation rate, (d) PO_4-P concentration, (e) Ca concentration, and (f) removed Ca/P molar ratio. The red triangles represent the performance data for the G reactor, and the green dots represent the performance data for the G+B reactor. The black dash lines in (a), (b), (d), and (e) represent the corresponding values of the feeds, and the error bars of the black dash lines represent the standard deviations. The solid lines in (c) and (f) represent the average values of the scattered data.

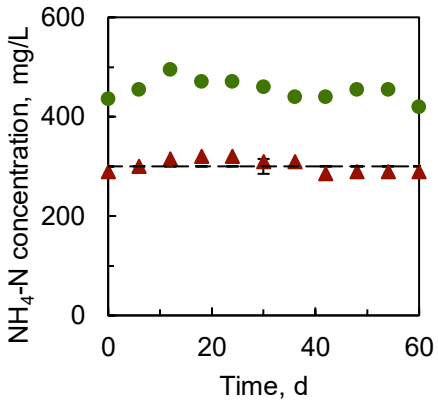

Figure 8-2. Reactor performance: NH_4-N concentration in effluent. The red triangles represent the values for the G reactor which had glucose as the sole carbon source, and the green dots represent the values for the G+B reactor which had glucose and BSA as the carbon sources. The black dash line represents the average NH_4-N concentration in the feeds for the G reactor and the G+B reactor. The error bar represents the standard deviation.

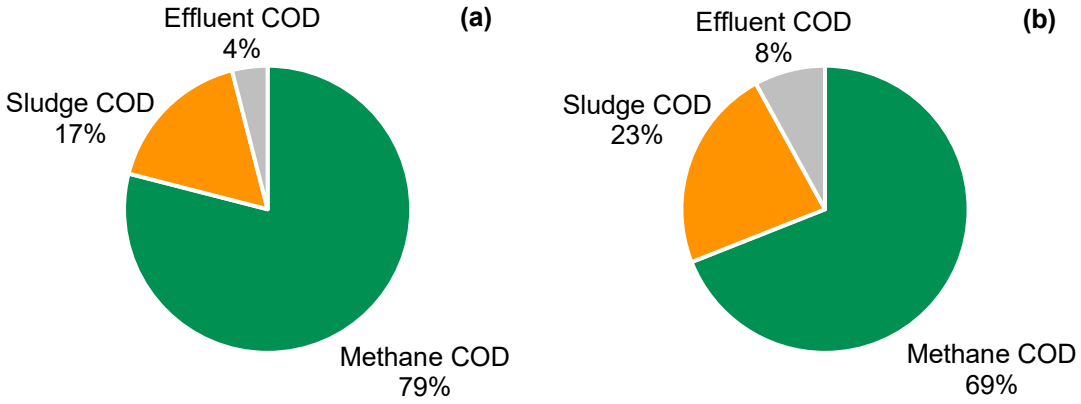

Figure 8-3. COD balance in (a) the G reactor and (b) the G+B reactor. The sludge COD includes COD accumulated in the sludge, COD in the discharged sludge, and COD lost due to the sludge washout.

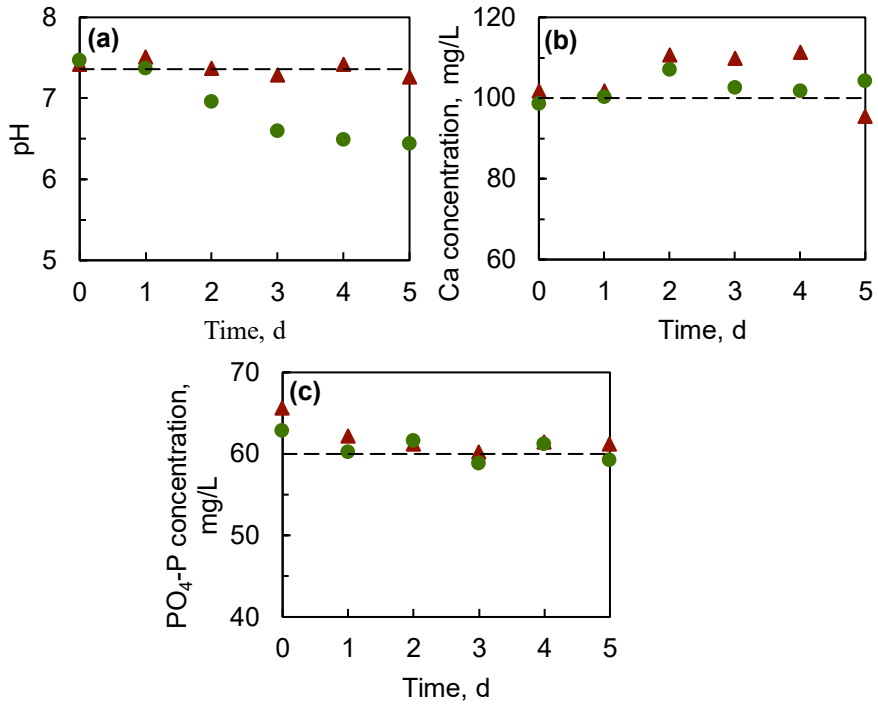

Figure 8-4. Variations of (a) pH, (b) Ca concentration, and (c) PO_4-P concentration with time in the feeds for the two reactors. The red triangles represent the values for the G reactor, and the green dots represent the values for the G+B reactor. The black dash lines represent the corresponding values which were used as the values of the feeds.

8.3.2 Sludge characterizations

The sludge characteristics of both reactors in terms of EPS contents, zeta potential, functional groups, and possible CaP species are shown in **Fig. 8–5**. EPS are complex mixture of polymers, and proteins and polysaccharides account for 70–80% of the total amount of EPS organic matters (Dignac et al., 1998). The EPS contents of the sludge in the two reactors [**Fig. 8–5(a)**] show that more proteins and polysaccharides were secreted by microbes in the G+B reactor, which was accompanied by the larger floc sizes in this reactor (**Fig. 8–6**). EPS secretion is often involved in the biomass aggregation (Liu et al., 2010; Ding et al., 2015; Cunha et al., 2018), and the higher

EPS contents in the G+B reactor may help explain the larger flocs observed. The presence of BSA as the carbon source in the G+B reactor may be correlated to the enhanced microbial EPS secretion.

The XRD pattern in **Fig. 8–5(b)** demonstrated the extracellular CaP precipitation in the G+B reactor, as well as its possible CaP species. Generally, the CaP species of interest have a Ca/P molar ratio of 0.50–2.00 (Tung, 1998). The CaP species mainly include DCPD ($CaHPO_4 \cdot 2H_2O$, Ca/P=1.00), DCP ($CaHPO_4$, Ca/P=1.00), OCP ($Ca_8H_2(PO_4)_6 \cdot 5H_2O$, Ca/P=1.33), TCP ($Ca_3(PO_4)_2$, Ca/P=1.50), HAP ($Ca_5(PO_4)_3OH$, Ca/P=1.67), and ACP ($Ca_3(PO_4)_2 \cdot xH_2O$, Ca/P=1.50). The sludge is a complex mixture, and it is difficult to identify its exact composition. Based on the molar ratio of removed Ca and P and the peaks detected by the XRD analysis [**Fig. 8–5(d)**], the CaP minerals in the G+B reactor possibly contained HAP, ACP, TCP, and $CaCO_3$.

The impact of CaP precipitation on the sludge zeta potential is shown in **Fig. 8–5(c)**. The zeta potential of sludge in the G+B reactor (-19.2 mV) was less negative than that of sludge in the G reactor (-22.1 mV), which likely arose from the neutralization of negatively charged functional groups by Ca^{2+} in the G+B reactor.

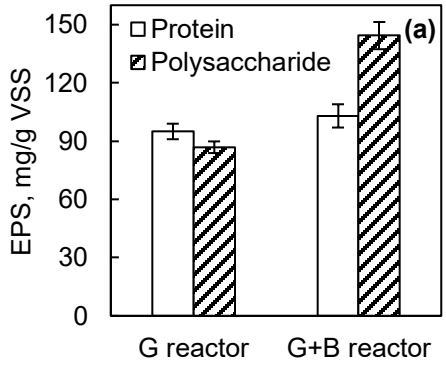

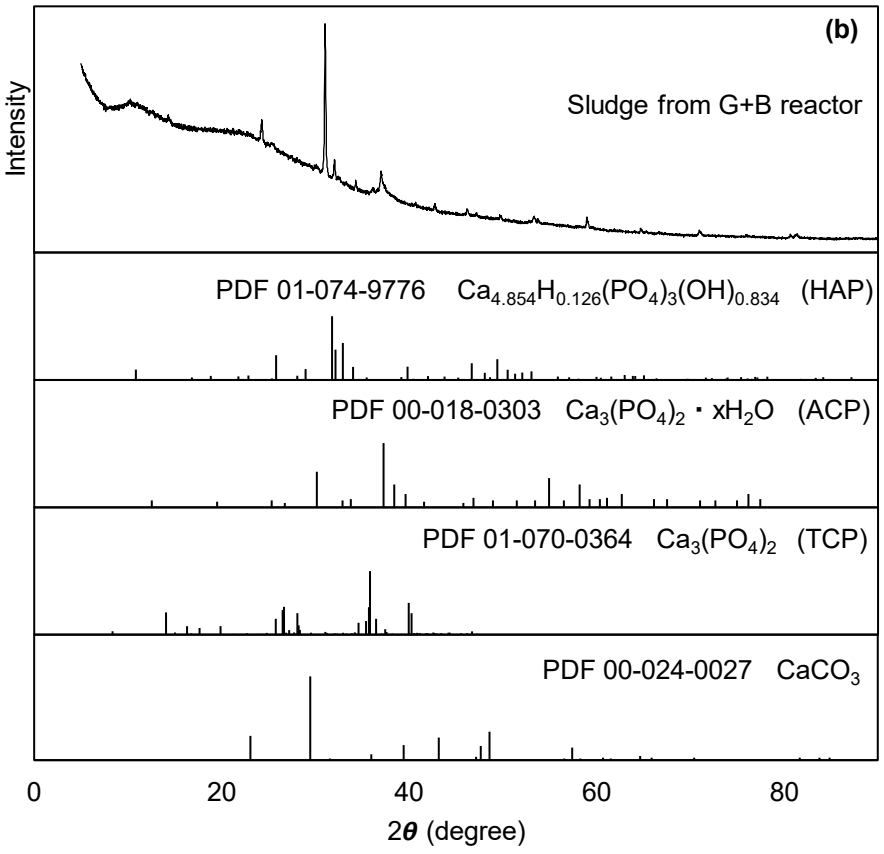
(b)
Sludge from G+B reactor
Intensity
PDF 01-074-9776 $Ca_{4.854}H_{0.126}(PO_4)_3(OH)_{0.834}$ (HAP)
PDF 00-018-0303 $Ca_3(PO_4)_2 \cdot xH_2O$ (ACP)
PDF 01-070-0364 $Ca_3(PO_4)_2$ (TCP)
PDF 00-024-0027 $CaCO_3$
0
20
40
60
80
2θ (degree)

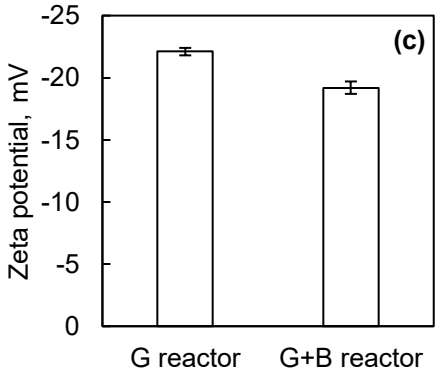
(c)
Zeta potential, mV
-25
-20
-15
-10
-5
0
G reactor
G+B reactor

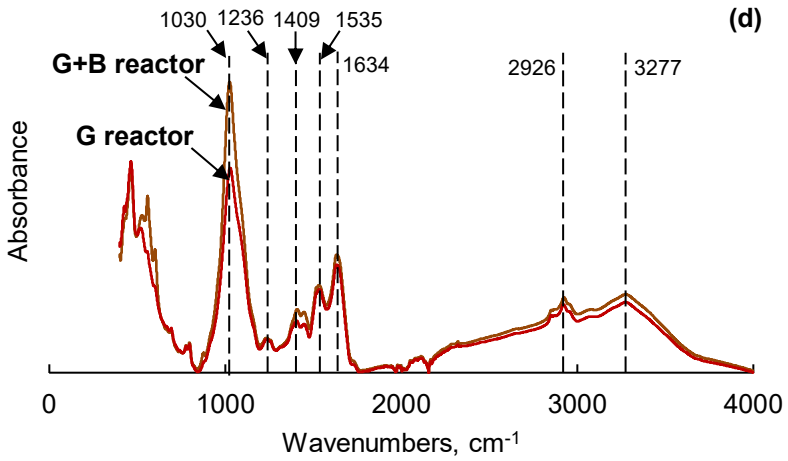

Figure 8-5. Sludge characterization for the two UASB reactors: (a) EPS contents, (b) XRD pattern, (c) zeta potential, and (d) FTIR spectra.

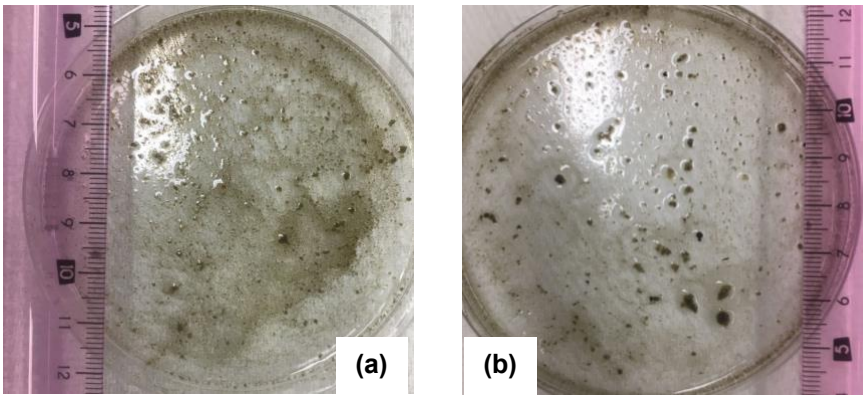

Figure 8-6. Flocs from (a) the G reactor and (b) the G+B reactor.

Further, as shown in **Fig. 8–5(d)**, the sludge in both reactors shared similar FTIR spectra. The possible stretchings including O–H (3,277 cm^{-1}), C–H (2,926 cm^{-1}), C=O (1,409 cm^{-1}), C=C (1,634 cm^{-1}), and C–O–C (1,030 cm^{-1}), and the N–H bendings (1,535 cm^{-1}, 1,236 cm^{-1}) were identified in both reactors (Cuetos et al., 2009; Wang et al., 2012; Liu et al., 2018; Lguirati et al., 2005; Carchesio et al., 2014). In the G+B reactor, these stretchings and bendings exhibited higher concentrations due to the higher peak values. It has been reported that the functional groups such

as –OH, –COOH, –NH, $–NH_2$, and –SH are responsible for the binding of metals (Javanbakht et al., 2014; Liu et al., 2018; Yang et al., 2019; Deng et al., 2019). The binding of Ca^{2+} with these relevant functional groups was likely to enrich the localized Ca in the sludge, increasing the localized supersaturation of CaP minerals and facilitating their nucleation. Although the sludge in both reactors shared similar functional groups, the P and Ca removals were only found in the G+B reactor, but not found in the G reactor. This observation may be explained by the fact that the binding of Ca^{2+} with the functional groups was affected by the concentration and the pH. At a higher pH environment, the deprotonation of the functional groups created larger active surfaces and higher availability of the groups that are able to bind Ca^{2+}, as also reported previously (Rogowska et al., 2018).

8.3.3 Microbial community analysis

Figs. 8–7 shows the richness and the relative abundances of archaeal and bacterial genera for both reactors. The more complex feed of the G+B reactor led to the richer archaeal and bacterial genera in this reactor [**Figs. 8–7(a)** and **(b)**]. *Methanolinea* (35.27%), *Methanosaeta* (29.37%), and an undefined genus of the family *WSA2* (14.62%) were the three dominant archaeal genera in the G reactor; while *Methanolinea* (37.88%), *Methanosaeta* (16.35%), an undefined genus of the family WSA2 (15.53%), and *Methanocorpusculum* (13.14%) were the four most abundance archaeal genera in the G+B reactor. *Methanolinea* is a hydrogenotrophic methanogen that utilizes H_2/CO_2 to produce methane (Sakai et al., 2012). *Methanosaeta* is an obligate acetoclastic methanogen which consumes acetate to generate methane (Smith and Ingram-Smith, 2007). The family *WSA2* is reported to be restricted to methanogenesis through methylated thiol reduction (Nobu et al., 2016). *Methanocorpusculum* is a versatile methanogen that can use both H_2/CO_2 and formate to

produce methane (KEGG, 2020). Therefore, in both reactors, the three major methanogenesis pathways, i.e., hydrogenotrophic, acetoclastic, and methylotrophic methanogenesis, coexisted.

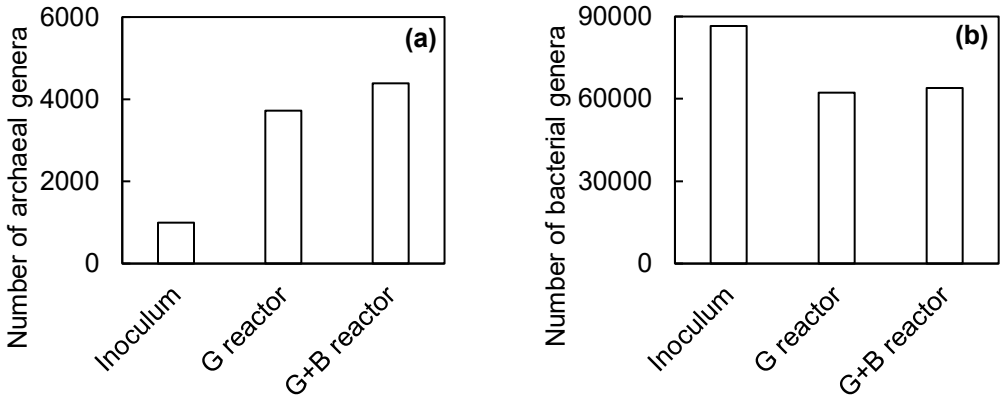

(c)

Inoculum	G reactor	G+B reactor	
6.52	35.27	37.89	Methanolinea
25.68	29.37	16.35	Methanosaeta
42.73	14.62	15.53	f_WSA2
0.00	0.75	13.14	Methanocorpusculum
6.32	3.00	7.06	o_WCHD3-30
4.01	1.31	3.23	Methanoculleus
3.61	2.31	1.59	Methanobacterium
1.20	4.59	1.48	f_Methanospirillaceae
1.91	1.74	1.23	f_[Methanomassiliicoccaceae]
2.91	1.29	0.98	Methanomassiliicoccus
0.00	0.27	0.87	Methanosphaerula
0.00	3.59	0.30	c_MBGB
1.71	0.89	0.25	o_pGrfC26
0.50	0.00	0.11	vadinCA11
0.90	0.00	0.00	Methanobrevibacter
2.01	0.64	0.00	Methanospirillum
0.00	0.35	0.00	Methanosarcina

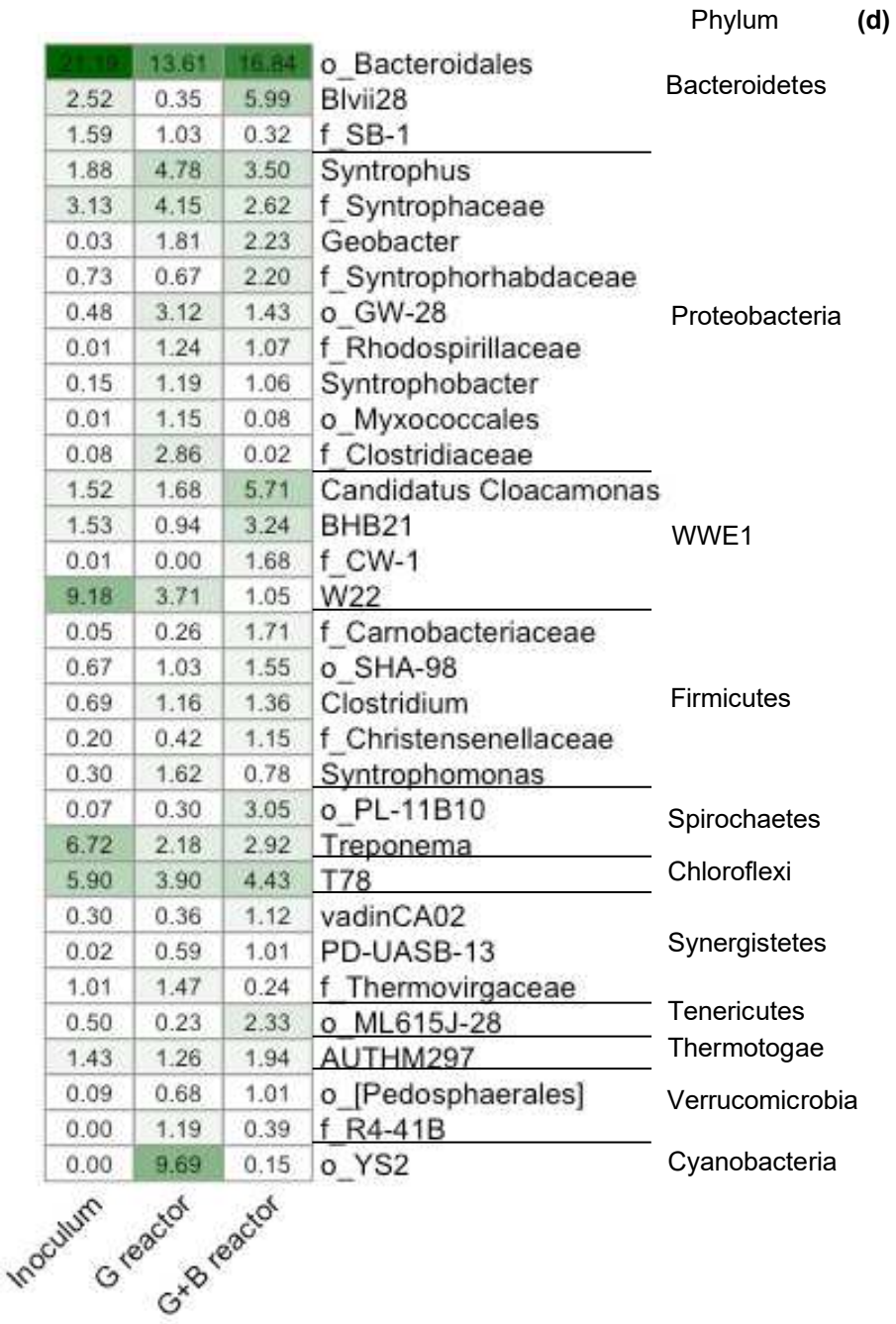

Figure 8-7. Microbial community analysis for the two UASB reactors: (a) the richness of archaeal genera, (b) the richness of bacterial genera, (c) the relative abundance of archaeal genera, and (d) the most abundant bacterial genera (relative abundance > 1%). Undefined genera were named using higher taxonomic levels such as family (f_) and order (o_).

In the bacterial genera, the microorganisms belonging to the phyla *Bacteroidetes*, *Proteobacteria*, *WWE1*, *Firmicutes*, *Spirochaetes*, and *Chloroflexi* were abundant. An undefined genus of the order *Bacteroidales* (the phylum *Bacteroidetes*) was the most abundant and accounted for 13.61% in the G reactor and 16.84% in the G+B reactor, respectively. The phylum *Bacteroidetes* consists of a broad group of microorganisms that are mainly responsible for the degradation of complex organic matters, especially in the form of proteins and carbohydrates (Thomas et al., 2011). The phyla *Bacteroidetes*, *Firmicutes*, *Proteobacteria*, and *Chloroflexi* contain most identified species of acidogenic bacteria (Venkiteshwaran et al., 2015). Syntrophic acetogenesis could play an important role in the two reactors since *Syntrophus* (4.78% in the G reactor and 3.50% in the G+B reactor), *Syntrophobacter* (1.19% in the G reactor and 1.06% in the G+B reactor), and *Candidatus Cloacamonas* (1.68% in the G reactor and 5.71% in the G+B reactor) were identified in high relative abundances. The syntrophic acetogenesis is efficient to maintain a rapid and stable anaerobic digestion process through consuming VFAs such as propionate and butyrate and producing H_2 or formate (Venkiteshwaran et al., 2015; Juste-Poinapen et al., 2015).

The metagenome and functional genes that belong to the groups of metabolism, cellular processes, genetic information processing, and environmental information processing were predicted based on the 16S rRNA gene amplicon data. The results can be found in **Fig. 8–8**. It showed that the presence of BSA in the G+B reactor promoted higher prevalence of the energy metabolism, the nucleotide metabolism, and the genetic information processing functions. The sole carbon source glucose in the G reactor led to higher prevalence of the cell motility, the membrane transport, and the signal transduction.

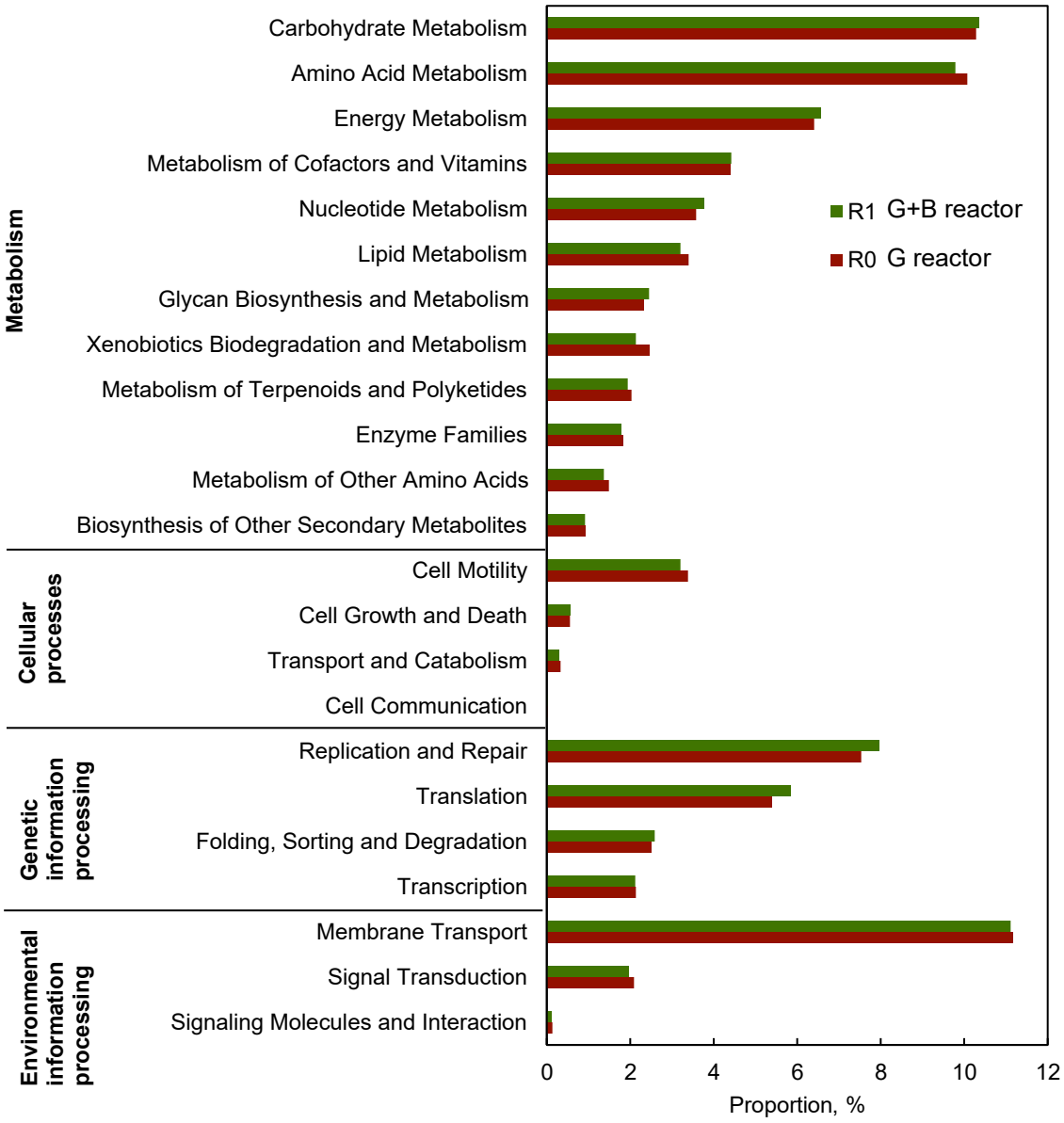

Figure 8-8. Predicted metagenome functions.

8.4 Discussion

8.4.1 A local microenvironment overcomes activation energy barriers for CaP mineral nucleation

As discussed above, the nucleation of CaP minerals must satisfy the thermodynamic and kinetic requirements (**Fig. 8–9**), including (1) the thermodynamic requirement on the supersaturation of specific CaP species (essentially same as ΔG, the difference of Gibbs free energies between a product and reactants); and (2) the kinetic energy requirement to overcome activation energy barriers for producing specific CaP species.

The supersaturation of CaP species is dependent on the chemical environment (including Ca^{2+}/PO_4^{3-}/HPO_4^{2-}/$H_2PO_4^-$ concentrations and the pH). As shown in **Table 8–2**, all the CaP species of interest (HAP, ACP, and TCP) had the SI values above 0 under the reactor operation conditions, indicating that these CaP species had the potential to precipitate upon mixing. However, CaP precipitation was observed neither in the feeding tanks (**Fig. 8–4**) nor in the G reactor, indicating that activation energy barriers must be overcome to allow CaP mineral precipitation.

Table 8-2. Supersaturation index (SI) of potential precipitates calculated based on MINTEQ.

Mineral	Formula	PH		
		6.0	7.0	8.0
HAP	$Ca_5(PO_4)_3OH$	3.58	9.46	13.83
ACP	$Ca_3(PO_4)_2 \cdot xH_2O$	<0	2.16	4.57
DCP	$CaHPO_4$	<0	0.38	0.52
TCP	$Ca_3(PO_4)_2$	<0	2.04	4.29
Calcite	$CaCO_3$	<0	0.42	1.35

The activation energy is the minimum energy required to form precipitation through bring reactant molecules together and placing them in an exactly right orientation. Generally,

accelerating the motion of molecules and increasing the frequency and force of molecule collisions help overcome the activation energy barrier. In the G+B reactor, the activation energies may be overcome through (i) the elevated pH and the increased availability of OH^- as a result of BSA fermentation, and (ii) the deprotonation of the negatively charged functional groups in the EPS due to the pH increase, which created active sites for EPS-Ca^{2+} complexation, leading to an increased local Ca concentration to trigger CaP nucleation.

To summarize, anaerobic digestion of BSA created a favorable environment that overcame activation energy barriers and enabled CaP precipitation.

8.4.2 Microbial community maintains a stabilized pH environment

The stabilized CaP mineralization also relied on the well-established microbial community in the bioreactor. The favorable pH environment can be correlated with VFA accumulation, and the timely consumption of VFAs is critical to prevent the dissociation of CaP minerals. The VFAs such as acetate, propionate, and butyrate are produced during the acidogenesis and acetogenesis stages of the anaerobic digestion process. Although acetate can be directly used by acetoclastic methanogen, other intermediates like propionate and butyrate have to be further degraded before they can be utilized by methanogens to produce methane (Venkiteshwaran et al., 2015).

The syntrophic acetogens can utilize propionate and butyrate to produce H_2 and formate (Venkiteshwaran et al., 2015; Juste-Poinapen et al., 2015), which can be further consumed by hydrogenotrophic methanogens to generate methane. The syntrophic bacteria and versatile methanogens developed in the G+B reactor are important in maintaining a stabilized pH environment for CaP mineralization.

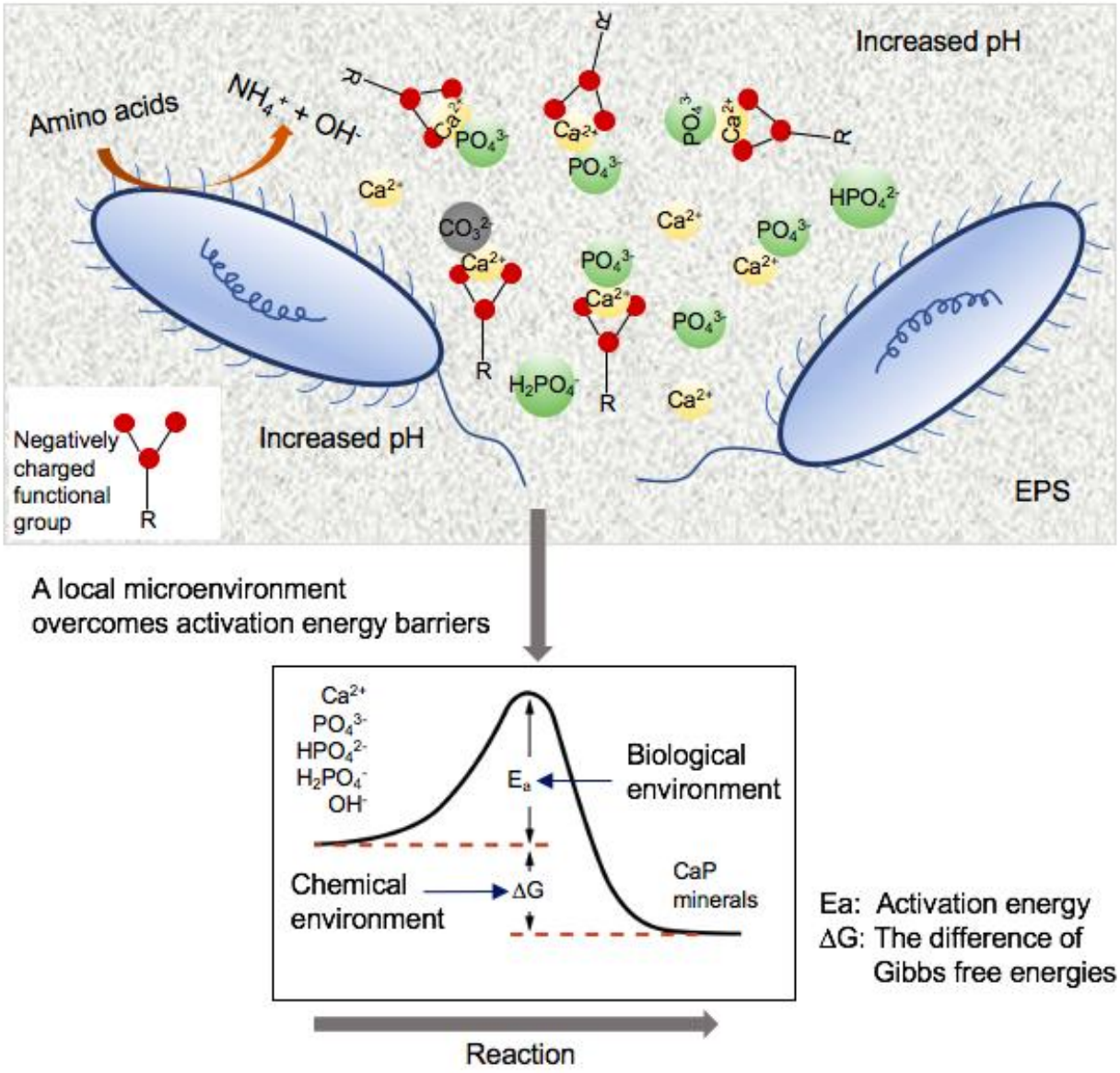

Figure 8-9. Schematic illustration of calcium phosphate mineralization in the UASB reactor (Castro-Alonso et al., 2019).

8.4.3 Implication

P is non-renewable resource and is essential to feed the growing planet. To relief the reliance on phosphate reserves, recovering P from waste sources is of particular importance. In practice, P can be recovered through various approaches such as phosphate salts precipitation, struvite

crystallization, and chemical phosphate leaching (Egle et al., 2016). The observations in this study could provide an alternative approach in enhanced CaP recovery in anerobic reactors. Source-diverted blackwater has been demonstrated to be a feasible source for CaP recovery in anaerobic digesters (Tervahauta et al., 2014; Cunha et al., 2018; Zhang et al., 2021a; Zhang et al., 2021b). Whey processing effluents and soybean protein wastewater with considerable PO_4-P and protein contents may be good sources for simultaneous recovery of biomethane and CaP. On the other hand, starch processing wastewater, low in protein contents, but with considerable PO_4-P contents, could be potential sources for P recovery through CaP precipitation if it is codigested with protein-enriched wastewater such as fishing, cheese, and poultry processing wastewater. While the ratio of different sources should be further investigated for achieving both energy and nutrient recovery efficiently and economically.

8.5 Conclusions

Chapter 8 demonstrated successfully the feasibility of recovering P and biomethane from blackwater simultaneously. It completed Objective 3.1. The present study showed the importance of protein contents on CaP mineralization in UASB reactors. In the G+B reactor, the degradation of amino acids led to elevated pH and enriched Ca concentration in EPS, which helped overcome the activation energy barriers for CaP nucleation. The stabilized CaP mineralization also relied on the well-shaped microbial community in the bioreactor. The versatile methanogenesis pathways and the presence of syntrophic acetogens could probably contribute to a stabilized pH environment to prevent the dissociation of the produced CaP minerals. In addition, the findings in this study could provide guidance on the selection of waste sources for CaP recovery economically.

Codigestion of potential waste sources and adjustment of their ratios for enhanced CaP recovery deserve further investigation.

References

Alisawi, H.A.O., 2020. Performance of wastewater treatment during variable temperature. Appl. Water Sci. 10, 89.

ATCC, 2021. Trace mineral supplement. atcc.org/products/md-tms.

Bradford, M.M., 1976. A rapid and sensitive method for the quantitation of microgram quantities of protein utilizing the principle of protein-dye binding. Anal. Biochem. 72 (1–2), 248–254.

Callahan, B.J., McMurdie, P.J., Rosen, M.J., Han, A.W., Johnson, A.M.A., Holmes, S.P., 2016. DADA2: high resolution sample inference from Illumina amplicon data. Nat. Methods 13 (7), 581–583.

Caporaso, J.G., Kuczynski, J., Stombaugh, J., Bittinger, K., Bushman, F.D., Costello, E.K., Fierer, N., Peña, A.G., Goodrich, J.K., Gordon, J.I., Huttley, G.A., Kelley, S.T., Knights, D., Koenig, J.E., Ley, R.E., Lozupone, C.A., McDonald, D., Muegge, B.D., Pirrung, M., Reeder, J., Sevinsky, J.R., Turnbaugh, P.J., Walters, W.A., Widmann, J., Yatsunenko, T., Zaneveld, J., Knight, R., 2010. QIIME allows analysis of high-throughput community sequencing data. Nat. Methods 7 (5), 335–336.

Carchesio, M., Tatàno, F., Lancellotti, I., Taurino, R., Colombo, E., Barbieri, L., 2014. Comparison of biomethane production and digestate characterization for selected agricultural substrates in Italy. Environ. Technol. 35 (17), 2212–2226.

Castro-Alonso, M.J., Montañez-Hernandez, L.E., Sanchez-Muñoz, M.A., Franco, M.R.M., Narayanasamy, R., Balagurusamy, N., 2019. Microbially induced calcium carbonate precipitation (MICP) and its potential in bioconcrete: microbiological and molecular concepts. Front. Mater. 6, 126.

Cuetos, M.J., Gómez, X., Otero, M., Morán, A., 2009. Anaerobic digestion of solid slaughterhouse waste: study of biological stabilization by Fourier Transform infrared spectroscopy and thermogravimetry combined with mass spectrometry. Biodegradation 21, 543–556.

Cunha, J.R., Tervahauta, T., van der Weijden, R.D., Temmink, H., Leal, L.H., Zeeman, G., Buisman, C.J.N., 2018. The effect of bioinduced increased pH on the enrichment of calcium phosphate in granules during anaerobic treatment of black water. Environ. Sci. Technol. 52, 13144–13154.

Deng, N., Stack, A.G., Weber, J., Cao, B., De Yoreo, J.J., Hu, Y., 2019. Organic-mineral interfacial chemistry drives heterogeneous nucleation of Sr-rich (Ba_x, Sr_{1-x})SO_4 from undersaturated solution. PNAS 116 (27), 13221–13226.

Dignac, M.-F., Urbain, V., Rybacki, D., Bruchet, A., Snidaro, D., Scribe, P., 1998. Chemical description of extracellular polymers: implication on activated sludge floc structure. Water Sci. Technol. 38 (8−9), 45−53.

Ding, Z., Bourven, I., Guibaud, G., van Hullebusch, E.D., Panico, A., Pirozzi, F., Esposito, G., 2015. Role of extracellular polymeric substances (EPS) production in bioaggregation: application to wastewater treatment. Appl. Microbiol. Biotechnol. 99 (23), 9883−9905.

DuBois, M., Gilles, K.A., Hamilton, J.K., Rebers, P.A., Smith, F., 1956. Colorimetric method for determination of sugars and related substances. Anal. Chem. 28 (3), 350−356.

Egle, L., Rechberger, H., Krampe, J., Zessner, M., 2016. Phosphorus recovery from municipal wastewater: an integrated comparative technological, environmental and economic assessment of P recovery technologies. Sci. Total Environ. 571 (2016) 522–542.

Fang, W., Zhang, P., Zhang, G., Jin, S., Li, D., Zhang, M., Xu, X., 2014. Effect of alkaline addition on anaerobic sludge digestion with combined pretreatment of alkaline and high pressure homogenization. Bioresour. Technol. 168, 167–172.

Javanbakht, V., Alavi, S. A., Zilouei, H., 2014. Mechanisms of heavy metal removal using microorganisms as biosorbent. Water Sci. Technol. 69 (9), 1775–1787.

Juste-Poinapen, N.M.S., Turner, M.S., Rabaey, K., Virdis, B., Batstone, D.J., 2015. Evaluating the potential impact of proton carriers o syntrophic propionate oxidation. Sci. Rep. 5, 18364.

KEGG, 2020. https://www.kegg.jp/kegg-bin/show_organism?org=mla.

Kolde, R., 2019. Package ‘pheatmap’. https://cran.r-project.org/package=pheatmap.

Lguirati, A., Baddi, G.A., El Mousadik, A., Gilard, V., Revel, J.C., Hafidi, M., 2005. Analysis of humic acids from aerated and non-aerated urban landfill composts. Int. Biodeterior. Biodegradation 56, 8–16.

Liu, H., Fang, H.H.P., 2002. Extraction of extracellular polymeric substances (EPS) of sludges. J. Biotechnol. 95, 249–256.

Liu, Y., Lv, W., Zhang, Z., Xia, S., 2018. Influencing characteristics of short-time aerobic digestion on spatial distribution and adsorption capacity of extracellular polymeric substances in waste activated sludge. RSC Adv. 8, 32172.

Liu, X., Sheng, G., Luo, H., Zhang, F., Yuan, S., Xu, J., Zeng, R., Wu, J., Yu, H., 2010. Contribution of extracellular polymeric substances (EPS) to the sludge aggregation. Environ. Sci. Technol. 44 (11), 4355−4360.

McDonald, D., Price, M.N., Goodrich, J., Nawrocki, E.P., DeSantis, T.Z., Probst, A., Andersen, G.L., Knight, R., Hugenholtz, P., 2012. An improved Greengenes taxonomy with explicit ranks for ecological and evolutionary analyses of bacteria and archaea. ISME J. 6 (3), 610–618.

R Core Team, 2020. R: A Language and Environment for Statistical Computing, R Foundation for Statistical Computing, Vienna, Austria.

Rice, E.W., Baird, R.B., Eaton, A.D., 2017. Standard Methods for the Examination of Water and Wastewater, 23rd edition. American Public Health Association (APHA), American Water Works Association, Water Environment Federation (WEF), Washington, DC, USA.

Rogowska, A., Pomastowski, P., Złoch, M., Railean-Plugaru, V., Król, A., Rafińska, K., Szultka-Młyńska, M., Buszewski, B., 2018. The influence of different pH on the electrophoretic behaviour of *Saccharomyces cerevisiae* modified by calcium ions. Sci. Rep. 8, 7261.

Sakai, S., Ehara, M., Tseng, I.-C., Yamaguchi, T., Bräuer, S. L., Cadillo-Quiroz, H., Zinder, S.H., Imachi, H., 2012. Methanolinea mesophila sp. nov., a hydrogenotrophic methanogen isolated from

rice field soil, and proposal of the archaeal family Methanoregulaceae fam. Nov. within the order Methanomicrobiales. Int. J. Syst. Evol. Microbiol. 62 (Pt 6), 1389–1395.

Smith, K.S., Ingram-Smith, C., 2007. *Methanosaeta*, the forgotten methanogen? Trends Microbiol. 15 (4), 150–155.

Tervahauta, T., van der Weijden, R.D., Flemming, R.L., Leal, L.H., Zeeman, G., Buisman, C.J.N., 2014. Calcium phosphate granulation in anerobic treatment of black water: a new approach to phosphorus recovery. Water Res. 48, 632–642.

Thomas, F., Hehemann, J.-H., Rebuffet, E., Czjzek, M., Michel, G., 2011. Environmental and gut *Bacteroidetes*: the food connection. Front. Microbiol. 2, 93.

Tung, M. S., 1998. Calcium phosphates: structure, composition, solubility, and stability, in: Amjad, Z. (Ed.), Calcium Phosphates in Biological and Industrial Systems. Springer, New York.

Venkiteshwaran, K., Bocher, B., Maki, J., Zitomer, D., 2015. Relating anaerobic digestion microbial community and process function. Microbiol Insights 8 (Suppl 2), 37–44.

Wang, L., Wang, L., Ren, X., Ye, X., Li, W., Yuan, S., Sun, M., Sheng, G., Yu, H., Wang, X., 2012. pH dependence of structure and surface properties of microbial EPS. Environ. Sci. Technol. 46, 737–744.

Werner, J.J., Koren, O., Hugenholtz, P., DeSantis, T.Z., Walters, W.A., Caporaso, J.G., Angenent, L.T., Knight, R., Ley, R.E., 2012. Impact of training sets on classification of high-throughput bacterial 16s rRNA gene surveys. ISME J. 6 (1), 94–103.

Yang, X., Wan, Y., Zheng, Y., He, F., Yu, Z., Huang, J., Wang, H., Ok, Y.S., Jiang, Y., Gao, B., 2019. Surface functional groups of carbon-based adsorbents and their roles in the removal of heavy metals from aqueous solutions: a critical review. Chem. Eng. J. 366 (15), 608–621.

Yao, Y., 2014. Use of Carbohydrate, Protein and Fat to Characterise Wastewater in terms of Its Major Elemental Constituents and Energy. University of Manchester, UK.

Zhang, L., Mou, A., Guo, B., Sun, H., Anwar, M.N., Liu, Y., 2021a. Simultaneous phosphorus recovery in energy generation reactor (SPRING): high rate thermophilic blackwater treatment. Resour. Conserv. Recycl. 164, 105163.

Zhang, L., Mou, A., Sun, H., Zhang, Y., Zhou, Y., Liu, Y., 2021b. Calcium phosphate granules formation: key to high rate of mesophilic UASB treatment of toilet wastewater. Sci. Total Environ. 773, 144972.

CHAPTER 9 THE ROLE OF PROTEIN CONTENTS IN PROMOTING PHOSPHORUS AND BIOMETHANE RECOVERY FROM BLACKWATER

A version of this chapter has been published in the *Biomass and Bioenergy*.

9.1 Synopsis

In comparison to blackwater, food processing wastewater like those from dairy, beverage, and fish-processing industry contains even higher protein contents (Duong et al., 2019). Protein-rich wastewater have outstanding biogas-producing potential, but it is usually challenging to handle protein-rich substrates in anaerobic digestion (AD) processes due to slow degradation, inefficient hydrolysis, unbalanced C/N ratio, foaming, and biomass washout (Kovács et al., 2013; Lin et al., 2018; Duong et al., 2019). If these issues could be solved, protein-rich wastewater would be extremely valuable for resource recovery because in addition to high protein content, they may also contain large quantities of nutrients such as P and Ca.

The role of proteins in P and bioenergy recovery from wastewater has not been well understood. Following Chapter 8, Chapter 9 aims to further examine the impact of feedwater protein content on CaP and biomethane production in AD processes. Four 1.0 L UASB reactors fed with different types of synthetic feeds were operated for 90 d under a mesophilic condition. According to the contributions of carbon sources to the COD, the four feeds comprised carbon sources of 100% glucose, 75% glucose + 25% bovine serum albumin (BSA), 50% glucose + 50% BSA, and 100% BSA, respectively. The effects of BSA content on pH change, Ca and P removals, and methane production were measured, and the community structures built at different BSA contents were identified.

9.2 Experimental Procedure and Analysis

9.2.1 UASB reactor operation

Four 1.0 L UASB reactors (R1, R2, R3, and R4) were operated under the mesophilic condition (35 ± 2 ºC) controlled by the water baths. Each reactor was fed with one of four types of synthetic feeds based on the percentage of the organic's COD in the feed's total COD: R1: 100% glucose, R2: 75% glucose + 25% BSA, R3: 50% glucose + 50% BSA, and R4: 100% BSA (**Table 9–1)**. Deionized water was used to prepare the synthetic feeds. The trace mineral stock in **Table 9–1** was prepared based on the Wolfe's formulation (ATCC, 2021). The vitamin supplement in **Table 9–1** contained, in mg/L: 20 biotin, 100 riboflavine, 100 nicotinamide, 100 p-aminobenzoic acid, 100 thiamin, 100 panthotenic acid, 100 pyridoxamine, and 100 cyanocobalamine. The four feeds were stored at 4 ºC and refilled every 2 d.

The digested sludge was collected from a local wastewater treatment plant (Edmonton, Canada). The reactors were each inoculated with 0.7 L digested sludge with a volatile suspended solid (VSS) concentration of 9.5 g/L. The reactors had a hydraulic retention time (HRT) of 3.6 d and an organic loading rate (OLR) of 1.1 g COD/L/d. The reactors were operated at a stabilized state for 90 d. The feed and effluent characteristics (pH value, COD concentration, Ca concentration, and PO_4-P concentration) and the methane production were monitored every 3 d. The startup periods (21 d) were not considered in the analysis.

9.2.2 Chemical analysis

The feed and effluent COD concentrations and the sludge VSS concentrations in the four reactors were tested following the Standard Methods (Rice et al., 2017). The feed and effluent Ca concentrations were tested using a Hach hardness reagent set (Hach, Loveland, US). The feed and

effluent pH values were measured with a pH meter (SympHony B40PCID, VWR, Radnor, US). The feed and effluent PO_4-P concentrations were determined using a Hach kit (TNT 844, Hach, Loveland, US). The generated biogas was collected in a 10 L foil sampling bag (Chromatographic Specialties Inc., Brockville, Canada), and its volume was measured every 3 d with a syringe. The biogas composition was identified with a gas chromatography (7890B, Agilent Technologies, Santa Clara, US). The methanisation rate was calculated based on the percentage of the feed's COD that was converted to the methane's COD, represented as % (also as g CH_4 COD/g feed COD).

Table 9-1. The feed recipes for the four reactors (R1, R2, R3, and R4).

Chemicals					Characteristics	
	R1	R2	R3	R4		
Glucose, %COD	100	75	50	0	COD, mg/L	4070.6± 185.0
BSA, %COD	0	25	50	100		
NaH_2PO_4					PO_4-P, mg/L	60.0±2.9
NH_4Cl					NH_4-N, mg/L	306.1±12.0
$CaCl_2$					Ca, mg/L	52.1±3.2
$MgCl_2 \cdot 6H_2O$					Mg, mg/L	10.0±0.7
KCl					K, mg/L	51.3±2.2
$NaHCO_3$					Alkalinity, mg $CaCO_3$/L	990.5±74.8
Trace mineral stock, mL/L						10
Vitamin stock, mL/L						1

9.2.3 Statistical analysis

All results are expressed as the mean value ± standard deviation. Single factor analysis of variance (ANOVA) was performed using Microsoft Excel® to determine the differences between the four reactors' effluent quality. A P-value less than 0.05 indicates statistically significant differences.

9.2.4 Sludge sampling and microbial analysis

At the end of the reactor operation, sludge samples of each reactor were collected from all sampling ports within the sludge bed and then mixed well. The mixed sludge (1.5 mL) was centrifuged at 4000 *g* for 10 min, and the supernatant was discarded. Genomic DNA was extracted from the retained sludge with a DNeasy Power-Soil Kit (QIAGEN, Hilden, Germany), according to the manufacturer's protocol. The extracted DNA concentrations were measured with NanoDrop One (Thermo Scientific, Waltham, USA). 16S rRNA genes were amplified using the universal primer pair 515F (GTGCCAGCMGCCGCGG) and 806R (GGACTACHVGGGTWTCTAAT). The pooled PCR products were sequenced on the Illumina MiSeq platform. The data sets generated by 16S rRNA gene amplicon sequencing were deposited in the NCBI Sequence Read Archive under the accession number PRJNA802873. Sequence analyses were performed based on the DADA2 pipeline (Callahan et al., 2016) using the Qiime2 workflow (Caporaso et al., 2010). OTUs were clustered with 99% similarity with reference to the Greengenes database, version 13_8 (McDonald et al., 2012; Werner et al., 2012). Heatmaps were generated using the "pheatmap" package, version 1.0.12 (Kolde, 2019) in RStuido, version 3.6.3 (R Core Team, 2020). Alpha diversity represented by the Shannon diversity index and beta diversity based on the principal coordinates analysis (PCoA) were calculated using the "vegan" package, version 2.5.7 (Oksanen et al., 2019). Predicted

metagenome and functional genes were determined using the Phylogenetic Investigation of Communities by Reconstruction of Unobserved States (PICRUSt) (Langille et al., 2013).

9.3 Results

9.3.1 UASB reactor performance

The performance of the four UASB reactors (after the startup phase), R1 (0% BSA), R2 (25% BSA), R3 (50% BSA), and R4 (100% BSA), is shown in **Fig. 9–1**. All reactors removed more than 90% COD (P-value = 0.01) [**Fig. 9–1(a)**]. A 25% BSA content in the R2 feed contributed to the highest methanisation rate (82.7% ± 5.6%). The feed COD mass balance for the four reactors can be found in Fig. **9–2**. A higher BSA content in the feed led to reduced methane production [**Fig. 9–1(b)**].

Compared to the feed pH value of the four reactors (7.3 ± 0.3), the pH value of R1 effluent did not change too much and varied around 7.2 (± 0.3). In comparison, the effluent pH values increased significantly to 7.8 ± 0.4, 7.9 ± 0.3, and 8.0 ± 0.2, for R2, R3, and R4, respectively (P-value = 0) [**Fig. 9–1(c)**]. The pH changes from the reactor feeds to the effluents showed that, in comparison to the feed without BSA, the presence of BSA in the feed significantly raised the effluent pH, and an increase in the BSA content brought about a slight effluent pH increment. As stated in previous studies (Lin et al., 2018), the release of free ammonia (NH_3) from the amino acid degradation and the dissolution of NH_3 in water that produces ammonium (NH_4^+) and OH^- may have caused the effluent pH increases in R2, R3, and R4. The effluent NH_4-N concentrations for the four reactors are shown in **Fig. 9–3**. In addition, the effluent pH value did not increase linearly with the BSA content, which may be explained by H^+ produced from the degradation of

amino acids present in the BSA (represented by $N_xH_yNO_z$) and the equilibrium between NH_3 and NH_4^+, as shown in the reactions below.

$$N_xH_yNO_z + H_2O \rightarrow CH_3COO^- + H^+ + NH_3 + CO_2 + H_2$$

$$CO_2 + H_2O \leftrightarrow HCO_3^- + H^+$$

$$NH_3 + H_2O \leftrightarrow NH_4^+ + OH^-$$

The Ca and P removals [**Figs. 9–1(d)** and **9–1(e)**] show that the highest CaP production was achieved in R4, followed by R3 and R2. The Ca and P removal efficiency was positively related to the pH increment in the reactor. Compared to the Ca concentration in the reactor feed (52.1 ± 3.2 mg/L), the effluent Ca concentrations of R1, R2, R3, and R4 were 50.9 ± 3.3, 41.0 ± 4.3, 38.0 ± 2.9, and 35.6 ± 3.1 mg/L, respectively (P-value =0). The feed P concentration of the four reactors was 60.0 ± 2.9 mg/L, and the effluent P concentrations of R1, R2, R3, and R4 were 59.2 ± 2.9, 51.9 ± 1.6, 49.4 ± 2.6, and 47.9 ± 2.5 mg/L, respectively (P-value =0). A higher pH increase brought about more Ca and P removals during the AD.

The removed Ca and P molar ratio (Ca/P) for R2, R3, and R4 was 1.1 ± 0.4 (P-value = 0.998) at the current low Ca concentration (52.1 ± 3.2 mg/L), shown in **Figs. 9–1(f)**. The CaP produced from anaerobic digesters includes $Ca_{10}(PO_4)_6(OH)_2$ (HAP), $Ca_3(PO_4)_2{\bullet}xH_2O$ (ACP), $Ca_3(PO_4)_2$ (TCP), $CaHPO_4$ (DCP), etc. (Daneshgar et al., 2018). The composition of produced CaP varies with pH, Ca concentration, P concentration, and temperature. In previous studies that produced CaP from blackwater with high Ca concentrations (100–250 mg/L) and high P concentrations (50–210.6 mg/L) (Cunha et al., 2018; Zhang et al., 2021), the removed Ca/P varied from 1.0 to 1.68.

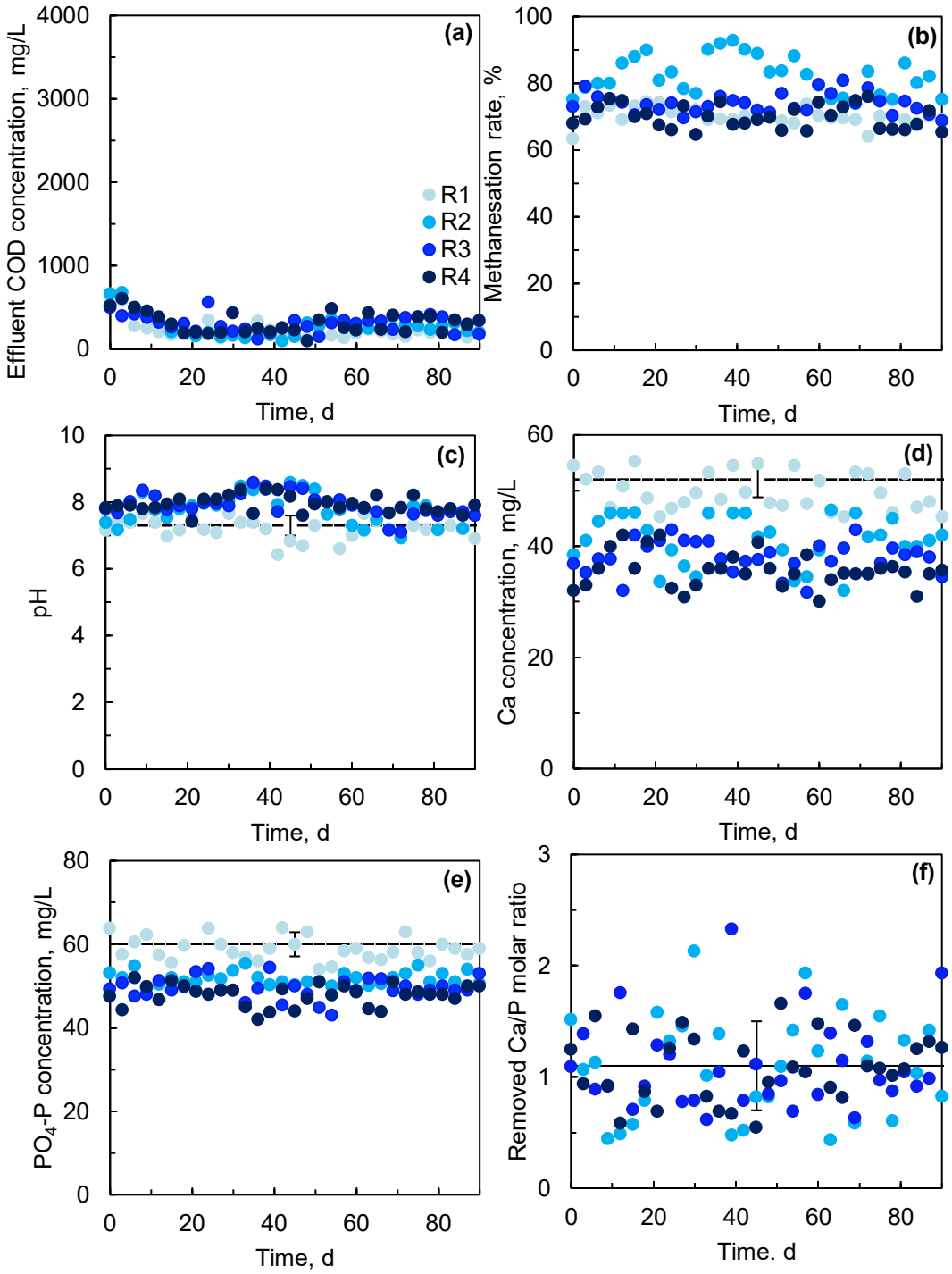

Figure 9-1. Performance of R1 (0% BSA), R2 (25% BSA), R3 (50% BSA), and R4 (100% BSA): (a) effluent COD concentration, (b) methanisation rate, (c) pH value, (d) Ca concentration, (e) PO_4-P concentration, and (f) removed Ca/P molar ratio. The dots represent the performance data for the effluent [(a), (c), (d) and (e)] or biogas (b). The solid lines in (c), (d) and (e) represent the corresponding values of the feeds, and the solid line in (f) represents the average value. The error bars of the solid lines represent the standard deviations. The legends of the six figures are the same as shown in (a).

Two mechanisms underlie the CaP precipitation that is induced by the protein degradation. One mechanism is the enhanced supersaturation condition for CaP species created by the pH elevation in the reactor. The hydrolysis of proteins brings about the pH increase. In the hydrolysis of proteins, hydroxyl ions are generated. When a hydroxyl ion is released from a reaction as a final product or an intermediate, it can be rapidly consumed by another reaction and not be reflected in the effluent characteristics. The dynamic biological reaction is difficult to capture or measure, while it helps build a local environment that facilitates the CaP precipitation. The other mechanism is the localized supersaturation condition for CaP species arising from the enriched Ca due to the complexation of Ca^{2+} and extracellular polymeric substances (EPS).

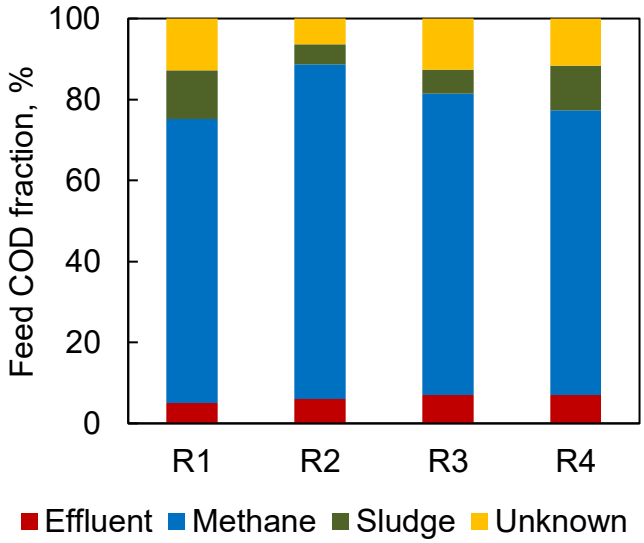

Figure 9-2. The feed COD mass balance for the four reactors.

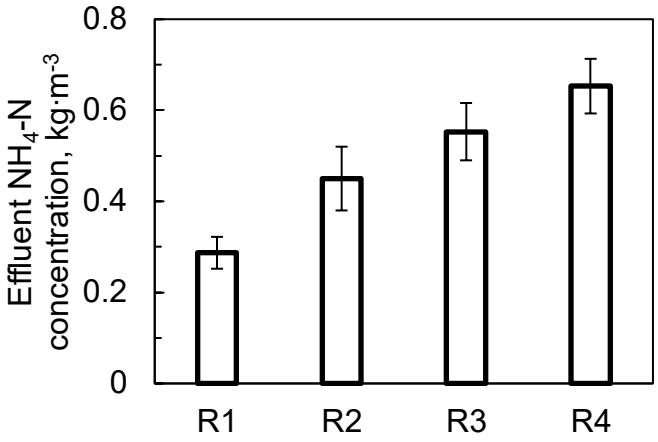

Figure 9-3. The effluent NH_4-N concentrations for the four reactors.

9.3.2 Microbial community analysis

Figs. 9–4 shows the richness and the diversity of microbial communities identified in the four reactors. As shown in **Fig. 9–4(a)**, R2 had the richest archaea and bacteria, which was in accordance with the highest methane production from R2. The microbial community diversity depends both the substrate type and the environmental factor (Hiibel et al., 2011; Wu et al., 2018). In a low stress environment, all reactors fed with either the simple substrate (in R1 and R4) or the complex substrate (in R2 and R3) performed well. The beta diversity calculated based on the PcoA in **Figs. 9–4(c)** and **9–4(d)** illustrated that the archaeal and bacterial communities were clustered into individual groups, and the clustering pattern was in close relation with the high methanogenesis efficiency of the four reactors (Yu et al., 2020).

Fig. 9–5 presents the relative abundances of archaeal and bacterial genera in the communities of the four reactors. As shown in **Fig. 9–5(a)**, *Methanosaeta* dominated the archaeal communities of the four reactors, with the relative abundances of 57.61%, 81.02%, 47.06%, and

41.91% in R1, R2, R3, and R4, respectively. An undefined genus of the family *Methanospirillaceae* (24.02%), *Methanobacterium* (12.98%), *Methanocorpusculum* (26.70%), and *VadinCA11* (24.88%) were the next abundant genera in R1, R2, R3, and R4, respectively. The acetoclastic and methylotrophic methanogenesis dominated in R1 and R4 which were fed with the single carbon sources. The acetoclastic and hydrogenotrophic methanogenesis dominated in R2 and R3 which were fed with the mixed carbon sources.

Fig. 9–5(b) shows that although the abundant bacterial genera varied among the four reactors, the dominant bacterial groups fell into several phyla, including *Firmicutes*, *Bacteroidetes*, *Proteobacteria*, and *Synergistetes* [**Fig. 9–5(c)**]. In R1 (0% BSA), the genera belonging to the phyla *Firmicutes* (30.12%), *Bateroidetes* (10.22%), and *Proteobacteria* (10.05%) were the most prevalent. In R2 (25% BSA), the genera belonging to the phylum *Synergistetes* alone comprising 44.23% of the bacteria, and *Proteobacteria* and *Firmicutes* accounted 15.35% and 11.80%, respectively. In R3 (75% BSA), members of the phylum *Bacteroidetes* (29.3%) were dominant, followed by *Synergistetes* (14.17%) and *WWE1* (13.66%). In R4 (100% BSA), the most abundant phyla were *Bacteroidetes* (25.48%), *Proteobacteria* (20.70%), and *Synergistetes* (17.83%). Species of the phyla *Bacteroidetes* and *Synergistetes* are known to play prominent roles in protein and/or amino acid degradation (Tang et al., 2005; Militon et al., 2015). *Firmicutes* and *Bacteroidetes* communities have been found to be robust during the digestion of substrates like casein, starch and cream in biogas-producing reactors (Kampmann et al., 2012); however, their competition, quantified by the population abundance ratio of *Firmicutes* to *Bacteroidetes* (F/B ratio), has been reported to be an indicator of AD process performance, such as the methane generation (Chen et al., 2016). The prevalence of acidogenic fermentative populations of Bacteroidetes usually indicates the volatile fatty acid accumulation and, consequently, inhibits the

methane production. In contrast, the relative abundance of Firmicutes was positively correlated with the methane production (Chen et al., 2016). Therefore, a higher F/B ratio would suggest greater methane production. R2 had the highest F/B ratio (26.2) and accounted for the greatest methane production. The F/B ratio decreased at both lower and higher BSA concentrations, leading to lower methane production in R1, R3, and R4 compared to R2. The high methane production in R2 was also related to the highest prevalence of *Synergistetes*. *Synergistetes* have been shown to utilize acetate (Ito et al., 2011). The presence of *Synergistetes* and *Methanosaeta* was likely linked to an efficient utilization of acetate to produce methane in R2.

The metagenome and functional genes involved in metabolism, cellular processes, genetic information processing, and environmental information processing were predicted based on the 16S rRNA gene amplicon data, shown in **Fig. 9–6**. **Fig. 9–6** indicates that BSA (present in R2, R3, and R4) promoted a higher prevalence of almost all types of metabolism except carbohydrate metabolism. R2 (75% glucose + 25% BSA) had the highest prevalence of amino acid metabolism, cell motility, signal transduction, and predicted methane metabolism.

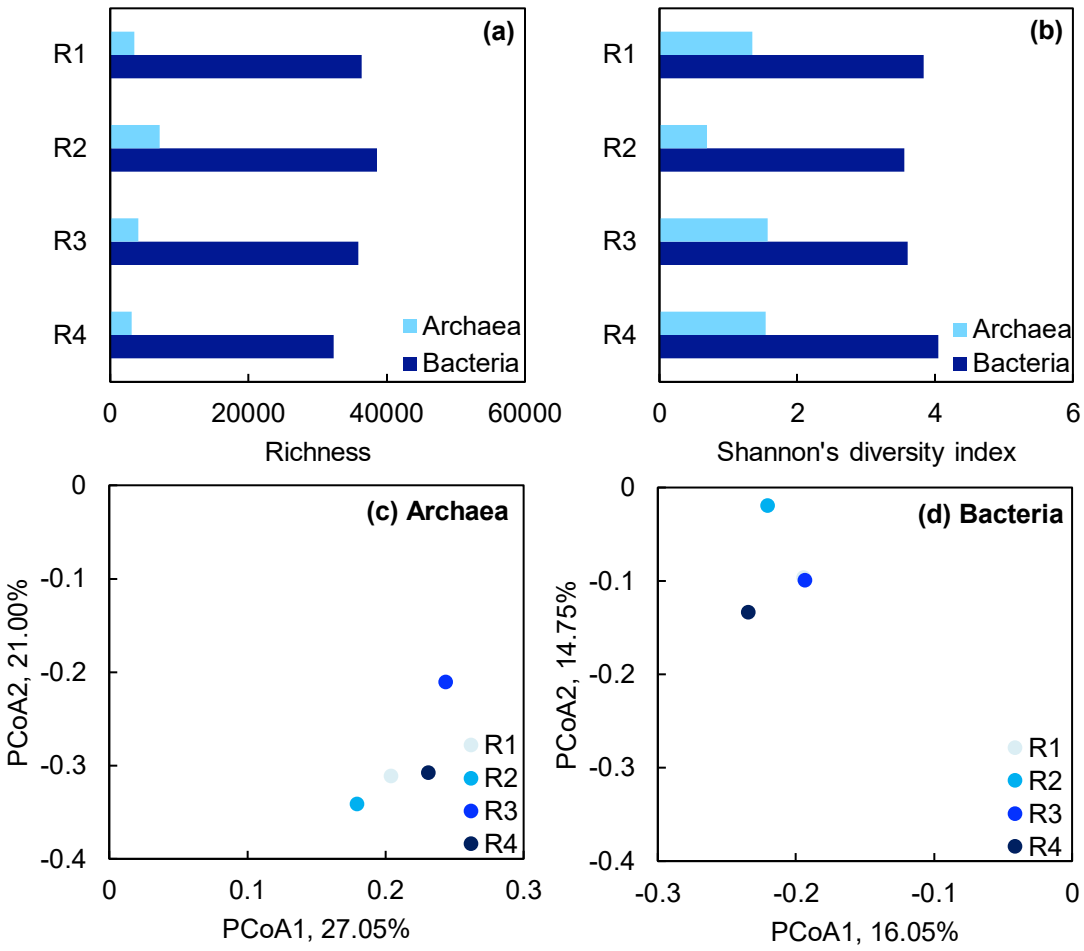

Figure 9-4. Microbial community richness and diversity for R1 (0% BSA), R2 (25% BSA), R3 (50% BSA), and R4 (100% BSA): (a) community richness indicated by the number of genera, (b) alpha diversity represented by the Shannon's diversity index, (c) beta diversity of archaeal community based on the PCoA, and (d) beta diversity of bacterial community based on the PCoA.

(a)

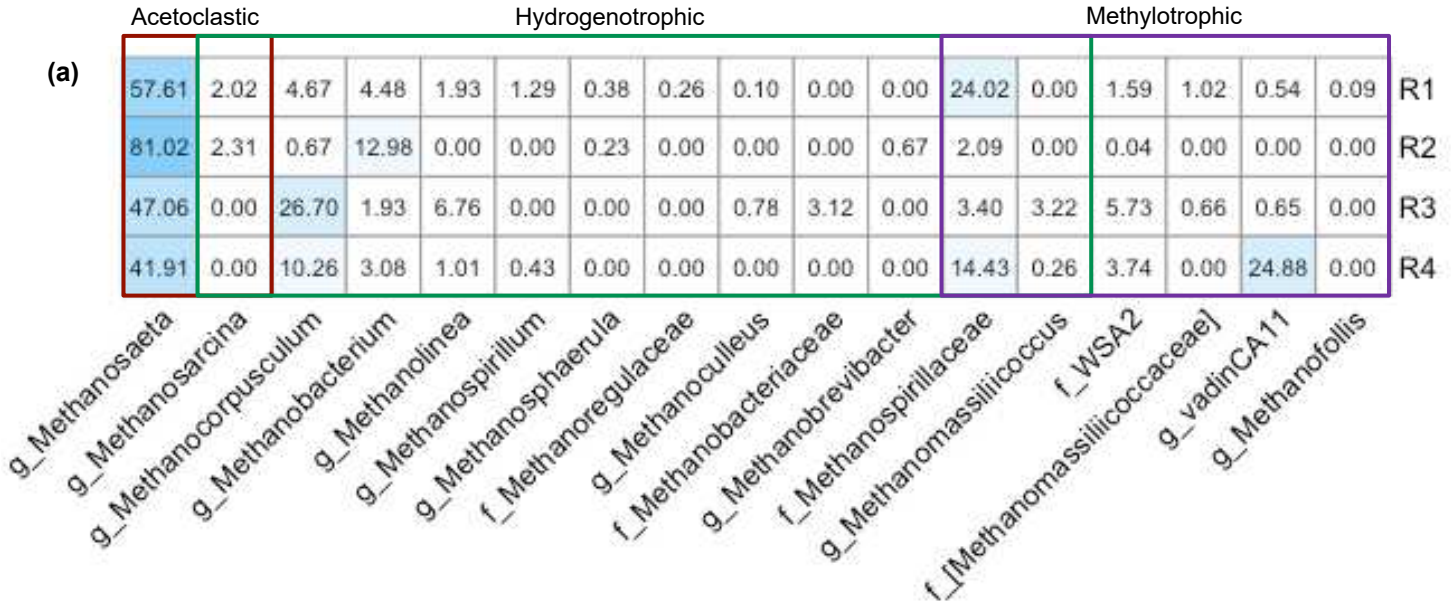
Acetoclastic
Hydrogenotrophic
Methylotrophic
57.61 2.02 4.67 4.48 1.93 1.29 0.38 0.26 0.10 0.00 0.00 24.02 0.00 1.59 1.02 0.54 0.09 R1
81.02 2.31 0.67 12.98 0.00 0.00 0.23 0.00 0.00 0.00 0.67 2.09 0.00 0.04 0.00 0.00 0.00 R2
47.06 0.00 26.70 1.93 6.76 0.00 0.00 0.00 0.78 3.12 0.00 3.40 3.22 5.73 0.66 0.65 0.00 R3
41.91 0.00 10.26 3.08 1.01 0.43 0.00 0.00 0.00 0.00 0.00 14.43 0.26 3.74 0.00 24.88 0.00 R4
g_Methanosaeta
g_Methanosarcina
g_Methanocorpusculum
g_Methanobacterium
g_Methanolinea
g_Methanospirillum
g_Methanosphaerula
f_Methanoregulaceae
g_Methanoculleus
f_Methanobacteriaceae
g_Methanobrevibacter
f_Methanospirillaceae
g_Methanomassiliicoccus
f_WSA2
f_[Methanomassiliicoccaceae]
g_vadinCA11
g_Methanofollis

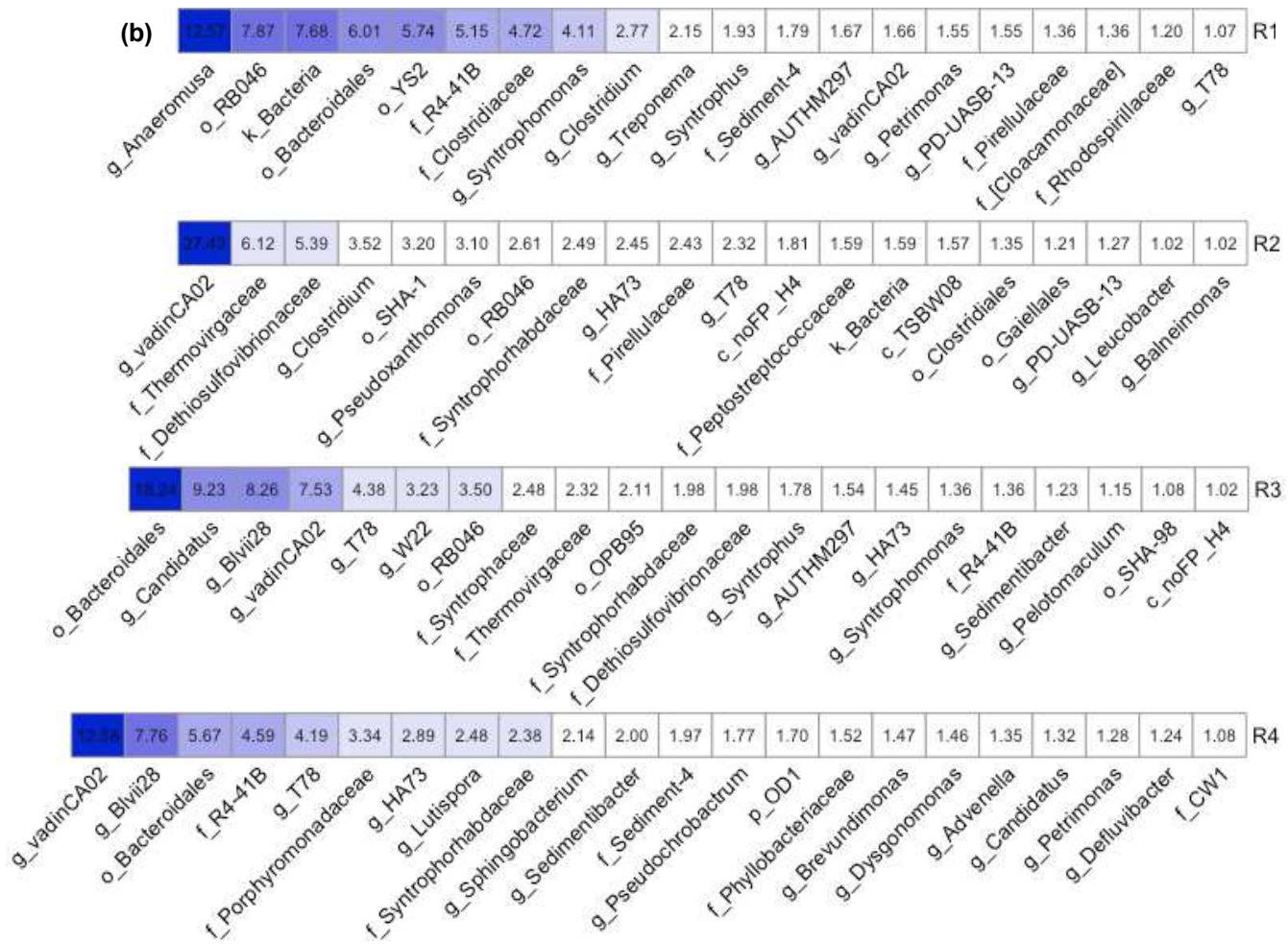
(b)
12.57 7.87 7.68 6.01 5.74 5.15 4.72 4.11 2.77 2.15 1.93 1.79 1.67 1.66 1.55 1.55 1.36 1.36 1.20 1.07 R1
g_Anaeromusa o_RB046 k_Bacteria o_Bacteroidales o_YS2 f_R4-41B f_Clostridiaceae g_Syntrophomonas g_Clostridium g_Treponema g_Syntrophus f_Sediment-4 g_AUTHM297 g_vadinCA02 g_Petrimonas g_PD-UASB-13 f_Pirellulaceae f_[Cloacamonaceae] f_Rhodospirillaceae g_T78
27.43 6.12 5.39 3.52 3.20 3.10 2.61 2.49 2.45 2.43 2.32 1.81 1.59 1.59 1.57 1.35 1.21 1.27 1.02 1.02 R2
g_vadinCA02 f_Thermovirgaceae f_Dethiosulfovibrionaceae g_Clostridium o_SHA-1 g_Pseudoxanthomonas o_RB046 f_Syntrophorhabdaceae g_HA73 f_Pirellulaceae g_T78 c_noFP_H4 f_Peptostreptococcaceae k_Bacteria c_TSBW08 o_Clostridiales o_Gaiellales g_PD-UASB-13 g_Leucobacter g_Balneimonas
19.24 9.23 8.26 7.53 4.38 3.23 3.50 2.48 2.32 2.11 1.98 1.98 1.78 1.54 1.45 1.36 1.36 1.23 1.15 1.08 1.02 R3
o_Bacteroidales g_Candidatus g_Blvii28 g_vadinCA02 g_T78 g_W22 o_RB046 f_Syntrophaceae f_Thermovirgaceae o_OPB95 f_Syntrophorhabdaceae f_Dethiosulfovibrionaceae g_Syntrophus g_AUTHM297 g_HA73 g_Syntrophomonas f_R4-41B g_Sedimentibacter g_Pelotomaculum o_SHA-98 c_noFP_H4
12.84 7.76 5.67 4.59 4.19 3.34 2.89 2.48 2.38 2.14 2.00 1.97 1.77 1.70 1.52 1.47 1.46 1.35 1.32 1.28 1.24 1.08 R4
g_vadinCA02 g_Blvii28 o_Bacteroidales f_R4-41B g_T78 f_Porphyromonadaceae g_HA73 g_Lutispora f_Syntrophorhabdaceae g_Sphingobacterium g_Sedimentibacter f_Sediment-4 g_Pseudochrobactrum p_OD1 f_Phyllobacteriaceae g_Brevundimonas g_Dysgonomonas g_Advenella g_Candidatus g_Petrimonas g_Defluvibacter f_CW1

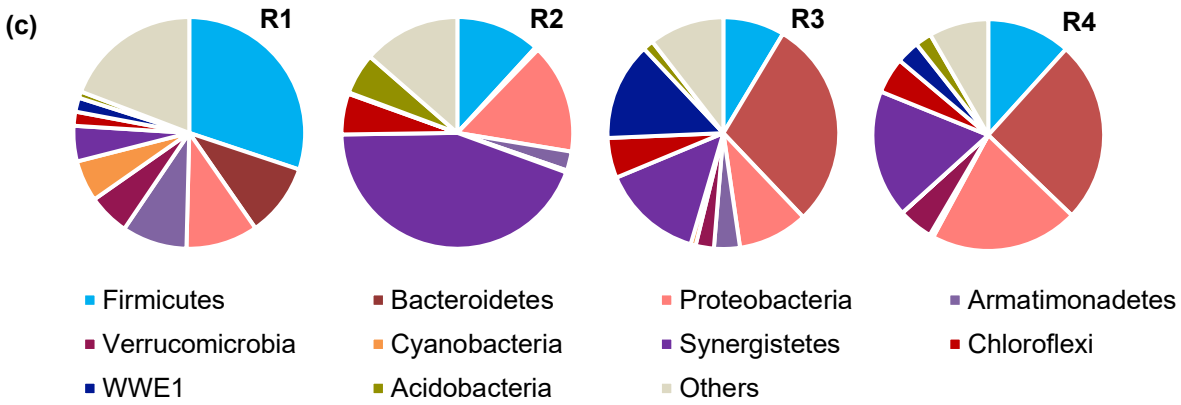

Figure 9-5. Microbial community analysis for R1 (0% BSA), R2 (25% BSA), R3 (50% BSA), and R4 (100% BSA): (a) the relative abundances (%) of archaeal genera, (b) the most abundant bacterial genera (individual relative abundance > 1%), and (c) bacterial groups classified based on phylum and their percentages of the total bacterial community. Genera were named using the taxonomic levels such as genus (g_), family (f_) order (o_), class (c_), and kingdom (k_).

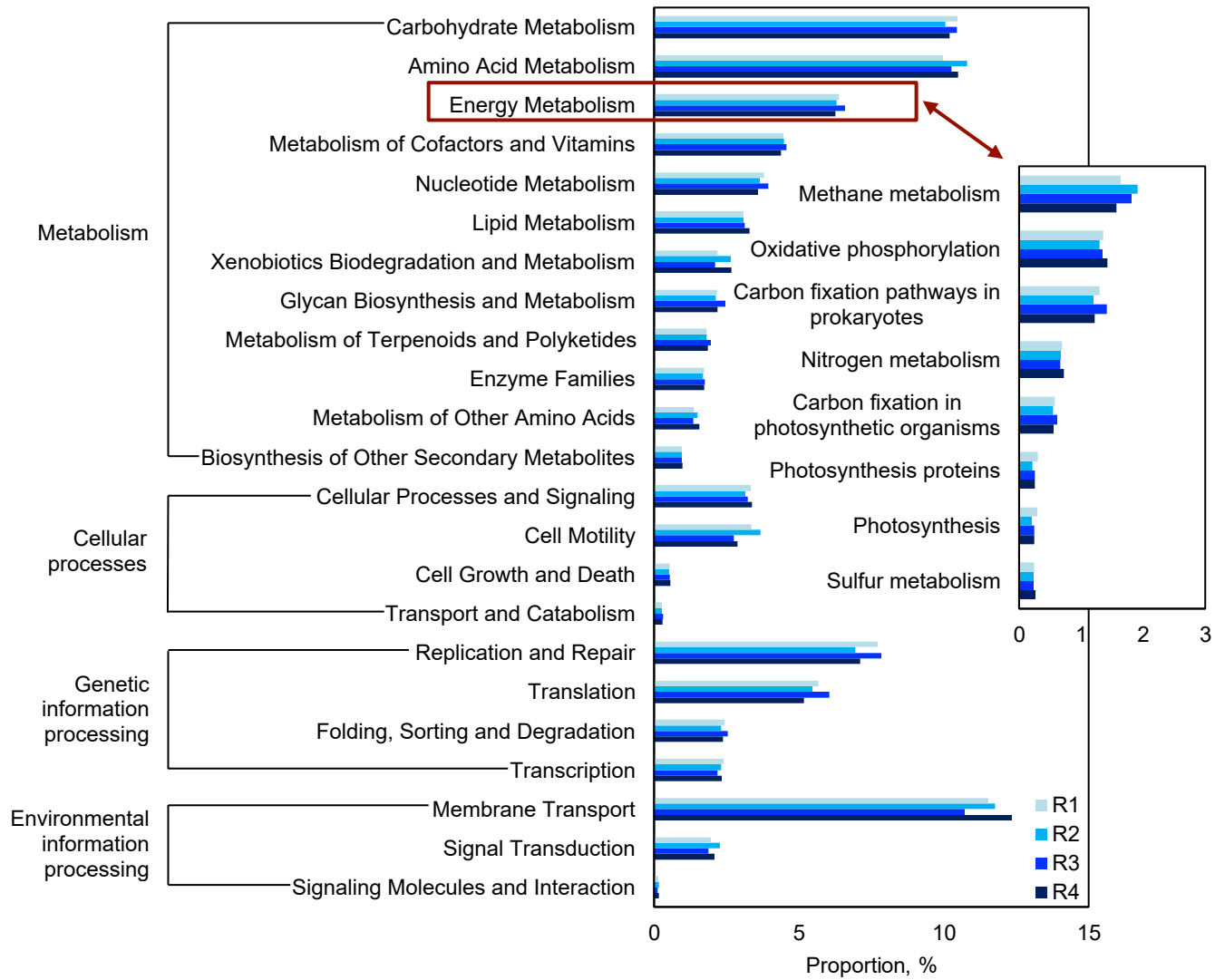

Figure 9-6. Predicted metagenome functions for R1 (0% BSA), R2 (25% BSA), R3 (50% BSA), and R4 (100% BSA).

9.4 Implication

The Ca and P concentrations used in this study are representative for a range of wastewater types such as blackwater (de Graaff et al., 2010; Tervahauta et al., 2014). In comparison to the studies that focused on the CaP precipitation facilitated by the high Ca concentration (Szogi et al., 2018) or the Ca addition (Cunha et al., 2018), this study demonstrated that the CaP precipitation is possible even under the low Ca (52.1 mg/L) and P (60.0 mg/L) concentration conditions. The CaP production does not only rely on a high Ca concentration or Ca addition, but also depends on the feedstock and other factors like the operational condition and the reactor configuration. An alternative is to achieve an optimum feedstock to create a localized supersaturation condition to facilitate the CaP precipitation at low P and Ca concentration conditions. A bio-induced pH elevation can trigger the CaP precipitation at a low or even below supersaturation requirement. The reactors with higher BSA concentrations had higher protein degradation and thus higher pH levels, therefore greater CaP production. However, due to the production of protons and the equilibrium between free ammonia and ammonium, the pH increment is limited even for a feed with a very high BSA content.

The total ammonia nitrogen/free ammonia nitrogen with a high concentration generated from a high-content BSA feed might adversely impact the AD process stability and reduce the methane production (Morozova et al., 2020). The C/N ratio of substrates has been recognized to be one of the most important factors affecting the total ammonia nitrogen/free ammonia nitrogen accumulation and the methane production. An optimum C/N ratio of 15–32 is usually recommended for an AD process (Kovács, 2013; Morozova et al., 2020; Wang et al., 2014). According to the molecular weight of BSA (66430.3 Da) and its 583 amino acid residues (Hirayama et al., 1990; Huang et al., 2018), the theoretical C/N ratios in R2, R3, and R4 feeds,

calculated with Eq. (9–1), were 15.3, 7.2, and 3.2, respectively. The R2 feed, consisting of 25% BSA and 75% glucose, had the optimum C/N ratio for maximized methane production. However, whether the C/N ratio is very important for the biomethane yield is questionable. Previous studies (Kovács, 2015; Guarino et al., 2016) demonstrated that even at a wide range of the C/N ratio (*e.g.*, 9–50), the biomethane yield was not affected. Some other factors like the COD-based percentage of individual organic in substrates rather than the C/N ratio alone might deserve further study. Further analysis demonstrated that the R2 feed helped shape a microbial community favorable for the energy recovery through efficient acetate utilization. The co-digestion of various waste streams of different natures could potentially enhance the P recovery and maximize the biogas production.

$$C/N = \frac{W_{\text{glucose}} \times C_{\text{glucose}} + W_{\text{BSA}} \times C_{\text{BSA}}}{W_{\text{BSA}} \times N_{\text{BSA}}} \quad (9\text{–}1)$$

where W_{glucose} and W_{BSA} were the weight of glucose and BSA (g VS), respectively. C_{glucose}, C_{BSA}, and N_{BSA} were the organic carbon content in glucose, organic carbon content in BSA, and nitrogen content in BSA (g/g VS), respectively.

Although the present study focused on the CaP precipitation from wastewater with low Ca and P concentrations, the observation can be useful when evaluating the CaP precipitation from wastewater with high Ca and P concentrations, as the localized supersaturation also exists under these conditions. In addition to proteins, other organics such as urea (Zhang et al., 2021) can also lead to a pH increase after the hydrolysis. CaP precipitation and energy recovery from wastewater can be efficient and economical through the co-digestion of streams containing considerable P and Ca and complex organic constituents. The anaerobic degradation of organics such as proteins and urea provides a moderate to high pH, which, together with Ca^{2+} and $PO_4^{3-}/HPO_4^{2-}/H_2PO_4^-$, could induce a favorable chemical environment for enhanced CaP production. The anaerobic degradation

of organics with proportional proteins could also create a biological environment for efficient methanogenesis. Co-digestion of targeted waste streams can provide efficient and economical P and energy recovery and promote sustainable waste management, while the ratio of these streams deserves further study.

9.5 Conclusions

Chapter 9 explored the role of feedwater protein content in the simultaneous biomethane production and CaP precipitation in a UASB reactor. It completed Objective 3.2. The hydrolysis of BSA in the reactor feed increased the pH, creating a local environment that triggered the CaP precipitation under a low supersaturation condition; however, the pH elevation was limited even at 100% BSA content. A BSA content of 25% created a microbial community favorable for the methanogenesis, mainly through the acetate utilization, and led to the greatest methane production. This study contributes to the process design and operation of anaerobic digesters for enhanced biomethane and P recovery by clarifying the impact of feedstock characteristics.

References

ATCC, 2021. Trace mineral supplement. atcc.org/products/md-tms (Accessed 5 June 2021).

Callahan, B.J., McMurdie, P.J., Rosen, M.J., Han, A.W., Johnson, A.M.A., Holmes, S.P., 2016. DADA2: high resolution sample inference from Illumina amplicon data. Nat. Methods 13 (7), 581–583.

Caporaso, J.G., Kuczynski, J., Stombaugh, J., Bittinger, K., Bushman, F.D., Costello, E.K., Fierer, N., Peña, A.G., Goodrich, J.K., Gordon, J.I., Huttley, G.A., Kelley, S.T., Knights, D., Koenig, J.E., Ley, R.E., Lozupone, C.A., McDonald, D., Muegge, B.D., Pirrung, M., Reeder, J., Sevinsky, J.R., Turnbaugh, P.J., Walters, W.A., Widmann, J., Yatsunenko, T., Zaneveld, J., Knight, R., 2010. QIIME allows analysis of high-throughput community sequencing data. Nat. Methods 7 (5), 335–336.

Chen, S., Cheng, H., Wyckoff, K.N., He, Q., 2016. Linkages of Firmicutes and Bacteroidetes populations to methanogenic process performance. J. Ind. Microbiol. 43 (6), 771–781.

Cunha, J.R., Schott, C., van der Weijden, R.D., Leal, L.H., Zeeman, G., Buisman, C., 2018. Calcium addition to increase the production of phosphate granules in anaerobic treatment of black water. Water Res. 130, 333–342.

Daneshgar, S., Buttafava, A., Capsoni, D., Callegari, A., Capodaglio, A. G., 2018. Impact of pH and ionic molar ratios on phosphorus forms precipitation and recovery from different wastewater sludges. Resources 7 (4), 71.

de Graaff, M.S., Temmink, H., Zeeman, G., Buisman, C.J.N., 2010. Anaerobic treatment of concentrated black water in a UASB reactor at a short HRT. Water 2, 101–119.

Duong, T.H., Grolle, K., Nga, T.T.V., Zeeman, G., Temmink, H., van Eekert, M., 2019. Protein hydrolysis and fermentation under methanogenic and acidifying conditions. Biotechnol. Biofuels 12, 254.

Eisenhauer, N., Scheu, S., Jousset, A., 2012. Bacterial diversity stabilizes community productivity. PLoS One 7(3), e34517.

Guarino, G., Carotenuto, C., di Cristofaro, F., Papa, S., Morrone, B., Minale, M., 2016. Does the C/N ratio really affect the bio-methane yield? a three years investigation of buffalo manure digestion. Chem. Eng. Trans. 49, 463–468.

Hiibel, S.R., Pereyra, L.P., Breazeal, M.V.R., Reisman, D.V., Reardon, K.F., Pruden, A., 2011. Effect of organic substrate on the microbial community structure in pilot-scale sulfate-reducing biochemical reactors treating mine drainage. Environ. Eng. Sci. 28 (8), 563–572.

Hirayama, K., Akashi, S., Furuya, M., Fukuhara, K., 1990. Rapid confirmation and revision of the primary structure of bovine serum albumin by ESIMS and frit-FAB LC/MS. Biochem. Biophys. Res. Commun. 173 (2), 639–646.

Huang, Z., Gengenbach, T., Tian, J., Shen, W., Garnier, G., 2018. Effect of bovine serum albumin treatment on the aging and activity of antibodies in paper diagnostics. Front. Chem. 6, 161.

Ito, T., Yoshiguchi, K., Ariesyady, H.D., Okabe, S., 2011. Identification of a novel acetate-utilizing bacterium belonging to Synergistes group 4 in anaerobic digester sludge. ISME J. 5(12), 1844–1856.

Kampmann, K., Ratering, S., Kramer, I., Schmidt, M., Zerr, W., Schnell, S., 2012. Unexpected stability of Bacteroidetes and Firmicutes communities in laboratory biogas reactors fed with different defined substrates. App. Environ. Microbiol. 78 (7), 2016–2119.

Kehrein, P., van Loosdrecht, M., Osseweijer, P., Garfí, M., Dewulf, J., Posada, J., 2020. A critical review of resource recovery from municipal wastewater treatment plants-market supply potentials, technologies and bottlenecks. Environ. Sci.: Water Res. Technol. 6, 877.

Kolde, R., 2019. Package ‘pheatmap’. https://cran.r-project.org/package=pheatmap.

Kovács, E., Wirth, R., Maróti, G., Bagi, Z., Nagy, K., Minárovits, J., 2015. Augmented biogas production from protein-rich substrates and associated metagenomic changes. Bioresour. Technol. 178, 254–261.

Kovács, E., Wirth, R., Maróti, G., Bagi, Z., Rákhely, G., Kovács, K.L., 2013. Biogas production from protein-rich biomass: fed-batch anaerobic fermentation of casein and of pig blood and associated changes in microbial community composition. PLoS one 8 (10), e77265.

Langille, M.G., Zaneveld, J., Caporaso, J.G., McDonald, D., Knights, D., Reyes, J.A., Clemente, J.C., Burkepile, D.E., Vega Thurber, R.L., Knight, R., Beiko, R.G., Huttenhower, C., 2013. Predicted functional profiling of microbial communities using 16S rRNA marker gene sequences. Nat. Biotechnol. 31 (9), 814–821.

Lin, R., Deng, C., Cheng, J., Xia, A., Lens, P.N.L., Jackson, S.A., Dobson, A.D.W., Murphy, J.D., 2018. Graphene facilitates biomethane production from protein-derived glycine in anaerobic digestion. iScience 10, 158–170.

McDonald, D., Price, M. N., Goodrich, J., Nawrocki, E. P., DeSantis, T. Z., Probst, A., Andersen, G. L., Knight, R., Hugenholtz, P., 2012. An improved Greengenes taxonomy with explicit ranks for ecological and evolutionary analyses of bacteria and archaea. ISME J. 6 (3), 610–618.

Militon, C., Hamdi, O., Michotey, V., Fardeau, M.-L., Ollivier, B., Bouallagui, H., Hamdi, M., Bonin, P., 2015. Ecological significance of Synergistetes in the biological treatment of tuna cooking wastewater by an anerobic sequencing batch reactor. Environ. Sci. Pollut. Res. Int. 22, 18230–18238.

Morozova, I., Nikulina, N., Oechsner, H., Krümpel, J., Lemmer, A., 2020. Effects of increasing nitrogen content on process stability and reactor performance in anaerobic digestion. Energies 13(5), 1139.

Oksanen, J., Blanchet, F.G., Friendly, M., Kindt, R., Legendre, P., McGlinn, D., Minchin, P.R., O'Hara, R. B., Simpson, G.L., Solymos, P., Stevens, M.H.H., Szoecs, E., Wagner, H., 2019. Vegan: Community Ecology Package.

Puyol, D., Batstone, D.J., Hülsen, T., Astals, S., Peces, M., Krömer J.O., 2017. Resource recovery from wastewater by biological technologies: opportunities, challenges, and prospects. Front. Microbiol. 7, 2016.

R Core Team, 2020. R: A Language and Environment for Statistical Computing. R Foundation for Statistical Computing, Vienna, Austria.

Rice, E.W., Baird, R.B., Eaton, A.D., 2017. Standard Methods for the Examination of Water and Wastewater, 23rd edition. American Public Health Association (APHA), American Water Works Association, Water Environment Federation (WEF), Washington, DC, USA.

Royal Society of Chemistry. BSA. http://www.chemspider.com/Chemical-Structure.4523073.html, 2022 (Accessed 3 January 2022).

Szogi, A.A., Vanotti, M.B., Shumaker, P.D., 2018. Economic recovery of calcium phosphates from swine lagoon sludge using quick wash process and geotextile filtration. Front. Sustain. Food Syst. 2, 37.

Tang, Y., Shigematsu, T., Morimura, S., Kida, K., 2005. Microbial community analysis of mesophilic anaerobic protein degradation process using bovine serum albumin (BSA)-fed continuous cultivation. J. Biosci. Bioeng. 99, 150–164.

Tervahauta, T., van der Weijden, R.D., Flemming, R.L., Leal, L.H., Zeeman, G., Buisman, C.J.N., 2014. Calcium phosphate granulation in anaerobic treatment of black water: a new approach to phosphorus recovery. Water Res. 48, 632–642.

Wang, X., Lu, X., Li, F., Yang, G., 2014. Effects of temperature and carbon-nitrogen (C/N) ratio on the performance of anaerobic co-digestion of dairy manure, chicken manure and rice straw: focusing on ammonia inhibition. PLoS One 9(5), e97265.

Werner, J.J., Koren, O., Hugenholtz, P., DeSantis, T.Z., Walters, W.A., Caporaso, J.G., Angenent, L.T., Knight, R., Ley, R.E., 2012. Impact of training sets on classification of high-throughput bacterial 16s rRNA gene surveys. ISME J. 6 (1), 94–103.

Wu, Z., Liu, Q., Li, Z., Cheng, W., Sun, J., Guo, Z., Li, Y., Zhou, J., Meng, D., Li, H., Lei, P., Yin, H., 2018. Environmental factors shaping the diversity of bacterial communities that promote rice production. BMC Microbiology 18, 51.

Yu, N., Guo, B., Zhang, Y., Zhang, L., Zhou, Y., Liu, Y., 2020. Different micro-aeration rates facilitate production of different end-products from source-diverted blackwater. Water Res. 177, 115783.

Zhang, L., Mou, A., Guo, B., Sun, H., Anwar, M.N., Liu, Y., 2021. Simultaneous phosphorus recovery in energy generation reactor (SPRING): high rate thermophilic blackwater treatment. Resour. Conserv. Recycl. 164, 105163.

CHAPTER 10 CONCLUSIONS AND RECOMMENDATIONS

10.1 Overview

Nutrient such as P and N and energy recovery from wastewater is one of the targets of next-generation wastewater treatment plant. The geological P availability, socio-economic and environmental vulnerabilities, and future P crisis drive the P recovery from waste streams to relieve the dependence of phosphate rock reserves (Alewell et al., 2020). P can be recovered from wastes in different forms through chemical or bio-induced chemical precipitation. To achieve efficient P recovery, the chemical addition is usually applied. The use of chemicals will greatly increase the operating cost. An efficient and economical P recovery is required for sustainable wastewater management.

Aiming at achieving efficient and economical P and bioenergy recovery from wastewater, this thesis mainly studied the P and biomethane recovery directly from blackwater. Specifically, it tested the feasibility of recovering P through struvite precipitation and simultaneously recovering P through CaP precipitation and biomethane from blackwater. This thesis also studied the impact of one important operational condition, mixing, on biomethane recovery from synthetic blackwater in a UASB reactor. First, the feasibility of producing struvite from concentrated blackwater without alkali addition was examined. The purity and heavy-metal contents of produced struvite were assessed. The impact of TSS concentration of blackwater on struvite purity and size was studied. Second, the impact of effluent recirculation strategy on biomethane production in a UASB reactor treating synthetic blackwater of different solid contents was assessed. The hydrolysis

efficiency of particulate organic matter was calculated. The involved microbial community's evolution and dynamic shift was identified. An ecology model, based on a non-steady-state mass balance (16S rRNA MiSeq reads normalized by volatile suspended solids), was developed to quantify microbiome responses to disturbances in the UASB reactor treating blackwater. Finally, as a typical content in blackwater, proteins' role in simultaneous P and bioenergy recovery was examined.

10.2 Conclusions

The results drawn from this thesis demonstrated that raw concentrated blackwater is an economically-viable and environmentally-sustainable waste source for P recovery through both struvite precipitation and bio-induced CaP precipitation. The major conclusions are summarized as follows.

Feasibility of P recovery through struvite precipitation from raw blackwater

The feasibility of P recovery through struvite precipitation from raw concentrated blackwater was successfully demonstrated in Chapter 3. Among various blackwater sources, including concentrated blackwater collected from vacuum toilet systems, low-dilution blackwater collected from dual-flush toilet systems, and low-dilution blackwater anaerobically digested by the UASB reactor, P recovery percentage was the highest from concentrated blackwater. A P removal efficiency exceeding 90 % was achieved as a result of both an appropriate supersaturation ratio of struvite (>4.0) and a high initial pH value (close to 9.0 after storage). The high quality of the produced struvite was demonstrated by a purity of 94.9 %, the Mg/P/N mass ratio of 10:12:4.7 based on the EDS analysis, and low heavy-metal contents. The moderate PO_4-P concentration,

high NH_4-N concentration, relatively low Ca concentration, strong buffering capacity, and ideal pH enable concentrated blackwater to be a potential source candidate for producing struvite.

The impact of TSS concentration of blackwater on produced struvite quality was studied in Chapter 4. A fluidized bed reactor (FBR) was operated in a batch mode. At appropriate water quality (e.g., pH = 8.9) and operational conditions (e.g., Mg/P molar ratio = 1.5), neither blackwater TSS nor FBR upflow velocity significantly affected the P recovery efficiency. TSS had a significant impact on the purity and size of the struvite product. The struvite purity increased with the decrease of TSS concentration within the studied range of 120 to 1,600 mg/L. At higher TSS levels (520–1,600 mg/L), the struvite crystal remained small (<5 μm) with the FBR upflow velocity ranging from 18 to 90 m/h. When the TSS concentration was lower than 220 mg/L, the struvite crystal was able to grow continuously (up to 100 μm), and its size was directly impacted by the FBR upflow velocity. A greater upflow velocity was unfavorable to the agglomeration of struvite crystals. The studies in Chapters 3 and 4 put forward an economical method for struvite production from concentrated blackwater through saving the chemical cost associated with pH adjustment and suggest strategies to enhance P recovery in decentralized wastewater management systems.

Impact of effluent recirculation strategy on biomethane production

The impact of effluent recirculation on methane production from UASB reactors treating substrates of different solid contents was studied in Chapter 5. Two 2.0 L UASB reactors were operated for 219 d under a mesophilic condition. When the UASB reactors were fed with a high-solid content substrate, effluent recirculation led to significantly reduced methanisation rate (from 47.9% without recirculation to 25.5% with recirculation) and hydrolysis efficiency of particulate

organic matter (from 45.5% without recirculation to 22% with recirculation). In comparison to the high-solid content substrate, a low-solid content substrate led to an increase in methanisation rate for both UASB reactors with and without effluent recirculation, but the difference in methane production for with and without effluent recirculation operation reduced significantly. The lower methane production in the presence of effluent recirculation arose from the inefficient hydrolysis of particulate organic matter, which was mitigated when the reactors were fed with a low-solid content substrate. Turbulence due to effluent recirculation enhanced biomass transport but limited the accessibility of adsorption sites on particulate matter. It was concluded that mixing due to effluent recirculation caused an insufficient attachment between microorganisms/enzymes and particles, which could have lowered the hydrolysis efficiency of particulate organic matter.

An ecology model, based on a non-steady-state mass balance (16S rRNA MiSeq reads normalized by volatile suspended solids), to quantify microbiome responses to disturbances in wastewater bioreactors was developed in Chapter 6. For the first time, this new model helped identify active species (different from dominant species) responding to a changed environment based on the calculation of individual microbe's net growth rate during the community evolution.

Based on the model, the importance of low-abundance species in maintaining biosystem stability in response to the effluent recirculation was demonstrated in Chapter 7. Sludge samples were taken from the top and bottom layers of the reactors every half hydraulic retention time after the initiation/termination of effluent recirculation, and the microbial community evolution was assessed. Community evolution studies showed that directly following the initiation/termination of effluent recirculation, the microbial communities reached the highest diversity. The net growth rates of individual microbes during community evolution illustrated that low-abundance species played a critical role in response to the disturbance induced by initiating or discontinuing effluent

recirculation. This novel model demonstrated the role of low-abundance microorganisms in maintaining the biosystem stability when the system is undergoing disturbances.

Role of proteins in enhanced simultaneous P and bioenergy recovery from blackwater

As a major content in blackwater, proteins' role in the bio-induced CaP precipitation in a UASB reactor was revealed in Chapter 8. Two UASB reactors fed with two types of synthetic wastewater were operated under a mesophilic condition. The feed of one reactor (G reactor) had glucose as the sole carbon source, and the feed of the other reactor (G+B reactor) had glucose (60% COD) and BSA, (40% COD) as the combined carbon sources. P and Ca removals were only observed in the G+B reactor. The main difference between the two reactors was the elevated pH in the G+B reactor, which may be attributed to the degradation of amino acids. The elevated pH caused the deprotonation of the negatively charged functional groups in the sludge, creating available active surfaces for Ca^{2+} complexation. The high availability of OH^- and the enriched Ca in the G+B reactor built a favorable microenvironment to overcome the activation energy barriers hindering the CaP nucleation. The stabilized CaP mineralization largely depended on the well-established microbial community, where the efficient hydrogenotrophic methanogens and syntrophic acetogens may maintain a stabilized pH environment to prevent the dissociation of CaP minerals. It was concluded that the degradation of proteins led to elevated pH and enriched Ca in the EPS, which helped create a localized supersaturation environment to facilitate the CaP formation even under a low supersaturation condition.

The impact of protein content on CaP and methane production in a UASB reactor was further examined in Chapter 9. Four 1.0 L UASB reactors fed with different types of synthetic feeds were operated for 90 d under a mesophilic condition. According to the contributions of

carbon sources to the COD, the four feeds comprised carbon sources of 100% glucose, 75% glucose + 25% bovine serum albumin (BSA), 50% glucose + 50% BSA, and 100% BSA, respectively. The amino acid degradation caused pH elevation, leading to the CaP precipitation at a low supersaturation condition, whereas compared to a lower BSA content (25% BSA), an increase in BSA content (75% or 100% BSA) only brought about a slightly pH increase. A 25% BSA content in feedwater helped shape a superior microbial community that contributed to the maximized methane production (the methanisation rate of 82.7%). The high prevalence of bacterial species of the phylum *Synergistetes* and the methanogen *Methanosaeta* demonstrated that methane was mainly produced through the acetate utilization. In summary, a higher protein content led to higher CaP production, while an optimum protein content existed for maximized biomethane yield.

10.3 Recommendations

Generally, although the concept of P recovery through struvite and CaP precipitation is not new, P recovery is still facing challenges hindering its full-scale application at a level of industrial maturity. Moreover, shifts towards a more technologically and economically feasible P recovery process are needed.

This thesis demonstrated the feasibility of producing struvite from raw concentrated blackwater without alkali addition for pH adjustment. The use of raw blackwater with an appropriate pH value rather than anaerobically digested blackwater helps save operating cost. However, struvite production from raw blackwater in an up-scaled FBR should be further studied. For instance, these issues should be considered carefully: the necessity of blackwater TSS

separation, the design of the FBR for the requirement of struvite size, the safety of using struvite produced from blackwater, and the post-treatment of produced struvite.

P recovery does not only rely on a high P concentration and a chemical addition, an alternative economical way can be to achieve an optimum feedstock/operational condition for the creation of a local supersaturation condition, facilitating P product production at a low or even below supersaturation requirement. A specific wastewater composition can facilitate the bio-induced CaP precipitation at a low supersaturation condition, which makes efficient CaP precipitation free of Ca addition possible. Blackwater is a good waste source for simultaneous CaP precipitation and bioenergy recovery because it contains proteins and urea and has a high COD concentration. Co-digestion of various streams with considerable P and Ca concentration and complex organic constituents is potentially feasible for maximized simultaneous CaP precipitation and bioenergy recovery in an efficient and economical way, which deserves further study.

Moreover, in addition to the wastewater composition, the reactor configuration and operational condition (e.g., recirculation, temperature, and OLR) also impact positively or adversely the localized supersaturation environment in an anaerobic digester. The maintenance and deterioration of localized environment deserve more efforts.

References

Alewell, C., Ringeval, B., Ballabio, C., Robinson, D.A., Panagos, P., Borrelli, P., 2020. Global phosphorus shortage will be aggravated by soil erosion. Nat. Commun. 11, 4546.

BIBLIOGRAPHY

Alewell, C., Ringeval, B., Ballabio, C., Robinson, D.A., Panagos, P., Borrelli, P., 2020. Global phosphorus shortage will be aggravated by soil erosion. Nat. Commun. 11, 4546.

Ali, M., Wang, Z., Salam, K.W., Hari, A.R., Pronk, M., van Loosdrecht, M.C.M., Saikaly, P.E., 2019. Importance of species sorting and immigration in the bacterial assembly of different-sized aggregates in a full-scale aerobic granular sludge plant. Environ. Sci. Technol. 53, 8291–8301.

Alisawi, H.A.O., 2020. Performance of wastewater treatment during variable temperature. Appl. Water Sci. 10, 89.

Alp, Ö., 2010. Further Treatment of Digested Blackwater for Extraction of Valuable Components. PhD Thesis, Hamburg University of Technology, Germany.

ATCC. Trace mineral supplement. atcc.org/products/md-tms, 2021.

Baird, R.B., Eaton, A.D., Rice, E.W., 2017. Standard Methods for the Examination of Water and Wastewater, 23rd ed. American Public Health Association, Washington.

Banerjee, S., Schlaeppi, K., van der Heijden, M.G., 2018. Keystone taxa as drivers of microbiome structure and functioning. Nat. Rev. Microbiol. 16 (9), 567–576.

Bartkiene, E., Lele, V., Ruzauskas, M., Domig, K.J., Starkute, V., Zavistanaviciute, P., Bartkevics, V., Pugajeva, I., Klupsaite, D., Juodeikiene, G., Mickiene, R., Rocha, J.M., 2020. Lactic acid bacteria isolation from spontaneous sourdough and their characterization including antimicrobial and antifungal properties evaluation. Microorganisms 8, 64.

Batstone, D.J., Hülsen, T., Mehta, C.M., Keller, J., 2015. Platforms for energy and nutrient recovery from domestic wastewater: a review. Chemosphere 140, 2–11.

Batstone, D.J., Keller, J., Angelidaki, R.I., Kalyuzhnyi, S.V., Pavlostathis, S.G., Rozzi, A., Sanders, W.T.M., Siegrist, H., Vavilin, V.A., 2002. The Anerobic Digestion Model No 1(ADM1). Water Sci. Technol. 45 (10), 65-73.

Benjamino, J., Lincoln, S., Srivastava, R., Graf, J., 2018. Low-abundant bacteria drive compositional changes in the gut microbiota after dietary alteration. Microbiome 6, 86.

Bhuiyan, M.I.H., Mavinic, D.S., Beckie, R.D., 2008. Nucleation and growth kinetics of struvite in a fluidized bed reactor. J. Cryst. Growth 310 (6), 1187–1194.

Bhuiyan, M.I.H., Mavinic, D.S., Koch, F.A., 2008. Thermal decomposition of struvite and its phase transition. Chemosphere 70 (8), 1347–1356.

Bickel, S., Or, D., 2021. The chosen few—variations in common and rare soil bacteria across biomes. ISM J. 15, 3315–3325.

Boanini, E., Gazzano, M., Nervi, C., Chierotti, M.R., Rubini, K., Gobetto, R., Bigi, A., 2019. Strontium and zinc substitution in *β*-tricalcium phosphate: an X-ray diffraction, solid state NMR and ATR-FTIR study. J. Funct. Biomater. 10 (2), 20.

Boiocchi, R., Zhang, Q., Gao, M., Liu, Y., 2022. Modeling and optimization of an upflow anaerobic sludge blanket (UASB) system treating blackwater. J. Environ. Chem. Eng. 10 (3), 107614.

Borgerding, J., 1972. Phosphate deposits in digestion systems. J. Water Pollut. Control Fed. 44, 813-819.

Bradford, M.M., 1976. A rapid and sensitive method for the quantitation of microgram quantities of protein utilizing the principle of protein-dye binding. Anal. Biochem. 72, 248–254.

Buzzini, A.P., Pires, E.C., 2007. Evaluation of a upflow anaerobic sludge blanket reactor with partial recirculation of effluent used to treat wastewaters from pulp and paper plants. Bioresour. Technol. 98, 1838–1848.

Callahan, B.J., McMurdie, P.J., Rosen, M.J., Han, A.W., Johnson, A.M.A., Holmes, S.P., 2016. DADA2: high resolution sample inference from Illumina amplicon data. Nat. Methods 13 (7), 581–583.

Calusinska, M., Goux, X., Fossépré, M., Muller, E.E.L., Wilmes, P., Delfosse, P., 2018. A year of monitoring 20 mesophilic full-scale bioreactors reveals the existence of stable but different core microbiomes in bio-waste and wastewater anaerobic digestion systems. Biotechnol. Biofuels 11, 196.

Campbell, B.J., Kirchman, D.L., 2013. Bacterial diversity, community structure and potential growth rates along an estuarine salinity gradient. ISME J. 7 (1), 210–220.

Campos, J.L., Crutchik, D., Franchi, Ó., Pavissich, J.P., Belmonte, M., Pedrouso, A., Mosquera-Corral, A., Val del Río, Á., 2019. Nitrogen and phosphorus recovery from anaerobically pretreated agro-food wastes: a review. Front. Sustain. Food Syst. 2, 91.

Capdevielle, A., Sýkorová, E., Béline, F., Daumer. M.L., 2016. Effects of organic matter on crystallization of struvite in biologically treated swine wastewater. Environ. Technol. 37 (7), 880–892.

Capodaglio, A.G., 2020. Taking the water out of "wastewater": an ineluctable oxymoron for urban water cycle sustainability. Water Environ. Res. 92 (12), 2030–2040.

Caporaso, J.G., Kuczynski, J., Stombaugh, J., Bittinger, K., Bushman, F.D., Costello, E.K., Fierer, N., Peña, A.G., Goodrich, J.K., Gordon, J.I., Huttley, G.A., Kelley, S.T., Knights, D., Koenig, J.E., Ley, R.E., Lozupone, C.A., McDonald, D., Muegge, B.D., Pirrung, M., Reeder, J., Sevinsky, J.R., Turnbaugh, P.J., Walters, W.A., Widmann, J., Yatsunenko, T., Zaneveld, J., Knight, R., 2010. QIIME allows analysis of high-throughput community sequencing data. Nat. Methods 7 (5), 335–336.

Carchesio, M., Tatàno, F., Lancellotti, I., Taurino, R., Colombo, E., Barbieri, L., 2014. Comparison of biomethane production and digestate characterization for selected agricultural substrates in Italy. Environ. Technol. 35, 2212–2226.

Castro-Alonso, M.J., Montañez-Hernandez, L.E., Sanchez-Muñoz, M.A., Franco, M.R.M., Narayanasamy, R., Balagurusamy, N., 2019. Microbially induced calcium carbonate precipitation (MICP) and its potential in bioconcrete: microbiological and molecular concepts, Front. Mater. 6, 126.

Chen, S., Cheng, H., Wyckoff, K.N., He, Q., 2016. Linkages of Firmicutes and Bacteroidetes populations to methanogenic process performance. J. Ind. Microbiol. 43 (6), 771–781.

Cheng, H., Cheng, D., Mao, J., Lu, T., Hong, P.-Y., 2019. Identification and characterization of core sludge and biofilm microbiota in anaerobic membrane bioreactors. Environ. Int. 133, 105165.

Chernicharo, C.A.L., 2006. Post-treatment options for the anaerobic treatment of domestic wastewater. Rev. Environ. Sci. Biotechnol. 5, 73–92.

Christensen, M.L., Hjorth, M., Keiding, K., 2009. Characterization of pig slurry with reference to flocculation and separation. Water Res. 43 (3), 773–783.

Claussen, J.C., Skiecevičienė, J., Wang, J., Rausch, P., Karlsen, T.H., Lieb, W, Baines, J.F., Franke, A., Hütt, M.-T., 2017. Boolean analysis reveals systematic interactions among low-abundance species in the human gut microbiome. PLoS Comput. Biol. 13 (6), e1005361.

Cordell, D., Drangert, J.-O., White, S., 2009. The story of phosphorus: global food security and food for thought. Global Environ. Change 19 (2), 292–305.

Cornel, P., Schaum, C., 2009. Phosphorus recovery from wastewater: needs, technologies and costs. Water Sci. Technol. 59 (6), 1069–1076.

Cuetos, M.J., Gómez, X., Otero, M., Morán, A., 2009. Anaerobic digestion of solid slaughterhouse waste: study of biological stabilization by Fourier Transform infrared spectroscopy and thermogravimetry combined with mass spectrometry. Biodegradation 21, 543–556.

Cunha, J.R., Morais, S., Silva, J.C., van der Weijden, R.D., Leal, L.H., Zeeman, G., Buisman, C., 2019. Bulk pH and carbon source are key factors for calcium phosphate granulation. Environ. Sci. Technol. 53, 1334–1343.

Cunha, J.R., Schott, C., van der Weijden, R.D., Leal, L.H., Zeeman, G., Buisman, C., 2018. Calcium addition to increase the production of phosphate granules in anaerobic treatment of black water. Water Res. 130, 333–342.

Cunha, J.R., Schott, C., van der Weijden, R.D., Leal, L.H., Zeeman, G., Buisman, C., 2019. Recovery of calcium phosphate granules from black water using a hybrid upflow anaerobic sludge bed and gas-lift reactor. Environ Res. 178, 108671.

Cunha, J.R., Schott, C., van der Weijden, R.D., Leal, L.H., Zeeman, G., Buisman, C., 2020. Calcium phosphate granules recovered from black water treatment: a sustainable substitute for mined phosphorus in soil fertilization. Resour. Conserv. Recycl. 158, 104791.

Cunha, J.R., Tervahauta, T., van der Weijden, R.D., Temmink, H., Leal, L.H., Zeeman, G., Buisman, C.J.N., 2018. The effect of bioinduced increased pH on the enrichment of calcium phosphate in granules during anaerobic treatment of black water. Environ. Sci. Technol. 52, 13144–13154.

Dai, H., Tan, X., Zhu, H., Sun, T., Wang, X., 2018. Effects of commonly occurring metal ions on hydroxyapatite crystallization for phosphorus recovery from wastewater. Water 10 (11), 1619.

Daneshgar, S., Buttafava, A., Capsoni, D., Callegari, A., Capodaglio, A.G., 2018. Impact of pH and ionic molar ratios on phosphorus forms precipitation and recovery from different wastewater sludges. Resources 7 (4), 71.

Daneshgar, S., Callegari, A., Capodaglio, A.G., Vaccari, D., 2018. The potential phosphorus crisis: resource conservation and possible escape technologies: a review. Resources 7 (2), 37.

Dang, H., Yu, N., Mou, A., Zhang, L., Guo, B., Liu, Y., 2022. Metagenomic insights into direct interspecies electron transfer and quorum sensing in blackwater anaerobic digestion reactors supplemented with granular activated carbon. Bioresour. Technol. 352, 127113.

Dawson, W., Hör, J., Egert, M., van Kleunen, M., Pester, M., 2017. A small number of low-abundance bacteria dominate plant species-specific responses during rhizosphere colonization. Front. Microbiol. 8, 875.

de Cena, J.A., Zhang, J., Deng, D., Damé-Teixeira, N., Do, T., 2021. Low-abundant microorganisms: the human microbiome's dark matter, a scoping review. Front. Cell. Infect. Microbiol. 11, 689197.

de Graaff M.S., Temmink, H., Zeeman, G., Buisman, C.J.N., 2010. Anaerobic treatment of concentrated blackwater in a UASB reactor at a short HRT. Water 2 (1), 101–119.

de Graaff M.S., Temmink, H., Zeeman, G., Buisman, C.J.N., 2011. Energy and phosphorus recovery from black water. Water Sci. Technol. 63 (11), 2759–2765.

de Ridder, M., de Jong, S., Polchar, J., Lingermann, S., 2012. Risks and Opportunities in the Global Phosphate Rock Market. The Hague Centre for Strategic Studies, The Hague, The Netherlands.

De Vrieze, J., Hennebel, T., Boon, N., Verstraete, W., 2012. Methanosarcina: the rediscovered methanogen for heavy duty biomethanation. Bioresour. Technol. 112, 1–9.

De Vrieze, J., Verstraete, W., 2016. Perspectives for microbial community composition in anaerobic digestion: from abundance and activity to connectivity. Environ. Microbiol. 18 (9), 2797–2809.

Deng, N., Stack, A.G., Weber, J., Cao, B., De Yoreo, J.J., Hu, Y., 2019. Organic-mineral interfacial chemistry drives heterogeneous nucleation of Sr-rich (Ba_x, Sr_{1-x})SO_4 from undersaturated solution. PNAS 116, 13221–13226.

Dignac, M.-F., Urbain, V., Rybacki, D., Bruchet, A., Snidaro, D., Scribe, P., 1998. Chemical description of extracellular polymers: implication on activated sludge floc structure. Water Sci. Technol. 38, 45−53.

Ding, Z., Bourven, I., Guibaud, G., van Hullebusch, E.D., Panico, A., Pirozzi, F., Esposito, G., 2015. Role of extracellular polymeric substances (EPS) production in bioaggregation: application to wastewater treatment. Appl. Microbiol. Biotechnol. 99, 9883−9905.

DuBois, M., Gilles, K.A., Hamilton, J.K., Rebers, P.A., Smith, F., 1956. Colorimetric method for determination of sugars and related substances. Anal. Chem. 28, 350−356.

Duong, T.H., Grolle, K., Nga, T.T.V., Zeeman, G., Temmink, H., van Eekert, M., 2019. Protein hydrolysis and fermentation under methanogenic and acidifying conditions. Biotechnol. Biofuels 12, 254.

Egle, L., Rechberger, H., Krampe, J., Zessner, M., 2016. Phosphorus recovery from municipal wastewater: an integrated comparative technological, environmental and economic assessment of P recovery technologies. Sci. Total Environ. 571, 522–542.

Eisenhauer, N., Scheu, S., Jousset, A., 2012. Bacterial diversity stabilizes community productivity. PLoS One 7 (3), e34517.

Fang, W., Zhang, P., Zhang, G., Jin, S., Li, D., Zhang, M., Xu, X., 2014. Effect of alkaline addition on anaerobic sludge digestion with combined pretreatment of alkaline and high pressure homogenization. Bioresour. Technol. 168, 167–172.

Farag, I.F., Davis, J.P., Youssef, N.H., Elshahed M.S., 2014. Global patterns of abundance, diversity and community structure of the *Aminicenantes* (candidate phylum OP8). PLoS One 9 (3), e92139.

Fattah, K.P., Mavinic, D.S., Koch, F.A., 2012. Influence of process parameters on the characteristics of struvite pellets. J. Environ. Eng. 138 (12), 1200–1209.

Fattah, K.P., Mavinic, D.S., Koch, F.A., Jacob, C., 2008. Determining the feasibility of phosphorus recovery as struvite from filter press centrate in a secondary wastewater treatment plant. J. Environ. Sci. Health Part A 43, 756–764.

Flint, H.J., Stewart, C.S., 1999. Bacteroides and prevotella, in: Robinson, R.K. (Ed.), Encyclopedia of Food Microbiology, pp. 198–203.

Florentino, A.P., Sharaf, A., Zhang, L., Liu, Y., 2019. Overcoming ammonia inhibition in anaerobic blackwater treatment with granular activated carbon: the role of electroactive microorganisms. Environ. Sci.: Water Res. Technol. 5, 383.

Florentino, A.P., Xu, R., Zhang, L., Liu, Y., 2019. Anaerobic digestion of blackwater assisted by granular activated carbon: from digestion inhibition to methanogenesis enhancement. Chemosphere 233, 462–471.

Frigon, D., Wells, G., 2019. Microbial immigration in wastewater treatment systems: analytical considerations and process implications. Curr. Opin. Biotechnol. 57, 151–159.

Gao, M., 2020. Anaerobic Treatment of Source-diverted Blackwater-maximizing Biomethane Recovery. University of Alberta, Canada.

Gao, M., Guo, B., Zhang, L., Zhang, Y., Liu, Y., 2019. Microbial community dynamics in anaerobic digesters treating conventional and vacuum toilet flushed blackwater. Water Res. 160 (1), 249–258.

Gao, M., Zhang, L., Florentino, A.P., Liu, Y., 2019. Performance of anaerobic treatment of blackwater collected from different toilet flushing systems: can we achieve both energy recovery and water conservation? J. Hazard. Mater. 365, 44–52.

Gao, M., Zhang, L., Guo, B., Zhang, Y., Liu, Y., 2019. Enhancing biomethane recovery from source-diverted blackwater through hydrogenotrophic methanogenesis dominant pathway. Chem. Eng. J. 378, 122258.

Gao, M., Zhang, L., Liu, Y., 2020. High-loading food waste and blackwater anaerobic co-digestion: maximizing bioenergy recovery. Chem. Eng. J. 394, 124911.

Gao, M., Zhang, L., Zhang, H., Florentino, A.P., Liu, Y., 2019. Energy recovery from municipal wastewater: impacts of temperature and collection systems. J. Environ. Eng. Sci. 141 (1), 24–31.

Garcia, M.C., Vanotti, M.B., Szogi, A.A., 2007. Simultaneous separation of phosphorus sludge and manure solids with polymers. Trans. ASABE 50 (6), 2205–2215.

García-García, N., Tamames, J., Linz, A.M., Pedrós-Alió, C., Puente-Sánchez, F., 2019. Microdiversity ensures the maintenance of functional microbial communities under changing environmental conditions. ISME J. 13 (12), 2969–2983.

Gell, K., de Ruijter, F.J., Kuntke, P., de Graaff, M., Smit, A.L., 2011. Safety and effectiveness of struvite from black water and urine as a phosphorus fertilizer. J. Agric. Sci. 3 (3), 67–80.

Ghosh, S., Lobanov, S., Lo, V.K., 2019. Impact of supersaturation ratio on phosphorus recovery from synthetic anaerobic digester supernatant through a struvite crystallization fluidized bed reactor. J. Environ. Technol. 40 (15), 2000–2010.

Guarino, G., Carotenuto, C., di Cristofaro, F., Papa, S., Morrone, B., Minale, M., 2016. Does the C/N ratio really affect the bio-methane yield? a three years investigation of buffalo manure digestion. Chem. Eng. Trans. 49, 463–468.

Guo, B., 2019. Cellular Metabolic Markers and Growth Dynamics Definition of Functional Groups in Activated Sludge Wastewater Treatment Heterotrophic Population. McGill University, Montreal.

Guo, H., Oosterkamp, M.J., Tonin, F., Hendriks, A., Nair, R., van Lier, J.B., de Kreuk, M., 2021. Reconsidering hydrolysis kinetics for anaerobic digestion of waste activated sludge applying cascade reactors with ultra-short residence times. Water Res. 202, 117398.

Guo, B., Yu, N., Weissbrodt, D.G., Liu, Y., 2021. Effects of micro-aeration on microbial niches and antimicrobial resistances in blackwater anaerobic digesters. Water Res. 196, 117035.

Guo, B., Zhang, L., Sun, H., Gao, M., Yu, N., Zhang, Q., Mou, A., Liu, Y., 2022. Microbial co-occurrence network topological properties links with reactor parameters and reveals importance of low-abundance genera. NPJ Biofilms Microbiomes 8, 3.

Hallas, J.F., Mackowiak, C.L., Wilkie, A.C., Harris, W.G., 2019. Struvite phosphorus recovery from aerobically digested municipal wastewater. Sustainability 11 (2), 376.

Hiibel, S.R., Pereyra, L.P., Breazeal, M.V.R., Reisman, D.V., Reardon, K.F., Pruden, A., 2011. Effect of organic substrate on the microbial community structure in pilot-scale sulfate-reducing biochemical reactors treating mine drainage. Environ. Eng. Sci. 28 (8), 563–572.

Hirayama, K., Akashi, S., Furuya, M., Fukuhara, K., 1990. Rapid confirmation and revision of the primary structure of bovine serum albumin by ESIMS and frit-FAB LC/MS. Biochem. Biophys. Res. Commun. 173 (2), 639–646.

Hjorth, M., Christensen, M.L., Christensen, P.V., 2008. Flocculation, coagulation, and precipitation of manure affecting three separation techniques. Bioresour. Technol. 99 (18), 8598–8604.

Hol, W.H.G., Garbeva, P., Hordijk, C., Hundscheid, M.P.J., Gunnewiek, P.J.A.K., van Agtmaal, M., Kuramae, E.E., de Boer, W., 2015. Non-random species loss in bacterial communities reduces antifungal volatile production. Ecology 96 (8), 2042–2048.

Hooper, D.U., Chapin III, F.S., Ewel, J.J., Hector, A., Inchausti, P., Lavorel, S., Lawton, J.H., Lodge, D.M., Loreau, M., Naeem, S., Schmid, B., Setälä, H., Symstad, A.J., Vandermeer J., Wardle, D.A., 2005. Effects of biodiversity on ecosystem functioning: a consensus of current knowledge. Ecol. Monogr. 75(1), 3–35.

Huang, Z., Gengenbach, T., Tian, J., Shen, W., Garnier, G., 2018. Effect of bovine serum albumin treatment on the aging and activity of antibodies in paper diagnostics. Front. Chem. 6, 161.

Huang, Q., Zakaria, B.S., Zhang, Y., Zhang, L., Liu, Y., Dhar, B.R., 2021. A high-rate anaerobic biofilm reactor for biomethane recovery from source-separated blackwater at ambient temperature. Water Environ. Res., 93 (1), 61–74.

Hussain, A., Dubey, S.K., 2014. Specific methanogenic activity test for anaerobic treatment of phenolic wastewater. Desalin. Water Treat. 52 (37–39), 7015–7025.

International Energy Agency, 2021. The Role of Critical Minerals in Clean Energy Transitions. IEA Publications.

Iqbal, M., Bhuiyan, H., Mavinic, D.S., 2008. Assessing struvite precipitation in a pilot-scale fluidized bed crystallizer. Environ. Technol. 29 (11), 1157–1167.

Ito, T., Yoshiguchi, K., Ariesyady, H.D., Okabe, S., 2011. Identification of a novel acetate-utilizing bacterium belonging to Synergistes group 4 in anaerobic digester sludge. ISME J. 5 (12), 1844–1856.

Jarzyna, M.A., Norman, K.E.A., LaMontagne, J.M., Helmus, M.R., Li, D., Parker, S.M., Rocha, M.P., Record, S., Sokol, E.R., Zarnetske, P.L., Surasinghe, T.D., 2022. Community stability is related to animal diversity change. Ecosphere 13 (3), e3970.

Javanbakht, V., Alavi, S.A., Zilouei, H., 2014. Mechanisms of heavy metal removal using microorganisms as biosorbent. Water Sci. Technol. 69, 1775–1787.

Jiang, Y., Dennehy, C., Lawlor, P.G., Hu, Z., McCabe, M., Cormican, P., Zhan, X., Gardiner, G.E., 2019. Exploring the roles of and interactions among microbes in dry co-digestion of food waste and pig manure using high-throughput 16S rRNA gene amplicon sequencing. Biotechnol. Biofuels 12, 5.

Jolis, D., 2008. High-solids anaerobic digestion of municipal sludge pretreated by thermal hydrolysis. Water Environ. Res. 80 (7), 654–662.

Jousset, A., Bienhold, C., Chatzinotas, A., Gallien, L., Gobet, A., Kurm, V., Küsel, K., Rillig, M.C., Rivett, D.W., Salles, J.F., van der Heijden, M.G.A., Youssef, N.H., Zhang, X., Wei, Z., Hol, W.H.G., 2017. Where less may be more: how the rare biosphere pulls ecosystems strings. ISME J. 11 (4), 853–862.

Juste-Poinapen, N.M.S., Turner, M.S., Rabaey, K., Virdis, B., Batstone, D.J., 2015. Evaluating the potential impact of proton carriers on syntrophic propionate oxidation. Sci. Rep. 5, 18364.

Kalyanaraman, R., 2008. Nucleation energetics during homogeneous solidification in elemental metallic liquids. J. Appl. Phys. 104, 033506.

Kampmann, K., Ratering, S., Kramer, I., Schmidt, M., Zerr, W., Schnell, S., 2012. Unexpected stability of Bacteroidetes and Firmicutes communities in laboratory biogas reactors fed with different defined substrates. App. Environ. Microbiol. 78 (7), 2016–2119.

KEGG, https://www.kegg.jp/kegg-bin/show_organism?org=mla, 2020.

Kim, M., Ahn, Y.-H., Speece, R.E., 2002. Comparative process stability and efficiency of anaerobic digestion; mesophilic vs. thermophilic. Water Res. 36 (17), 4369–4385.

Knerr, H., Rechenburg, A., Kistemann, T., Schmitt, T.G., 2011. Performance of a MBR for the treatment of blackwater. Water Sci Technol. 63 (6), 1247–1254.

Kok, D.-J.D., Pande, S., van Lier, J.B., Ortigara, A.R.C., Savenije, H., Uhlenbrook, S., 2018. Global phosphorus recovery from wastewater for agricultural reuse. Hydrol. Earth Syst. Sci. 22, 5781–5799.

Kolde, R., Package 'pheatmap'. https://cran.r-project.org/package=pheatmap, 2019.

Konopka, A., Lindemann, S., Fredrickson, J., 2015. Dynamics in microbial communities: unraveling mechanisms to identify principles. ISME J. 9, 1488–1495.

Kovács, E., Wirth, R., Maróti, G., Bagi, Z., Nagy, K., Minárovits, J., 2015. Augmented biogas production from protein-rich substrates and associated metagenomic changes. Bioresour. Technol. 178, 254–261.

Kovács, E., Wirth, R., Maróti, G., Bagi, Z., Rákhely, G., Kovács, K.L., 2013. Biogas production from protein-rich biomass: fed-batch anaerobic fermentation of casein and of pig blood and associated changes in microbial community composition. PLoS one 8 (10), e77265.

Kristensen, J.M., Singleton, C., Clegg, L.-A., Petriglieri, F., Nielsen, P.H., 2021. High diversity and functional potential of undescribed "Acidobacteriota" in Danish wastewater treatment plants. Front. Microbiol. 12, 643950.

Kujawa-Roeleveld, K., Zeeman, G., 2006. Anaerobic treatment in decentralised and source-separation-based sanitation concepts. Rev. Environ. Sci. Biotechnol. 5 (1), 115–139.

Kuo, J., Dow, J., 2017. Biogas production from anaerobic digestion of food waste and relevant air quality implications. J. Air Waste Manag. Assoc. 67, 1000–1011.

Kurm, V., van der Putten, W.H., de Boer, W., Naus-Wiezer, S., Hol, W.H.G., 2017. Low abundant soil bacteria can be metabolically versatile and fast growing. Ecology 98 (2), 555–564.

Langille, M.G., Zaneveld, J., Caporaso, J.G., McDonald, D., Knights, D., Reyes, J.A., Clemente, J.C., Burkepile, D.E., Vega Thurber, R.L., Knight, R., Beiko, R.G., Huttenhower, C., 2013. Predicted functional profiling of microbial communities using 16S rRNA marker gene sequences. Nat. Biotechnol. 31 (9), 814–821.

Lee, S.-H., Kumar, R., Jeon, B.-H., 2016. Struvite precipitation under changing ionic conditions in synthetic wastewater: experiment and modeling. J. Colloid Interface Sci. 474, 93–102.

Lei, Y., Song, B., van der Weijden, R.D., Saakes, M., Buisma, C.J.N., 2017. Electrochemical induced calcium phosphate precipitation: importance of local pH. Environ. Sci. Technol. 51 (19), 11156–11164.

Lennon, J.T., Jones, S.E., 2011. Microbial seed banks: the ecological and evolutionary implications of dormancy. Nat. Rev. Microbiol. 9 (2), 119–130.

Lguirati, A., Baddi, G.A., El Mousadik, A., Gilard, V., Revel, J.C., Hafidi, M., 2005. Analysis of humic acids from aerated and non-aerated urban landfill composts. Int. Biodeterior. Biodegradation 56, 8–16.

Li, B., Boiarkina, I., Yu, W., Huang, H., Munir, T., Wang, G., Yong, B.R., 2019. Phosphorus recovery through struvite crystallization: challenges for future design. Sci. Total Environ. 648, 1244–1256.

Li, L., He, Q., Ma, Y., Wang, X., Peng, X., 2016. A mesophilic anaerobic digester for treating food waste: process stability and microbial community analysis using pyrosequencing. Microb. Cell Fact. 15, 65.

Li, P., Liu, J., Jiang, C., Wu, M., Liu, M., Li, Z., 2019. Distinct successions of common and rare bacteria in soil under humic acid amendment—a microcosm study. Front. Microbiol. 10, 1–14.

Liang, H., Ye, D., Luo, L., 2017. Unravelling diversity and metabolic potential of microbial consortia at each stage of leather sewage treatment. RSC Adv. 7, 41727–41737.

Lin, R., Deng, C., Cheng, J., Xia, A., Lens, P.N.L., Jackson, S.A., Dobson, A.D.W., Murphy, J.D., 2018. Graphene facilitates biomethane production from protein-derived glycine in anaerobic digestion. iScience 10, 158–170.

Lissens, G., Verstraete, W., Albrecht, T., Brunner, G., Creuly, C., Seon, J., Dussap, G., Lasseur, C., 2004. Advanced anaerobic bioconversion of lignocellulosic waste for bioregenerative life

support following thermal water treatment and biodegradation by *Fibrobacter succinogenes*. Biodegradation 15, 173–183.

Liu, Z., Cichocki, N., Bonk, F., Günther, S., Schattenberg, F., Harms, H., Centler, F., Müller, S., 2018. Ecological stability properties of microbial communities assessed by flow cytometry. mSphere 3 (1), e00564-17.

Liu, H., Fang, H.H.P., 2002. Extraction of extracellular polymeric substances (EPS) of sludges. J. Biotechnol. 95, 249–256.

Liu, Y., Lv, W., Zhang, Z., Xia, S., 2018. Influencing characteristics of short-time aerobic digestion on spatial distribution and adsorption capacity of extracellular polymeric substances in waste activated sludge. RSC Adv. 56, 32172–32177.

Liu, X., Sheng, G., Luo, H., Zhang, F., Yuan, S., Xu, J., Zeng, R., Wu, J., Yu, H., 2010. Contribution of extracellular polymeric substances (EPS) to the sludge aggregation. Environ. Sci. Technol. 44, 4355−4360.

López-López, A., León-Becerril, E., Rosales-Contreras, M. E., Villegas-García, E., 2015. Influence of alkalinity and VFAs on the performance of an UASB reactor with recirculation for the treatment of Tequila vinasses. Environ. Technol. 36 (19), 2468–2476.

Lukitawesa, Wikandari, R., Millati, R., Taherzadeh, M.J., Niklasson, C., 2018. Effect of effluent recirculation on biogas production using two-stage anaerobic digestion of citrus waste. Molecules 23 (12), 3380.

Lynch, M.D.J., Neufeld, J.D., 2015. Ecology and exploration of the rare biosphere. Nat. Rev. Microbiol. 13, 217–229.

Ma, S., Ma, H., Hu, H., Ren, H., 2019. Effect of mixing intensity on hydrolysis and acidification of sewage sludge in two-stage anaerobic digestion: characteristics of dissolved organic matter and the key microorganisms. Water Res. 148, 359–367.

Maleki, E., Bokhary, A., Liao, B.Q., 2018. A review of anaerobic digestion bio-kinetics. Rev. Environ. Sci. Biotechnol. 17, 691–705.

Manzoor, M.A.P., Singh, B., Agrawal, A.K., Arun, A.B., Mujeeburahiman, M., Rekha, P.-D., 2018. Morphological and micro-tomographic study on evolution of struvite in synthetic urine infected with bacteria and investigation of its pathological biomineralization. PLoS One 13 (8), e0202306.

Martinez, C., La Gattina, G., Garrido, L., Gilabert, U., Ozols, A., 2015. Hydroxyapatite microsphere production by plasma spray. Procedia Mater. Sci. 8, 319–323.

Maurer, M., Rothenberger, D., Larsen, T.A., 2005. Decentralised wastewater treatment technologies from a national perspective: at what cost are they competitive? Water Supply 5 (6), 145–154.

McDonald, D., Price, M.N., Goodrich, J., Nawrocki, E.P., DeSantis, T.Z., Probst, A., Andersen, G.L., Knight, R., Hugenholtz, P., 2012. An improved Greengenes taxonomy with explicit ranks for ecological and evolutionary analyses of bacteria and archaea. ISME J. 6 (3), 610–618.

Mei, R., Liu, W.-T., 2019. Quantifying the contribution of microbial immigration in engineered water systems. Microbiome 7, 144.

Mei, R., Narihiro, T., Nobu, M.K., Kuroda, K., Liu, W.-T., 2016. Evaluating digestion efficiency in full-scale anaerobic digesters by identifying active microbial populations through the lens of microbial activity. Sci. Rep. 6, 34090.

Mei, R., Nobu, M.K., Narihiro, T., Liu, W.-T., 2020. Metagenomic and metatranscriptomic analyses revealed uncultured Bacteroidales populations as the dominant proteolytic amino acid degraders in anaerobic digesters. Front. Microbiol. 11, 593006.

Meinzinger, F., Oldenburg, M., 2009. Characteristics of source-separated household wastewater flows: a statistical assessment. Water Sci. Technol. 59 (9), 1785–1791.

Militon, C., Hamdi, O., Michotey, V., Fardeau, M.-L., Ollivier, B., Bouallagui, H., Hamdi, M., Bonin, P., 2015. Ecological significance of Synergistetes in the biological treatment of tuna cooking wastewater by an anerobic sequencing batch reactor. Environ. Sci. Pollut. Res. Int. 22, 18230–18238.

Mitani, Y., Sakai, Y., Mishina, F., Ishiduka, S., 2003. Struvite recovery from wastewater having low phosphate concentration. J. Water Environ. Technol. 1 (1), 13–18.

Moges, M.E., Todt, D., Heistad, A., 2018. Treatment of source-separated blackwater: a decentralized strategy for nutrient recovery towards a circular economy. Water 10, 463.

Morozova, I., Nikulina, N., Oechsner, H., Krümpel, J., Lemmer, A., 2020. Effects of increasing nitrogen content on process stability and reactor performance in anaerobic digestion. Energies 13(5), 1139.

Nelson, N. O., Mikkelsen, R.L., Hesterberg, D.L., 2003. Struvite precipitation in anaerobic swine lagoon liquid: effect of pH and Mg:P ratio and determination of rate constant. Bioresour. Technol. 89 (3), 229-236.

Ni, M., Ratner, B.D., 2008. Differentiation of calcium carbonate polymorphs by surface analysis techniques-an XPS and TOF-SIMS study. Surf. Interface Anal. 40 (10), 1356–1361.

Nobu, M.K., Narihiro, T., Kuroda, K., Mei, R., Liu, W.-T., 2016. Chasing the elusive Euryarchaeota class WSA2: genomes reveal a uniquely fastidious methyl-reducing methanogen. ISME J. 10, 2478–2487.

Nsavyimana, G., Kaboneka, S., Bigumandondera, P., Ngahane, E.L., Ndikumana, T., Vasel, J.L., 2020. Exploring a new approach of the population equivalent concept through a detailed characterization of grey and black waters. IJASRE 6 (1), 32–49.

Obileke, K., Nwokolo, N., Makaka, G., Mukumba, P, Onyeaka, H., 2021. Anaerobic digestion: technology for biogas production as a source of renewable energy- a review. Energy Environ. 32 (2), 191–225.

Ofiţeru, I.D., Lunn, M., Curtis, T.P., Wells, G.F., Criddle, C.S., Francis, C.A., Sloan, W.T., 2010. Combined niche and neutral effects in a microbial wastewater treatment community. PNAS 107 (35), 15345–15350.

Ohlinger, K.N., Young, T.M., Schroeder, E.D., 2000. Postdigetion struvite precipitation using a fluidized bed reactor. J. Environ. Eng. 126 (4), 361–368.

Oksanen, J., Blanchet, F.G., Friendly, M., Kindt, R., Legendre, P., McGlinn, D., Minchin, P.R., O'Hara, R. B., Simpson, G.L., Solymos, P., Stevens, M.H.H., Szoecs, E., Wagner, H., 2019. Vegan: Community Ecology Package.

Palmquist, H., Hanæus, J., 2005. Hazardous substances in separately collected grey- and blackwater from ordinary Swedish households. Sci. Total Environ. 348 (1-3), 151–163.

Peng, L., Dai, H., Wu, Y., Peng, Y., Lu, X., 2018. A comprehensive review of the available media and approaches for phosphorus recovery from wastewater. Water Air Soil Pollut. 229 (4), 115.

Ping, Q., Li, Y., Wu, X., Yang, L., Wang, L., 2016. Characterization of morphology and component of struvite pellets crystallized from sludge dewatering liquor: effects of total suspended solid and phosphate concentrations. J. Hazard. Mater. 310, 261–269.

Pust, M.-M., Tümmler, B., 2022. Bacterial low-abundant taxa are key determinants of a healthy airway metagenome in the early years of human life. Comput. Struct. Biotechnol. J. 20, 175–186.

R Core Team, 2020. R: A Language and Environment for Statistical Computing, R Foundation for Statistical Computing, Vienna, Austria.

Rahaman, Md. S., 2009. Phosphorus Recovery from Wastewater through Struvite Crystallization in a Fluidized Bed Reactor: Kinetics, Hydrodynamics and Performance. PhD Thesis, University of British Columbia, Canada.

Rahaman, Md.S., Mavinic, D.S., Ellis, N., 2014. Fluidisation behaviour of struvite recovered from wastewater. J. Environ. Eng. Sci. 9 (2), 137–149.

Rice, E.W., Baird, R.B., Eaton, A.D., 2017. Standard Methods for the Examination of Water and Wastewater, 23rd ed., American Public Health Association (APHA), American Water Works Association, Water Environment Federation (WEF), Washington, DC.

Rogowska, A., Pomastowski, P., Złoch, M., Railean-Plugaru, V., Król, A., Rafińska, K., Szultka-Młyńska, M., Buszewski, B., 2018. The influence of different pH on the electrophoretic behaviour of *Saccharomyces cerevisiae* modified by calcium ions. Sci. Rep. 8, 7261.

Ronteltap, M., Maurer, M., Gujer, W., 2007. The behaviour of pharmaceuticals and heavy metals during struvite precipitation in urine. Water Res. 41 (9), 1859–1868.

Royal Society of Chemistry. BSA. http://www.chemspider.com/Chemical-Structure.4523073.html, 2022.

Sakai, S., Ehara, M., Tseng, I.-C., Yamaguchi, T., Bräuer, S.L., Cadillo-Quiroz, H., Zinder, S.H., Imachi, H., 2012. *Methanolinea mesophila* sp. nov., a hydrogenotrophic methanogen isolated from rice field soil, and proposal of the archaeal family *Methanoregulaceae* fam. Nov. within the order *Methanomicrobiales*. Int. J. Syst. Evol. Microbiol. 62, 1389–1395.

Samreen, S., Kausar, S., 2019. Phosphorus fertilizer: the original and commercial sources, in: Zhang, T. (Ed.), Phosphorus-Recovery and Recycling. IntechOpen, London, UK.

Santillan, E., Seshan, H, Constancias, F., Drautz-Moses, D.I., Wuertz, S., 2019. Frequency of disturbance alters diversity, function, and underlying assembly mechanisms of complex bacterial communities. npj Biofilms Microbiomes 5, 8.

Saunders, A.M., Albertsen, M., Vollertsen, J., Nielsen, P.H., 2016. The activated sludge ecosystem contains a core community of abundant organisms. ISME J. 10, 11–20.

Sawyer, C.N., McCarty, P.L., Parkin, G.F., 2003. Chemistry for Environmental Engineering and Science, fifth ed., McGraw-Hill Inc.

Schauder, R., Schink, B., 1989, *Anaerovibrio glycerini* sp. nov., an anerobic bacterium fermenting glycerol to propionate, cell matter, and hydrogen. Arch. Microbiol. 152, 473–478.

Seifan, M., Seifan, T., Jeltsch, F., Tielbörger, K., 2012. Combined disturbances and the role of their spatial and temporal properties in shaping community structure. Perspect. Plant Ecol. Evol. Syst. 14 (3), 217–229.

Shaddel, S., Ucar, S., Andreassen, J.-P., Østerhus, S.W., 2019. Engineering of struvite crystals by regulating supersaturation-correlation with phosphorus recovery, crystal morphology and process efficiency. J. Environ. Chem. Eng. 7 (1), 102918.

Shade, A., Peter, H., Allison, S.D., Baho, D.L., Berga, M., Bürgmann, H., Huber, D.H., Langenheder, S., Lennon, J.T., Martiny, J.B.H., Matulich, K.L., Schmidt, T.M., Handelsman, J., 2012. Fundamentals of microbial community resistance and resilience. Front. Microbiol. 3, 417.

Shih, K., Yan, H., 2016, The crystallization of struvite and its analog (K-struvite) from waste streams for nutrient recycling, in: Prasad, M.N.V., Shih, K. (Eds.), Environmental Material and Waste. Academic Press, Elsevier, pp. 665–686.

Shim, S., Won, S., Reza, A., Kim, S., Ahmed, N., Ra, C., 2020. Design and optimization of fluidized bed reactor operating conditions for struvite recovery process from swine wastewater. Processes 8, 422.

Siegel, F.R., 1961. Factors influencing the precipitation of dolomitic carbonates. State Geol. Surv. Kansas Bull. 152 (Pt. 5), 127–158.

Silva, L., Calleja, M.L., Huete-Stauffer, T.M., Ivetic, S., Ansari, M.I., Viegas, M., Morán, X.A.G., 2019. Low abundances but high growth rates of coastal heterotrophic bacteria in the red sea. Front. Microbiol. 9, 3244.

Singh, B., Szamosi, Z., Siménfalvi, Z., 2020. Impact of mixing intensity and duration on biogas production in an anaerobic digester: a review. Crit. Rev. Biotechnol. 40 (4), 508–521.

Siriwongrungson, V., Zeng, R.J., Angelidaki, I., 2007. Homoacetogenesis as the alternative pathway for H_2 sink during thermophilic anaerobic degradation of butyrate under suppressed methanogenesis. Water Res. 41 (18), 4204–4210.

Sitthi, S., Hatamoto, M., Watari, T., Yamaguchi, T., 2020. Enhancing anaerobic syntrophic propionate degradation using modified polyvinyl alcohol gel beads. Heliyon 6, e05665.

Smith, K.S., Ingram-Smith, C., 2007. *Methanosaeta*, the forgotten methanogen? Trends Microbiol. 15, 150–155.

Sloan, W.T., Lunn, M., Woodcock, S., Head, I.M., Nee, S., Curtis, T.P., 2006. Quantifying the roles of immigration and chance in shaping prokaryote community structure. Environ. Microbiol. 8, 732–740.

Speece, R.E., 2008. Anaerobic Biotechnology and Odor/Corrosion Control for Municipalities and Industries. Archae Press, Tennessee, US.

Stępień, A., Pabis, K., Sobczyk, R., Serigstad, B., 2022. High species richness and extremely low abundance of Cumacean communities along the shelf and slope of the Gulf of Guinea (West Africa). Front. Mar. Sci. 8, 703547.

Stroot, P.G., McMahon, K.D., Mackie, R.I., Raskin, L., 2001. Anaerobic codigestion of municipal solid waste and biosolids under various mixing conditions–I. digester performance. Water Res. 35 (7), 1804–1816.

Swain, G., Maurya, K.L., Sonwani, R.K., Singh, R.S., Jaiswal, R.P., Nai, B.N., 2022. Effect of mixing intensity on biodegradation of phenol in a moving bed biofilm reactor: process optimization and external mass transfer study. Bioresour. Technol. 351, 126921.

Szogi, A.A., Vanotti, M.B., Shumaker, P.D., 2018. Economic recovery of calcium phosphates from swine lagoon sludge using quick wash process and geotextile filtration. Front. Sustain. Food Syst. 2, 37.

Tai, C.Y., Chien, W.-C., Chen, C.Y., 1999. Crystal growth kinetics of calcite in a dense fluidized-bed crystallizer. AIChE J. 45 (8), 1605–1614.

Tang, Y., Shigematsu, T., Morimura, S., Kida, K., 2005. Microbial community analysis of mesophilic anaerobic protein degradation process using bovine serum albumin (BSA)-fed continuous cultivation. J. Biosci. Bioeng. 99, 150–164.

Tarragó, E., Puig, S., Ruscalleda, M., Balaguer, M.D., Colprim, J., 2016. Controlling struvite particles' size using the up-flow velocity. Chem. Eng. J. 302, 819–827.

Tarragó, T., Sciarria, T.P., Ruscalleda, M., Colprim, J., Balaguer, M.D., Adani, F., Puig, S., 2018. Effect of suspended solids and its role on struvite formation from digested manure. J. Chem. Technol. Biotechnol. 93, 2758–2765.

Tervahauta, T., Trang, H., Hernández, L., Zeeman, G., Buisman, C.J.N., 2013. Prospects of source-separation-based sanitation concepts: a model-based study. Water 5, 1006–1035.

Tervahauta, T., van der Weijden, R.D., Flemming, R.L., Leal, L.H., Zeeman, G., Buisman, C.J.N., 2014. Calcium phosphate granulation in anerobic treatment of black water: a new approach to phosphorus recovery. Water Res. 48, 632–642.

Theregowda, R.B., González-Mejía, A.M., Ma, X., Garland, J., 2019. Nutrient recovery from municipal wastewater for sustainable food production systems: an alternative to traditional fertilizers. Environ. Eng. Sci. 36 (7), 833–842.

Thomas, F., Hehemann, J.-H., Rebuffet, E., Czjzek, M., Michel, G., 2011. Environmental and gut *Bacteroidetes*: the food connection. Front. Microbiol. 2, 93.

Todt, D., Heistad, A., Jenssen, P.D., 2015. Load and distribution of organic matter and nutrients in a separated household wastewater stream. Environ. Technol. 36 (12), 1584–1593.

Tung, M.S., 1998. Calcium phosphates: structure, composition, solubility, and stability, in: Z. Amjad (Ed.), Calcium Phosphates in Biological and Industrial Systems, Springer, New York, pp. 1–19.

Turnbaugh, P.J., Walters, W.A., Widmann, J., Yatsunenko, T., Zaneveld, J., Knight, R., 2010. QIIME allows analysis of high-throughput community sequencing data. Nat. Methods 7 (5), 335–336.

Uludag-Demirer, S., Othman, M., 2009. Removal of ammonium and phosphate from the supernatant of anaerobically digested waste activated sludge by chemical precipitation. Bioresour. Technol. 100 (13), 3236-3244.

Van Kauwenbergh, S.J., Stewart, M., Mikkelsen, R., 2013. World reserves of phosphate rock-a dynamic and unfolding story. Better Crops 97 (3), 18–20.

Vavilin, V.A., Fernandez, B., Palatsi, J., Flotats, X., 2008. Hydrolysis kinetics in anaerobic degradation of particulate organic material: an overview. Waste Manage. 28 (6), 939–951.

Venkiteshwaran, K., Bocher, B., Maki, J., Zitomer, D., 2016. Relating anaerobic digestion microbial community and process function. Microbiol Insights 8, 37–44.

Verberk, W.C.E.P., 2011. Explaining general patterns in species abundance and distributions. Nature Education Knowledge 3(10), 38.

Vuono, D.C., Benecke, J., Henkel, J., Navidi, W.C., Cath T.Y., Munakata-Marr, J., Spear, J.R., Drewes, J.E., 2015. Disturbance and temporal partitioning of the activated sludge metacommunity. ISME J. 9, 425–435.

Wang, J., Burken, J.G., Zhang, X., 2006. Effect of seeding materials and mixing strength on struvite precipitation. Water Environ. Res. 78 (2), 125–132.

Wang, X., Chen, J., Li, Z., Cheng, S., Mang, H.-P., Zheng, L., Jan, I., Harada, H., 2023. Nutrient recovery technologies for management of blackwater: a review. Front. Environ. Sci. 10, 1080536.

Wang, X., Lu, X., Li, F., Yang, G., 2014. Effects of temperature and carbon-nitrogen (C/N) ratio on the performance of anaerobic co-digestion of dairy manure, chicken manure and rice straw: focusing on ammonia inhibition. PLoS One 9(5), e97265.

Wang, L.-L., Wang, L.-F., Ren, X.-M., Ye, X.-D., Li, W.-W., Yuan, S.-J., Sun, M., Sheng, G.-P., Yu, H.-Q., Wang, X.K., 2012. pH dependence of structure and surface properties of microbial EPS. Environ. Sci. Technol. 46, 737–744.

Wang, W., Xie, L., Luo, G., Zhou, Q., Angelidaki, I., 2013. Performance and microbial community analysis of the anaerobic reactor with coke oven gas biomethanation and in situ biogas upgrading. Bioresour. Technol. 146, 234–239.

Wei, J., Ge, J., Rouff, A.A., Wen, X., Meng, X., Song, Y., 2019. Phosphorus recovery from wastewater using light calcined magnesite, effects of alkalinity and organic acids. J. Environ. Chem. Eng. 7 (5), 103334.

Weiss, S., Zankel, A., Lebuhn, M., Petrak, S., Somitsch, W., Guebitz, G.M., 2011. Investigation of microorganisms colonising activated zeolites during anaerobic biogas production from grass silage. Bioresour. Technol. 102 (6), 4353–4359.

Werner, J.J., Koren, O., Hugenholtz, P., DeSantis, T.Z., Walters, W.A., Caporaso, J.G., Angenent, L.T., Knight, R., Ley, R.E., 2012. Impact of training sets on classification of high-throughput bacterial 16s rRNA gene surveys. ISME J. 6 (1), 94–103.

Wilsenach, J.A., van Loosdrecht, C.M., 2006. Integration of processes to treat wastewater and source-separated urine. J. Environ. Eng. 132 (3), 331–341.

Wintsche, B., Jehmlich, N., Popp, D., Harms, H., Kleinsteuber, S., 2018. Metabolic adaptation of methanogens in anaerobic digesters upon trace element limitation. Front. Microbiol. 9, 405.

Wu, Z., Liu, Q., Li, Z., Cheng, W., Sun, J., Guo, Z., Li, Y., Zhou, J., Meng, D., Li, H., Lei, P., Yin, H., 2018. Environmental factors shaping the diversity of bacterial communities that promote rice production. BMC Microbiology 18, 51.

Xia, Y., Chin, F.Y.L., Chao, Y., Zhang, T., 2015. Phylogeny-structured carbohydrate metabolism across microbiomes collected from different wastewater treatment process. Biotechnol. Biofuels 8, 172.

Xu, Z., Shi, Z., Jiang, L., 2011. Industrial biotechnology and commodity products, in: Moo-Young, M. (Ed.), Comprehensive Biotechnology, pp. 189–199.

Yan, Y., Connolly, J., Liang, M., Jiang, L., Wang, S., 2021. Mechanistic links between biodiversity effects on ecosystem functioning and stability in a multi-site grassland experiment. J. Ecol. 109, 3370–3378.

Yang, X., Wan, Y., Zheng, Y., He, F., Yu, Z., Huang, J., Wang, H., Ok, Y.S., Jiang, Y., Gao, B., 2019. Surface functional groups of carbon-based adsorbents and their roles in the removal of heavy metals from aqueous solutions: a critical review. Chem. Eng. J. 366, 608–621.

Yao, Y., 2014. Use of Carbohydrate, Protein and Fat to Characterise Wastewater in terms of Its Major Elemental Constituents and Energy, University of Manchester, UK.

Yee, R.A., Alessi D.S., Ashbolt, N.J., Hao, W., Konhauser, K., Liu, Y., 2019. Nutrient recovery from source-diverted blackwater: optimization for enhanced phosphorus recovery and reduced co-precipitation. J. Clean. Prod. 235 (20), 417–425.

Yee, R.A., Leifels, M., Scott, C., Ashbolt, N.J., Liu, Y., 2019. Evaluating microbial and chemical hazards in commercial struvite recovered from wastewater. Environ. Sci. Technol. 53 (9), 5378–5386.

Yu, N., Guo, B., Zhang, Y., Zhang, L., Zhou, Y., Liu, Y., 2020. Different micro-aeration rates facilitate production of different end-products from source-diverted blackwater. Water Res. 177, 115783.

Yuan, Z., Pratt, S., Batstone D.J., 2012. Phosphorus recovery from wastewater through microbial processes. Curr. Opin. Biotechnol. 23 (6), 878–883.

Zamanzadeh, M., Hagen, L.H., Svensson, K., Linjordet, R., Horn, S.J., 2016. Anaerobic digestion of food waste–effect of recirculation and temperature on performance and microbiology. Water Res. 96, 246–254.

Zeeman, G., Kujawa, K., de Mes, T., Hernandez, L., de Graaff, M., Abu-Ghunmi, L., Abu-Ghunmi, L., Mels, A., Meulman, B., Temmink, H., Buisman, C., van Lier, J., Lettinga, G., 2008. Anaerobic

treatment as a core technology for energy, nutrients and water recovery from source separated domestic waste(water). Water Sci. Technol. 57 (8), 1207-1212.

Zhang, H., Gong, W., Luo, X., Xie, B., Li, G., Liang, H., 2019. Obtaining high-purity struvite from anaerobically digested wastewater: effects of pH, Mg/P, and Ca^{2+} interactions. Environ. Eng. Sci. 36 (1), 102–113.

Zhang, L., Guo, B., Mou, A., Li, R., Liu, Y., 2020. Blackwater biomethane recovery using a thermophilic upflow anaerobic sludge blanker reactor: impacts of effluent recirculation on reactor performance. J. Environ. Manage. 274, 111157.

Zhang, L., Guo, B., Zhang, Q., Florentino, A., Xu, R., Zhang, Y., Liu, Y., 2019. Co-digestion of blackwater with kitchen organic waste: effects of mixing ratios and insights into microbial community. J. Clean. Prod. 236, 117703.

Zhang, L., Mou, A., Guo, B., Sun, H., Anwar, M.N., Liu, Y., 2021. Simultaneous phosphorus recovery in energy generation reactor (SPRING): high rate thermophilic blackwater treatment. Resour. Conserv. Recycl. 164, 105163.

Zhang, L., Mou, A., Sun, H., Zhang, Y., Zhou, Y., Liu, Y., 2021. Calcium phosphate granules formation: key to high rate of mesophilic UASB treatment of toilet wastewater. Sci. Total Environ. 773, 144972.

Zhang, L., Vrieze, J.D., Hendrickx, T.L.G., Wei, W., Temmink, H., Rijnaarts, H., Zeeman, G., 2018. Anaerobic treatment of raw domestic wastewater in a UASB-digester at 10°C and microbial community dynamics. Chem. Eng. J. 334, 2088–2097.

Zhang, L., Zhang, Y., Yuan, Y., Mou, A., Park, S., Liu, Y., 2022. Impacts of granular activated carbon addition on anaerobic granulation in blackwater treatment. Environ. Res. 206, 112406.

Zhao, X., Yang, Y., Feng, K., Wang, X., Liu, B., Xie, G., Xing, D., 2012. Self-regulating microbiome networks ensure functional resilience of biofilms in sand biofilters during manganese load fluctuations. Water Res. 188, 116473.